INVESTIGATION OF MOLECULAR MAGNETIC COMPOUNDS INCORPORATING 4D AND 5D TRANSITION METAL CYANOMETALLATES

A Dissertation

by

HEATHER IRENE SOUTHERLAND

Submitted to the Office of Graduate Studies of
Texas A&M University
in partial fulfillment of the requirements for the degree of

DOCTOR OF PHILOSOPHY

Chair of Committee,	Kim R. Dunbar
Committee Members,	Timothy R. Hughbanks
	Hong-Cai Zhou
	Igor V. Roshchin
Head of Department,	David H. Russell

August 2013

Major Subject: Chemistry

ABSTRACT

The field of molecular magnetism has expanded rapidly since the discovery of single molecule magnets (SMMs) in the 1990's and has witnessed extraordinary advances in the last several decades. One of the current trends in molecular magnetic research is to incorporate metal ions that have pronounced single-ion anisotropy in an effort to improve magnetic exchange interactions. The 4d and 5d transition metal ions have large spin-orbit coupling parameters which contribute to the orbital angular momentum effects that lead to anisotropic behavior. The work herein describes efforts to synthesize and characterize new cyanide-bridged molecular materials incorporating 4d and 5d transition metal ions, specifically the $[Os(CN)_6]^{3-}$, $[Mo(CN)_6]^{3-}$ and $[W(CN)_8]^{3-}$ ions.

The 5d hexacyanometallate $[Os(CN)_6]^{3-}$ was incorporated into a trinuclear cyanide bridged molecule and the $[Fe(CN)_6]^{3-}$ analog was prepared as a reference compound for assessing the effect of the 5d versus 3d metal ion on the magnetic properties. Both molecules exhibit SMM bistability with a pronounced increase (~90 %) in the blocking temperature (T_B) of the Os^{III} analogue. In addition to typical SMM behavior, both compounds exhibit exchange-biased SMM behavior, a shift in the quantum tunneling of the magnetization (QTM) from zero field. This exchange-bias can be turned "on" or "off" depending on the presence of interstitial methanol molecules.

New trigonal bipyramidal (TBP) molecules incorporating the rarely studies hexacyanomolybdate(III) ion are presented in chapter III of this dissertation. The molecules of general formula $[M(tmphen)_2]_3[Mo(CN)_6]_2$ (M = V^{II}, Mn^{II} and Fe^{II}; tmphen

= 3,4,7,8-tetramethyl-1,10-phenanthroline), represent additions to a large homologous family of TBP molecules reported by the Dunbar group over the years. The $[Mo(CN)_6]^{3-}$ ion was prepared *in situ* by loss of one cyanide ligand from $[Mo(CN)_7]^{4-}$. Of particular interest among the compounds reported is the V_3Mo_2 analog which exhibits extraordinarily strong antiferromagnetic coupling (estimated J = -134 cm^{-1}). The observed exchange coupling parameter is more than twice the current record for the antiferromagnetic coupling parameter for a cyanide-bridged magnetic molecule.

Another set of results were obtained using the octacyanometallate anion $[W^V(CN)_8]^{3-}$ as a building block for the synthesis and magnetic studies of a family of new cyanide-bridged magnetic materials. The compounds exhibit several different structural motifs including three 0-D molecular compounds (two pentanuclear molecules and a linear trinuclear molecule) and a 1-D chain, findings that illustrate the structural versatility of the octacyanotungstate(V) ions. The TBP molecule, $[Mn(tmphen)_2]_3[W(CN)_8]_2$, exhibits evidence for an out-of-phase signal when subjected to ac measurements in zero applied field. The 1-D chain also reveals evidence for the beginning of an out-of-phase signal under zero applied field which hints at single chain magnet behavior.

DEDICATION

To Imogen for reminding me of the important things in life.

~ Jellyfish Skew
~ Rayfish Ay
~ Snails Ooooo

ACKNOWLEDGEMENTS

First and foremost I would like to thank my advisor Prof. Kim R. Dunbar for her support and guidance throughout this process. It was Prof. Dunbar's research that first drew me to Texas A&M -- the enthusiasm and passion she has for research is contagious. I appreciate her patience and understanding with my non-traditional situation; her flexibility allowed me to be a full time researcher while being a full time mom.

I would like to thank my committee members, Prof. Timothy R. Hughbanks, Prof. Joe Zhou and Prof. Igor V. Roshchin for their support and time spent on this process. I would also like to thank Prof. Winfried Teizer for his time spent on my committee during my literature seminar and preliminary exam. Some of the research presented in this dissertation would not be possible without the measurements and theoretical calculations performed by our collaborators. I would like to thank Dr. Wolfgang Wernsdorfer for the micro-SQUID measurements in Chapter II and Dr. Mironov for the theoretical calculations in Chapter III.

I would like to thank the people who helped in guiding my meandering path on the road to pursue a Ph. D. Thanks to Dr. Robin McRae, the professor of the first chemistry class I was forced to take as a biology major – his enthusiasm in teaching was such that I fell in love with chemistry and changed my major. I am especially grateful to my undergraduate research advisor, Dr. Jamie Manson, who introduced me the world of research and helped me discover my love of inorganic chemistry.

I thank the members of the Dunbar group for their help and support of over the years, especially Dr. Andrey Prosvirin for teaching as he helped work up my magnetic data and for measuring my samples “just one more time” so we could verify the properties; Dr. Hanhua Zhao for his patience and help in the lab, without which the work in Chapter IV would not have been possible; and Dr. Xinyi Wang who taught me an incredible amount about synthesis. Thank you to all of the former Dunbar group members - Dr. Dafhne Aguire, Dr. Carolina Avendaño, Dr. Maryfer Ballesteros Rivas, Charlene Campbell, Dr. Kristen Funk, Ed Funck, Dr. Matt Hilfiger, Dr. Ferdi Karadas, Sarah Lane, Dr. Nazario Lopez, Dr. Eric Reinheimer and Dr. Qing-Lun Wang – for everything you taught me and for your support inside the lab and out. Thank you to all the current Dunbar group members – Francisco Birk, Andrew Brown, Mayela Canales, Amanda David, Jill Frank, David Kempe, Zhanyong Li, Bruno Peña-Maceda, Mohamed Saber, Codi Sanders, Toby Woods, Xuan Zhang, Zhongyue Zhang, Dr. Helen Chifotides and Dr. Dawid Pinkowicz – for being a great group to work with.

Thank you to all of my friends both near and far who have supported me through this process. Thanks to those at home who continue to be among my closest friends despite the distance, Delena Meyer and Lisa Ratzesberger. Thank you to Dr. Brendan Twamley for your friendship and encouragement, even when it came in the form of sarcasm. Thank you to my good friend Dr. Ian Giles, for the daily coffee break.

I wish to thank my family for their unconditional love and support—I am the person I am today because of you. I want to thank my parents, Steve and Lura Southerland, for their loving support and constant prayers. I thank my mom, Barbara

Austin, who followed me halfway across the country to help me pursue this dream and through the process has become one of my closest friends and confidants. I am grateful to my sister Steviee for her willingness to help with anything, especially during the home-stretch and for providing the occasional diversion in the form of afternoon shopping trips. I thank my brother John for his loving heart and slightly off-beat humor that always makes me smile. Thank you to my sister Amy for being my best friend and always being there with words of support or an appropriate movie quote.

Finally, I want to thank Tim Smallwood who helped me restore balance to my life and who has been my support in every way through this process. I look forward to facing many more challenges with you.

TABLE OF CONTENTS

Page

LIST OF FIGURES

Page

LIST OF TABLES

Page

CHAPTER I

INTRODUCTION AND LITERATURE REVIEW

Molecular magnetism is an emerging field of chemistry that has experienced a period of rapid growth over the last several decades[1-7] which is driven, in part, by the need for improved magnetic materials for use in developing modern technologies.[8-18] Computer hard drives, televisions, audio devices, motors and medical MRI equipment are just a few examples of common uses for magnets.[19,20] As technology develops, there is a continual push toward smaller lightweight devices that exhibit improved performances. Molecule-based magnets have certain advantages over classical magnets in that they can be synthesized at room temperature, have higher solubility, lower densities and have the possibility to be tuned *via* subtle modification of the linkers and metal centers.[21-29] The latter issue is most easily addressed if the synthesis of molecular magnets follows a building block or modular approach. By carefully selecting the molecular precursors the resulting materials are tailored to exhibit a particular geometry and to exhibit specific physical properties which depend on the magnetic interaction between building units, that is, both the metal centers and the bridging ligands that mediate exchange interactions. Of particular interest is the goal to synthesize multifunctional materials or bistable systems,[30] which are compounds that can exist in two stable states with the "on" and "off" states being controlled by heat, light, or an external magnetic field.[31,32]

Molecular Magnetism

Molecular magnetic materials behave in a similar fashion to their classical counterparts. That is, in an applied magnetic field, spin centers can interact in several ways: (a) ferromagnetic ordering occurs when spin centers align in a parallel fashion resulting in a net magnetic moment, (b) antiferromagnetic ordering is when spins align antiparallel to one another leading to an overall cancelation of the spin, (c) a ferrimagnet is the result of antiferromagnetic coupling between neighboring spins of unequal magnitude such that a net magnetic moment remains (Figure 1.1a).[33,34] These magnetic properties were first studied in bulk minerals and then, in the mid-1950s, Goodenough[35,36] and Kanamori[37] developed rules governing the expected exchange interactions between metal ions based on the symmetry of the involved orbitals. Magnetic exchange occurs through a pathway, either directly through space which is a special case involving bond formation (as in a metal-metal bond) or through a bridging ligand. The strength of the interaction is described by an exchange coupling constant, J, which can be either positive or negative. A large overlap between magnetic orbitals, i.e. interaction of orbitals of the same symmetry, tends to pair the spins, resulting in antiferromagnetic coupling. If the orbital overlap is minimal or zero, *i.e*. the orbitals are orthogonal, the spins will be parallel and ferromagnetic coupling results. The exchange interactions can be described using the Heisenberg-Dirac-Van Vleck[38] Hamiltonian (HDVV), $H = -2JS_AS_B$, where S is the local spins on metal centers M_A and M_B and the exchange coupling parameter, J, is positive for ferromagnetic exchange and negative for antiferromagnetic exchange (Figure 1.1b).

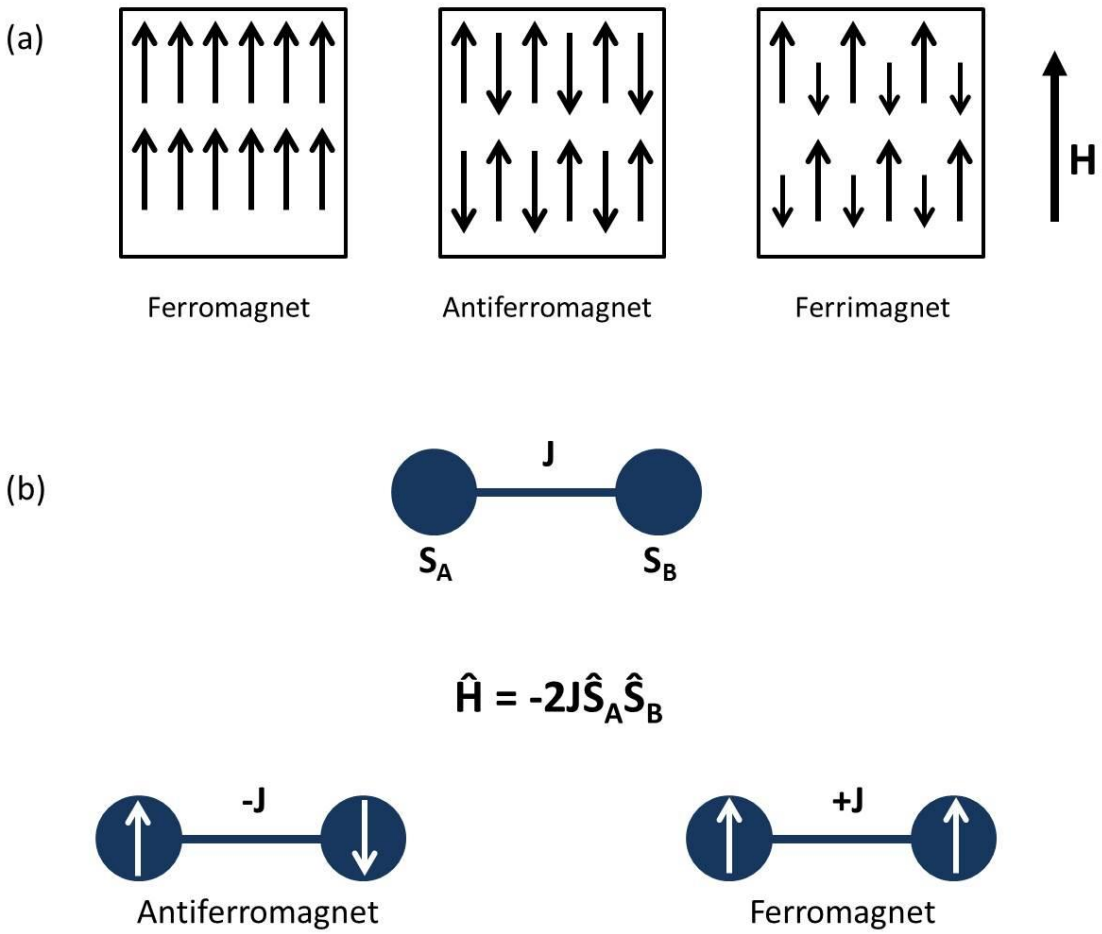

Figure 1.1 (a) Schematic representation of the different types of ordering. (b) The Heisenberg Hamiltonian describing exchange interactions between spin centers where J is negative for antiferromagnetic coupling and positive for ferromagnetic coupling.

In terms of synthesizing materials useful for technological devices, one of the initial goals of the field was to design materials that order at or above room temperature. A plethora of related research studies over the past several decades has spawned a library of compounds that order at high temperatures. The first room temperature molecule-based magnet, $V(TCNE)_2$, was reported by Miller in 1991,[39] with an ordering temperature, T_c, above 350 K and the first room temperature cyanide-based magnet, the Prussian Blue analog $V^{II}_{0.42}V^{III}_{0.58}[Cr^{III}(CN)_6]_{0.86}\bullet 2.8H_2O$ (T_C = 315K), was reported by Verdaguer's group in 1995.[40] Shortly thereafter, the independent groups of Girolami and Verdaguer reported that bimetallic Prussian Blue analogs can exhibit spontaneous magnetization at temperatures as high as 376 K.[41,42] Aside from their high ordering temperatures, Prussian-Blue analogs are known to exhibit a variety of interesting properties,[43,44] including photo-switchable magnetism,[45-50] spin-crossover behavior,[51-55] and charge-transfer induced spin transition.[56-62] Under external stimuli, these compounds undergo changes in the electronic state of one or more of the metal ions and consequently the observed magnetic properties are altered. Although Prussian Blue analogs often exhibit many interesting properties, the inability to determine their exact compositions presents a formidable obstacle to establishing structure-property relationships, as these materials are poorly crystalline products with many defects. This fact has prompted chemists to design cyanide-bridged compounds that mimic PB-type properties at the molecular level. Research in this field has progressed rapidly by employing the use of cyanometallates equipped with capping ligands as precursors, thereby preventing the formation of an extended three-dimensional network. This

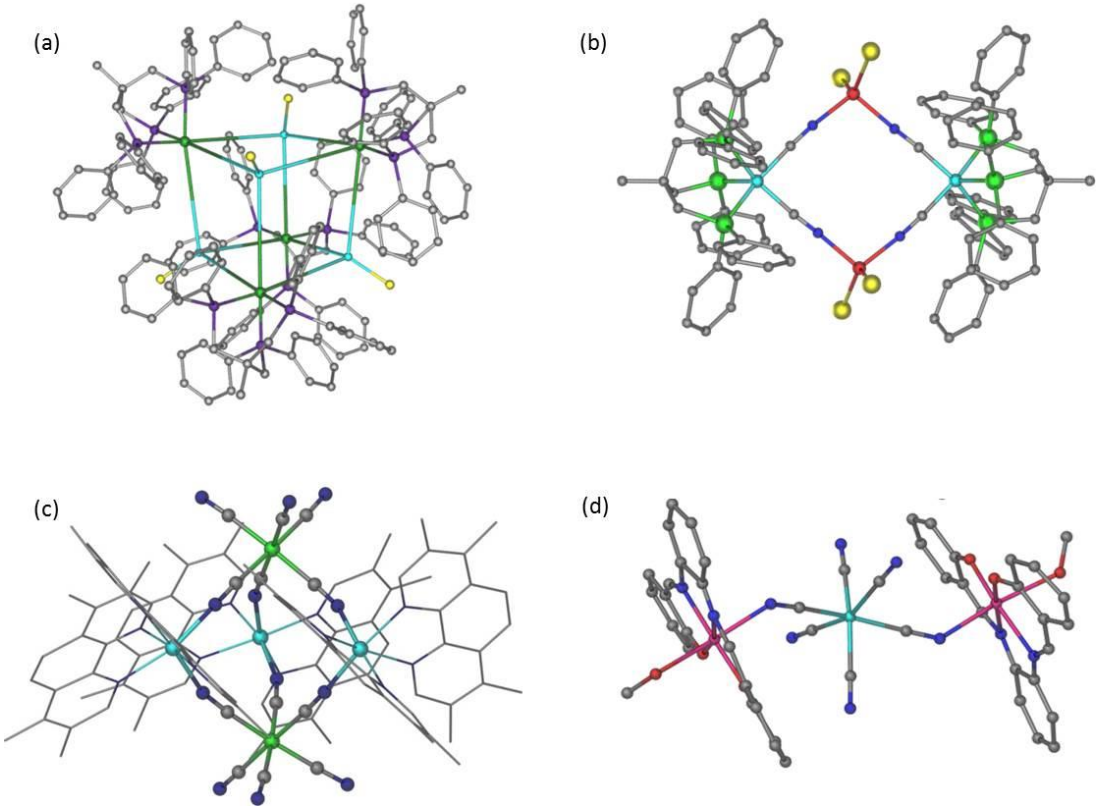

Figure 1.2 Ligand protected cyanide-bridged molecules (a) $M_4M'_4$ cube, (b) $M_2M'_2$ square, (c) $M_3M'_2$ trigonal bipyramid, (d) M_2M' trinuclear, illustrating the synthetic control afforded by the "building block" method of synthesis. Adapted from references 29, 44, 119 and 190.

"building-block approach" has thus far yielded a wide variety of model architectures, including molecular trinuclear compounds, squares, trigonal bipyramids, cubes and other more complex architectures (Figure 1.2).[1]

Single Molecule Magnets

Recently, the synthesis of magnetic materials on the nanometer scale has been the focus of considerable research efforts. The early 1990's was marked by the discovery of Single Molecule Magnets (SMMs), single-domain magnetic particles of molecular origin.[63,64] These SMMs retain their magnetization below a blocking temperature (T_B) in the absence of a magnetic field and exhibit magnetic hysteresis of molecular origin. SMMs are true 'mesoscale' particles that straddle the classical and quantum boundary;[65] along with classical magnetic behavior, they also exhibit a number of quantum effects: quantum size, quantum tunneling magnetization (QTM)[66-69] and quantum phase interference[70,71] which could render them useful as magnetic information storage units.[72] The slow reversal of their magnetization arises from both a high-spin ground state (S) and uniaxial anisotropy (D) (from axial zero-field splitting) resulting in an energy barrier for the inversion of the total spin of the molecule. The relaxation obeys two different processes, depending on the temperature. At high temperatures, the relaxation time (τ), is a thermally activated barrier (U), and is equal to $S^2|D|$ (integer spin systems) or $(S^2-1/4)|D|$ (half-integer spin systems).[72] At very low temperatures, QTM becomes the fastest relaxation pathway. A crossover between these two regimes, called thermally-assisted QTM, is often observed experimentally and an effective barrier (U_{eff}), much lower than U, is observed (Figure 1.3).[73]

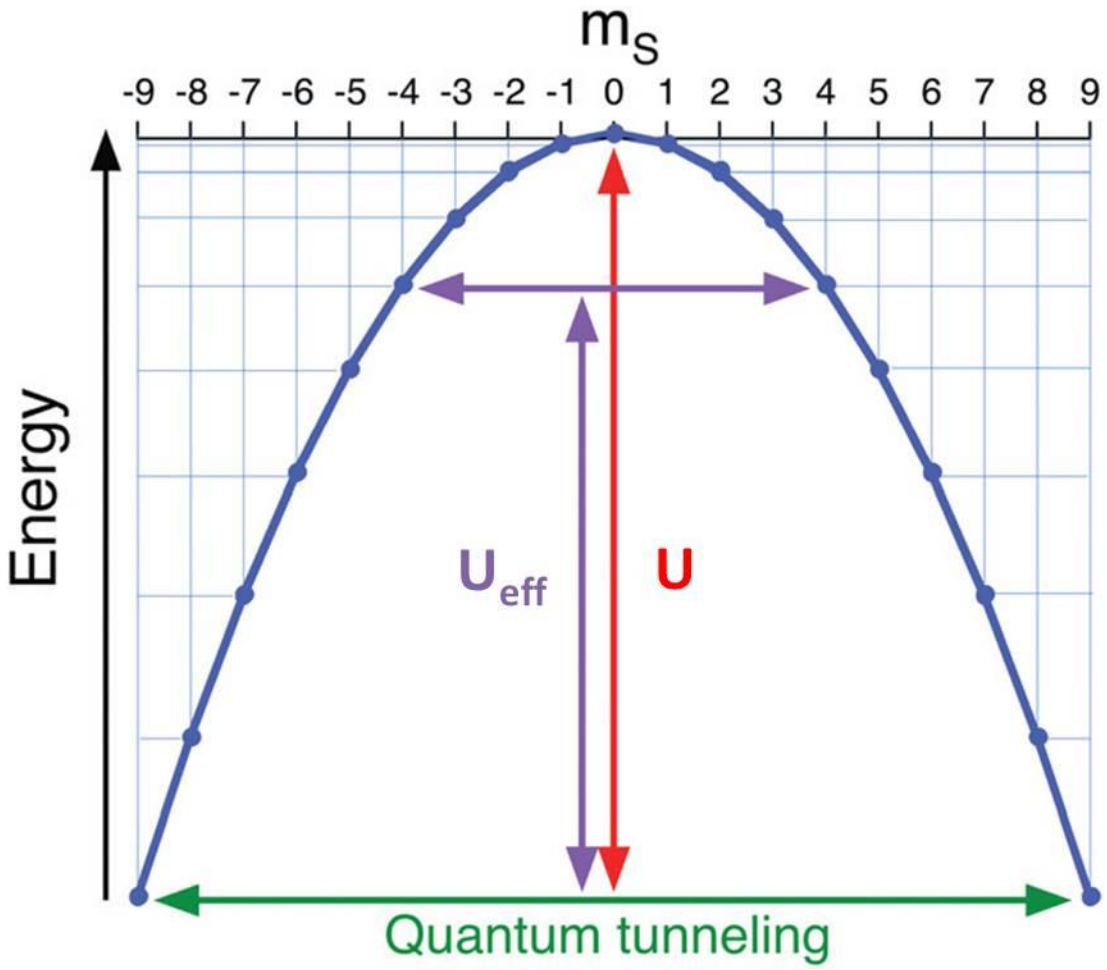

Figure 1.3 The energy diagram of an $S_T = 9$ SMM.[74] Red: The thermal energy barrier, U. Purple: The effective energy barrier, U_{eff}, due to thermally assisted QTM. Green: QTM. Adapted from reference 74.

The first molecule discovered to behave as an SMM is $[Mn_{12}O_{12}(O_2CCH_3)_{16}(H_2O)_4]$ ($Mn^{III}_8Mn^{IV}_4$) which was first reported by Lis in 1980[75] and later magnetically characterized by Christou and Hendrickson and independently by Gatteschi, Sessoli and co-workers (Figure 1.4).[63,64,76] Shortly thereafter Friedman, Sarachik and Barbara reported the observance of QTM in the Mn_{12}-Acetate molecule.[69,77] This discovery was followed by a family of the S = 10 mixed-valent compounds $[Mn_{12}O_{12}(O_2CR)_{16}(H_2O)_4]$ (R = Et, Ph, etc.), which were, until recently, the SMMs with the highest reported blocking temperatures (T_B = 3.5 K) and U_{eff} values (up to 51.4 cm^{-1}).[64,78-95] It was not until 15 years after the first discovery that Christou and co-workers reported a compound that had a higher blocking temperature (T_B = 4.5 K) and larger effective barrier (U_{eff} = 60.0 cm^{-1}) than the Mn_{12} series.[96] The molecule $[Mn^{III}_6O_2(sao)_6(O_2CPh)_2(EtOH)_4]$ ($saoH_2$ = salicylaldoxime or 2-hydroxybenzaldehyde oxime), possesses a structural distortion of the core of the hexametallic complex which was shown to switch the dominant magnetic exchange interactions among metal centers from antiferromagnetic to ferromagnetic, resulting in a molecule with S = 12 and D = -0.43 cm^{-1} in the ground state, giving rise to improved SMM properties (Figure 1.5).

Single Molecule Magnets: Spin versus Anisotropy

As presented earlier, the magnitude of the thermal barrier for reversal of the magnetization of SMMs is related to both the spin ground state, S, and the axial zero-field splitting parameter, D_Z, with a relationship of $U = S^2|D|$. It follows then, since the barrier height is dependent on the square of S, that it should have the largest effect. Much of the early research on SMMs focused on increasing the nuclearity and the spin

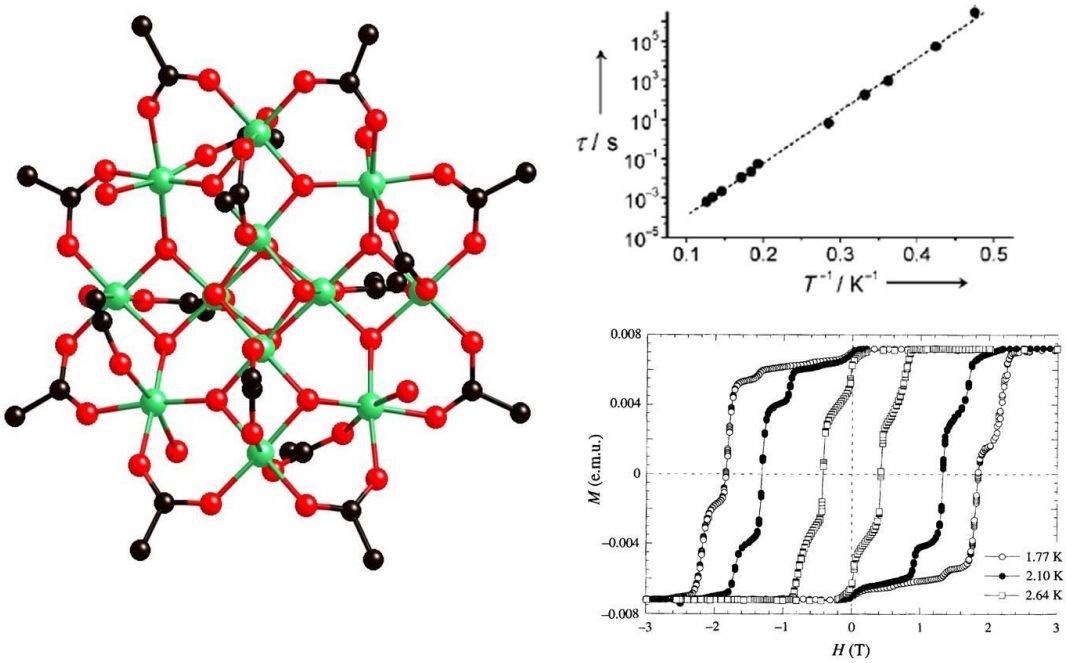

Figure 1.4 Molecular representation of the $Mn_{12}Ac$ SMM, Green = Mn, Red = O, Black = C. Top right: Arrhenius Law fit for the ac susceptibility data of $Mn_{12}Ac$ giving a barrier of 43.2 cm^{-1} and $\tau_0 = 2.1 \times 10^{-7}$ s. Bottom right: Hysteresis loop for $Mn_{12}Ac$ showing QTM through the barrier. Adapted from references 66 and 73.

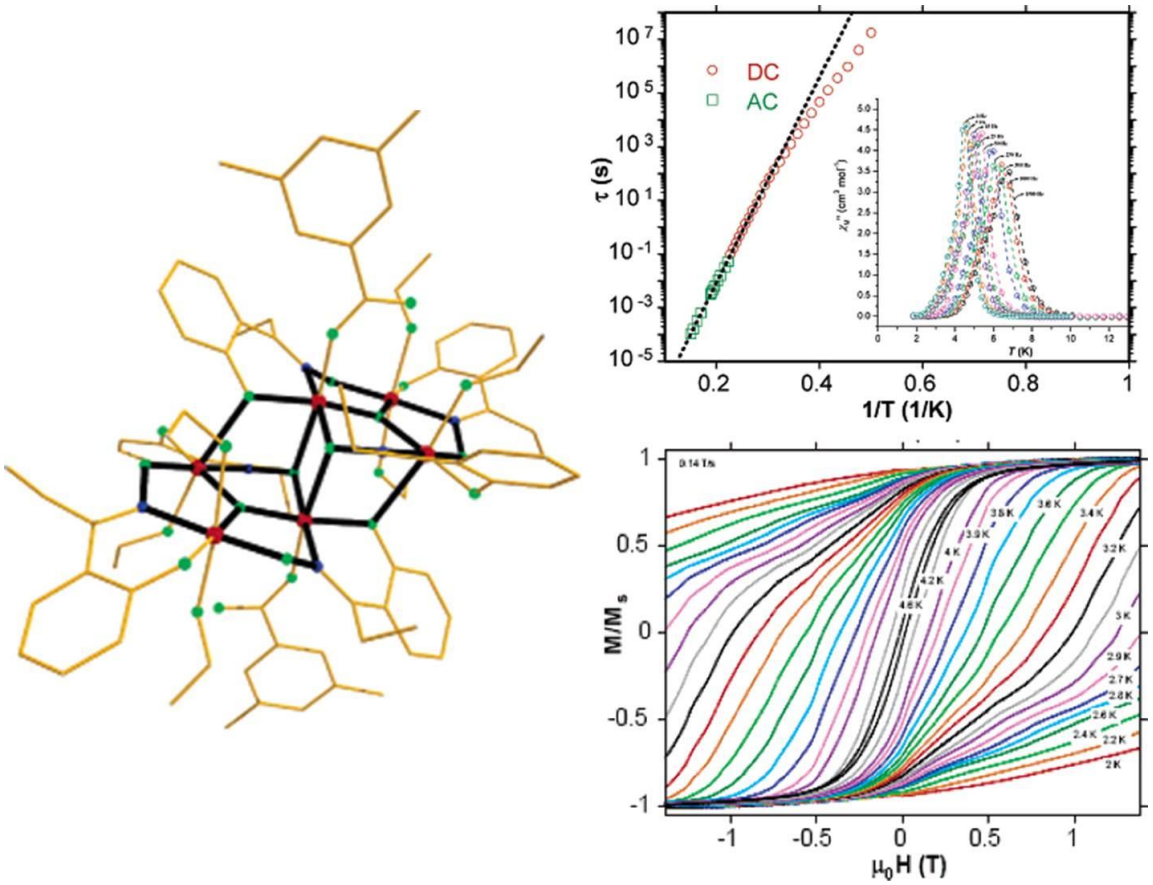

Figure 1.5 The molecule $[Mn^{III}_6O_2(sao)_6(O_2CPh)_2(EtOH)_4]$ ($saoH_2$ = salicylaldoxime or 2-hydroxybenzaldehyde oxime) showing the trigonal distortion of the Mn_6 core. Top right: ac susceptibility, χ" vs. T and the Arrhenius Law fit, U_{eff} = 60 cm^{-1}. Bottom right: Hysteresis loops of the SMM. Adapted from reference 95.

ground state of the molecules, such as those reported by Powell *et al*.[97] with a Mn_{19} molecule exhibiting a ground state of 83/2 and Christou *et al*. with Mn_{25} and Mn_{84} molecules having spin ground states of S = 51/2 and S = 6, respectively (Figure 1.6).[98,99] While these results represent an impressive array of large spin and/or high nuclearity molecules, all of these molecules are extremely low temperature SMMs with blocking temperatures less than 1 K. Recent theoretical work has suggested that focusing on the inherent anisotropy of the clusters should be a much more promising method for increasing the blocking temperature of SMM materials rather than the more traditional approach of increasing the ground state spin value.[100-109] The issue of the dependence of the barrier height relying mainly on S was addressed by Waldmann[106] in 2007. He pointed out that relying on the interpretation of the barrier height as $U = S^2|D|$, which results in the "golden rule" that spin has more of an influence on the magnitude of the barrier, is not exactly correct, but instead may be on the order of unity with D. In 2008, a paper by Ruiz and Alvarez argued that it may not even be possible to have high anisotropy and high ground state spin value coexist.[107] The theoretical work clearly indicates that it is more important for chemists to focus on increasing the anisotropy parameter, D, than the spin, S, for obtaining higher barriers in SMMs.

Anisotropy in 4d and 5d Transition Metals

One of the ways to increase the anisotropy is to use building blocks based on the heavier 4d and 5d transition metal ions which have larger spin-orbit interactions than their 3d counterparts resulting in the ground state being more isolated than the excited states. Moreover the larger, more diffuse orbitals of the 4d/5d metal ions provide better

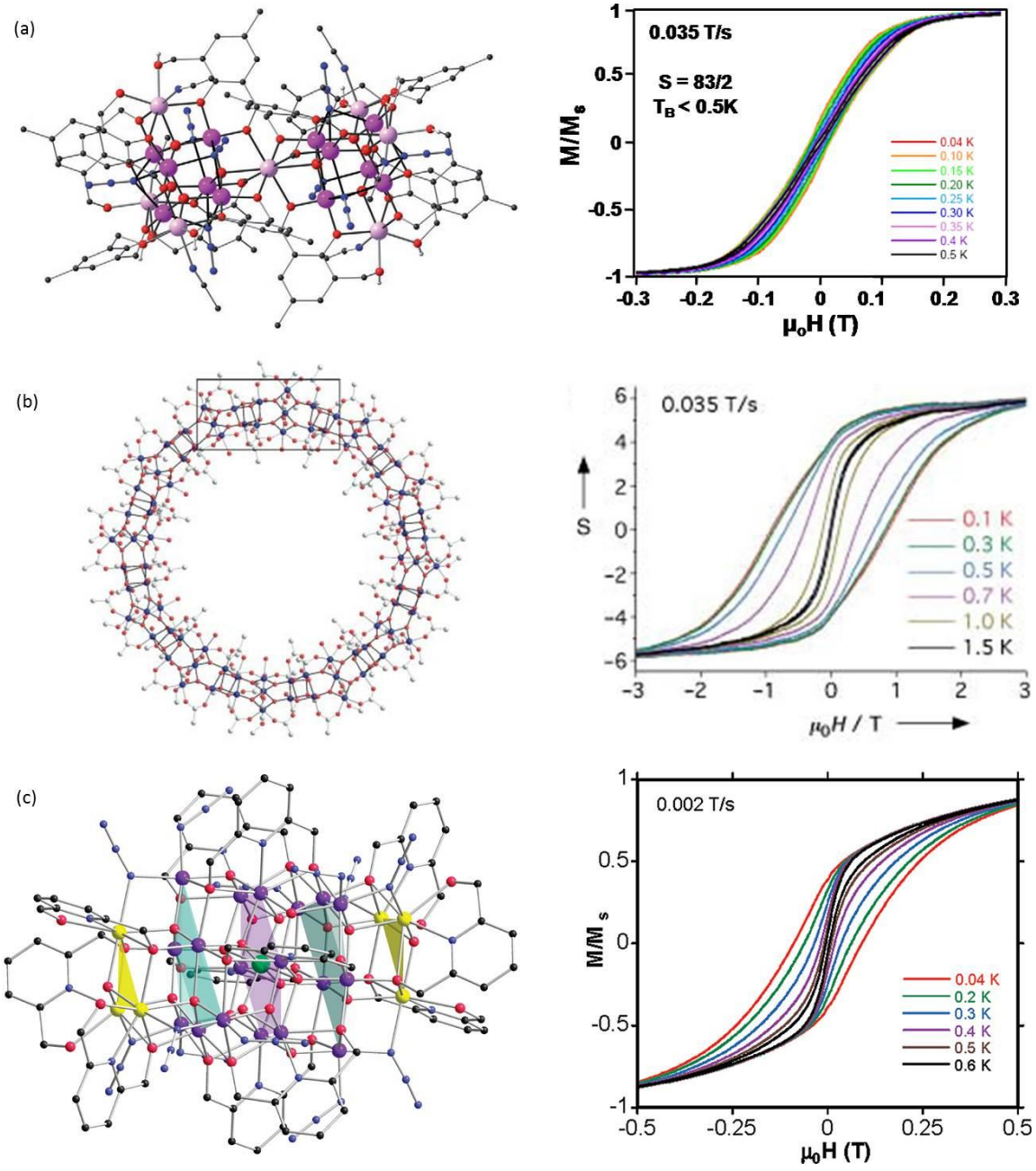

Figure 1.6 Examples of giant spin/large nuclearity compounds. (a) Mn_{19}, S = 83/2 molecule,[97] (b) Mn_{84}, S = 6 molecule[99], (c) Mn_{25}, S = 51/2 molecule.[98]

overlap and thus increase the strength of the exchange interaction and this interaction is expected to be anisotropic due to the orbitally dependent contributions to the exchange.[4,110-113] Despite it being known for some time that incorporation of the heavier cyanometallate congeners would most likely lead to enhanced magnetic properties, there have been relatively few SMMs reported incorporating these metal ions. The majority of compounds studied containing these ions are based on the precursors $[Mo^{V}(CN)_8]^{3-}$,[114,115] $[W^{V}(CN)_8]^{3-}$,[114-116] $[Nb^{IV}(CN)_8]^{4-}$,[117] $[(triphos)Re^{II}(CN)_3]^{-}$ [118-120] and $[Re^{IV}(CN)_7]^{3-}$.[110] The most widely studied of these being compounds synthesized from the octacyanometallates $[Mo^{V}(CN)_8]^{3-}$ and $[W^{V}(CN)_8]^{3-}$.[121,122] These octacyanometallates most often form large pentadecanuclear M'_6M_9 molecules of general formula $\{M^{II}[M^{II}(MeOH)_3]_8(\mu\text{-}CN)_{30}[M'^{V}(CN)_3]_6\}_x \cdot 4MeOH_y \cdot H_2O$ where M'^{V} = Mo, W and M^{II} = Ni, Mn, Co, several of which have been shown to exhibit SMM properties.[114,123-125] The first molecule incorporating Re^{II} to show SMM behavior is the distorted cube complex $\{[Mn^{II}Cl]_4[Re^{II}(triphos)(CN)_3]_4\}$ (Figure 1.7a).[118,119] Several years later Long's group reported the first compound based on the homoleptic $[Re^{IV}(CN)_7]^{3-}$ anion, specifically a star-like molecule with a formula of $[(PY_5Me_2)_4Mn^{II}_4Re^{IV}(CN)_7](PF_6)_2 \cdot 6H_2O$ and a blocking temperature of 5 K and U_{eff} = 33 cm^{-1} which is the highest effective barrier reported for a cyanide based SMM to date (Figure 1.7b).[110]

The Use of 4d and 5d Hexacyanometallates in Molecular Magnetic Materials

The overarching goal of molecular magnetism is to synthesize materials that exhibit specific tailored properties so it is of critical importance to have a deeper

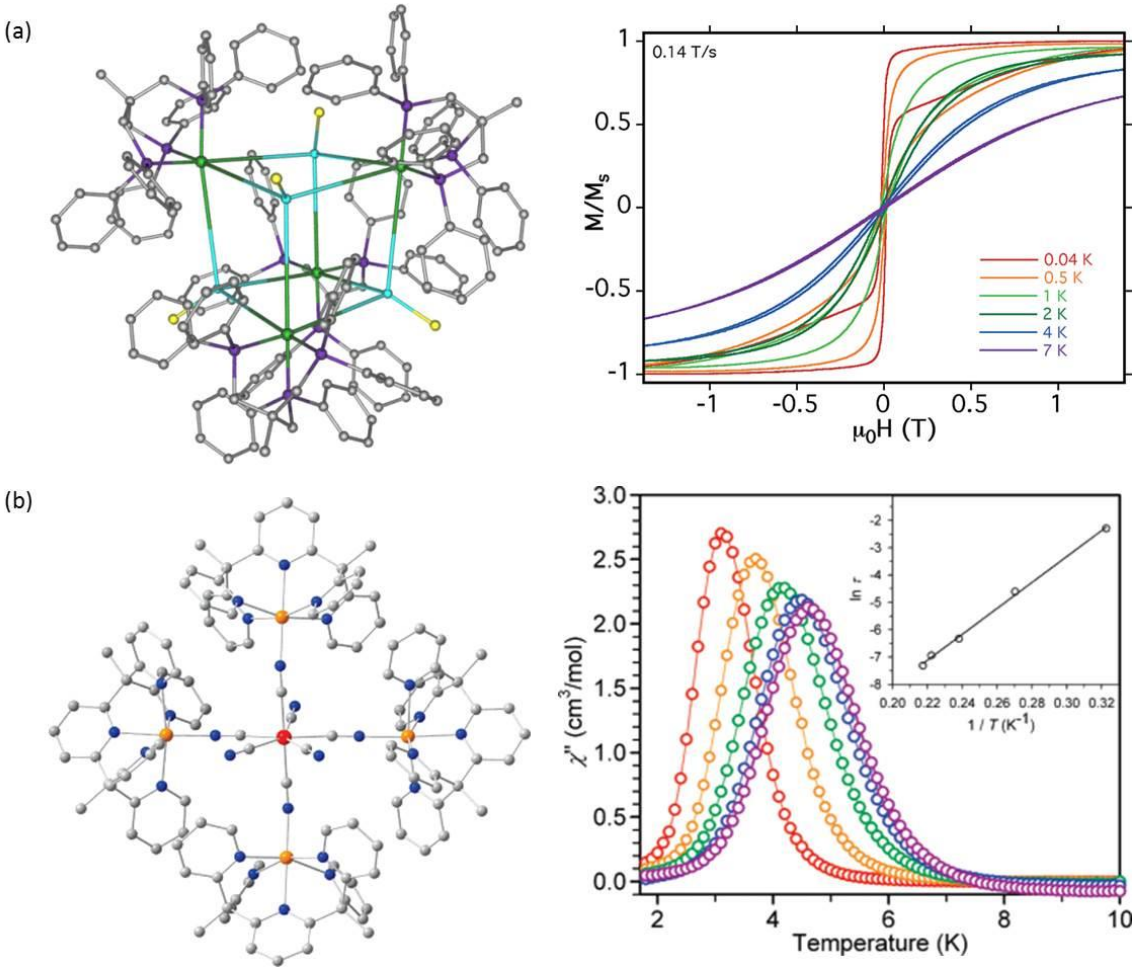

Figure 1.7 (a) The first molecule incorporating Re^{II}, $[Mn^{II}Cl]_4[Re^{II}(triphos)(CN)_3]_4\}$, to exhibit SMM behavior.[118] (b) The molecule $[(PY_5Me_2)_4Mn^{II}{}_4Re^{IV}(CN)_7](PF_6)_2 \cdot 6H_2O$ which holds the current record barrier for a CN-bridged molecule, U_{eff} = 33 cm^{-1}.[110]

understanding of structure-property relationships that are inherent to the materials. Mixed-metal cyanide compounds constitute an excellent platform for studying the magnetic bistability in SMMs. Although use of the cyanide ligand produces comparatively smaller nuclearity clusters than the oxo-bridged counterparts, cyanide is an excellent diamagnetic linker for use in the synthesis of molecular magnets for several reasons: (1) the cyanide ligand is known to bridge two transition metal atoms, M-CN-M' in a linear or nearly linear fashion; (2) the unsymmetrical cyanide ion allows for the selective binding of two different transition metal ions; (3) the polycyanometallate precursors are usually stable in solution making them useful building blocks for controlled syntheses.[22] In addition to these chemical advantages, the cyanide ion allows for predictable exchange coupling through the linear bridge. By considering the symmetry of the contributing metal-based magnetic orbitals and their possibility of mixing, the nature of the magnetic interactions usually can be predicted. If the magnetic orbitals are of the same symmetry, exchange is mediated through the CN^- ligand and antiferromagnetic coupling is observed. If the magnetic orbitals are orthogonal to each other, exchange cannot be mediated through the cyanide ligand and a ferromagnetic exchange is observed (figure 1.8). [22,126]

The synthetic control and predictability of the cyanide ligand have led many researchers to turn their efforts toward designing molecules using cyanometallates. This situation has resulted in a huge number of new cyanide-based SMM molecules, in addition to other interesting classes of paramagnetic cyanide-based compounds. Most of the SMMs reported, however, exhibit low blocking temperatures and small barriers.

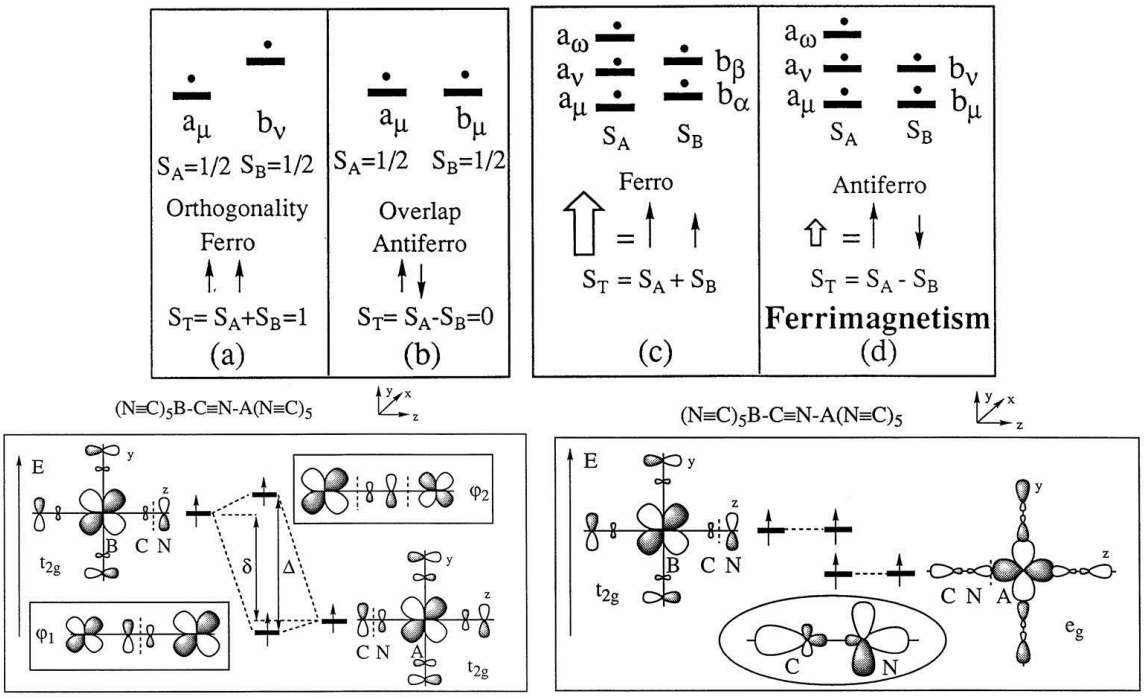

Figure 1.8 Top: Spin interactions between two identical spins (a) orthogonal orbitals result in ferromagnetic coupling, (b) orbital overlap (orbitals of the same symmetry) results in antiferromagnetic coupling; spin coupling between different spins (c) orthogonal orbitals result in ferromagnetism, (c) orbitals of the same symmetry result in antiferromagnetic coupling but with different spins leads to a magnetic ground state. Bottom: Molecular magnetic orbital diagrams to illustrate bridging through the cyanide ligand (left) built from the t_{2g} orbitals in a $(NC)_5B$-CN-$A(NC)_5$ unit, the orbital interaction results in antiferromagnetic interactions. The larger the $(\Delta-\delta)$ gap, the larger the $|J|$. (right) built from orthogonal t_{2g} and e_g orbitals of a $(NC)_5B$-CN-$A(NC)_5$ unit, the orbital interaction results in ferromagnetic interactions. Adapted from reference 22.

This is, in part, due to magnetic coupling (J) through the cyanide bridge generally being much weaker than for oxide bridges (|J| values below 10 cm^{-1}) resulting in the population of excited states, consequently introducing accessible levels of states that enhance relaxation effects. Therefore, there is a need to explore new metal ion combinations for cyanide and cyanide-containing linkers in order to search for improved superexchange interactions that would serve to stabilize a well-isolated ground state. To address this issue, theoreticians have recently begun studying lesser known metal building blocks such as those of V^{II} and Cr^{II}. These early, low-valent transition metals have more diffuse orbitals which may lead to increased overlap between the π and π^* orbitals of cyanide.[127,128] In addition, the lesser studied 4d and 5d cyanometallates, $[Mo(CN)_7]^{4-}$, $[Mo(CN)_6]^{3-}$ and $[Os(CN)_6]^{3-}$ exhibit large spin orbit coupling effects in addition to more diffuse orbitals which gives rise to increased anisotropy. Theoretical calculations published by Mironov suggest that compounds containing $[Mo(CN)_7]^{4-}$ will have strong anisotropic magnetic exchange which could lead to high blocking temperature SMMs.[102] Another study by Ruiz *et al*. led to the prediction that superexchange interactions between the hexacyanomolybdate(III) ion and the early 3d metal centers, V^{II} and Cr^{II}, should be extremely strong (J = -422 cm^{-1} for $Mo^{III}V^{II}$ and J = -186 cm^{-1} for $Mo^{III}Cr^{II}$) and that these metal combinations could lead to Prussian Blue phases that have critical temperatures well above room temperature.[126] Compounds containing the $[Os(CN)_6]^{3-}$ ion have also been the recent subject of theoretical calculations. Mironov showed that orbital contributions to the kinetic exchange would cause the exchange coupling in Os^{III}-CN-M^{II} groups to be strongly anisotropic.[100,101]

Despite promising theoretical predictions, the starting materials $[Mo(CN)_7]^{4-}$, $[Mo(CN)_6]^{3-}$, $[Os(CN)_6]^{3-}$ and $[Ru(CN)_6]^{3-}$ have been far less studied than the octacyanometallates, presumably because these ions are notoriously sensitive and difficult to handle synthetically. There have been several advances synthetically in this area and a number of research groups have reported new coordination compounds incorporating these scarcely reported cyanometallates. The heptacyanomolybdate ion was first reported in 1932[129] but it was not until the mid-1990's that Kahn reported using it in coordination compounds.[130] This group and a few others reported only several 2D and 3D magnets.[131-138] Dunbar *et al*. reported the first discrete molecule incorporating the $[Mo(CN)_7]^{4-}$ ion; a docosanuclear heterometallic Mo_8Mn_{14} cluster containing a record twenty-two paramagnetic centers and exhibiting the largest ground-state spin value (S = 31) reported for a cyanide-bridged molecule (Figure 1.9).[139] Reports of the hexacyanomolybdate ion are even scarcer in the literature. The $[Mo(CN)_6]^{3-}$ species was reported in 2002 by Beauvais and Long[140] and it was not until 2009 that they reported the first compound containing the ion.[141] The star-like molecule, $[(PY_5Me_2)_4V^{II}_4Mo^{III}(CN)_6](PF_6)_5$, (Figure 1.10) exhibits exceptionally strong antiferromagnetic coupling between the V^{II} and Mo^{III} centers ($J = -61\ cm^{-1}$), though not as strong as was predicted by theoretical calculations published by Ruiz and Alvarez in 2005.[126] The first compounds incorporating the rarely used cyanometallate $[Os(CN)_6]^{3-}$, were reported by the Dunbar group in the form of trigonal bipyramidal (TBP) compounds[142,143] one of which, $[Fe^{II}(tmphen)_2]_3[Os(CN)_6]_2$ (tmphen = 3,4,7,8-tetramethyl-1,10-phenanthroline), shows charge-transfer induced spin transition

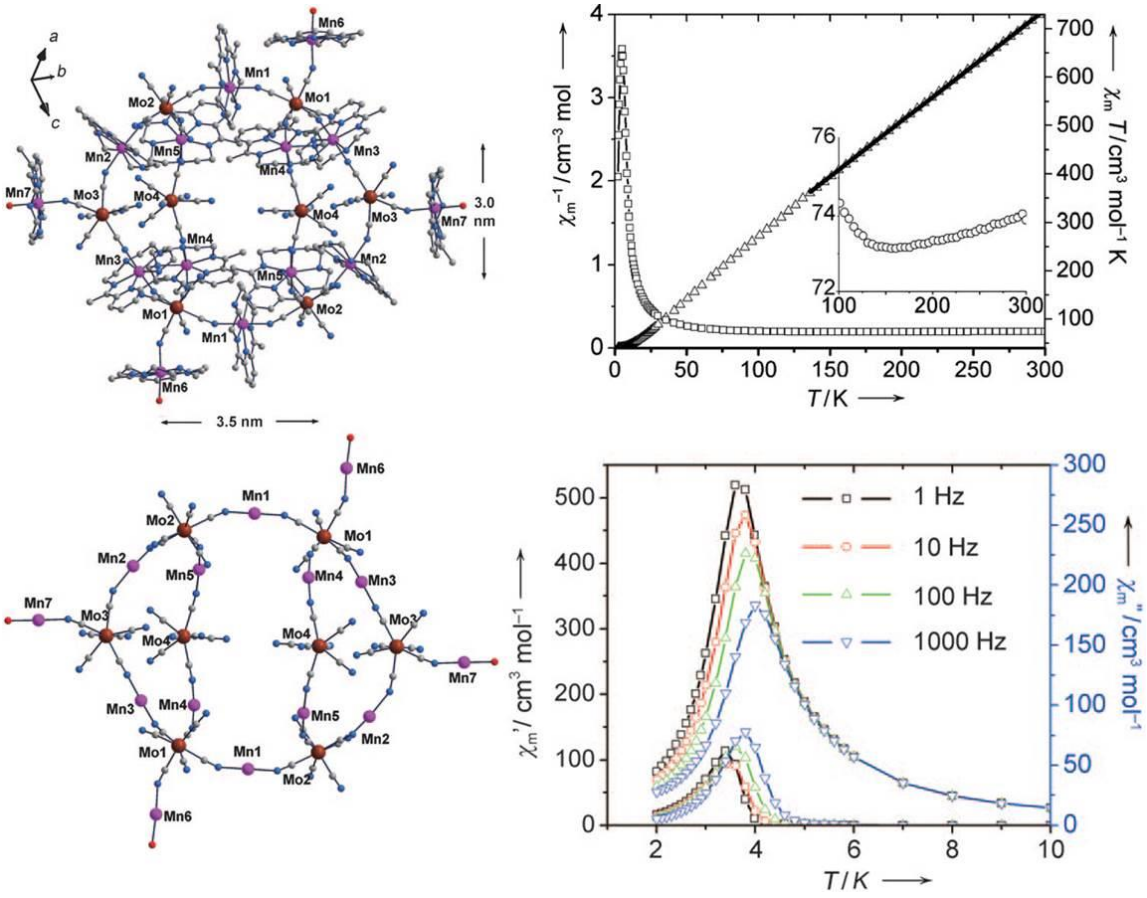

Figure 1.9 Molecular representation of the backbone of the first discrete molecule incorporating $[Mo(CN)_7]^{4-}$ reported by Dunbar *et al.* a docosanuclear heterobimetallic Mo_8Mn_{14} cluster (top left) and the skeletal backbone showing the record 22 metal centers (bottom left). The χT curve (top right) and ac plots (bottom right) showing glassy magnetic behavior. Adapted from reference 139.

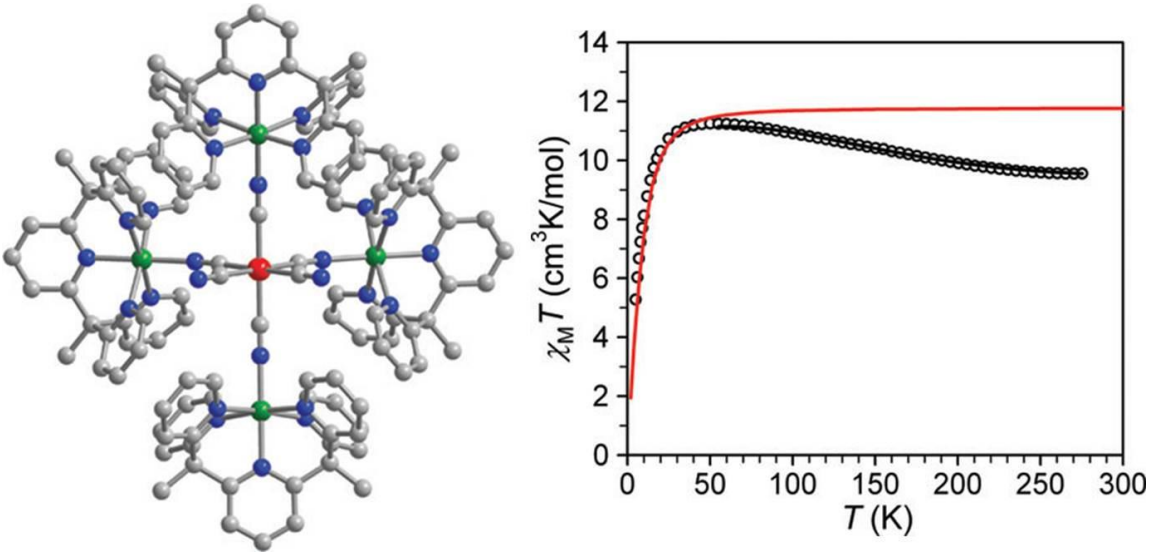

Figure 1.10 The molecule $[(PY_5Me_2)_4V^{II}_4Mo^{III}(CN)_6](PF_6)_5$, reported by Long *et al*.[141] A fitting to the variable-temperature data collected in an applied field of 5 T gives a strong antiferromagnetic exchange coupling parameter of J = -61 cm^{-1} with a g = 1.86.

behavior (CTIST)[142]. Recently, Bendix *et al*. reported three isostructural, trinuclear SMMs, $NEt_4[Mn^{III}_2(5\text{-Brsalen})_2(MeOH)_2M^{III}(CN)_2]$ (M = Fe, Ru, Os),[111,112,144,145] with effective barriers of 11.8 cm^{-1} and 13.2 cm^{-1} for the Ru and Os compounds, respectively and a much lower barrier for the Fe compound (Figure 1.11). This work helps support theoretical predictions that the 4d and 5d metal ions lead to stronger, more anisotropic exchange interactions and, in turn, a marked increase in blocking temperatures.

Recent Advances in Molecular Magnetism

The discovery of SMMs created an active research arena in the fields of both chemistry and physics. Collaborations between the fields have led to teams of researchers working together to improve SMM characteristics with incredible advances being made over the last 20 years. Extraordinary results were published recently, including the discovery of slow magnetic relaxation of the magnetization in mononuclear compounds, a phenomenon termed as "Single Ion Magnets" (SIMs). SIMs have been reported using lanthanides,[146-153] actinides[154,155] and 3d transition metals (Figure 1.12).[156-164] Another exciting development in the field of molecular magnets is the realization that molecules containing dysprosium have experimentally demonstrated the possibility of having extremely large energy barriers as high as 368 cm^{-1} [153] and magnetic hysteresis up to 14 K.[165-169]

With the field of molecular magnets moving towards device applications, it becomes imperative to have a controlled arrangement of SMMs in two dimensions. There have been several strategies developed for controlling these molecules; the most promising approach being to attach them to surfaces (Figure 1.13)[170-177] or arranging

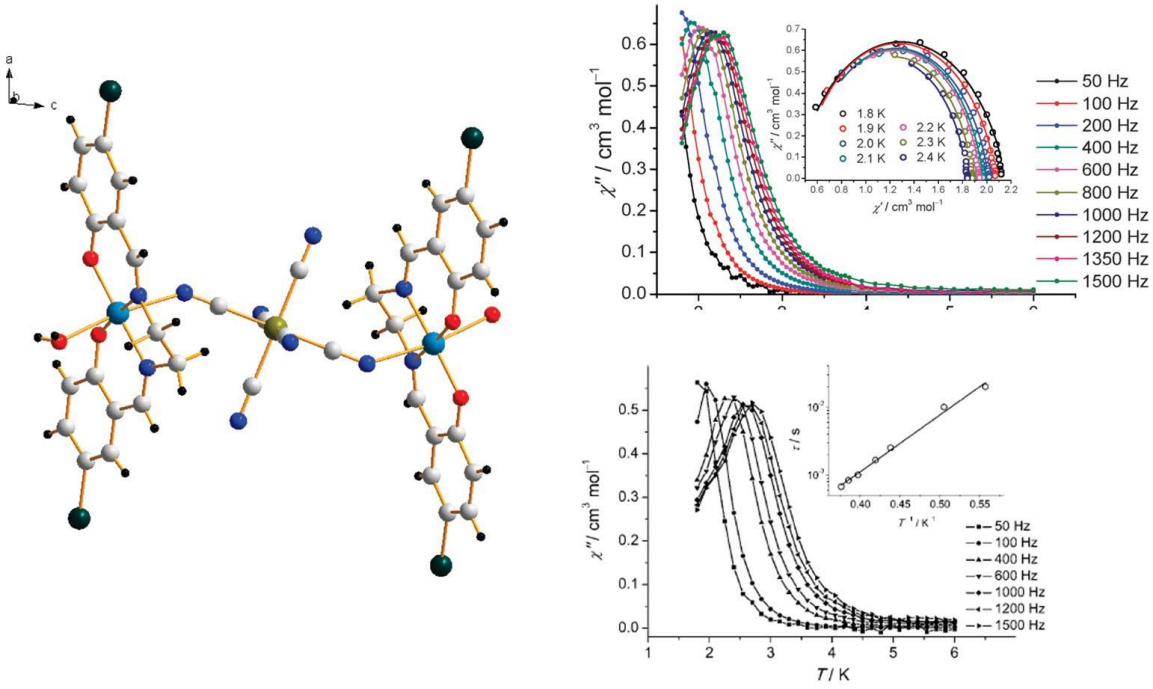

Figure 1.11 Structure of the Mn-M-Mn unit (M = Ru, Os).[144] Top right: out-of-phase ac susceptibility of the Mn_2Ru SMM, the data indicates an effective barrier of 11.8 cm^{-1}.[111] Bottom right: out-of-phase ac susceptibility of the Mn_2Os SMM giving a U_{eff} = 13.2 cm^{-1}.[112]

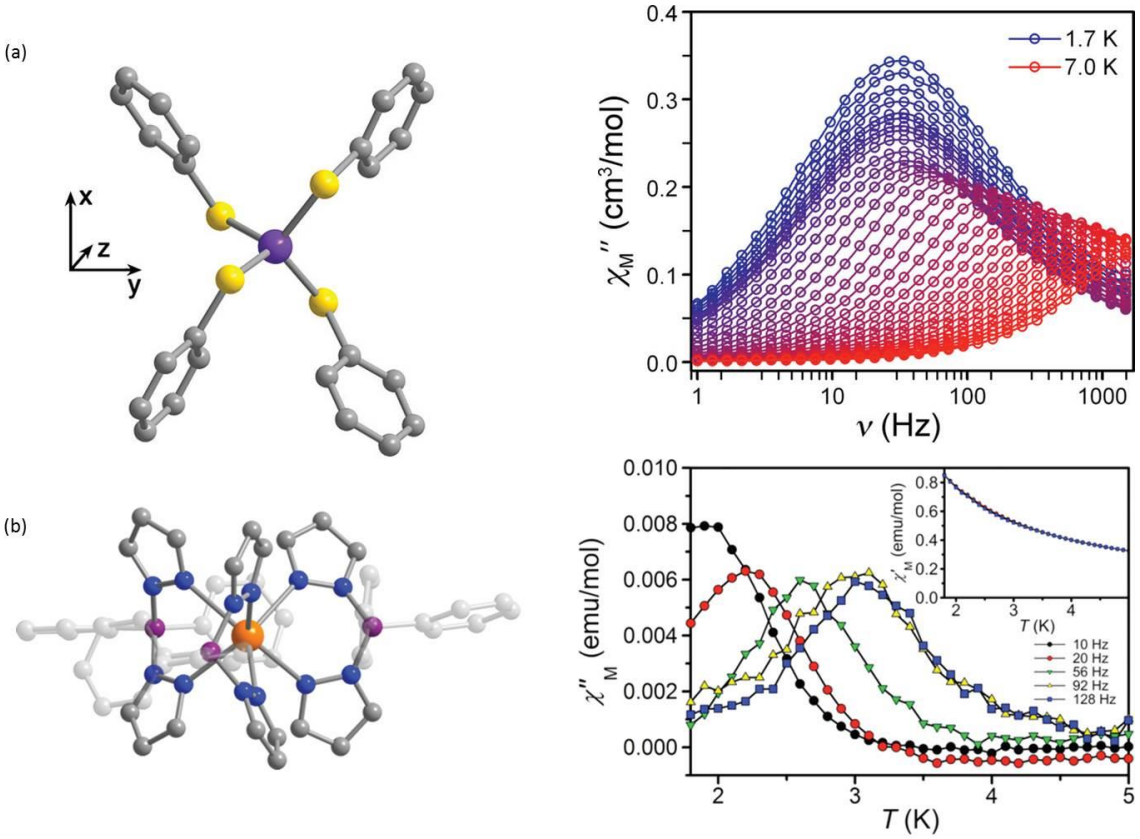

Figure 1.12 (a) (left) The SIM $[Co(SPh)_4]^{2-}$ an S = 3/2 molecule possessing D_{2d} symmetry. (right) frequency dependence of the out-of-phase ac susceptibility in zero applied dc field. An Arrhenius law gives U_{eff} = 21 cm^{-1} with τ_0 = 1.0 x 10^{-7} s.[163] (b) (left) Trigonal prismatic $U(Ph_2BPz_2)_3$ a SIM with D_{3h} symmetry. (right) frequency dependence of the out-of-phase component of the ac susceptibility in zero dc field. An Arrhenius law gives an effective barrier of U_{eff} = 20 cm^{-1} and τ_0 = 1 x 10^{-9} s.[155]

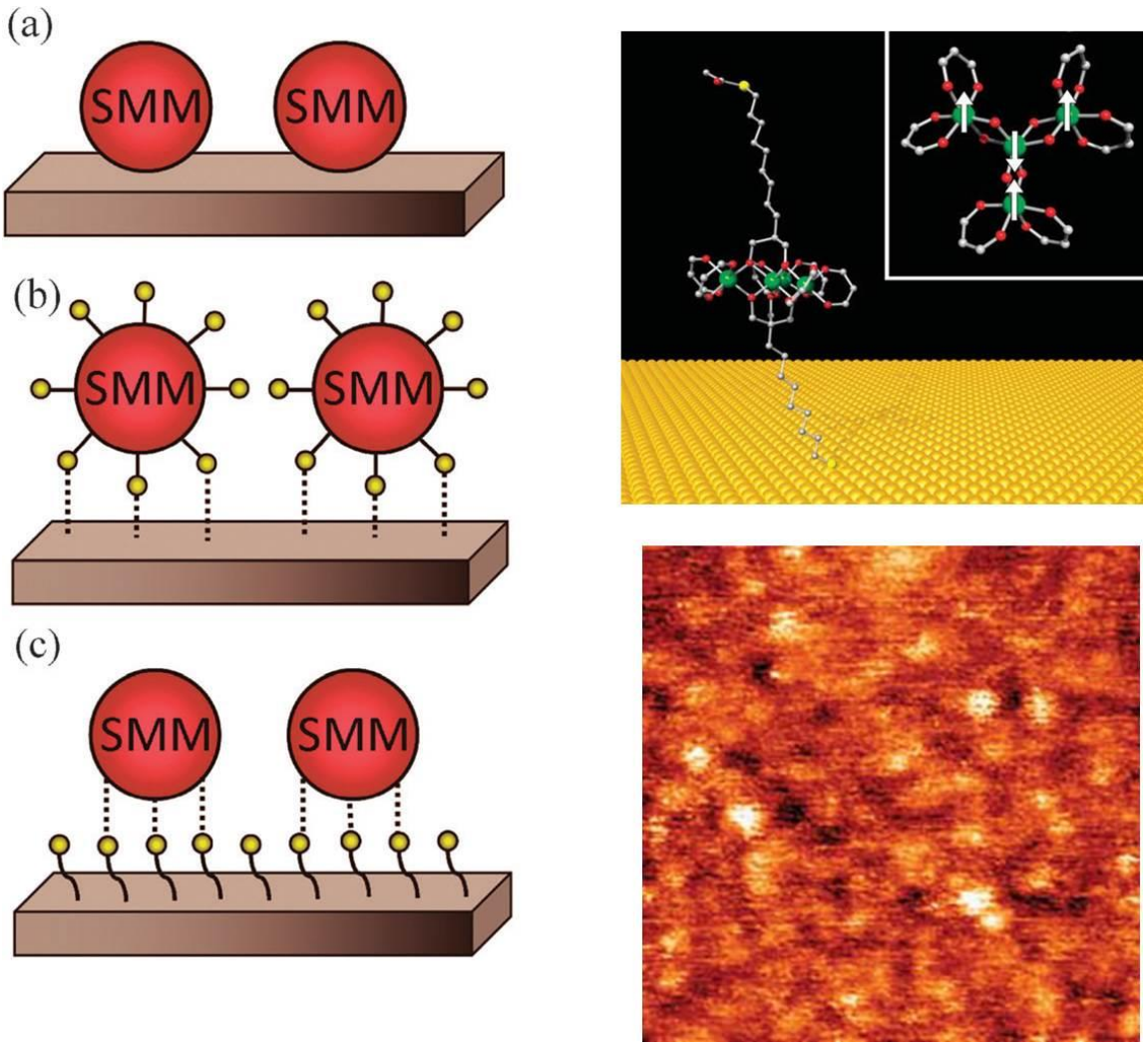

Figure 1.13 Left: Representation of different strategies for use of SMMs on surfaces. (a) SMM directly deposited on a bare surface; SMM immobilized by weak covalent interactions. (b) Pre-functionalization of the SMMs with functional groups able to interact with the bare surface. (c) Pre-functionalization of the surface with groups able to interact with the SMMs.[171] Right: (top) representation of pre-functionalized Fe_4 SMMs attached to a bare gold surface. (bottom) Room temperature STM image of Fe_4 SMMs attached to a gold surface.[174] Adapted from references 171 and 174.

them in extended coordination networks.[74,178-186] Wernsdorfer *et al*. showed that weak interactions between SMMs, *i.e*. hydrogen bonds, can modify the intrinsic SMM properties and give rise to new magnetic behavior.[187-190] Each SMM was discovered to have a weak exchange interaction with its neighbors which shifts the QTM from zero field, a phenomenon known as exchange bias. The interactions between the reported exchange bias SMMs are strong enough to influence the quantum properties but are not so strong as to produce ordering, or a transition to a classical magnetic material (Figure 1.14).[187-189,191-200] The investigation of these weak intermolecular interactions between SMMs could provide the ability to fine-tune the QTM and lead us closer to the use of SMMs in information storage and switching devices.

The work described in this dissertation focuses on the incorporation of 4d and 5d metal ions into cyanide-bridged materials for the study of magnetic properties. Chapter II presents extensive magnetic characterization of two trinuclear SMMs of formula, $PPN\{[Mn^{III}(salphen)(MeOH)]_2[M^{III}(CN)_6]\}\cdot 4MeOH$ (M^{III} = Fe and Os), that exhibit reversible exchange bias behavior. Chapter III describes the synthesis, structural characterization and magnetic studies of new TBP molecules incorporating the $[Mo(CN)_6]^{3-}$ ion. Chapter IV details a series of compounds incorporating the octacyanometallate anion, $[W(CN)_8]^{3-}$, which include two pentanuclear molecules, a trinuclear compound and a one-dimensional chain.

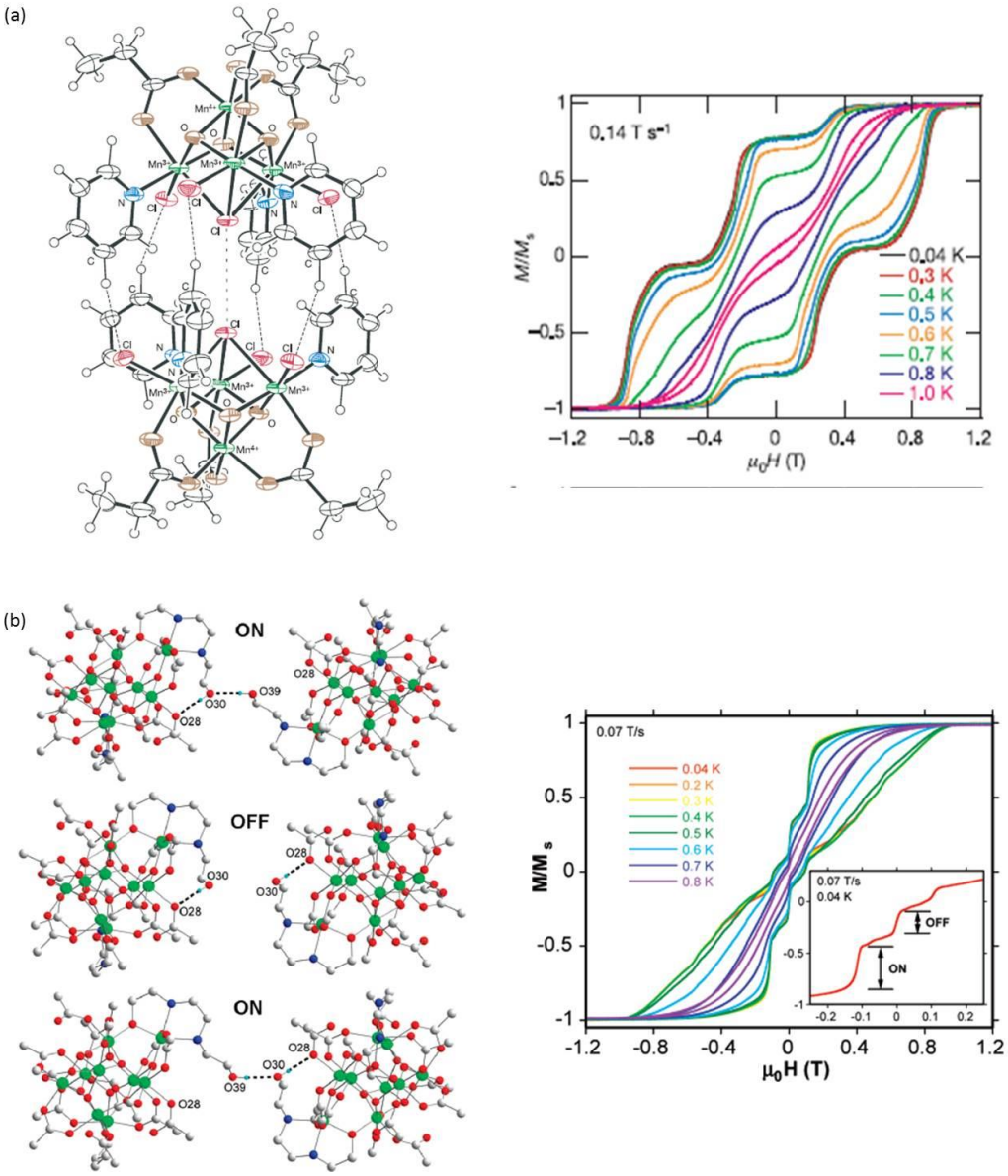

Figure 1.14 (a) Left: Molecular representation of the $[Mn_4O_3Cl_4(O_2CEt)_3(py)_3]_2$ supramolecular dimer. The dashed lines show the C-H···Cl hydrogen bonds connecting the SMMs. Right: Magnetization vs. applied magnetic field hysteresis loops showing the exchange bias behavior. The first QTM step is shifted from zero-field due to weak interactions between the SMMs.[189] (b) Left: The molecule $[Fe_9O_4(OH)_4(OCPh)_{13}(heenH)_2]$ ($heenH_2$ = N-N'-bis(2-hydroxyethyl)ethylenediamine) showing intermolecular interactions (top and bottom) and intramolecular interactions (middle) and the resultant ON anf OFF states with respect to the coupling of the molecules. Right: Magnetization vs. applied magnetic field hysteresis loops. The inset shows interpretation of QTM exhibited by the $[Fe_9]_2$ in the ON and OFF states.[191]

CHAPTER II

SINGLE MOLECULE MAGNETS BASED ON HEXACYANOMETALLATES OF FE(III) AND OS(III) THAT EXHIBIT REVERSIBLE SOLVENT DEPENDENT "ON" AND "OFF" EXCHANGE BIAS

Introduction

A recent development in the field of SMMs is the exploration of the effect of exchange-bias[187,189,191-197,199] which occurs when there are weak magnetic exchange interactions between neighboring SMMs causing a shift in the quantum tunneling of the magnetization (QTM) from zero-field. The magnetic exchange interactions in an exchange-coupled system are capable of breaking the degeneracy of the energy levels such that there is quantum interference associated with the spin length and QTM is shifted.[198] It has been suggested that the understanding and fine-tuning of weak intermolecular interactions could provide a means of control of the QTM in SMMs. The ability to control the shift of QTM could lead us one step closer to the use of SMMs in storage and switching devices.[189,197]

The simplest SMMs with bridging cyanide ligands are linear trinuclear species based on Mn^{III} Schiff base terminal units linked by hexacyanometallate building blocks.[144,180,201,202] Previously Carolina Avendaño from our group reported in her thesis the synthesis and structural characterization of two new trinuclear SMMs of Os^{III} and Fe^{III} using $\{Mn^{III}(salphen)(MeOH)\}^{+}$ as a capping group (salphen = *N*,*N*'-bis(salicylidene)-1,2-diaminobenzene).[190] The initial magnetic measurements reported

by the same student showed that these molecules exhibit SMM behavior. Furthermore, preliminary measurements indicated that the use of the salphen ligand promotes supramolecular interactions that are not present for the related known SMMS[111,112,144,180,201,202] giving rise to exchange bias SMM behavior in the Os^{III} congener. While the initial measurements revealed SMM behavior in both molecules and exchange bias SMM behavior in the Os^{III} molecule, the preliminary measurements were not extensive and provided insufficient data to fully describe the relationship between the Mn_2Fe and the Mn_2Os molecules. In addition, the previously reported study was incomplete in that it only reported exchange bias SMM behavior in the Mn_2Os molecule with only typical SMM behavior being observed in the Mn_2Fe molecule. In fact, the realization of the subtlety of the behavior of the crystals due to extent of solvation was not fully appreciated and no attempt was made to handle the solvated and desolvated samples in a consistent manner. Due to this situation, the study fell short of being able to explain the association between the traditional SMM and exchange bias behavior and some comparisons were made that I have demonstrated are no longer valid from the data collected for this dissertation research. The current chapter is a systematic study of the two SMMs, $PPN\{[Mn(salphen)(MeOH)]_2[M(CN)_6]\}\cdot 4MeOH$ ($M = Fe^{III}$ and Os^{III}), including a detailed magnetic study of the solvated and desolvated forms of the trinuclear molecules. The current results indicate that the supramolecular interactions present in these systems are crucial for controlling resonant quantum tunneling via weak intermolecular antiferromagnetic interactions.

Syntheses

Starting materials. Commercially available $K_3[Fe(CN)_6]$ (Aldrich) and PPNCl (Aldrich; PPN = bis(triphenylphosphine)nitrogen) were used as received. The tetradentate Schiff base ligand H_2-salphen was prepared according to literature procedure by mixing 2-salicylaldehyde and *o*-phenylenediamine in a 2:1 mol ratio and boiling in ethanol.[203] The $[Mn^{II}(H_2O)_4][BF_4]_2$ and $K_4[Os(CN)_6]$ salts were prepared as previously reported.[204,205]

$[PPN]_3[Os(CN)_6]$. The compound was synthesized following a previously reported procedure.[205] A quantity of $K_4Os(CN)_6$ (0.626 g, 1.2 mmol) was stirred in 50 mL of H_2O for 20 min. to give a clear, colorless solution. This solution was treated with $Ce^{IV}(SO_4)_2$ (0.827 g, 2.5 mmol) leading to a series of color changes: first to yellow followed by dark green and lastly to bright yellow. The solution was filtered and then added dropwise to a hot stirring solution of PPNCl (2.07 g, 3.4 mmol) resulting in the formation of a yellow precipitate. The solid was collected *via* suction filtration and washed with hot water (3 x 100 mL) followed by 100 mL of diethyl ether and dried *in vacuo*. Yield = 2.0 g, 82%. IR(Nujol): ν(C≡N) 2086, 2091 cm^{-1}.

$[Mn(salphen)(H_2O)_2][BF_4]$. This compound was synthesized using a modification of a previously reported procedure.[203] The ligand H_2salphen (1.0 g, 3.16 mmol) was added to a stirring solution of $Mn(BF_4)_2{\cdot}4H_2O$ (0.949 g, 3.16 mmol) in 80 mL of 95% ethanol to form and orange-yellow solution. The solution was stirred overnight to dissolve all H_2salphen and formed a dark red-brown solution. The solution was evaporated under a steady stream of N_2 at room temperature. The dark red-brown needles that formed after

several days were filtered in air, washed with diethyl ether, and air-dried. Yield = 0.896 g, 57%.

$PPN_3[Fe(CN)_6]$. This compound was synthesized by a previously reported procedure.[206] The salt $K_3[Fe(CN)_6]$ (1.0 g, 3.0 mmol) was dissolved in 30 mL of distilled water to form a yellow solution. The $[Fe(CN)_6]^{3-}$ solution was heated to ~45 °C and added dropwise to a warm stirring solution of PPNCl (5.1 g, 8.8 mmol in 125 mL of water) resulting in the formation of a microcrystalline yellow precipitate. The mixture was stirred for 10 minutes and filtered. The yellow solid was washed with warm water (3 x 20 mL and 3 x 100 mL) followed by diethyl ether (2 x 20 mL) and dried in air. Yield = 4.94 g, 92 %. IR(Nujol): ν(C≡N) 2104 cm^{-1}.

$PPN\{[Mn(salphen)(MeOH)]_2[Os(CN)_6]\}\cdot 4MeOH$ (1·4MeOH**).** This compound was prepared using a modification of a previously reported procedure.[190] A sample of $PPN_3[Os(CN)_6]$ (0.589 g, 0.30 mmol) was dissolved in methanol (60 mL) to form a yellow-green solution and 10 mL aliquots were placed into six separate 20 mL vials. A red-brown solution of $[Mn(salphen)(H_2O)_2][BF_4]$ (0.1476 g, 0.30 mmol) in methanol (60 mL) was prepared. An equal volume quantity of the methanol solution of $[Mn(salphen)(H_2O)_2][BF_4]$ (10 mL) was then layered over the 10 mL aliquots of the methanol solution of $PPN_3[Os(CN)_6]$. The layered solutions were placed in the freezer (-20° C) and left to stand undisturbed. Red-orange block crystals formed over several days. The crystals were collected *via* suction filtration and air dried. Yield = 0.077 g, 31 %. The unit cell of the crystals were checked and found to match previously reported

values: space group: C2/c; unit cell: a = 17.17 Å, b = 13.84 Å, c = 37.16 Å, β = 102.787°. IR(Nujol): ν(C=N) 1601 cm^{-1} (imine); ν(C≡N) 2086, 2092 cm^{-1} (cyanide).

PPN{[Mn(salphen)(MeOH)]$_2$[Fe(CN)$_6$]} (2·4MeOH**).** Compound **2**·4MeOH was prepared by a procedure parallel to the synthesis described for compound **1**·4MeOH.[190] The salt $(PPN)_3[Fe(CN)_6]$ was used as the source of $[Fe(CN)_6]^{3-}$ anions. Yield = 0.095 g, 41%. The unit cell of the crystals were checked and found to match previously reported values: space group: C2/c; unit cell: a = 17.03 Å, b = 13.82 Å, c = 37.13 Å, β = 102.650°. IR(Nujol): ν(C=N) 1601 cm^{-1} (imine); ν(C≡N) 2105, 2114 cm^{-1} (cyanide).

Results and Discussion

Syntheses

The trinuclear compounds **1**·4MeOH and **2**·4MeOH were synthesized as previously reported by a self-assembly reaction between $[Mn(salphen)(H_2O)_2][BF_4]$ and $(PPN)_3[M(CN)_6]$ ($M = Fe^{III}$, Os^{III}) in 1:1 molar ratio in methanol.[190] The synthesis of these molecules were attempted in other organic solvents (ethanol, acetonitrile, dichloromethane) in an attempt to change the coordinating solvent to investigate the role that coordinated methanol has on the properties of the isolated trinuclear molecules. In each case an insoluble tan precipitate was obtained that was thought to be the decomposition product MnO_2. The molecules are stable in air, but when removed from the mother liquor, a loss of interstitial solvent occurs, eliciting a change in the observed properties of the molecules. To ensure a complete removal of interstitial solvent, compounds **1**·4MeOH and **2**·4MeOH were dried *in vacuo* for 3 hours to obtain the

desolvated compounds **1** and **2**. Crystals of compounds **1**·4MeOH and **2**·4MeOH can be stored under the mother liquor in the freezer (-20° C) without decomposition for more than 6 months, but when left at room temperature in the mother liquor the compounds decompose to the tan powder of suspected MnO_2 after ~2 weeks. Desolvated and dried crystals of **1** and **2** are air stable and can be stored at ambient temperatures for more than 6 months.

Single Crystal Diffraction Studies

The structures of compounds **1** and **2** were reported previously[190] and found to crystallize in the monoclinic space group C2/c. The data were recollected and refined to give better R and GoF values. The linear trinuclear molecules consist of a central hexacyanometallate ($[Fe^{III}(CN)_6]^{3-}$ and $[Os^{III}(CN)_6]^{3-}$) anion bound to two terminal $[Mn(salphen)(MeOH)]^{+}$ units resulting in an overall negative charge balanced by PPN^{+} cations (Figure 2.1). Four of the CN^{-} ligands on the central hexacyanometallate are terminal and two trans CN^{-} ligands act as bridges to the Mn^{III} centers. The bridging CN^{-} ligands are considerably bent with an angle of 136.3(7)°. The coordination environment of the Mn^{III} centers is a square bipyramid with the N_2O_2 donor sites of the salphen ligand occupying the equatorial sites. One of the apical sites is occupied by the N-bound bridging CN^{-} ligand and the other is occupied by a coordinated methanol molecule. The Jahn-Teller axis of the Mn^{III} ions induces a significantly distorted square bipyramidal environment with a Mn - N(1) distance of 2.228 Å and a Mn - O(3) distance of 2.310 Å. The trinuclear molecules are arranged end to end in a pseudo 1D chain (Figure 2.2) composed of the trinuclear anions connected by a H-bond between the methanol

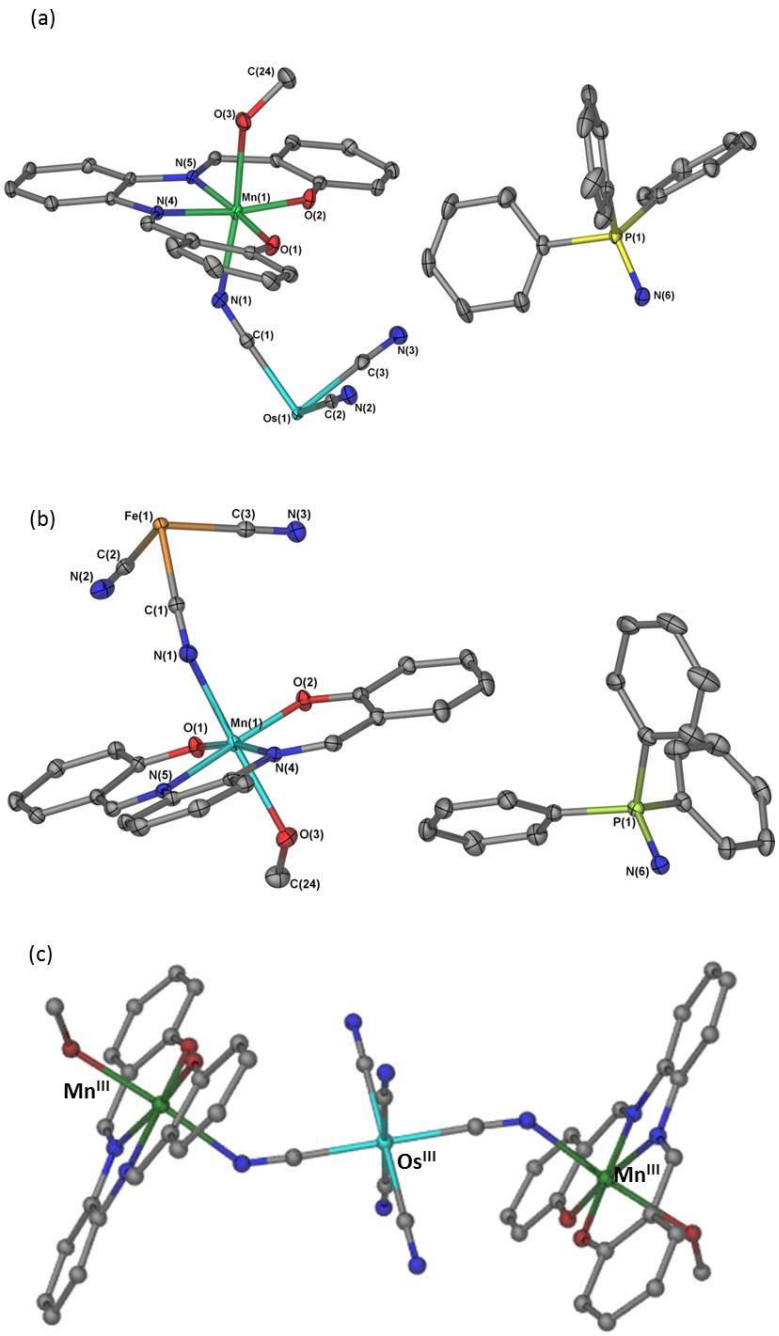

Figure 2.1 Thermal ellipsoid plot of the asymmetric unit of (a) (PPN){[Mn(salphen)(MeOH)]$_2$[Os(CN)$_6$]} and (b) (PPN){[Mn(salphen)(MeOH)]$_2$[Fe(CN)$_6$]}. Ellipsoids are projected at the 50% probability level. (c) Molecular representation of the trinuclear anion {[Mn(salphen)(MeOH)$_2$[Os(CN)$_6$]}$^-$ in **1**.

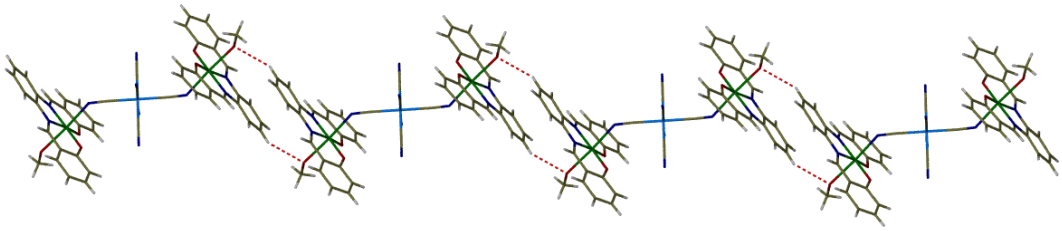

Figure 2. 2 Molecular representation of the trinuclear anion units of **1** arranged in a 1D chain. The dashed lines show the hydrogen bonding interactions between the salphen ligands and the coordinated methanol molecule.

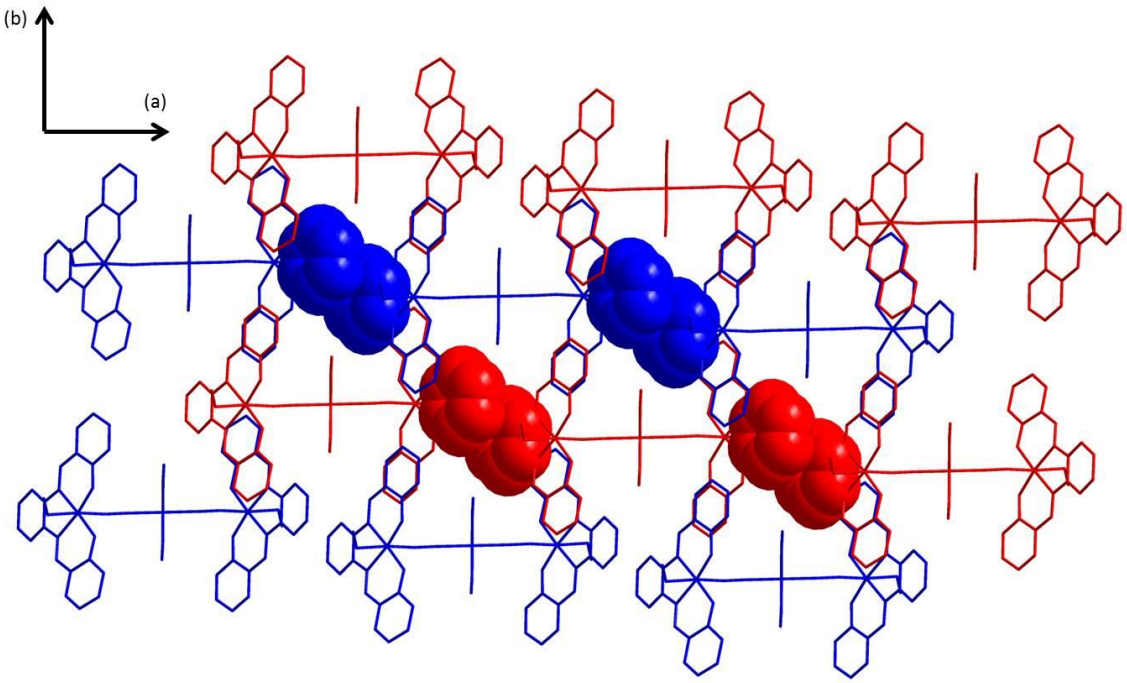

Figure 2.3 Molecular representation of the crystal packing of **1** in the ab plane illustrating the pi-pi stacking interactions between the trinuclear units. Interstitial methanol molecules and hydrogen atoms were omitted for clarity.

coordinated to Mn and the phenyl hydrogen of salphen on a neighboring molecule ($O_{MeOH}\cdots H_{salphen}$ 2.755Å) (Figure 2.2). The trinuclear anions are also involved in π-π stacking interactions with a salphen on the nearest trinuclear anion neighbor (Figure 2.3). In addition to the intermolecular H-bonding interaction, the coordinated MeOH ligand also participates in a stronger hydrogen bonding interaction with a nearby interstitial methanol solvent molecule. The Jahn-Teller axis of the Mn ions runs parallel to the pseudo 1D chain direction. The chains of SMMs are arranged in layers with the closest contact between the chains of trinuclear molecules being between the salphen ligands on neighboring molecules (3.896(2) Å) as illustrated in Figure 2.4. A packing diagram illustrating the PPN^+ cations located between layers of the psuedo chains is provided in Figure 2.5.

Thermogravimetric Analyses

Compounds **1**, **1**·4MeOH, **2** and **2**·4MeOH were evaluated for solvent content by thermogravimetric analysis. All compounds were scanned from 23 - 300° C at a rate of 2° C/min with the exception of compound **1** which was scanned from 23 - 450° C at a rate of 2° C per minute. Measurements of the solvated compounds were performed on freshly filtered crystals. Samples for the desolvated measurements were dried *in vacuo* for 3 hours to ensure removal of all interstitial solvent. The thermal curve for compound **1**·4MeOH (Figure 2.6) shows an initial mass loss of 15.2 % from 36 - 60° C which corresponds to 7 methanol molecules. This is attributed to the four crystallographically located interstitial methanol molecules as well as the surface methanol that is present on the still wet, freshly filtered crystals. The decomposition onset of compound **1**·4MeOH

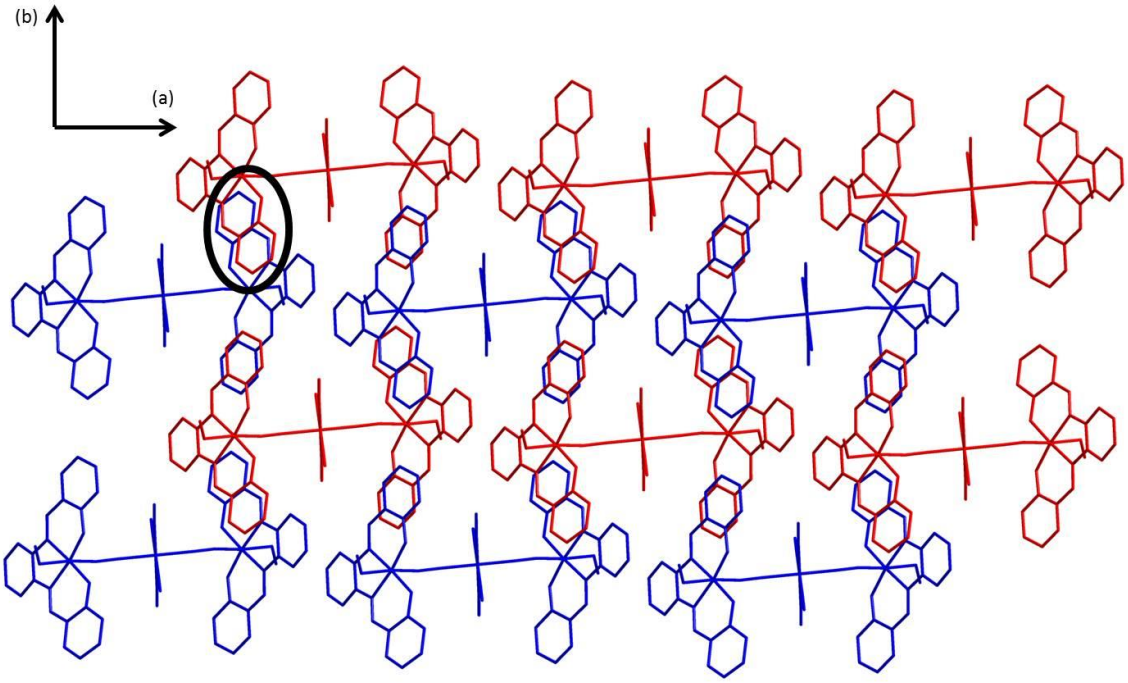

Figure 2.4 Molecular representation of the crystal packing of **1** in the ab-plane. The black circle highlights the closest contact between neighboring chains. Hydrogen atoms and interstitial methanol molecules were removed for the sake of clarity.

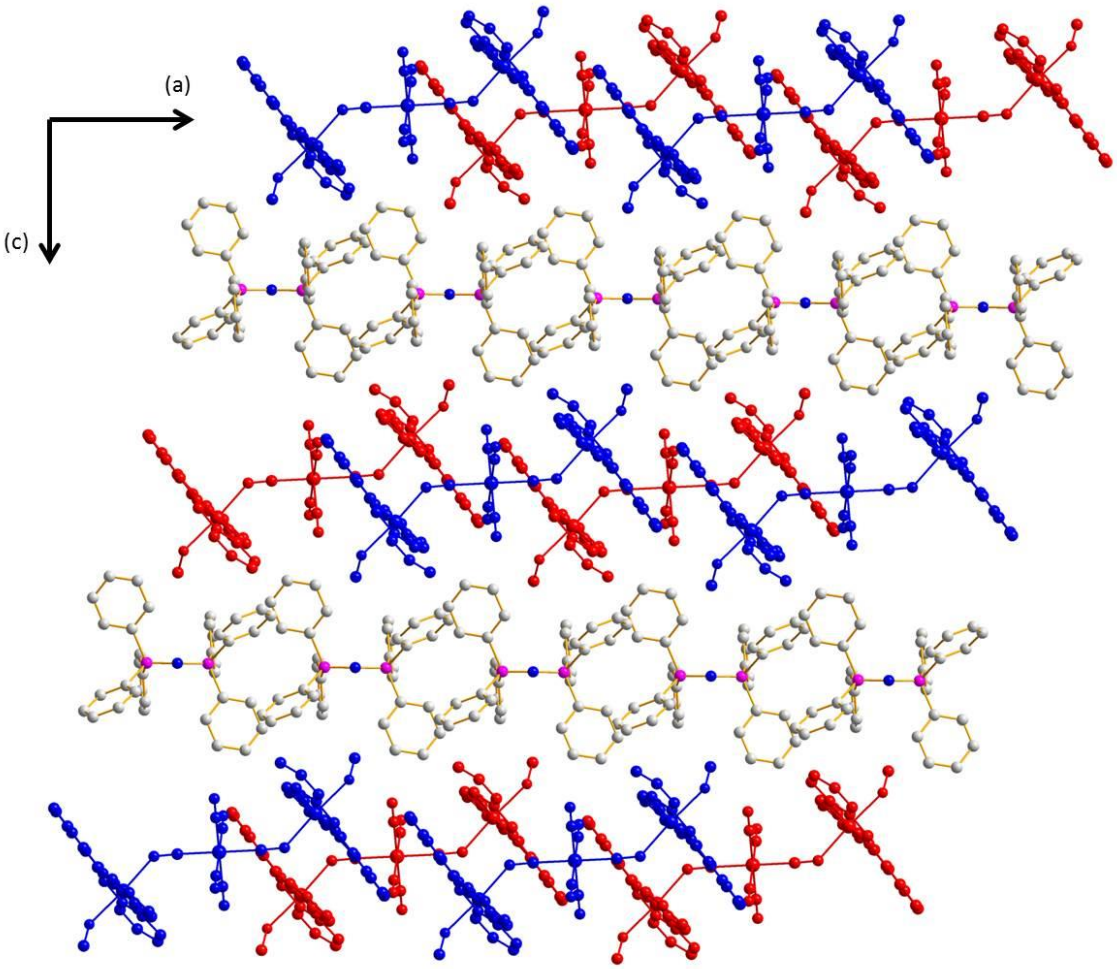

Figure 2.5 Molecular representation of the crystal packing of **1** in the ac-plane illustrating the layer arrangement of 1D chains with PPN^{+} cations packed between the layers of trinuclear molecules. The red and blue colors correspond to the colors from Figure 2.4 to highlight the corrugation of the pseudo-1-D arrangement of the molecules.

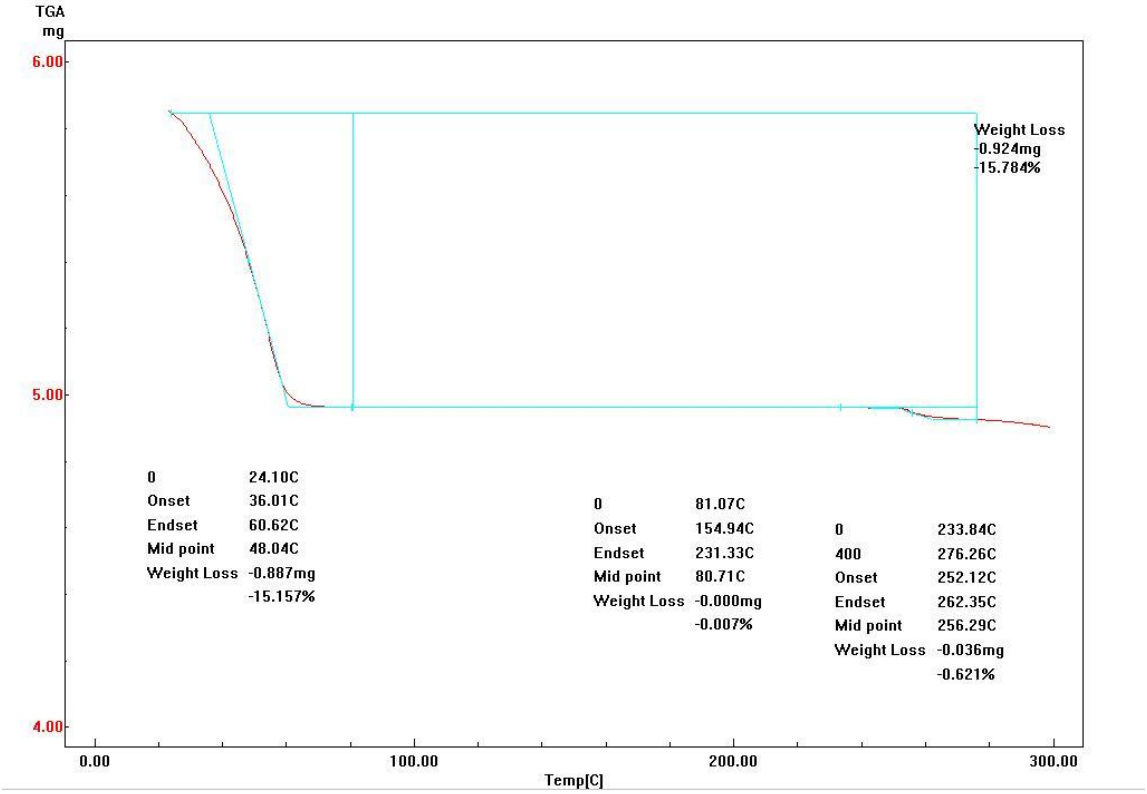

Figure 2.6 Thermal curve of **1**·4MeOH from 23-300° C. The blue lines indicate calculations for mass % loss of sample.

is 252° C and is marked by an initial mass drop that looks like it could be the loss of the coordinated methanol molecules, but with the mass loss of the initial drop being only 0.621 % (0.3 methanol molecules) this can only be attributed with certainty to the decomposition of the compound. Compound **2**·4MeOH (Figure 2.7), analogous to **1**·4MeOH, shows an initial mass loss of 16.9 % from 34 - 58° C which corresponds to 8 methanol molecules. Again, this is attributed to both the interstitial solvent and methanol on the surface of the freshly filtered crystals. The onset of decomposition at 230° C is marked by an initial decrease followed by the gradual curve that is common for decomposition curves. While the loss of the coordinated methanol molecules may trigger the decomposition of the product, this cannot be stated with certainty by analysis of the thermal curve. Compound **1** shows no initial mass loss and the thermal curve only shows a decrease in mass at the onset of decomposition of the product at 195° C (Figure 2.8). Compound **1** was measured to 450° C in order to observe the thermal curve for the complete decomposition of the product. The dried sample of compound **2** behaves in much the same manner as the dried sample of compound **1**. The thermal curve for compound **2** shows no loss of mass until the onset of decomposition at 225° C (Figure 2.9). By analyzing the thermal curves of the compounds, we can conclude that the solvated samples of **1**·4MeOH and **2**·4MeOH have interstitial solvent present whereas compounds **1** and **2** have been sufficiently dried to remove all interstitial solvent.

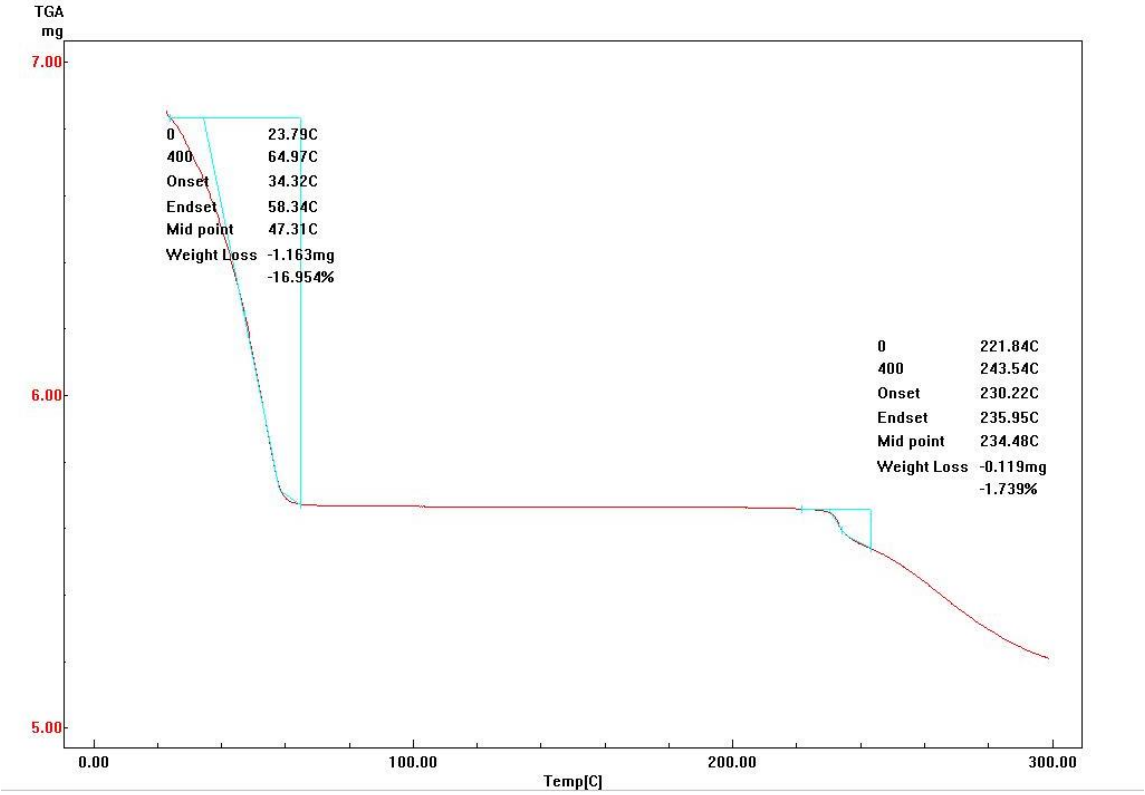

Figure 2.7 Thermal curve of **2**·4MeOH from 23-300° C. The blue lines indicate the calculated mass % loss.

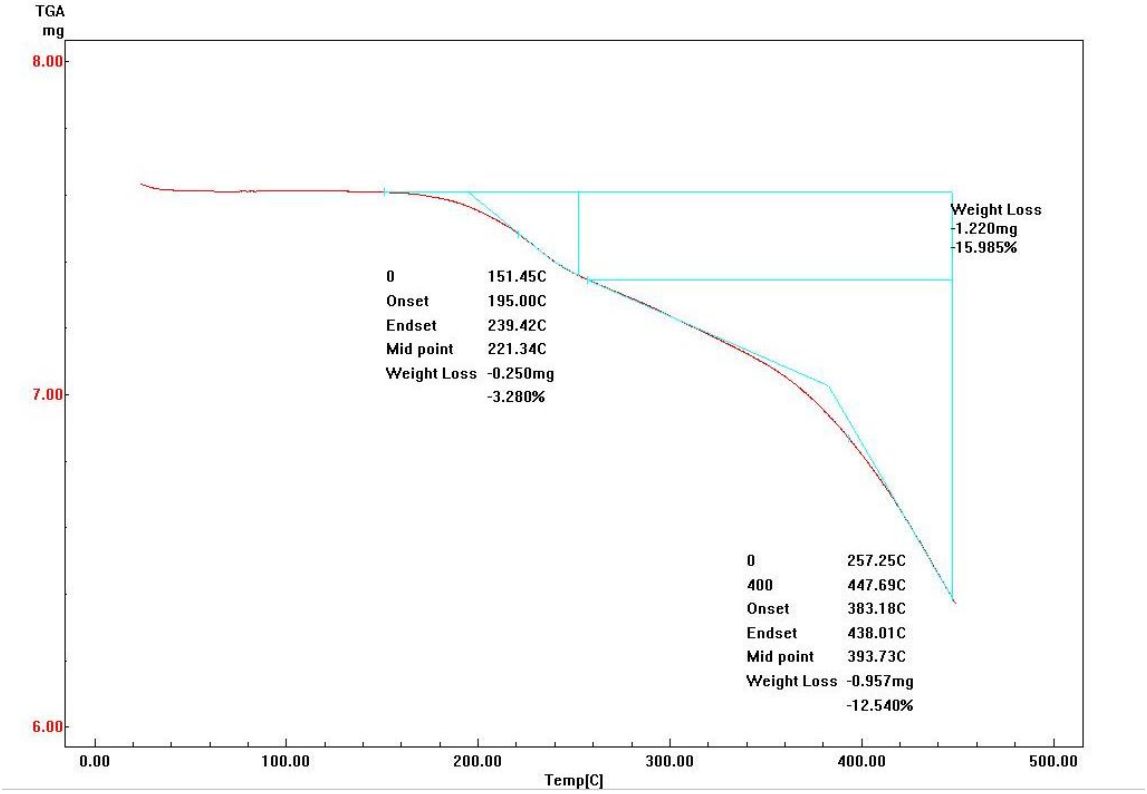

Figure 2.8 Thermal curve of compound **1** from 23-450° C. The blue lines indicate the mass % loss of the sample.

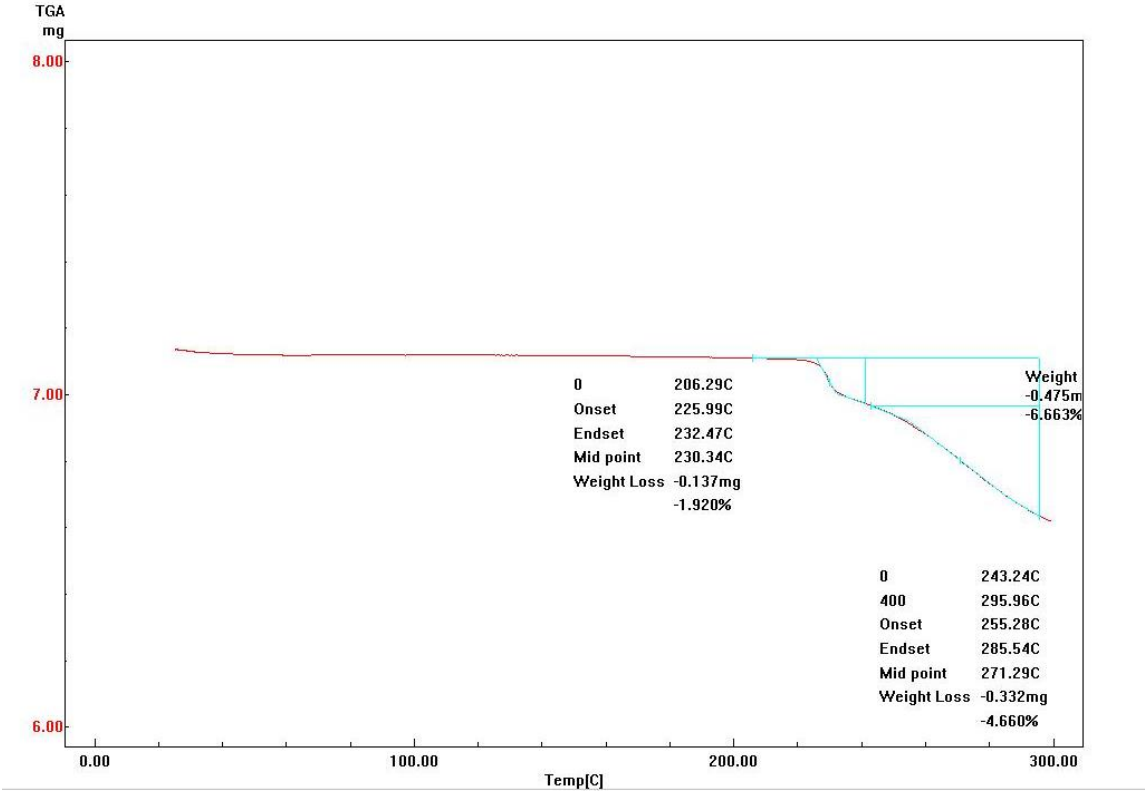

Figure 2.9 Thermal curve of **2** from 23-300° C. The blue lines indicate the mass % loss.

Magnetic Properties

The analysis of the magnetic data was performed with the assistance of Dr. Andrey Prosvirin in the Dunbar group. The measurements at mK temperatures were performed by Dr. Wolfgang Wernsdorfer in Grenoble, France using micro-SQUID techniques. The DC susceptibility data for compounds **1**, **1**·4MeOH, **2** and **2**·4MeOH were measured from 1.8-300 K in an applied magnetic field of 1000 G. All four compounds show an increase in χT as the temperature decreases indicative of ferromagnetic exchange interactions between the Mn^{III} centers and the trivalent hexacyanometallate (Fe^{III} or Os^{III}) mediated through the cyanide bridge. To avoid over-parameterization, the magnetic behavior was modeled using the isotropic Heisenberg-Dirac-Van Vleck Hamiltonian ignoring the spin-orbital contribution from the metal ions and assuming an external field (H) along the z-axis ($H = H_z$):

$$H = -2J_{Mn\text{-}M}(S_{Mn1}S_M + S_{Mn2}S_M) + \mu_B H_Z(2g_{Mn}S_{Mn} + g_M S_M) + D[S_T - (1/3)S_{Mn}(S_{Mn} + 1)] \quad \text{(Eq. 2.1)}$$

where $J_{Mn\text{-}M}$ is the isotropic exchange constant, M is the central Os^{III} or Fe^{III} atoms, and S_T is the total spin operator $S_T = S_{Mn1} + S_M + S_{Mn2}$. The simulation of the magnetic susceptibility data were carried out using MAGPACK[207] and inter-molecular interactions, zJ', were incorporated using the mean-field approximation:

$$\chi = \frac{\chi_{trimer}}{1 - \frac{2zJ'}{Ng^2\mu_B^2}\chi_{trimer}} \quad \text{(Eq. 2.2)}$$

As indicated earlier, the trinuclear compounds PPN{[Mn(salphen)(MeOH)]$_2$-[M(CN)$_6$]}·4MeOH (M = Fe^{III} and Os^{III}), were previously reported[190] and were shown to exhibit SMM behavior as has been observed for other compounds of general type A{[Mn(salen-type ligand)(solv)]$_2$[M(CN)$_6$]} (M= Cr, Fe, Ru, Os).[111,112,144,180,182,201,202] The previously reported ac susceptometry measurements of PPN{[Mn(salphen)-(MeOH)]$_2$[M(CN)$_6$]}·4MeOH (M = Fe^{III} and Os^{III}), while showing that these molecules behaved as SMMs, were preliminary data and additional measurements were required to obtain an accurate effective barrier for these molecules. All basic measurements (dc, magnetization, etc.) were repeated on carefully handled samples to verify the properties of the two compounds in both the SMM and exchange bias form. Detailed magnetic studies were also undertaken to probe the reversibility of the exhibited exchange bias behavior of these molecules.

PPN{[Mn(salphen)(MeOH)]$_2$[Os(CN)$_6$]} (1). The dc measurements of the Mn_2Os trinuclear molecule were previously measured and reported in Carolina Avendaño's thesis,[190] but were remeasured in this work with careful handling of solvated and desolvated samples. Measurements of compound **1** reported herein were performed on crystals that were dried *in vacuo* for three hours to ensure complete removal of interstitial solvent. Temperature dependent magnetic susceptibility data for **1** indicate ferromagnetic coupling between the high spin S = 2 Mn^{III} ions and the S = ½ Os^{III} ion (Figure 2.10). The room temperature χT vs. T value is 6.47 emu·K·mol^{-1} and is consistent with two isolated Mn^{III} ions and one isolated Os^{III} ion (6.35 emu·K·mol^{-1}). The values of χT first increases as temperature decreases, reaching a maximum value at

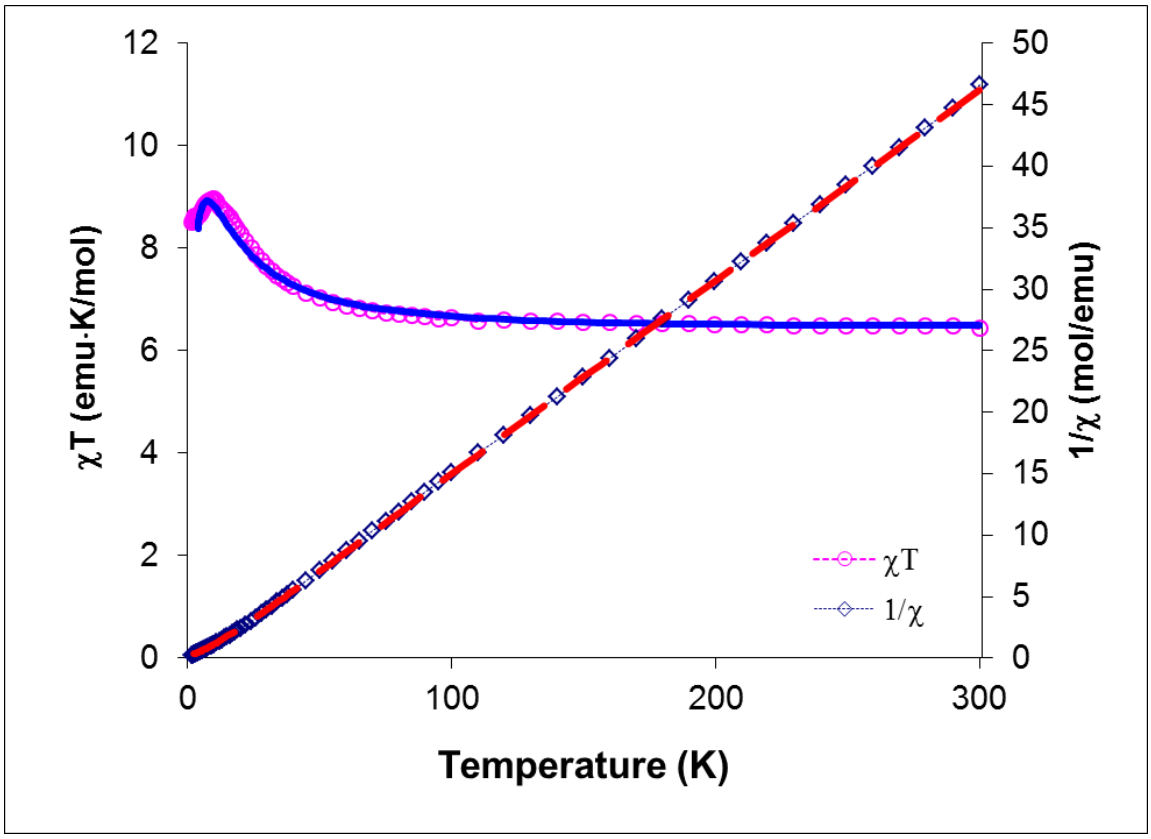

Figure 2.10 Temperature dependence of χT and $1/\chi$ for compound **1**. The solid line corresponds to the MAGPACK[207] simulation ($g_{Os} = 1.75$, $g_{Mn} = 2.0$, $J = 5.1\ cm^{-1}$, $zJ' = -0.12\ cm^{-1}$, $D = -0.03\ cm^{-1}$).

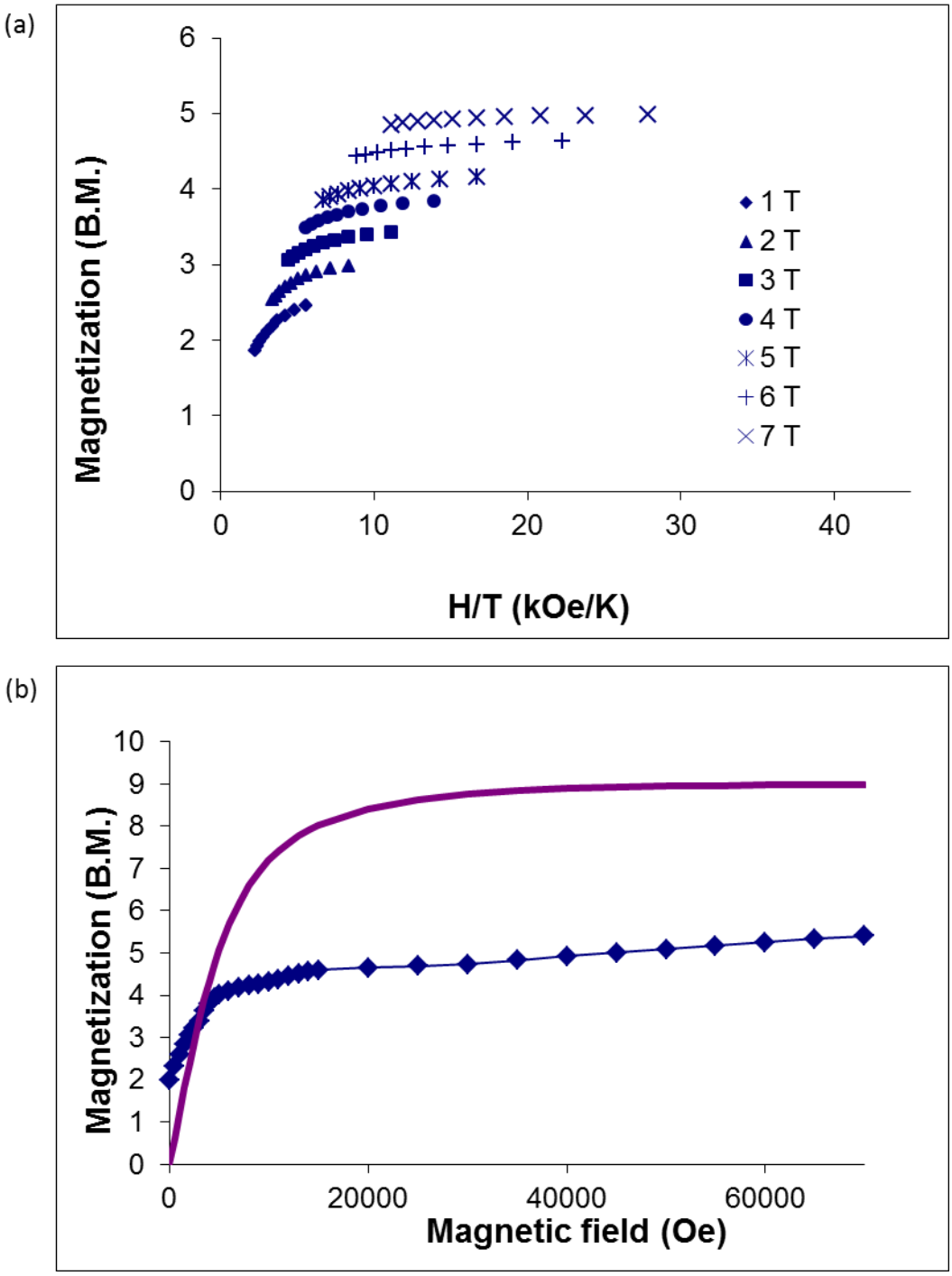

Figure 2.11 (a) Reduced magnetization data for compound **1** at applied external fields from 1 – 7 T. Adapted from ref 190 (b) Field dependent magnetization for **1**. The solid line corresponds to the Brillouin function for S = 9/2, g_{avg} = 2.0.

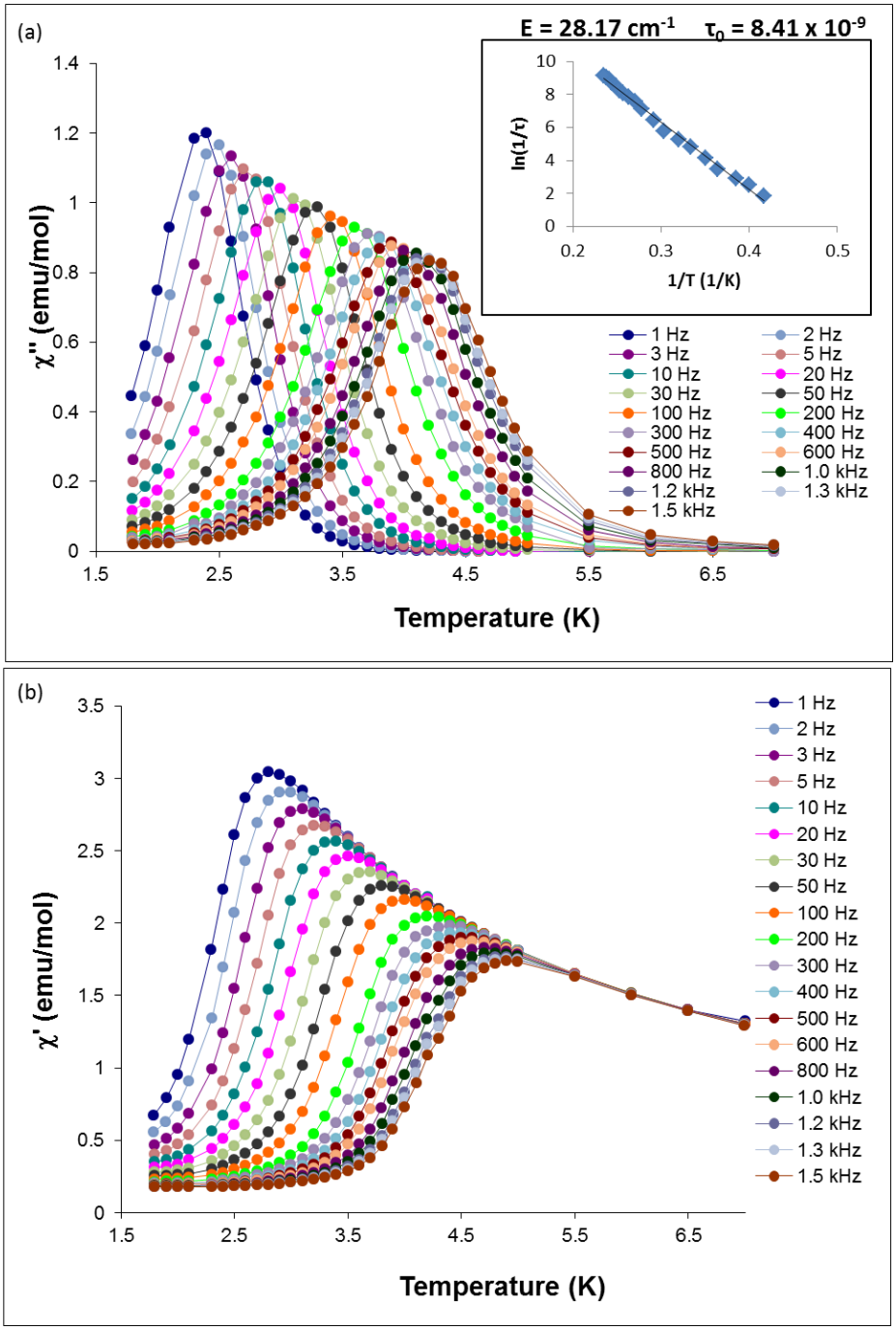

Figure 2.12 (a) Temperature dependence of the imaginary (χ") part of the ac susceptibility for **1** measured under various oscillating frequencies (1 – 1500 Hz). The solid lines are a guide for the eye. Inset: dependence of the logarithm of the relaxation rate (1/τ) on the inverse temperature (1/T). The solid line is a best linear fit to the Arrhenius law (U_{eff} = 28.17, τ_0 = 8.41 x 10^{-9} s). (b) Temperature dependence of the in-phase (χ') ac susceptibility signals for compound **1**.

~8 K, indicative of ferromagnetic coupling between the Mn^{III} and Os^{III} ions which results in an S = 9/2 ground state. The drop of χT at very low temperatures can be attributed to intermolecular interactions or zero field splitting. The field dependence of the magnetization data at temperatures between 2 and 20 K show a non-superposition between the isofield lines indicating the presence of significant anisotropy in the form of zero field splitting (Figure 2.11a). Even at 7 T and 2 K, however, the magnetization is much less than the expected saturation value of 9.0 μ_B for an S = 9/2 ground state with g = 2.0, (Figure 2.11b), indicating the population of low-lying excited states. Simulation of the magnetic susceptibility data using MAGPACK[207] and Eq. 1 results in the best fit parameters: J = 5.1 cm^{-1}, zJ' = -0.12 cm^{-1}, g_{Os} = 1.75, g_{Mn} = 2.0 , D = -0.3 cm^{-1}. These results for the dc measurements are consistent with the results of the Mn_2Os trinuclear molecule reported by Carolina Avendaño in her thesis.[190]

The ac magnetic susceptibility data of **1** in zero applied DC field exhibits slow relaxation of the magnetization (Figure 2.12a). The in-phase, χ', and out-of-phase signals, χ_M'' plotted vs. temperature, are depicted in Figure 2.12 for frequencies from 1 - 1500 Hz. Both χ' and χ'' are strongly frequency dependent below 5 K with χ_M'' achieving a maximum for each frequency measured. The maximum at 1.5 kHz in the χ_M'' data for **1** shows a blocking temperature of 4.3 K. The relaxation times follow an Arrhenius relationship: $\tau = \tau_o \exp(U_{eff}/k_BT)$ and a plot of $\ln(1/\tau)$ vs. 1/T is linear (Figure 2.12a inset) with a least-squares fit resulting in the values $\tau_o = 8.41 \times 10^{-9}$ s and U_{eff} = 28.2 cm^{-1}. The in-phase, χ', and out-of-phase, χ'', signals vs. frequency were also measured (Figure 2.13a and 2.14a). The relaxation times of the χ'' vs. ν data follow an

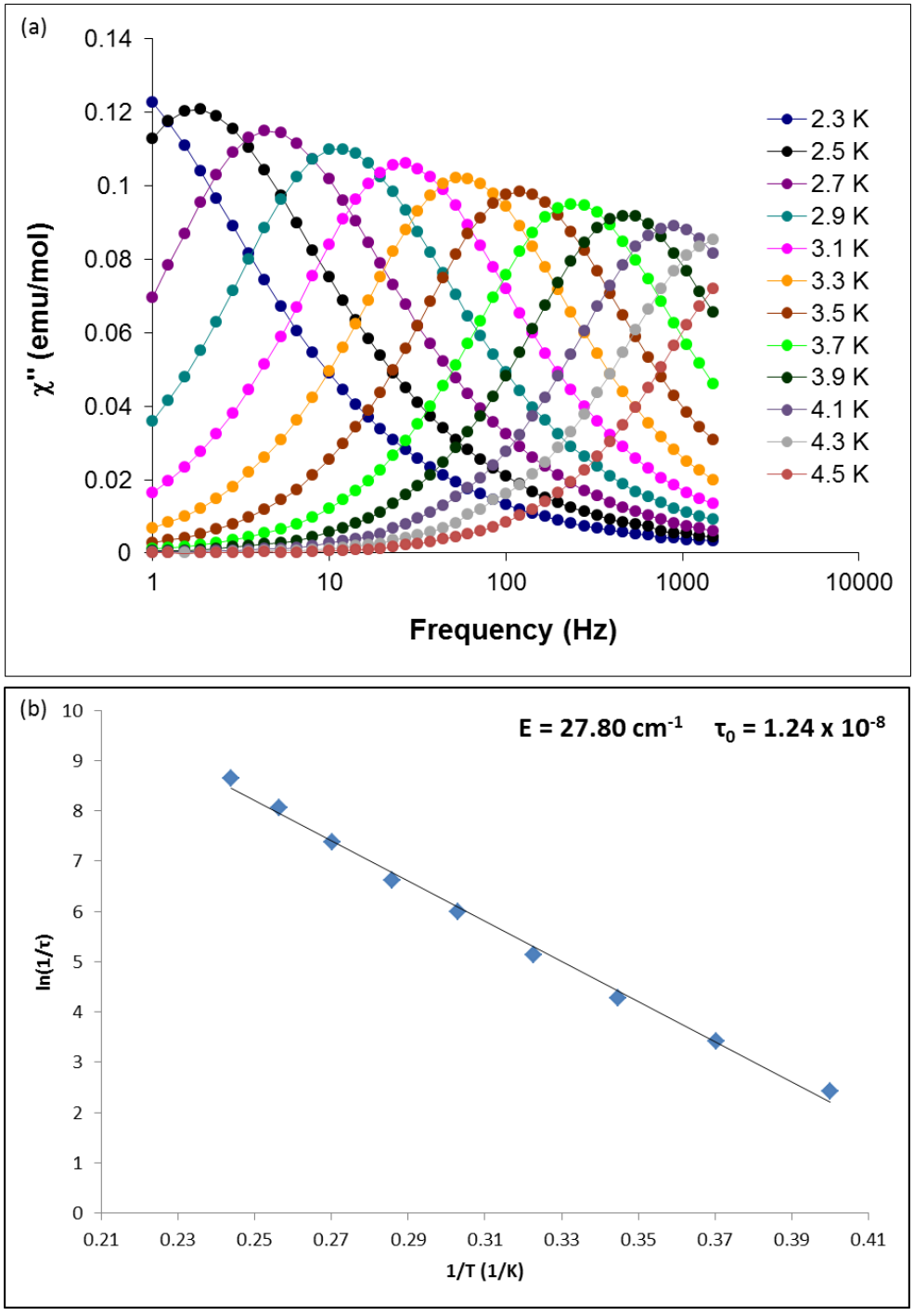

Figure 2.13 (a) Frequency dependence of the imaginary (χ") part of the ac susceptibility for **1** measured at various temperatures (2.3 – 4.5 K). (b) Dependence of the logarithm of the relaxation rate (1/τ) on the inverse temperature (1/T). The solid line is a best linear fit to the Arrhenius law (U_{eff} = 27.80 cm^{-1}, τ_0 = 1.24 x 10^{-8} s).

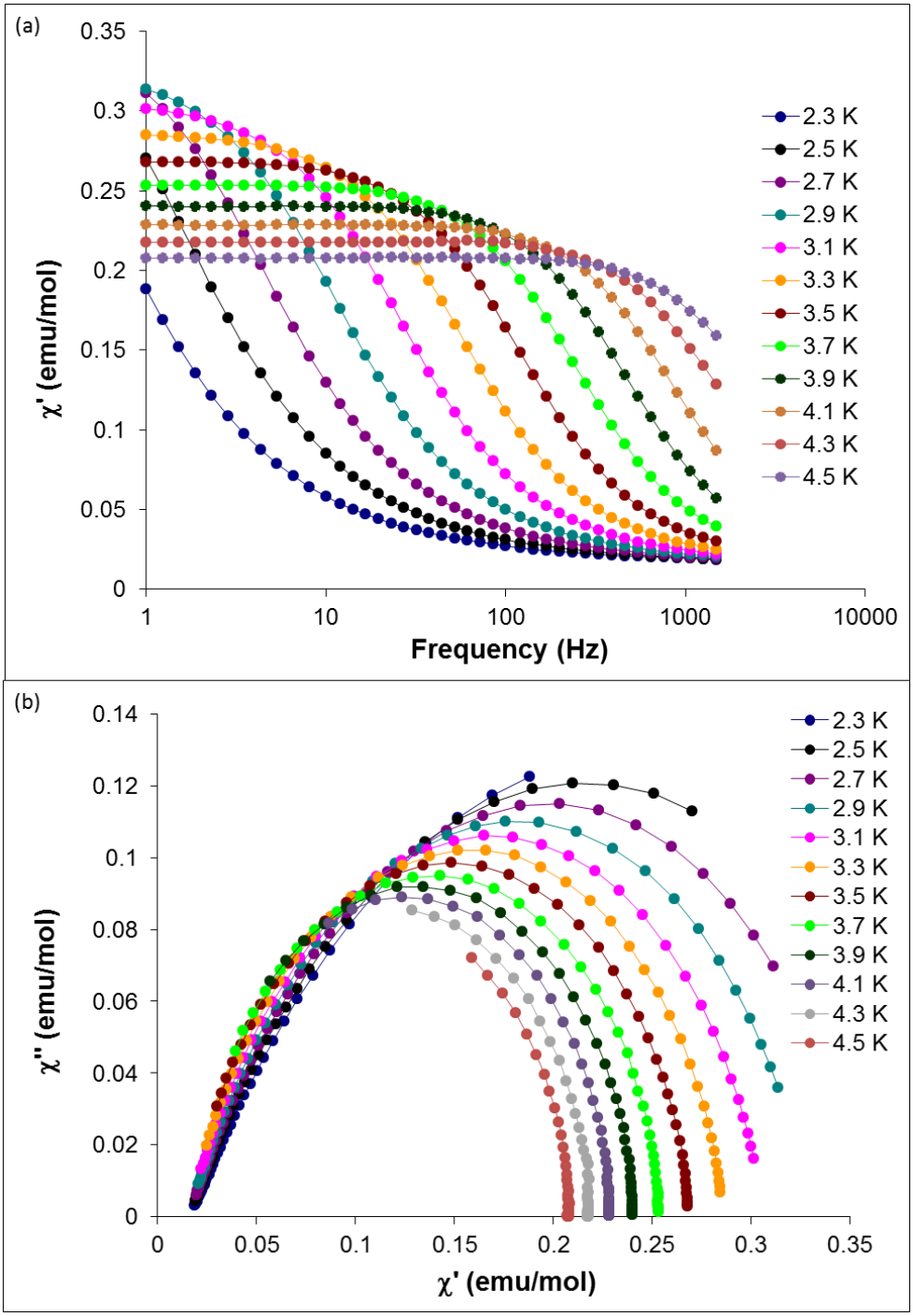

Figure 2.14 (a) Frequency dependence of the in-phase signals (χ') for compound **1** measured at various temperatures (2.3 – 4.5 K). The solid lines are a guide for the eye. (b) Cole-Cole plot for **1** at various temperatures (2.3 – 4.5 K). The solid lines are a guide for the eye.

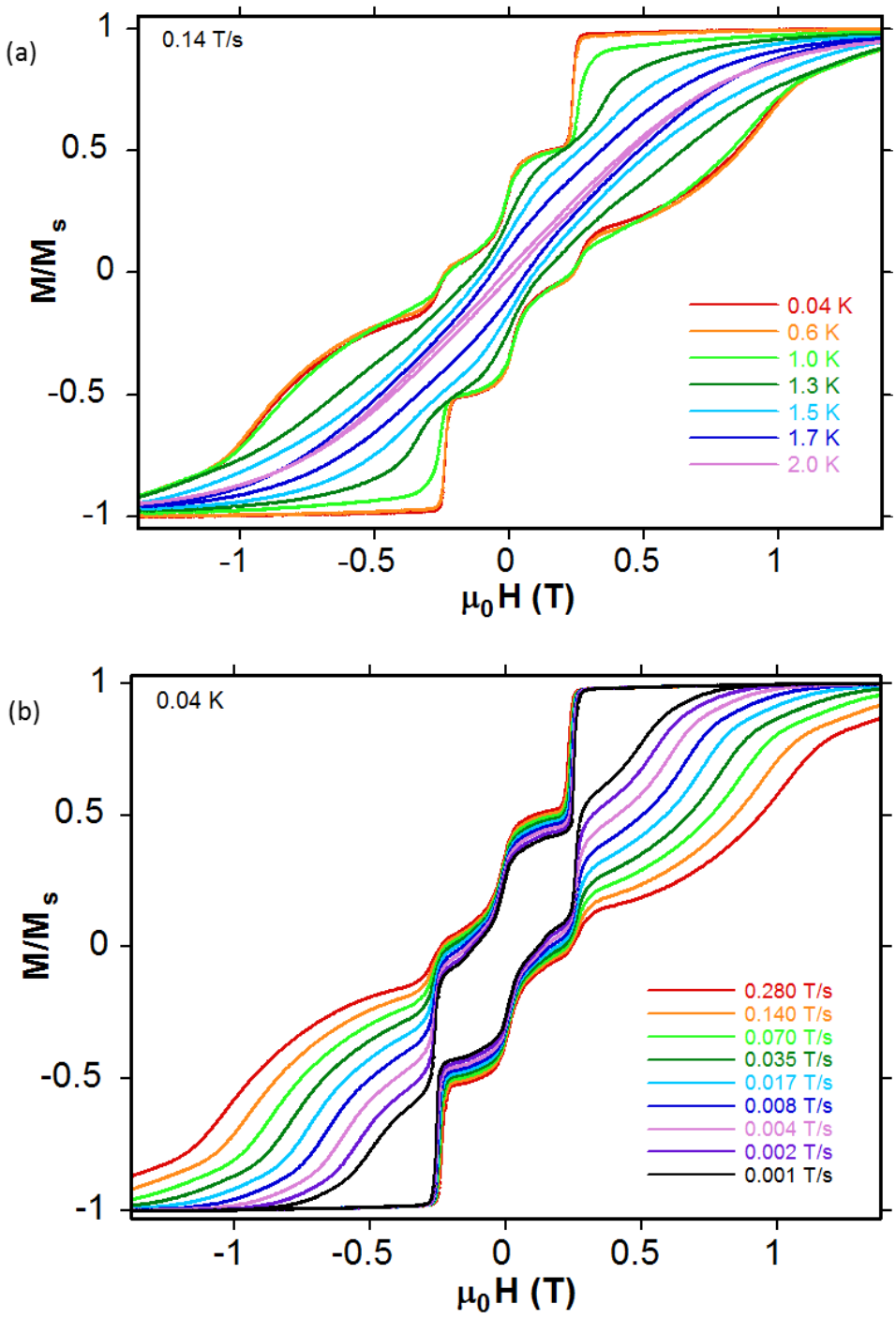

Figure 2.15 Magnetization (M) vs dc field (H) hysteresis loops for single crystals of **1** along the b-axis (a) below 2.0 K with a sweep field rate of 0.14 T/s and (b) below a sweep rate of 0.280 T/s at 0.04 K. Reprinted from reference 190.

Arrhenius relationship and a plot of $\ln(1/\tau)$ vs. 1/T (Figure 2.13b) is linear with a least-squares fit giving the values $U_{eff} = 27.80\ cm^{-1}$ with $\tau_0 = 1.24 \times 10^{-8}$ s. In addition, the shape of the Cole-Cole plot is nearly symmetrical (Figure 2.14b) showing that a single relaxation time, τ, is operating.

When it was initially discovered that these molecules behaved as SMMs, Carolina Avendaño sent the Os^{III} compounds to be measured on a micro-SQUID apparatus by Dr. Wernsdorfer in Grenoble, France to explore the relaxation dynamics of these SMMs further. The initial reports indeed showed that the compounds exhibited hysteresis below 2 K and that the Mn_2Os congener exhibited both typical SMM and exchange bias SMM behavior,[190] but because of the lack of systematic handling of the compounds for supporting measurements (*i.e.* ac measurements), it was unclear at the time how the history of the compounds related to the observed properties. The dc magnetization versus field scans on easy-axis oriented single crystals of dried samples of **1** were measured on a micro-SQUID apparatus. Hysteresis loops were observed below ~2 K (Figure 2.15) and the coercivities were observed to increase with decreasing temperatures and increasing field sweep rates, which is behavior typical of SMMs. The hysteresis loops exhibit a shift of the first QTM step, a phenomenon reminiscent of exchange-bias behavior due to intermolecular interactions between SMMs.[187,189,191-197,199] Typical SMMs are designed to have negligible intermolecular exchange interactions to prevent long range magnetic ordering. In these systems, the first step in the hysteresis loop upon scanning from negative to positive fields typically occurs at zero field. If, however, there are weak interactions between the SMMs present, (strong

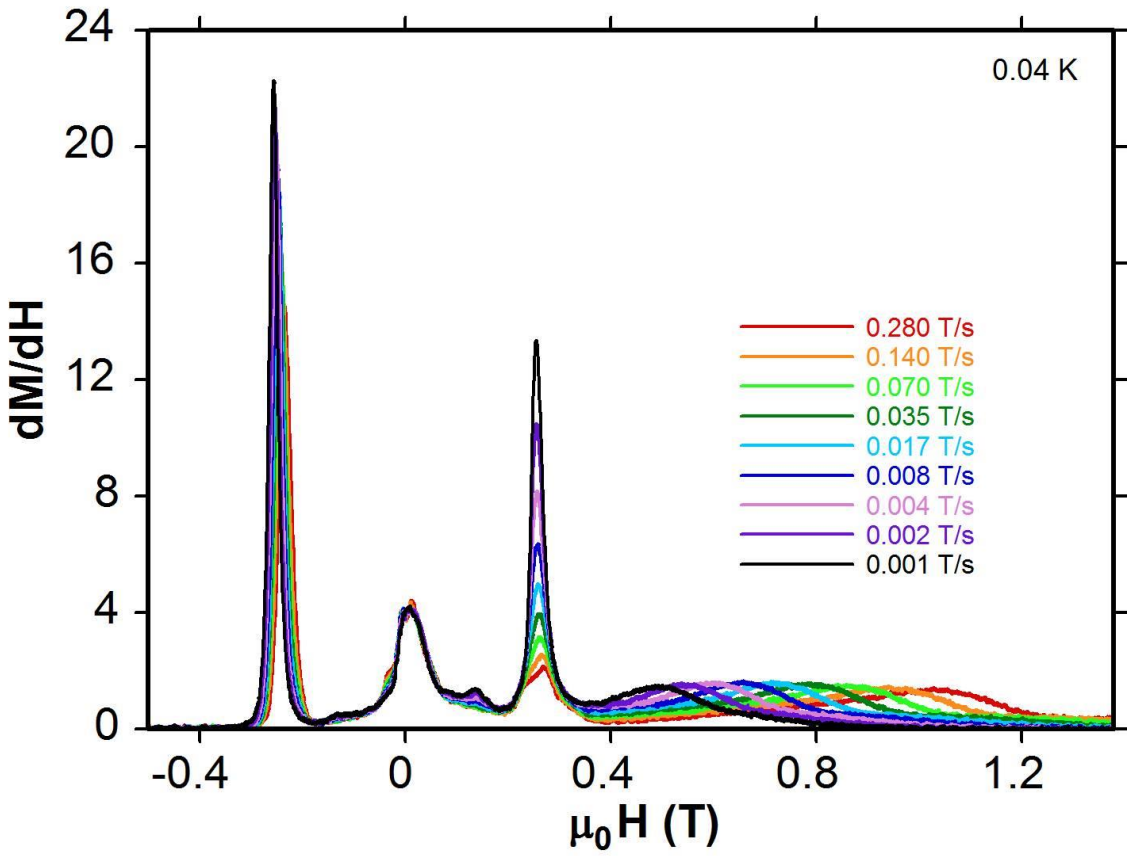

Figure 2.16 The derivative of the magnetization versus magnetic field (dM/dH) measured at 0.04 K below a sweep rate of 0.280 T/s for a single crystal of **1**.

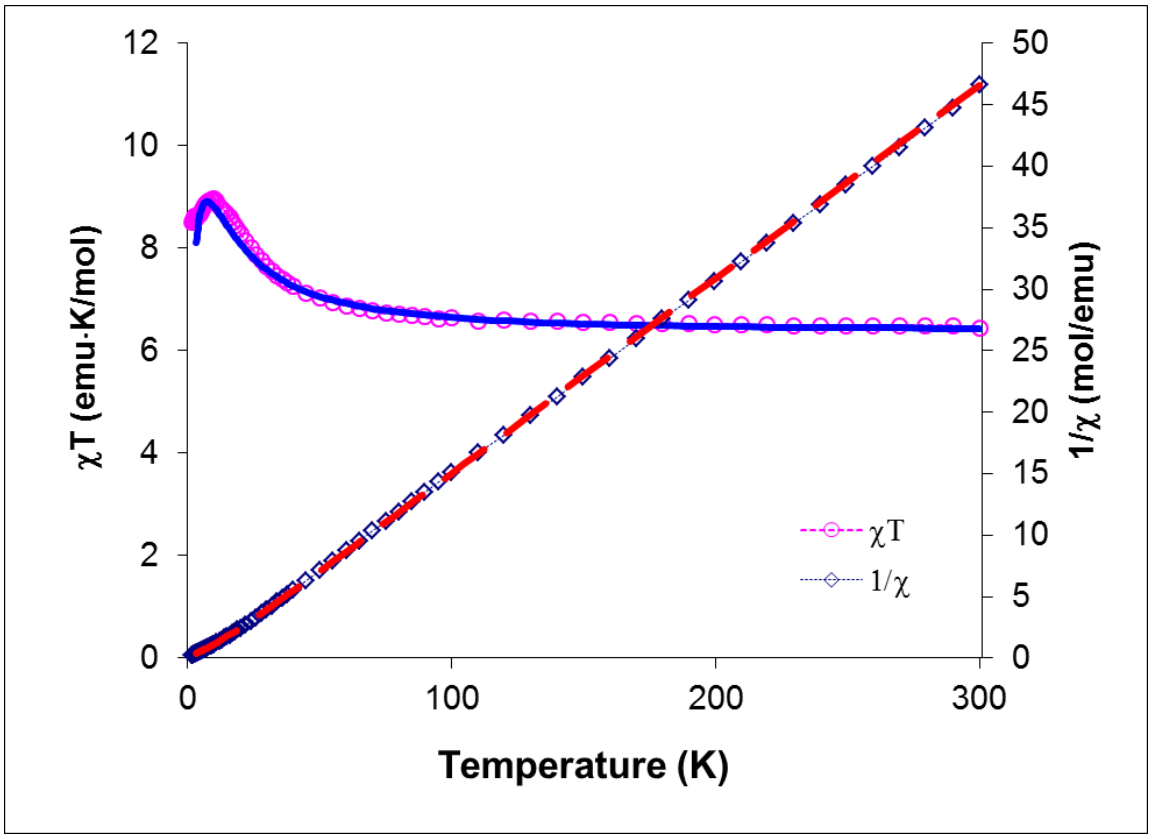

Figure 2.17 Temperature dependence of χT and $1/\chi$ for compound **1**·4MeOH. The solid line corresponds to the MAGPACK[207] simulation (g_{Os} = 1.75, g_{Mn} = 2.0, J = 5.5 cm^{-1}, zJ' = -0.06 cm^{-1}, D = -0.03 cm^{-1}).

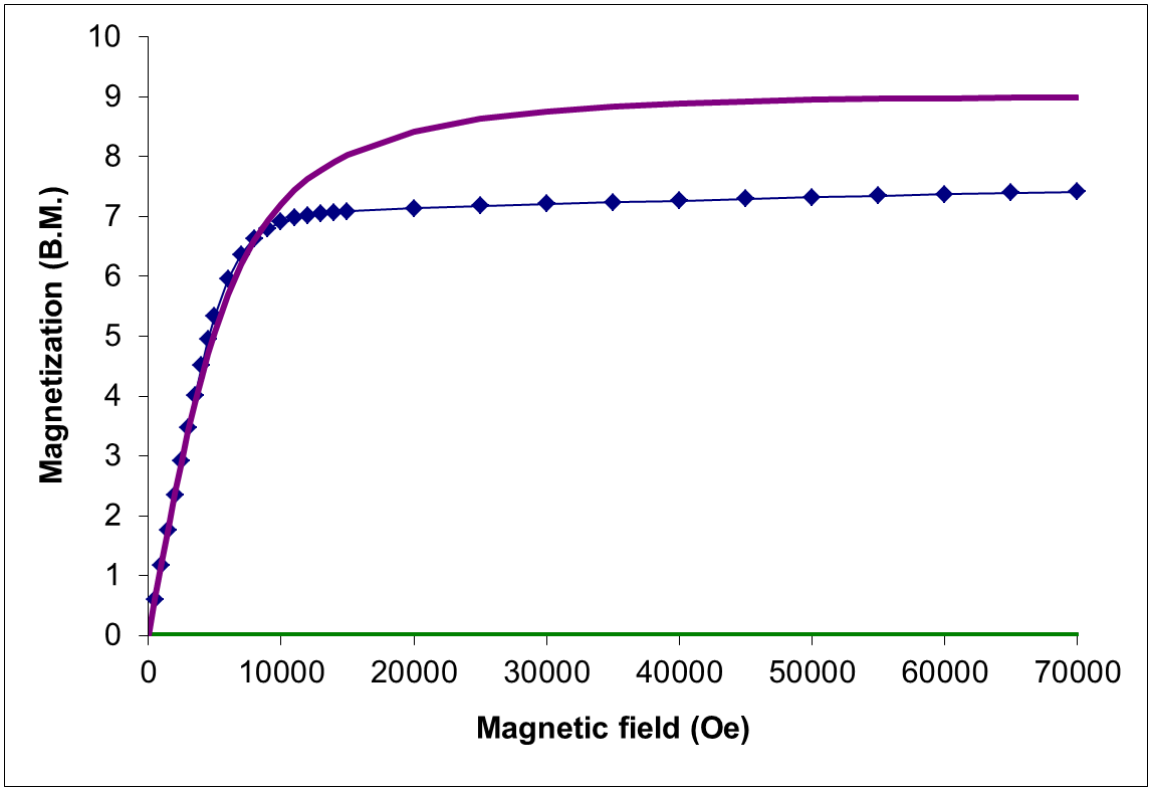

Figure 2.18 Field dependent magnetization for **1**·4MeOH. The solid line corresponds to the Brillouin function for S = 9/2, g_{avg} = 2.0.

enough to influence SMM behavior but too weak to induce long range magnetic ordering), a shift of the first QTM step occurs. This exchange bias behavior was first noted for the $[Mn_4]_2$ dimer of SMMs, $[Mn_4O_3Cl_4(O_2CEt)_3(py)_3]_2$[189] with subsequent examples being reported in the past few years.[187,189,191-197,199] In the case of compound **1**, the first QTM step observed in the hysteresis loop collected at 40 mK is shifted to -0.3 T which can clearly be observed in the derivative plot (Figure 2.16). This shift indicated the presence of antiferromagnetic interactions between the Mn_2Os SMMs. Below 1.0 K (Figure 2.15a) the hysteresis loops become temperature independent, but remain sweep-rate dependent at 40 mK (Figure 2.15b) indicating that QTM is occurring in the compound.

PPN{[Mn(salphen)(MeOH)]$_2$[Os(CN)$_6$]}·4MeOH (1·4MeOH**)**. In order to probe the role of interstitial solvent on the magnetic properties of **1**, magnetic measurements of **1**·4MeOH were carried out under the mother liquor. The χT vs T curve behaves very similarly to compound **1** as temperature is lowered from room temperature, however, the best fit parameter for compound **1**·4MeOH, (Figure 2.17) for the intermolecular interaction, $zJ' = -0.06$ cm^{-1}, is lower than the one observed for the dried sample, **1**, with coupled SMMs ($zJ' = -0.12$ cm^{-1}). Simulation of the magnetic susceptibility data for **1**·4MeOH using MAGPACK[207] and Eq. 1 results in the best fit parameters: $J = 5.5$ cm^{-1}, $zJ' = -0.06$ cm^{-1}, $g_{Os} = 1.75$, $g_{Mn} = 2.0$, $D = -0.3$ cm^{-1}. Also as in the case of compound **1**, the magnetization at 7 T is less than the expected saturation value of 9.0 μ_B for an S = 9/2 ground state with g = 2.0, (Figure 2.18), indicating the population of low-lying excited states. More importantly, the maxima of the out-of-phase frequency-dependent

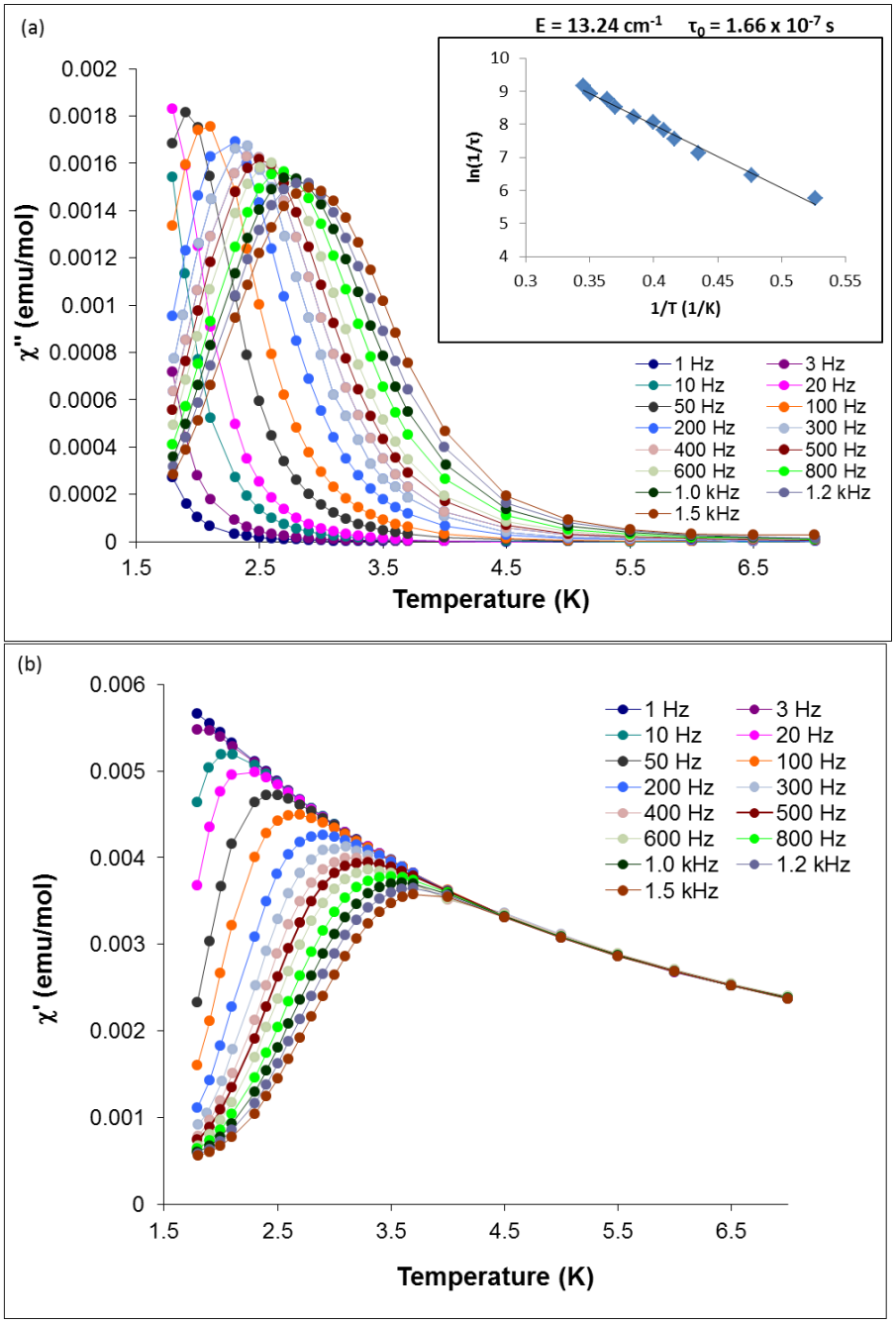

Figure 2.19 (a) Temperature dependence of the out-of-phase (χ") part of the ac susceptibility for **1**·4MeOH measured under various oscillating frequencies (1 – 1500 Hz). The solid lines are a guide for the eyes. Inset: dependence of the logarithm of the relaxation rate (1/τ) on the inverse temperature (1/T). The solid line is a best linear fit to the Arrhenius law (U_{eff} = 13.24, τ_0 = 1.66 x 10^{-7} s). (b) Temperature dependence of the in-phase (χ') ac susceptibility signals for compound **1**·4MeOH.

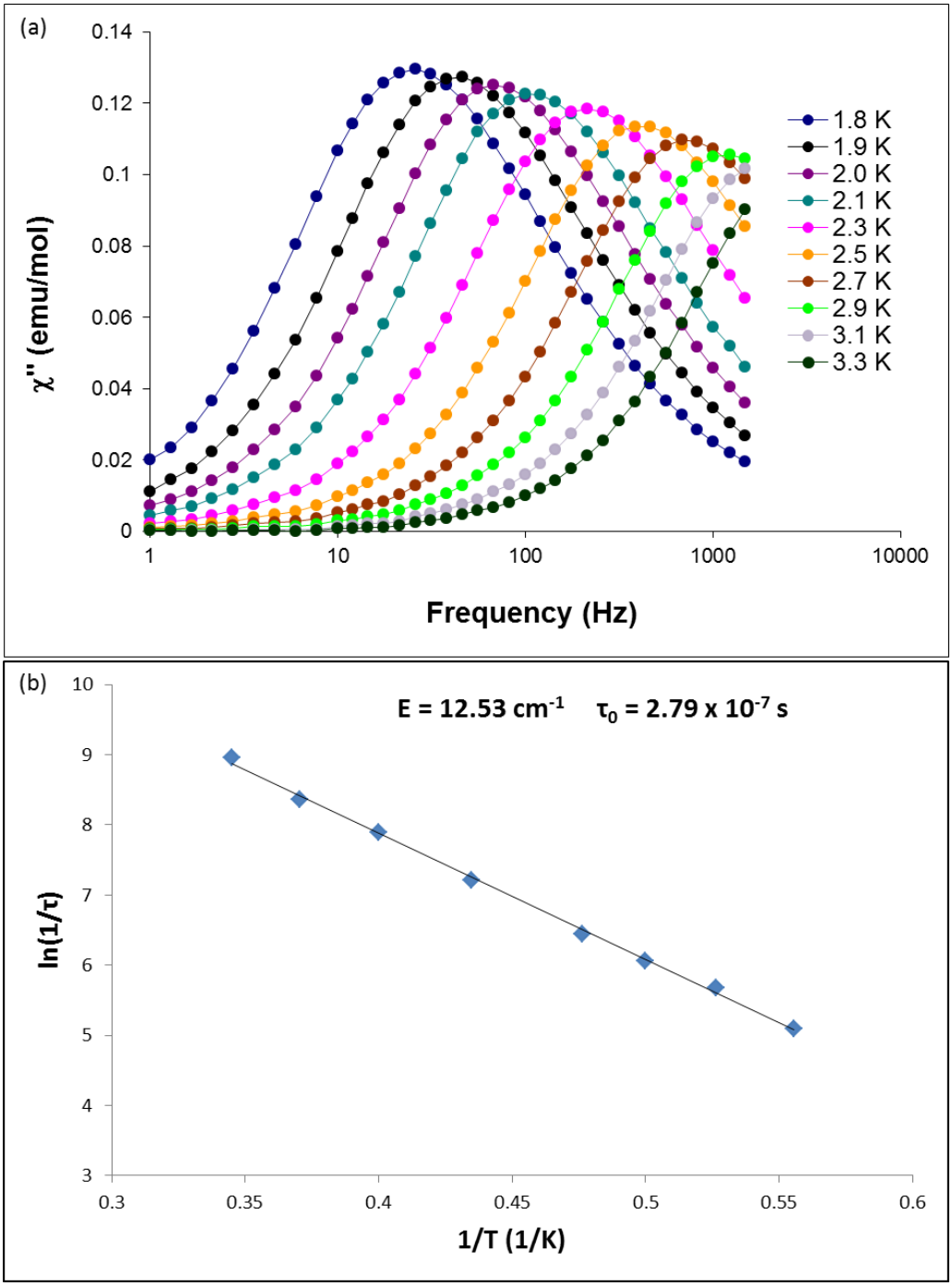

Figure 2.20 (a) Frequency dependence of the imaginary (χ") part of the ac susceptibility for **1**·4MeOH measured at various temperatures (1.8 – 3.3 K). (b) Dependence of the logarithm of the relaxation rate (1/τ) on the inverse temperature (1/T). The solid line is the best linear fit to the Arrhenius law (U_{eff} = 12.53 cm^{-1}, τ_0 = 2.79 x 10^{-7} s).

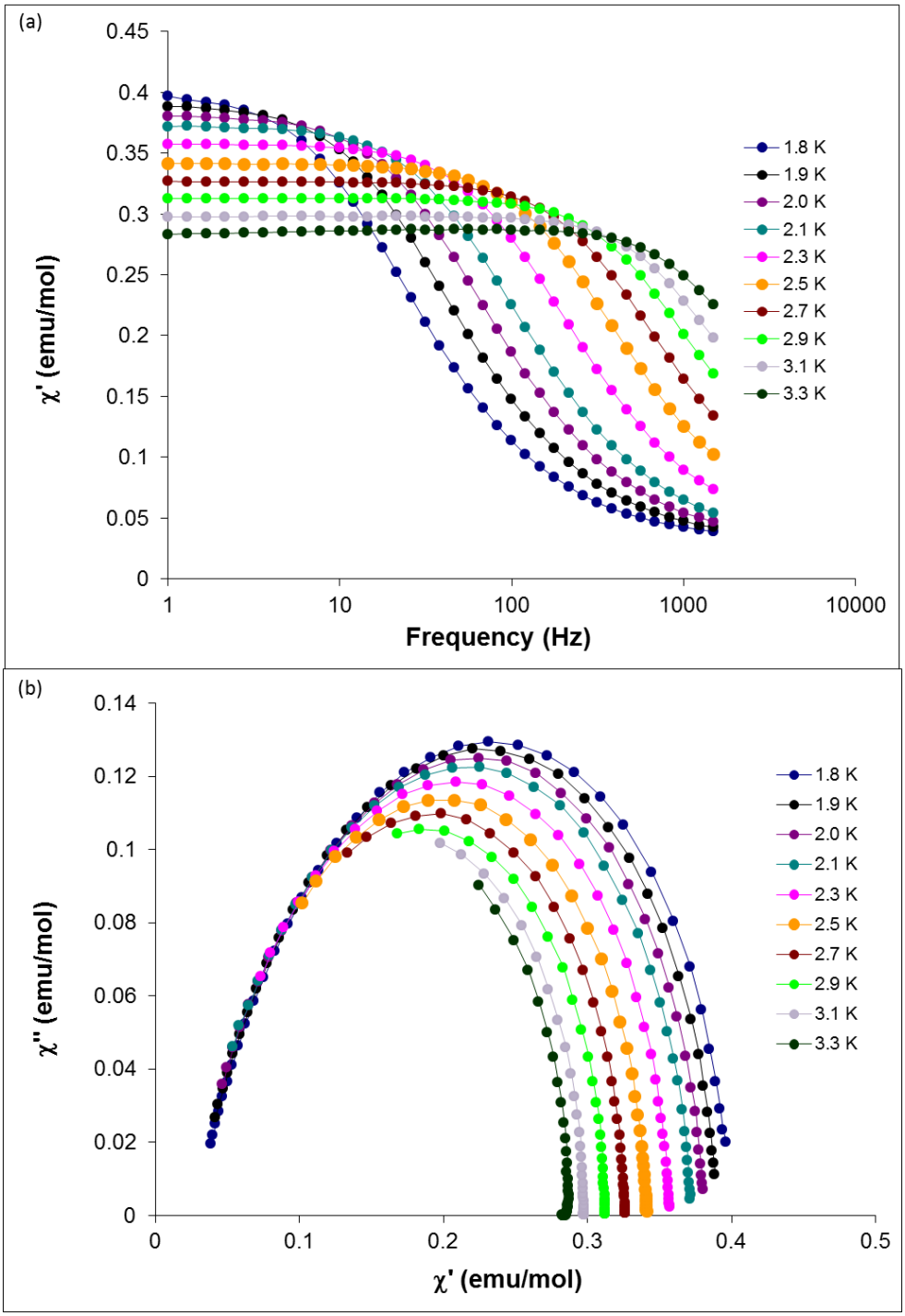

Figure 2.21 (a) Frequency dependence of the in-phase signals (χ') for compound **1**·4MeOH measured at various temperatures 1.8 – 3.3 K). The solid lines are a guide for the eyes. (b) Cole-Cole plot for **1**·4MeOH at various temperatures (1.8 - 3.3 K). The solid lines are a guide for the eye.

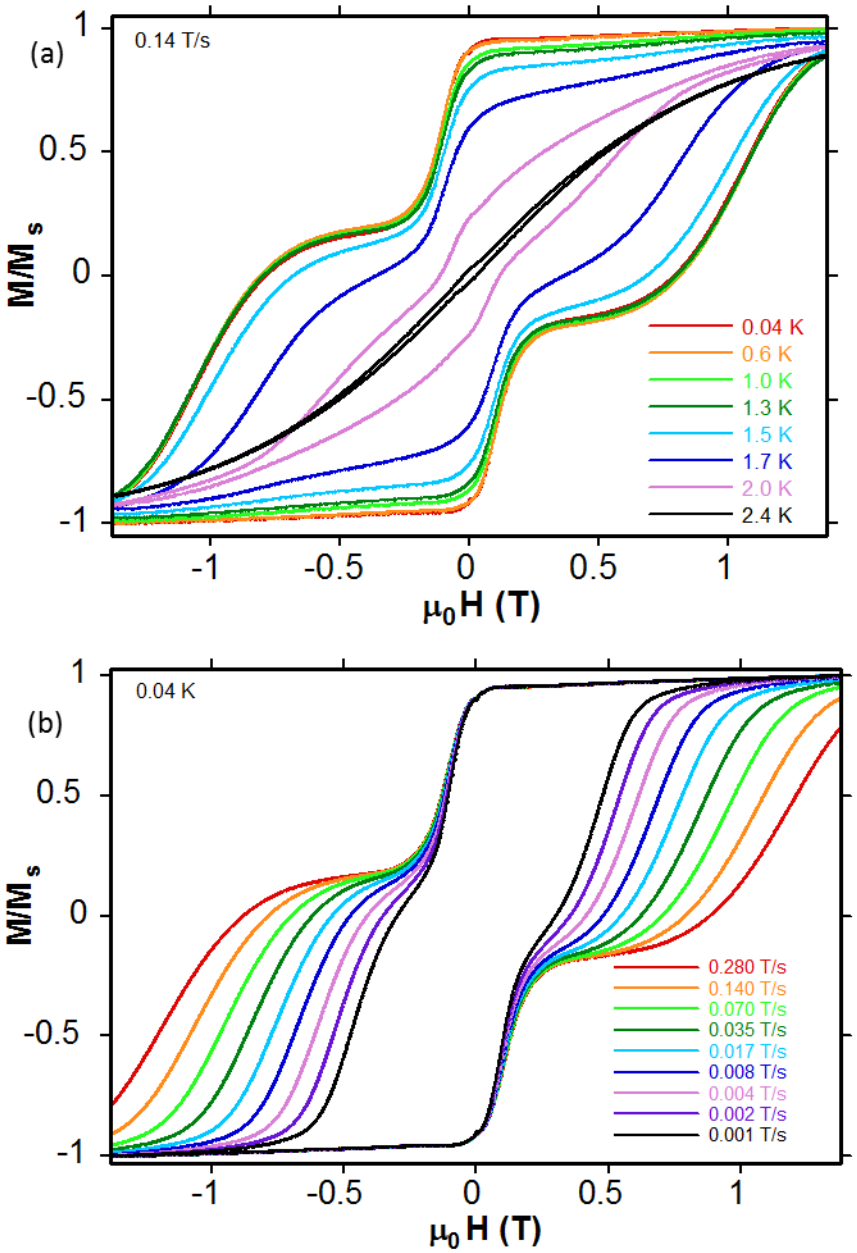

Figure 2.22 Magnetization (M) vs dc field (H) hysteresis loops for single crystals of **1**·4MeOH along the b-axis (a) below 2.4 K with a sweep field rate of 0.14 T/s and (b) below a sweep rate of 0.280 T/s at 0.04 K. Reprinted from reference 190.

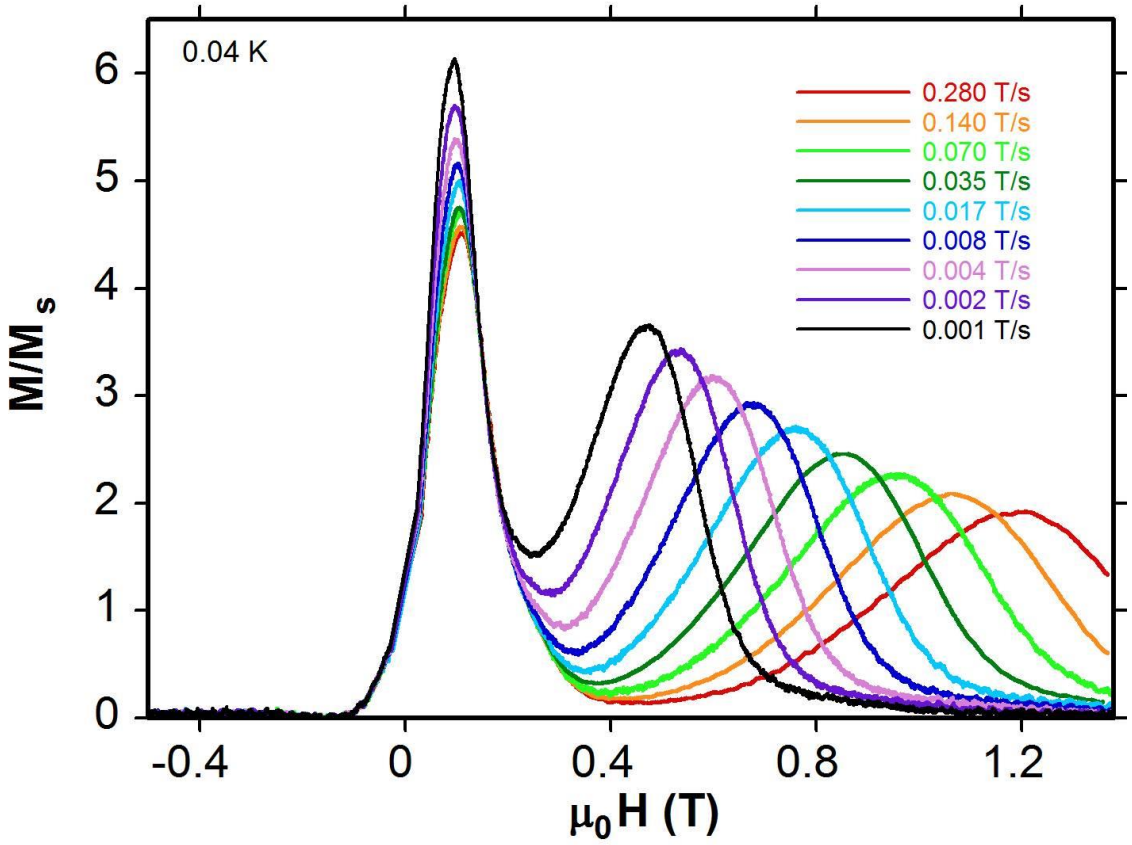

Figure 2.23 The derivative of the magnetization versus magnetic field (dM/dH) measured at 0.04 K below a sweep rate of 0.280 T/s for a single crystal of **1**·4MeOH.

ac susceptibility data on the sample of solvent-protected crystals of **1**·4MeOH indicate lower blocking temperatures (2.9 K at 1.5 kHz; Figure 2.19a) than for **1** and the peak temperatures, fitted to an Arrhenius relationship: $\tau = \tau_o \exp(U_{eff}/k_BT)$ (Figure 2.19a, inset), lead to an effective barrier height for magnetization reversal of $U_{eff} = 13.24$ cm^{-1} and a pre-exponential value $\tau_o = 1.66 \times 10^{-7}$ s, which is a much smaller barrier than the barrier exhibited by compound **1**. The barrier associated with **1**·4MeOH is comparable to the barrier of the Os^{III} congener of the K{[Mn(5-Brsalen)(H_2O)]$_2$[M$(CN)_6$]} series reported by Bendix, $U_{eff} = 13.2$ cm^{-1}.[112] The in-phase, χ', and out-of-phase, χ", signals vs. frequency were also measured and are plotted in Figure 2.20a and 2.21a. The peaks of the imaginary part of the out of phase signals, χ", were plotted and fit to an Arrhenius law. The plot of ln(1/τ) vs. 1/T (Figure 2.20b) is linear with a least-squares fit resulting in the values $U_{eff} = 12.53$ cm^{-1} and $\tau_0 = 2.79 \times 10^{-7}$ s. The shape of the Cole-Cole plot of **1**·4MeOH is symmetrical (Figure 2.21b) indicating that the solvated compound is undergoing a single relaxation event.

Samples of **1**·4MeOH, measured on a micro-SQUID, exhibit hysteresis loops typical for a SMM without exchange bias (Figure 2.22) with only two steps observed due to resonant QTM. As reported in Carolina Avendaño's thesis, based on behavior observed in previously reported, S = 9/2, A{[Mn(salen-type ligand)(solv)]$_2$[M$(CN)_6$]} molecules, the step at zero field is attributed to the fast relaxation between the lower energy levels, $m_s = \pm 9/2$[182] and the second relaxation that occurs around $\mu_0 H_1 = 0.7$ T is due to the first crossing between two energy levels, (i.e. $m_s = 9/2$ and $-7/2$)[190] (Figure 2.23). The hysteresis loops and the ac data collected show that **1**·4MeOH behaves as a

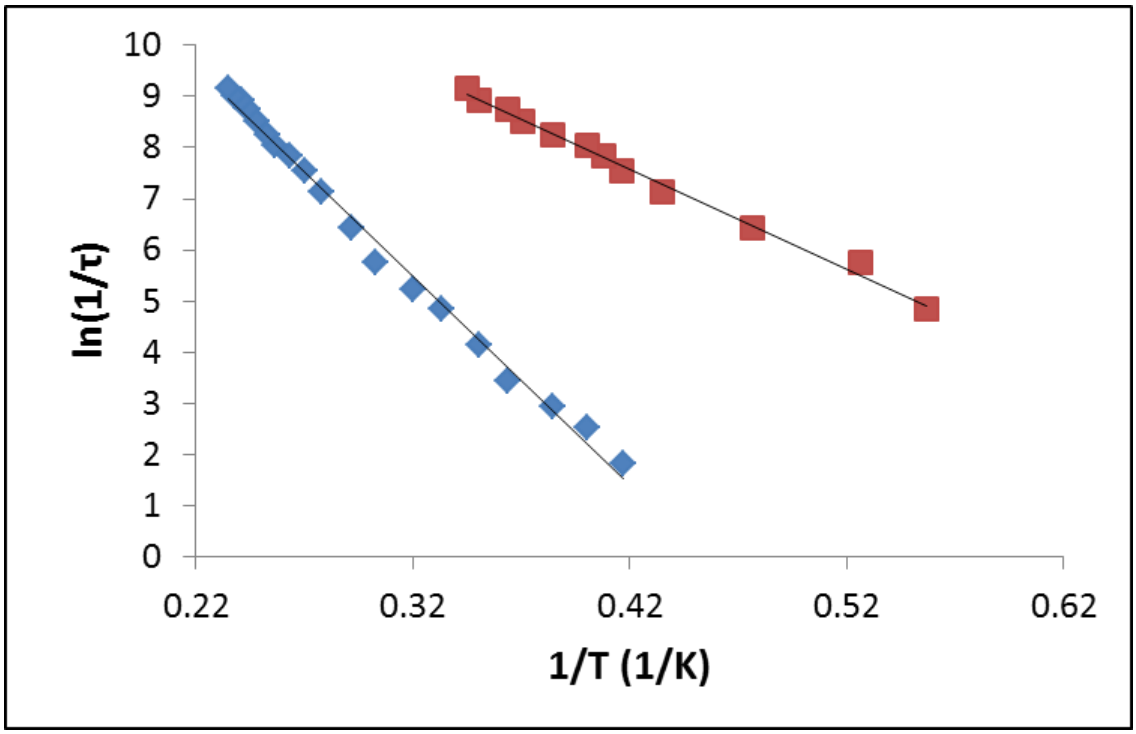

Figure 2.24 Logarithm of the relaxation rate (1/τ) versus the inverse temperature (1/T) plot for solvated 1·4MeOH (red) and dried (blue) **1**. The solid line represents the best linear fit to the Arrhenius law (red: U_{eff} = 13.24 cm^{-1} and τ_0 = 1.66 x 10^{-7} s; blue: U_{eff} = 28.17 cm^{-1} and τ_0 = 8.41 x 10^{-9} s). The data from the frequency dependent ac susceptibility (χ" vs. ν) were used to formulate this graph.

typical SMM without exchange bias behavior and, moreover, behaves similarly to previously reported compounds of the type A{[Mn(salen-type ligand)(solv)]$_2$[M(CN)$_6$]}.[112]

The observed properties in previously reported chains of ferro- or antiferromagnetically coupled SMMs, were influenced by the intrachain magnetic interactions. By applying the method described in ref 190 as defined for these previously reported 1D chain systems[70,178,208] to investigate the supramolecular pseudo-1D chains of antiferromagnetically coupled SMMs of **1**, the energy gap of the relaxation time is $\Delta_\tau = 2\Delta_\xi + \Delta_A$ (Eq. 2.3) within the Ising limit (where Δ_τ is the experimental energy gap for the exchange coupled SMMs and Δ_A is the experimental energy gap for an isolated SMM unit):

$$\Delta_A = |D| S_T^2/k_B \text{ and } \Delta_\xi = 4|zJ'|S_T^2\cos(\alpha) \quad \text{(Eq. 2.4)}$$

By rearranging Eq 2.3 and using the experimental values determined for the energy barriers for both the solvated SMM, **1**·4MeOH, ($U_{eff} = \Delta_A = 13.24$ cm^{-1}) and the exchange coupled (desolvated) SMMs, **1**, ($U_{eff} = \Delta_\tau = 28.17$ cm^{-1}), Δ_ξ is calculated to be 7.46 cm^{-1} (using $S_T = 9/2$ and $D = -0.03$ cm^{-1}). This this is consistent with a $zJ' = -0.12$ cm^{-1} ($\alpha = 37°$) which matches the value determined from the dc magnetic susceptibility measurements ($zJ' = -0.12$ cm^{-1}) of **1**.

The values obtained for the relaxation rate, τ, for both **1** and **1**·4MeOH were plotted together in (Figure 2.24). The thermal variations of the relaxation time observed for the solvated, **1**·4MeOH, and desolvated, **1**, samples are dramatically different

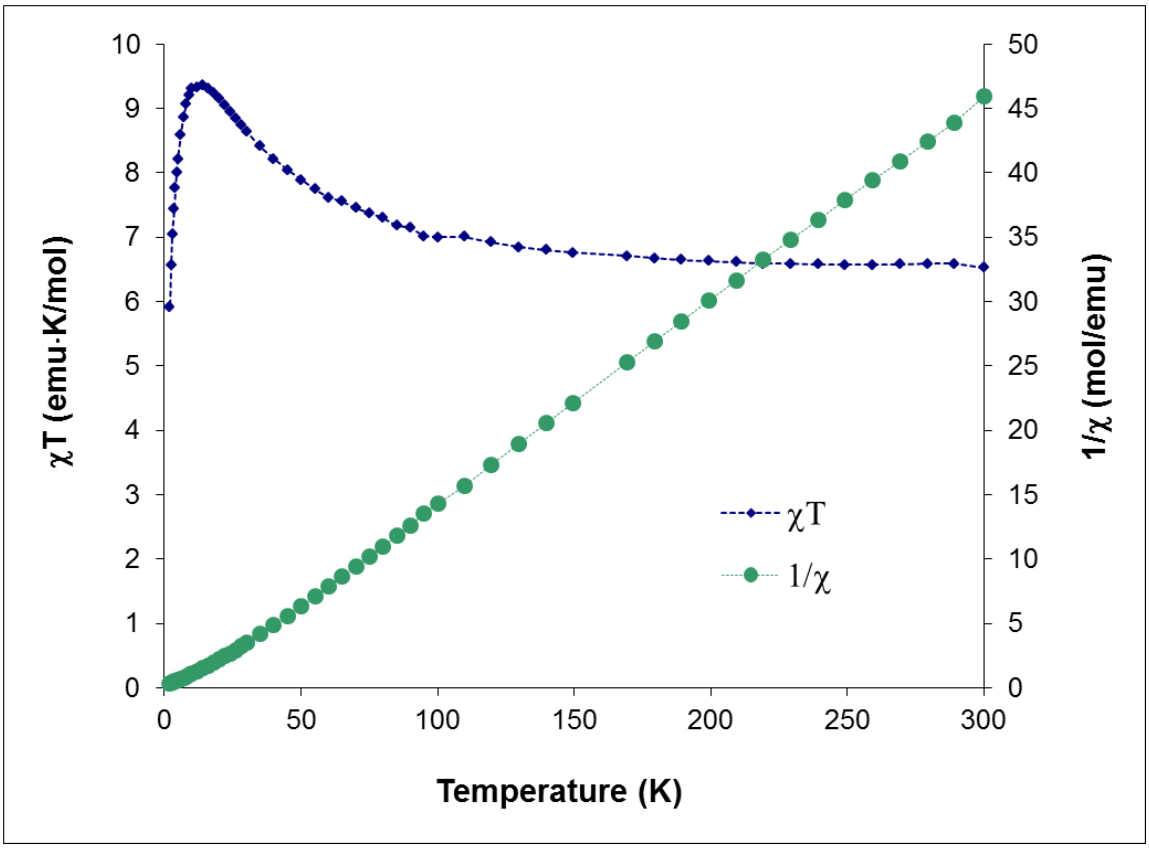

Figure 2.25 Temperature dependence of χT and $1/\chi$ for resolvated sample of compound **1**. Solid lines are a guide for the eye.

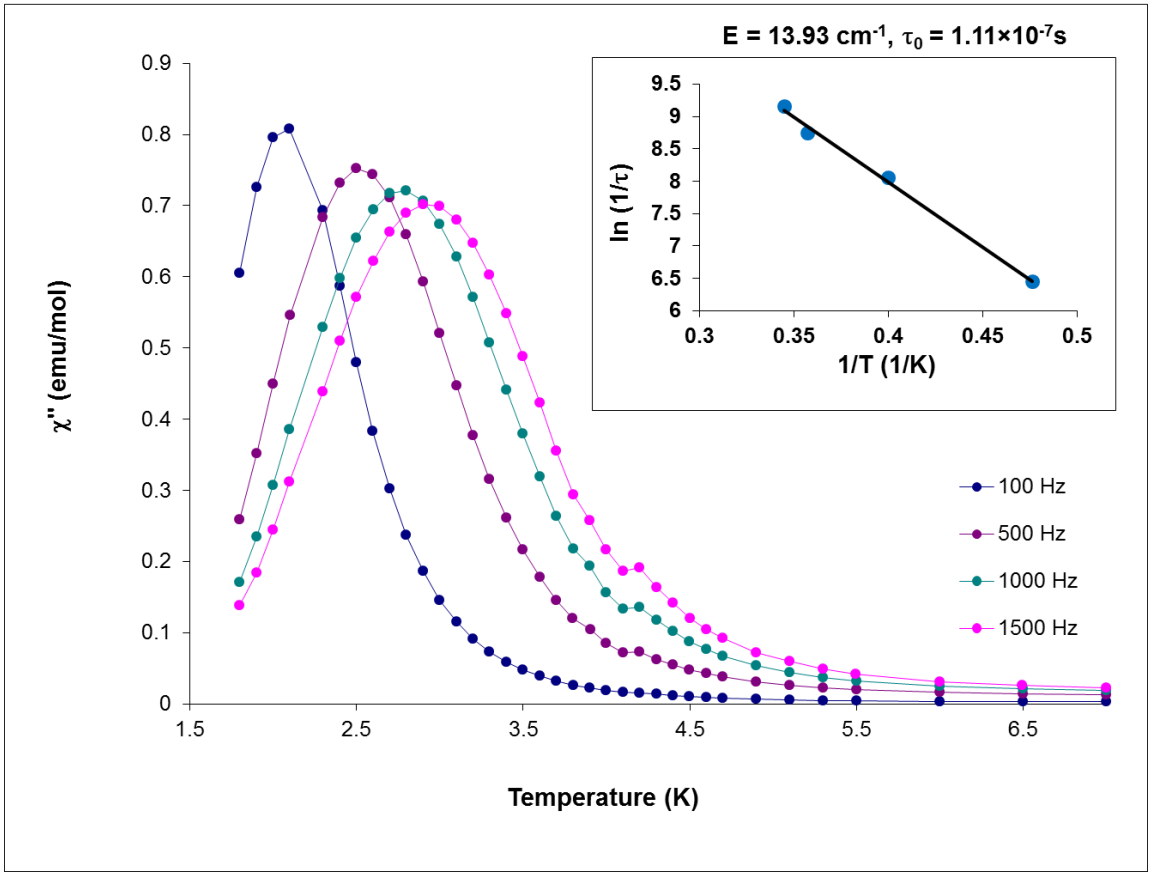

Figure 2.26 Temperature dependence of the out-of-phase (χ") part of the ac susceptibility for **1**·4MeOH measured under various oscillating frequencies (100 – 1500 Hz). The solid lines are a guide for the eye. Inset: dependence of the logarithm of the relaxation rate (1/τ) on the inverse temperature (1/T). The solid line is a best linear fit to the Arrhenius law (U_{eff} = 13.93, τ_0 = 1.11 x 10^{-7} s).

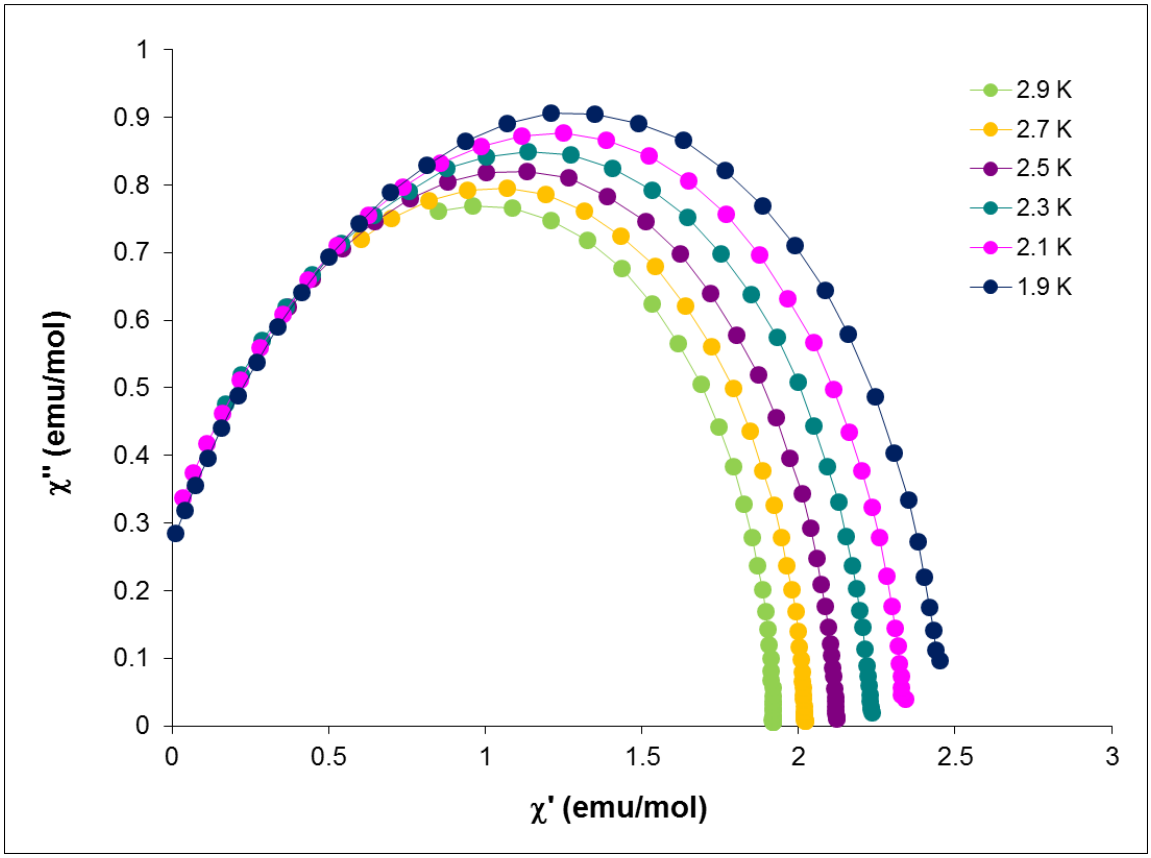

Figure 2.27 Cole-Cole plot for a "resolvated" sample of compound **1** at various temperatures (1.9 – 2.9 K). The solid lines are a guide for the eye.

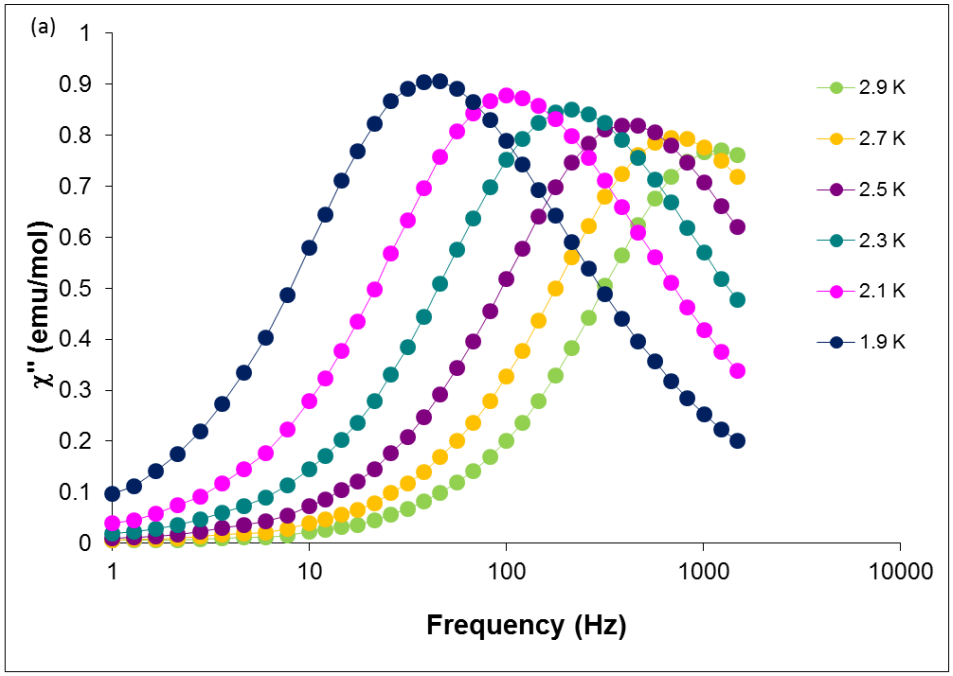

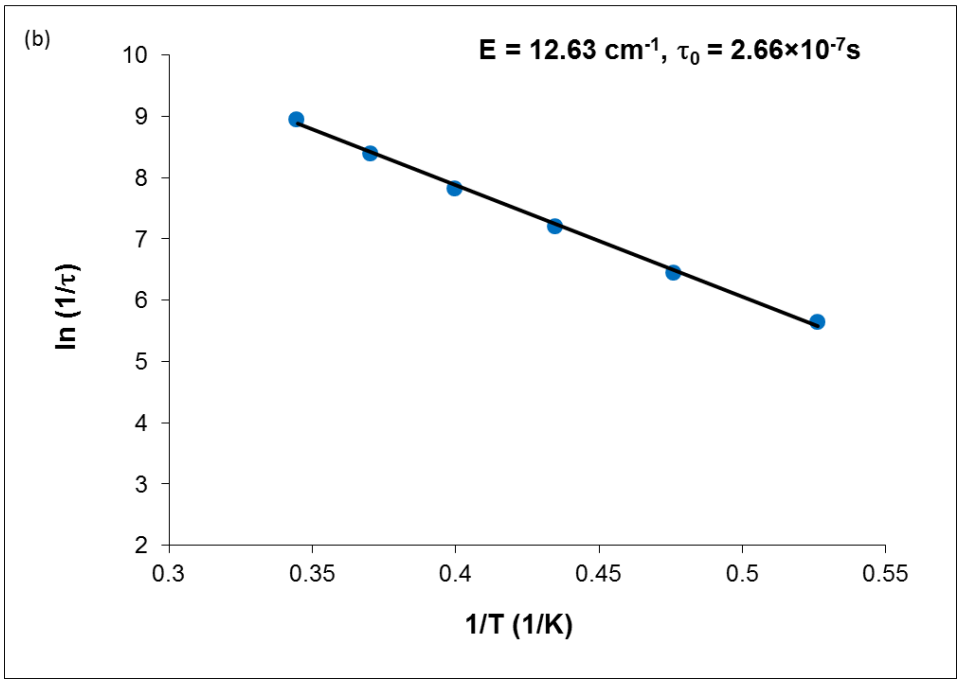

Figure 2.28 (a) Frequency dependence of the imaginary (χ") part of the ac susceptibility for a resolvated sample of **1** measured at various temperatures (1.9 – 2.9 K). (b) Dependence of the logarithm of the relaxation rate (1/τ) on the inverse temperature (1/T). The solid line is a best linear fit to the Arrhenius law (U_{eff} = 12.63 cm^{-1}, τ_0 = 2.66 x 10^{-7} s).

showing that the intermolecular exchange interactions between the SMM anions greatly effects the relaxation of the magnetization.

Reversibility of 1 and 1·4MeOH. The fact that two different behaviors are exhibited for dried samples of **1** and solvated samples **1**·4MeOH raises the question as to whether the exchange behavior is reversible. To address this question, the dried sample of **1** was soaked under methanol for several hours and magnetic measurements were acquired with the sample under solvent. The behavior of the χT plot shown in Figure 2.25 matches that of compound **1**·4MeOH with the value of χT reaching a maximum at ~ 8K. Analagous to **1**·4MeOH, the ac magnetic susceptibility data under a zero applied dc field exhibits slow relaxation of the magnetization (Figure 2.26). The out-of-phase signal, χ", for frequencies from 100 - 1500 Hz plotted vs. temperature, is shown in (Figure 2.26). The χ" data indicates a blocking temperature, T_B, of 3 K at 1.5 kHz. In addition, the shape of the Cole-Cole plot is nearly symmetrical (Figure 2.27) indicating that a single relaxation time, τ, is operative and that a complete conversion of the dried exchange bias **1** to the SMM **1**·4MeOH has occurred. A plot of ln(1/τ) vs. 1/T is linear (Figure 2.26, inset) and when fit to an Arrhenius law, gives a least-squares fit with the values $\tau_o = 1.11 \times 10^{-7}$ s and $U_{eff} = 13.9$ cm^{-1}. The χ" vs. T data, the out-of-phase signal, χ", vs. frequency was also measured and is shown in Figure 2.28a. The relaxation times of the χ" vs. ν data were plotted (Figure 2.28b) and fit to an Arrhenius relationship is with a least-squares fit giving $U_{eff} = 12.6$ cm^{-1} with $\tau_0 = 2.66 \times 10^{-7}$ s.

The measurement of compound **1** soaked under solvent shows that the Os^{III} compound exhibits SMM behavior with reversible exchange bias behavior. The extent

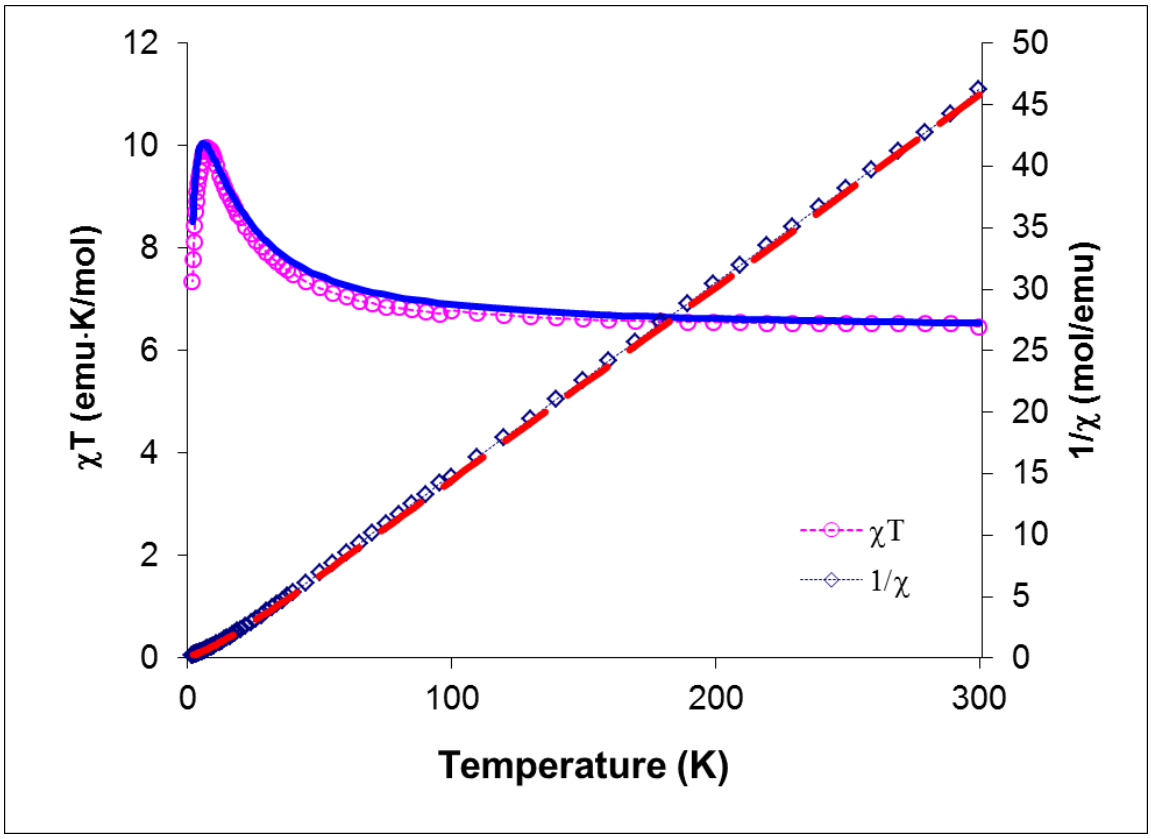

Figure 2.29 Temperature dependence of χT and $1/\chi$ for compound **2**. The solid line corresponds to the MAGPACK[207] simulation (g_{Fe} = 2.0, g_{Mn} = 2.0, J = 4.7 cm^{-1}, zJ' = -0.10 cm^{-1}, D = -0.3 cm^{-1}).

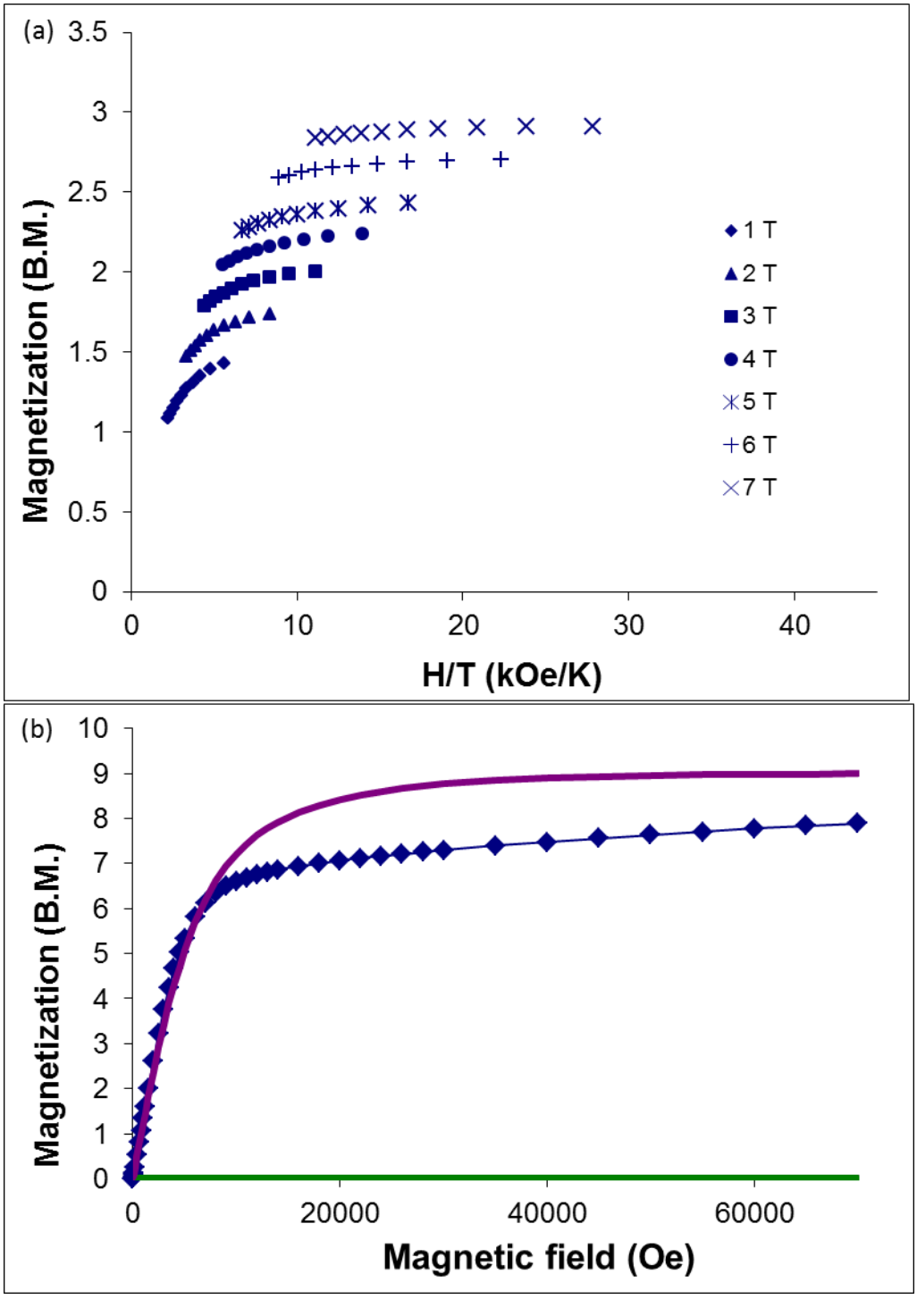

Figure 2.30 (a) Reduced magnetization data for compound **2** at applied external fields from 1 – 7 T Adapted from reference 190. (b) Field dependent magnetization for **2**. The solid line corresponds to the Brillouin function for S = 9/2, g_{avg} = 2.0.

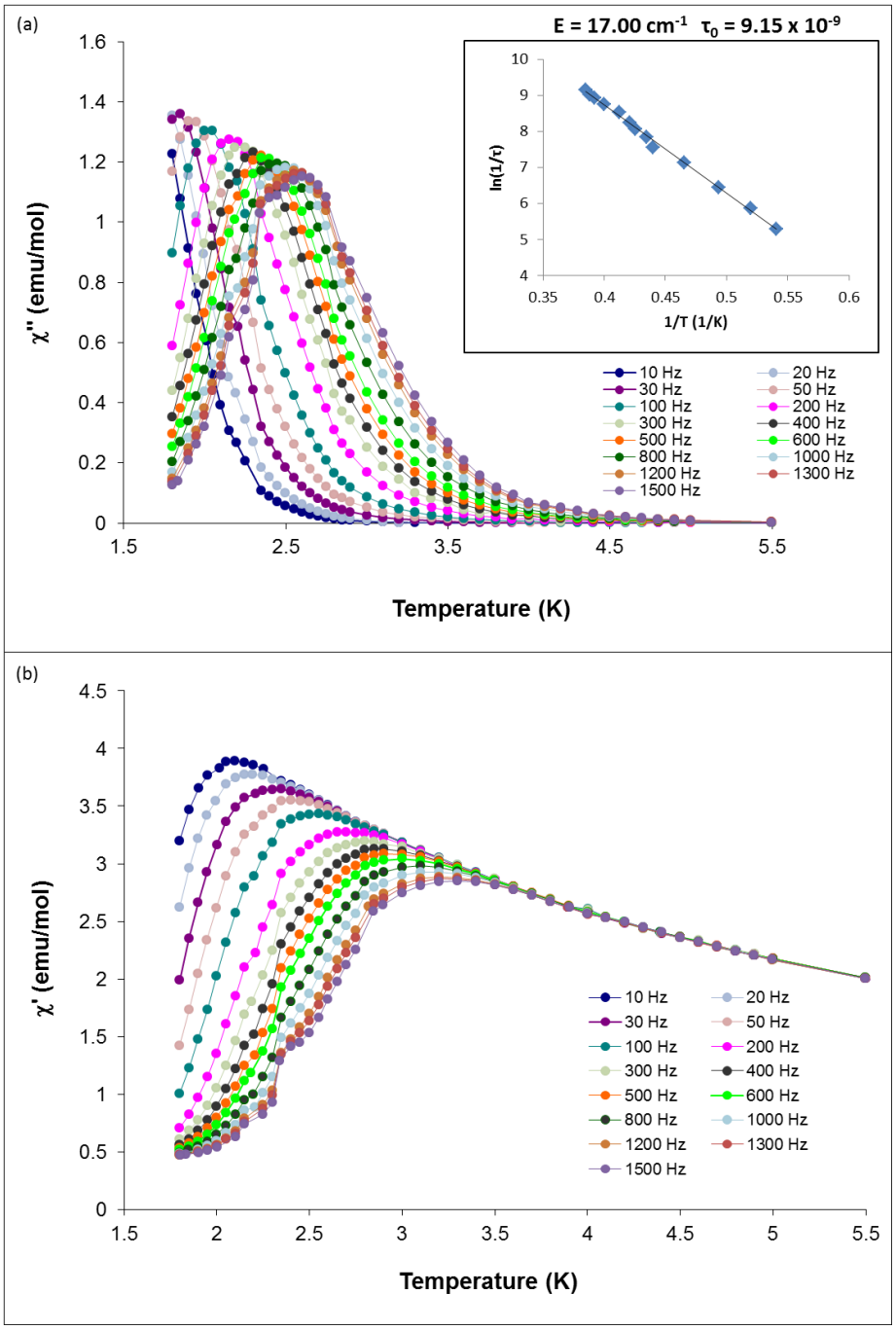

Figure 2.31 (a) Temperature dependence of the out-of-phase (χ") part of the ac susceptibility for **2** measured under various oscillating frequencies (10 – 1500 Hz). The solid lines are a guide for the eyes. Inset: dependence of the logarithm of the relaxation rate (1/τ) on the inverse temperature (1/T). The solid line is a best linear fit to the Arrhenius law (U_{eff} = 17.00, τ_0 = 9.15 x 10^{-9} s). (b) Temperature dependence of the in-phase (χ') ac susceptibility signals for compound **2**.

of solvation of the material, in this case, can provide a means of control for turning the interchain exchange interactions and the exchange bias behavior "on" and "off".

PPN{[Mn(salphen)(MeOH)]$_2$[Fe(CN)$_6$]} (2). The dc measurements of the Mn_2Fe trinuclear molecule were measured previously by Carolina Avendaño and reported in her thesis, but she measured the compound without regard to the solvation status of the crystals.[190] The Mn_2Fe compound was remeasured in this work with careful handling of the solvated and desolvated samples. Crystals of **2** were dried *in vacuo* for three hours prior to magnetic measurements to ensure complete removal of interstitial solvent. The magnetic properties of polycrystalline samples of **2** behave similarly to compound **1**. The temperature-dependent magnetic susceptibility data give a room temperature χT value of 6.51 emu·K·mol^{-1} which is consistent with two isolated high spin S = 2 Mn^{III} ions and one isolated S = ½ Fe^{III} ion (6.35 emu·K·mol^{-1}, Figure 2.29). The χT value increases as temperature is decreased to a maximum at ~8K and is indicative of ferromagnetic coupling between the Mn^{III} and Fe^{III} ions, giving an S = 9/2 ground state. The drop in χT at low temperatures can be attributed to zero field splitting or intermolecular interactions. The field dependence of the magnetization data between 2 and 20 K show non-superposition of the isofield lines which indicates the existence of zero-field splitting (Figure 2.30a). As in the case of compound **1**, even at 2 K, the magnetization data do not saturate indicating the population of low lying excited states (Figure 2.30b). Simulation of the susceptibility data using Eq. 1 and the program MAGPACK[207] resulted in best fit parameters of J = 4.7 cm-1, zJ′ = -0.10 cm-1, g_{Mn} = 2.0, g_{Fe} = 2.0, and D = -0.3 cm^{-1}.

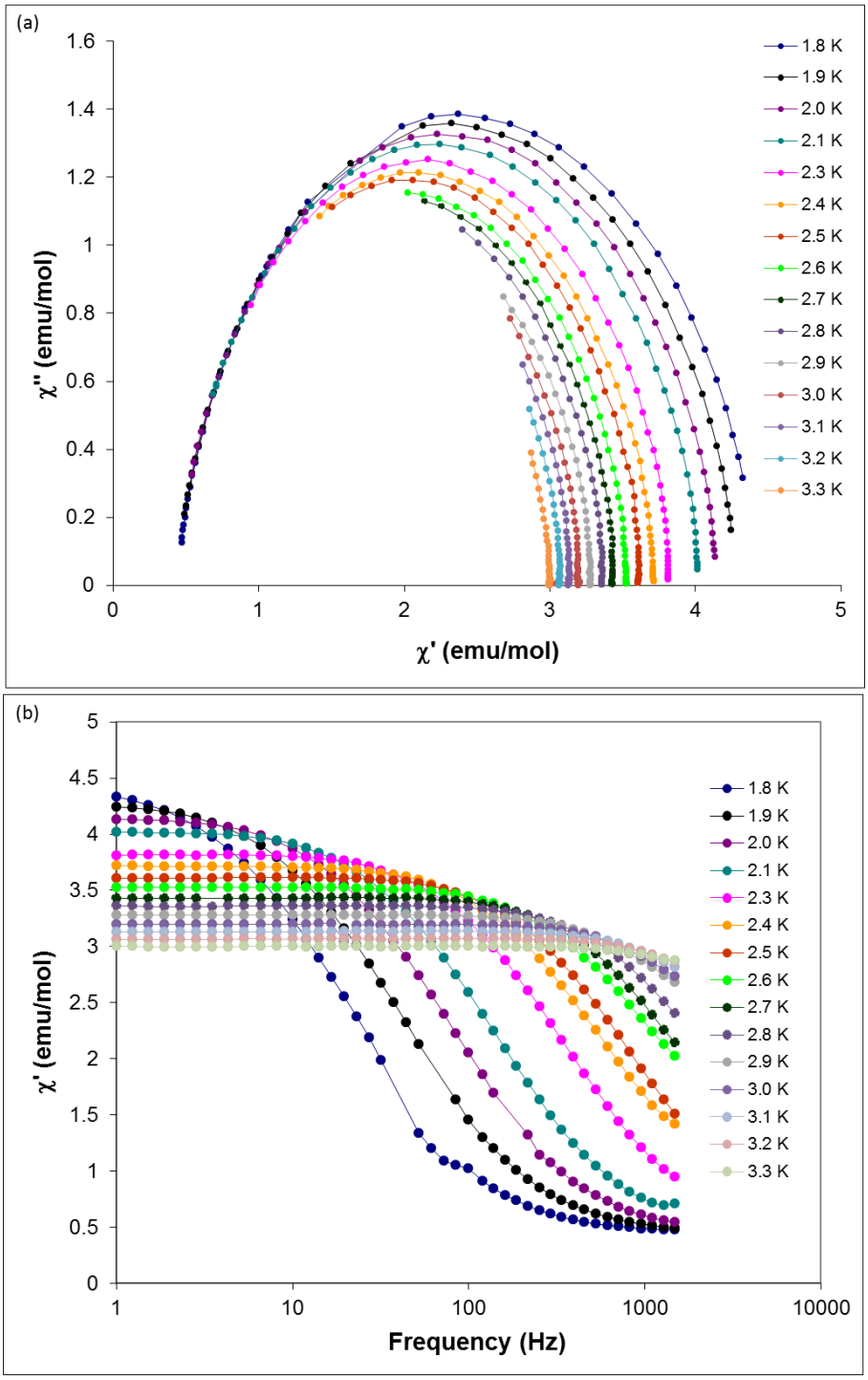

Figure 2.32 (a) Cole-Cole plot for **2** at various temperatures (1.8 - 3.3 K). The solid lines are a guide for the eye. (b) Frequency dependence of the in-phase signals (χ') for compound **2** measured at various temperatures 1.8 – 3.3 K). The solid lines are a guide for the eye.

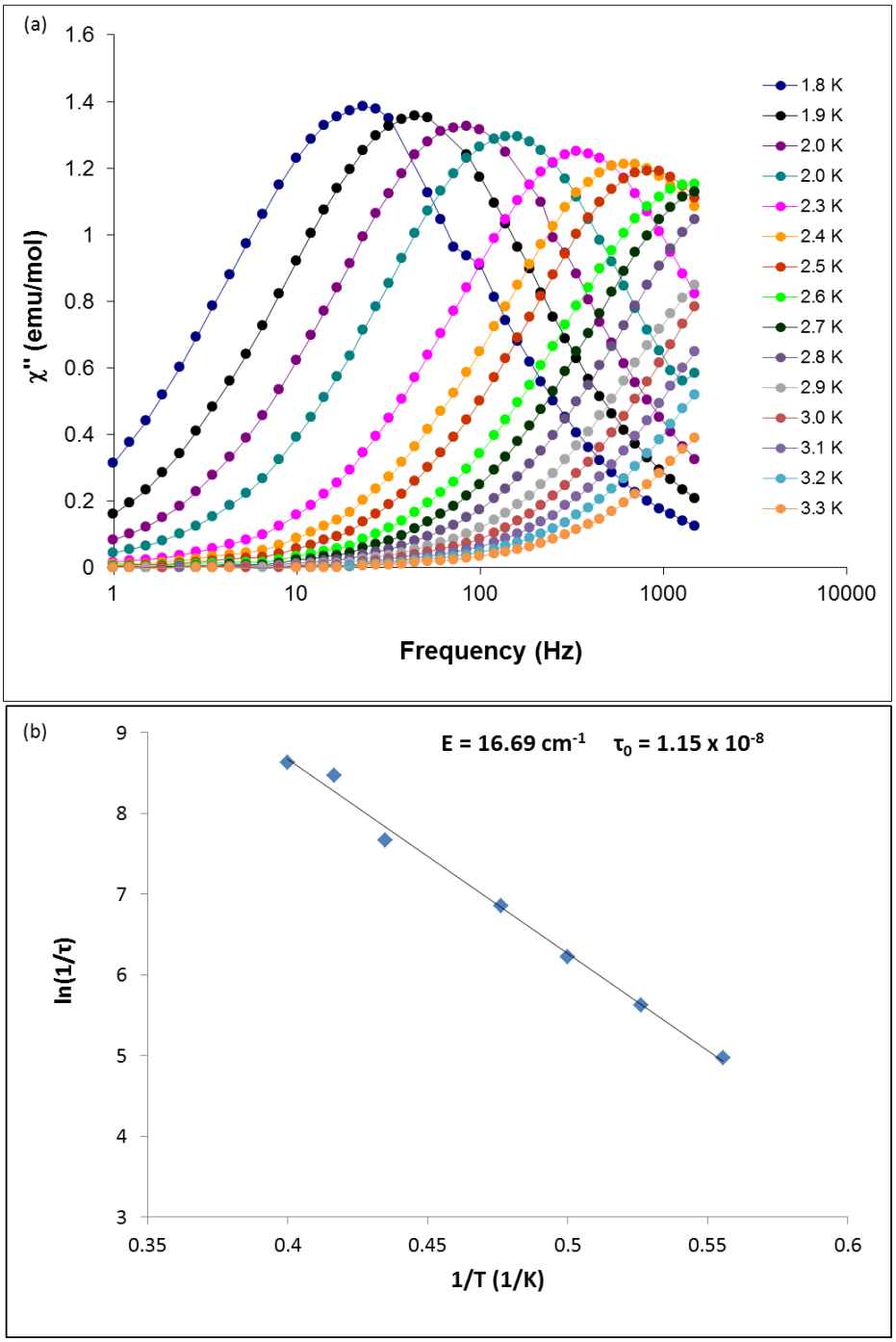

Figure 2.33 (a) Frequency dependence of the imaginary (χ") part of the ac susceptibility for **2** measured at various temperatures (1.8 – 3.3 K). (b) Dependence of the logarithm of the relaxation rate (1/τ) on the inverse temperature (1/T). The solid line is a best linear fit to the Arrhenius law (U_{eff} = 16.69 cm^{-1}, τ_0 = 1.15 x 10^{-8} s).

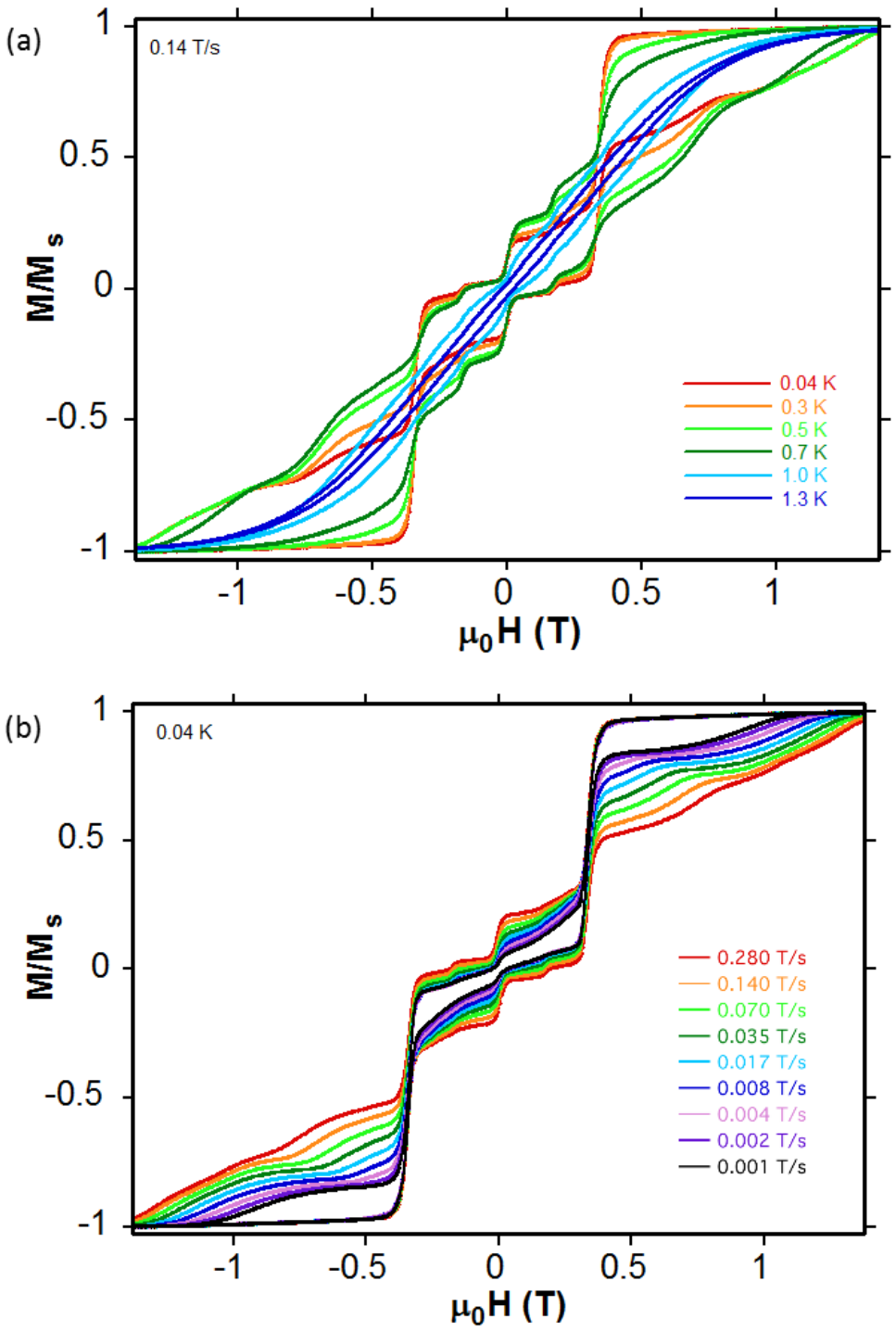

Figure 2.34 Magnetization (M) vs dc field (H) hysteresis loops for single crystals of **2** along the b-axis (a) below 1.3 K with a sweep field rate of 0.14 T/s and (b) below a sweep rate of 0.280 T/s at 0.04 K.

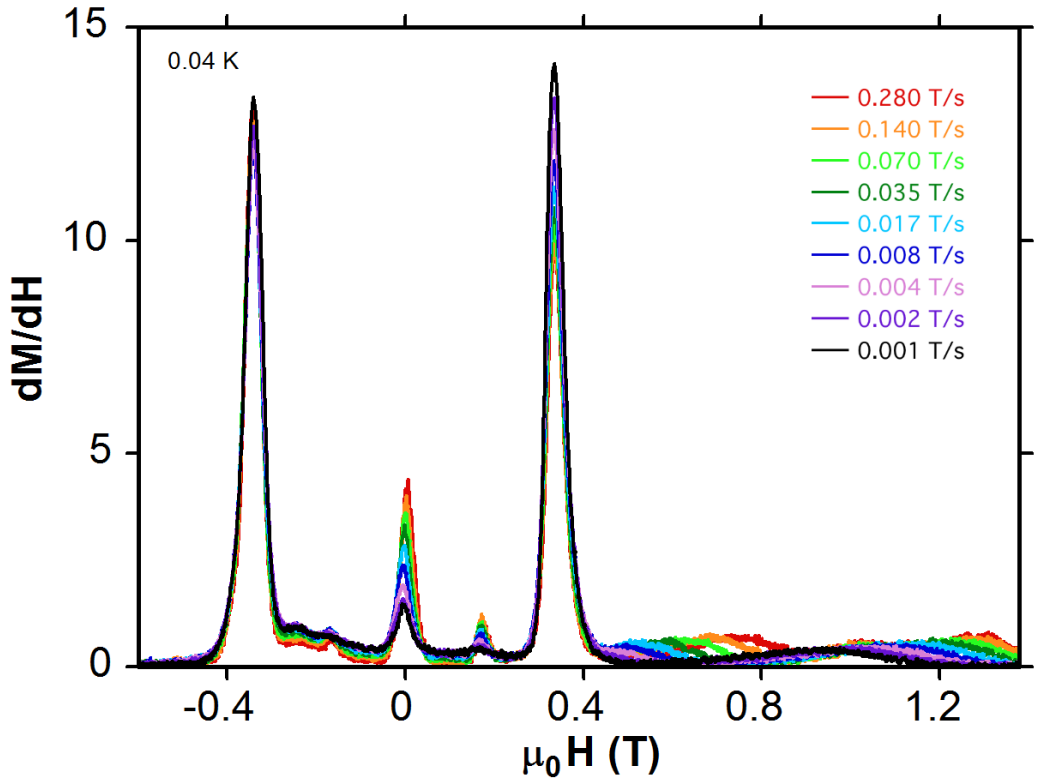

Figure 2.35 The derivative of the magnetization versus magnetic field (dM/dH) measured at 0.04 K below a sweep rate of 0.280 T/s for a single crystal of **2**.

The ac magnetic susceptibility data in zero applied DC field exhibit slow relaxation of the magnetization (Figure 2.31). The in-phase, χ', and out-of-phase signals, χ_M", for frequencies from 1 - 1500 Hz plotted vs. temperature, are both strongly frequency dependent below 3.5 K (Figure 2.31). The χ_M" data for **2** indicates a blocking temperature, T_B, of 2.6 K at 1.5 kHz. The relaxation times follow an Arrhenius relationship: $\tau = \tau_o \exp(U_{eff}/k_BT)$. A plot of $\ln(1/\tau)$ vs. 1/T is linear (Figure 2.31a, inset) with a least-squares fit resulting in the values $\tau_o = 9.15 \times 10^{-9}$ s and $U_{eff} = 17.0$ cm^{-1} s. The shape of the Cole-Cole plot is nearly symmetrical (Figure 2.32a) indicating that a single relaxation time, τ, can be considered. In addition to the χ' vs. T and χ" vs. T data, the in-phase, χ', and out-of-phase, χ", signals vs. frequency were measured (Figure 2.32b and 2.33a). The relaxation times of the χ" vs. ν data follow the Arrhenius relationship stated above and a plot of $\ln(1/\tau)$ vs. 1/T (Figure 2.33b) is linear with a least-squares fit giving the values $U_{eff} = 16.69$ cm^{-1} with $\tau_0 = 1.15 \times 10^{-8}$ s.

Hysteresis loops were collected on single crystals of **2** using a micro-SQUID. Temperature dependent scans reveal hysteretic behavior for **2** at low temperatures, with strongly temperature and sweep rate dependent coercivities. Compound **2** exhibits hysteresis loops for single crystals at mK temperatures (Figure 2.34), where the first step observed at 40 mK occurs at -0.4 T as a result of antiferromagnetic interactions between neighboring Mn_2Fe SMM anions. Below 1.0 K the hysteresis loops become temperature independent while remaining sweep-rate dependent even at 40 mK (Figure 2.34) indicating that quantum tunneling of the magnetization is still occurring. A derivative plot of the magnetization versus magnetic field (dM/dH) is shown in (Figure 2.35) and

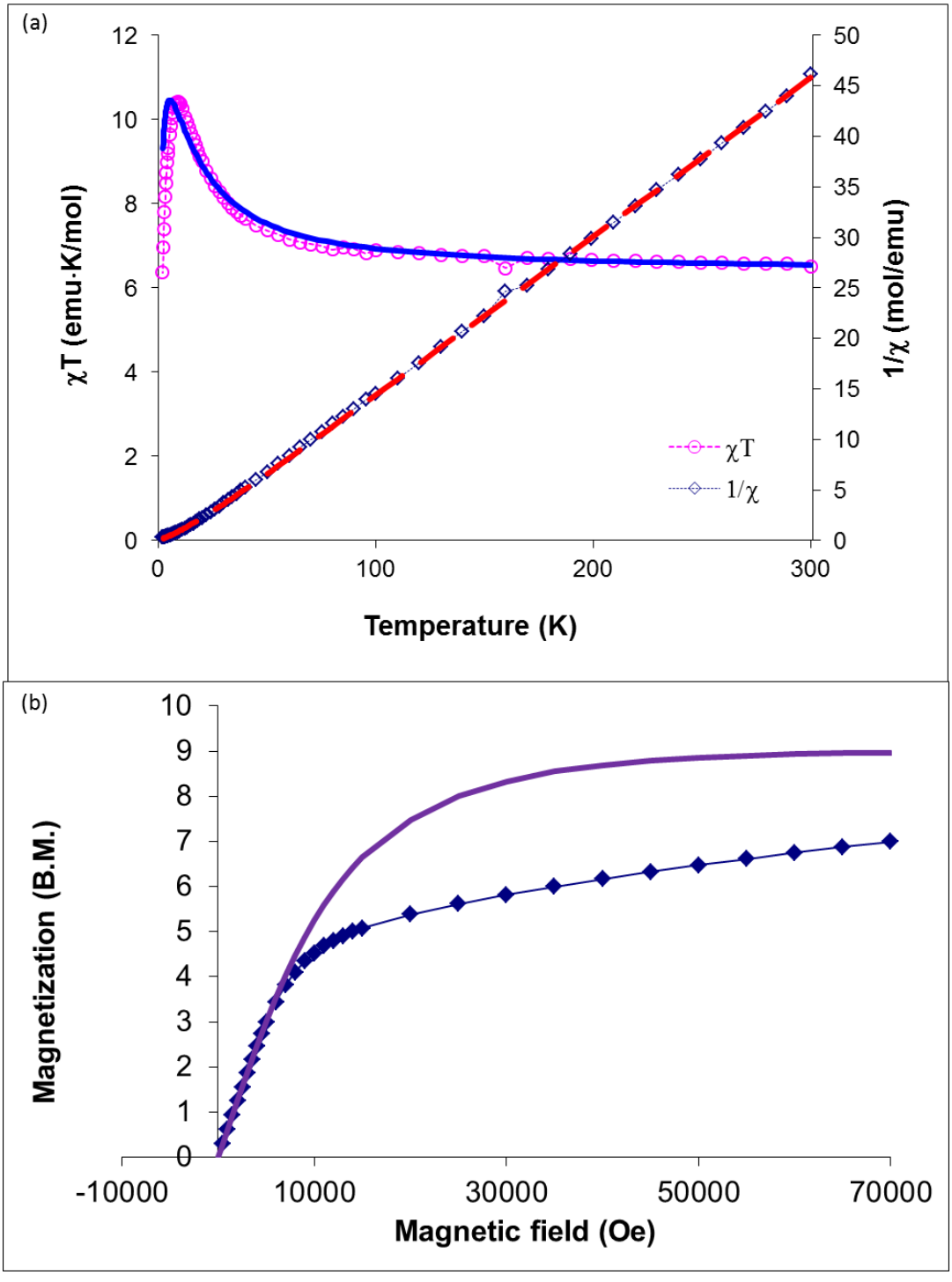

Figure 2.36 (a) Temperature dependence of χT and 1/χ for compound **2**·4MeOH. The solid line corresponds to the MAGPACK[207] simulation (g_{Fe} = 2.0, g_{Mn} = 2.0, J = 6.1 cm^{-1}, zJ' = -0.05 cm^{-1}, D = -0.3 cm^{-1}). (b) Field dependent magnetization for **2**·4MeOH. The solid line corresponds to the Brillouin function for S = 9/2, g_{avg} = 2.0.

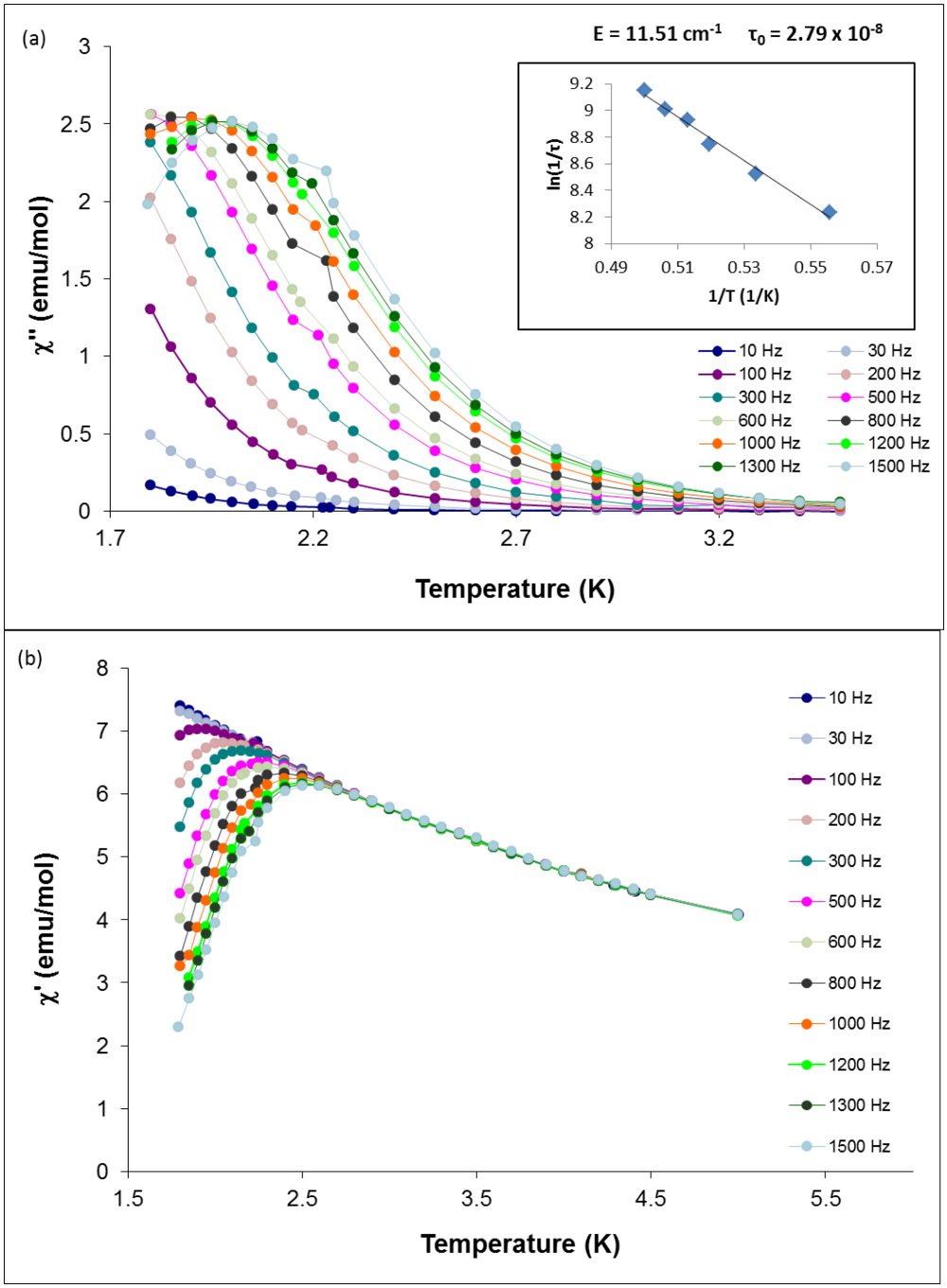

Figure 2.37 (a) Temperature dependence of the out-of-phase (χ") part of the ac susceptibility for **2**·4MeOH measured under various oscillating frequencies (10 – 1500 Hz). The solid lines are a guide for the eye. Inset: dependence of the logarithm of the relaxation rate (1/τ) on the inverse temperature (1/T). The solid line is a best linear fit to the Arrhenius law (U_{eff} = 11.51, τ_0 = 2.79 x 10^{-8} s). (b) Temperature dependence of the in-phase (χ') ac susceptibility signals for compound **2**·4MeOH.

illustrates the shift of the QTM from zero field indicating the exchange bias interactions occurring in compound **2**.

The combined AC, DC and micro-SQUID measurements gathered at low temperatures on **2** indicates that it exhibits exchange bias SMM behavior induced by a spin ground state of S = 9/2 and uniaxial anisotropy, D = -0.3 cm^{-1} and a weak intermolecular interaction, zJ' = -0.10 cm^{-1}.

PPN{[Mn(salphen)(MeOH)]$_2$[Fe(CN)$_6$]}·4MeOH (2·4MeOH**)**. Magnetic measurements of **2**·4MeOH were carried out under the mother liquor. Analogous to compound **2**, the temperature-dependent magnetic susceptibility data for compound **2**·4MeOH are dominated by the signature of ferromagnetic coupling between the high spin S = 2 Mn^{III} and S = ½ Fe^{III} ions (Figure 2.36a). The room temperature χT value of 6.55 emu·K·mol^{-1} is consistent with the value obtained for the dried **2** and the rise of χT as the temperature is lowered is evidence for ferromagnetic coupling and an S = 9/2 ground state. The magnetization curve is also similar to **2** and even at 7 T, the magnetization of **2**·4MeOH is well below the expected saturation level for an S = 9/2 ground state in the absence of zero field splitting (Figure 2.36b). The simulation of the magnetic susceptibility using Eq. 1 and MAGPACK[207] resulted in the best fit parameters of J = 6.1 cm^{-1}, zJ' = 0.05 cm^{-1}, g_{Mn} = 2.0, g_{Fe} = 2.0, and D = -0.3 cm^{-1} (Figure 2.36a). The intermolecular interaction, zJ' = -0.05 cm^{-1}, is significantly lower than the one observed for the desolvated SMM (zJ' = 0.10 cm^{-1}). This is an indicator that interstitial solvent plays a crucial role in the observation in observed intermolecular interactions, namely the presence of exchange bias behavior in the desolvated SMM.

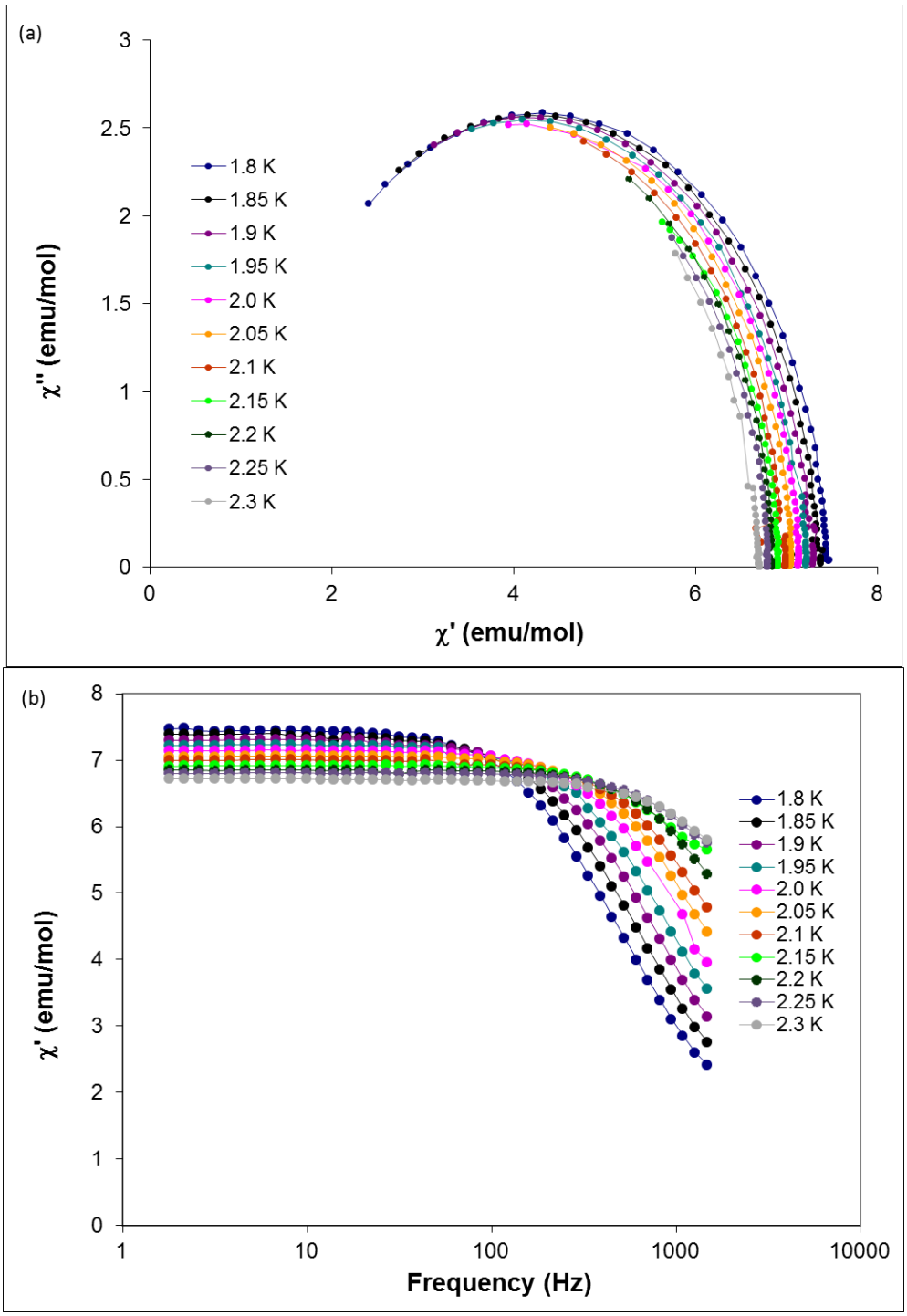

Figure 2.38 (a) Cole-Cole plot for **2**·4MeOH at various temperatures (1.8 - 2.3 K). The solid lines are a guide for the eye. (b) Frequency dependence of the in-phase signals (χ') for compound **2**·4MeOH measured at various temperatures 1.8 – 2.3 K). The solid lines are a guide for the eye.

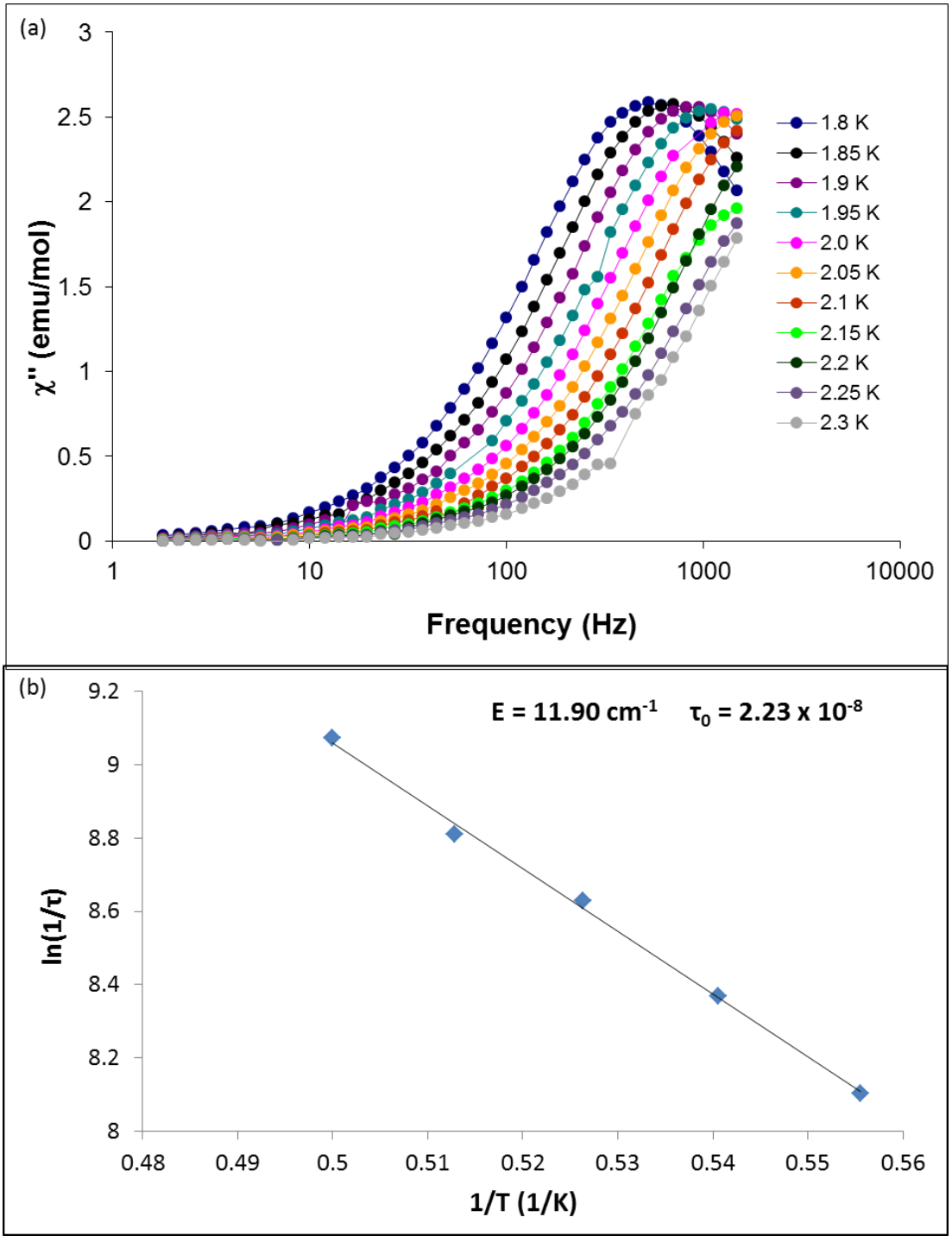

Figure 2.39 (a) Frequency dependence of the imaginary (χ") part of the ac susceptibility for **2**·4MeOH measured at various temperatures (1.8 – 2.3 K). (b) Dependence of the logarithm of the relaxation rate (1/τ) on the inverse temperature (1/T). The solid line is a best linear fit to the Arrhenius law (U_{eff} = 11.90 cm^{-1}, τ_0 = 2.23 x 10^{-8} s).

The magnetization reversal dynamics of compound **2**·4MeOH were probed with the use of ac susceptometry. As in the case for **2**, the ac magnetic susceptibility data under a zero applied DC field for **2**·4MeOH exhibits slow relaxation of the magnetization (Figure 2.37), with both χ' and χ" being strongly frequency dependent below 3.5 K. The χ_M" data for **2**·4MeOH indicates a blocking temperature, T_B, of 2.0 K at 1.5 kHz. In addition, the shape of the Cole-Cole plot is essentially symmetrical (Figure 2.38a) indicating that a single relaxation time, τ, can be considered. The peak temperatures were fit to an Arrhenius relationship: $\tau = \tau_o \exp(U_{eff}/k_BT)$ (Figure 2.37a, inset), leading to an effective barrier height for magnetic reversal of $U_{eff} = 11.51$ cm^{-1} with $\tau_0 = 2.79 \times 10^{-8}$ s. The barrier calculated for **2**·4MeOH is significantly lower than that exhibited for **2** ($U_{eff} = 17.0$ cm^{-1}). The in-phase, χ', and out-of-phase, χ", signals vs. frequency were also measured as shown in (Figure 2.38b, 2.39a). The relaxation times of the χ" vs. ν data follow an Arrhenius relationship and a plot of $\ln(1/\tau)$ vs. 1/T (Figure 2.39b) is linear with a least-squares fit giving the values $U_{eff} = 11.90$ cm^{-1} with $\tau_0 = 2.23 \times 10^{-8}$ s. The U_{eff} barrier is in good agreement with the findings for the related trinuclear SMM K{[Mn(5-Brsalen)(H_2O)]$_2$[Fe(CN)$_6$]} ($U_{eff} = 11.5$ cm^{-1}; 5-Brsalen = N,N′-(ethylene)bis-(5-bromosalicylidene-iminate))[144] and comparable to that reported by Miyasaka *et al.* for (Et_4N){[Mn(salmen)(MeOH)]$_2$[Fe(CN)$_6$]} ($U_{eff} = 10$ cm^{-1}; salmen = N,N′-(1-methylethylene)bis-(salicylideneiminate)).[182]

Although hysteresis loops of the solvated sample of **2**·4MeOH were not able to be collected due to the rapid loss of interstitial solvent from the crystals during sample preparation despite numerous attempts to prevent this occurrence, it is apparent from the

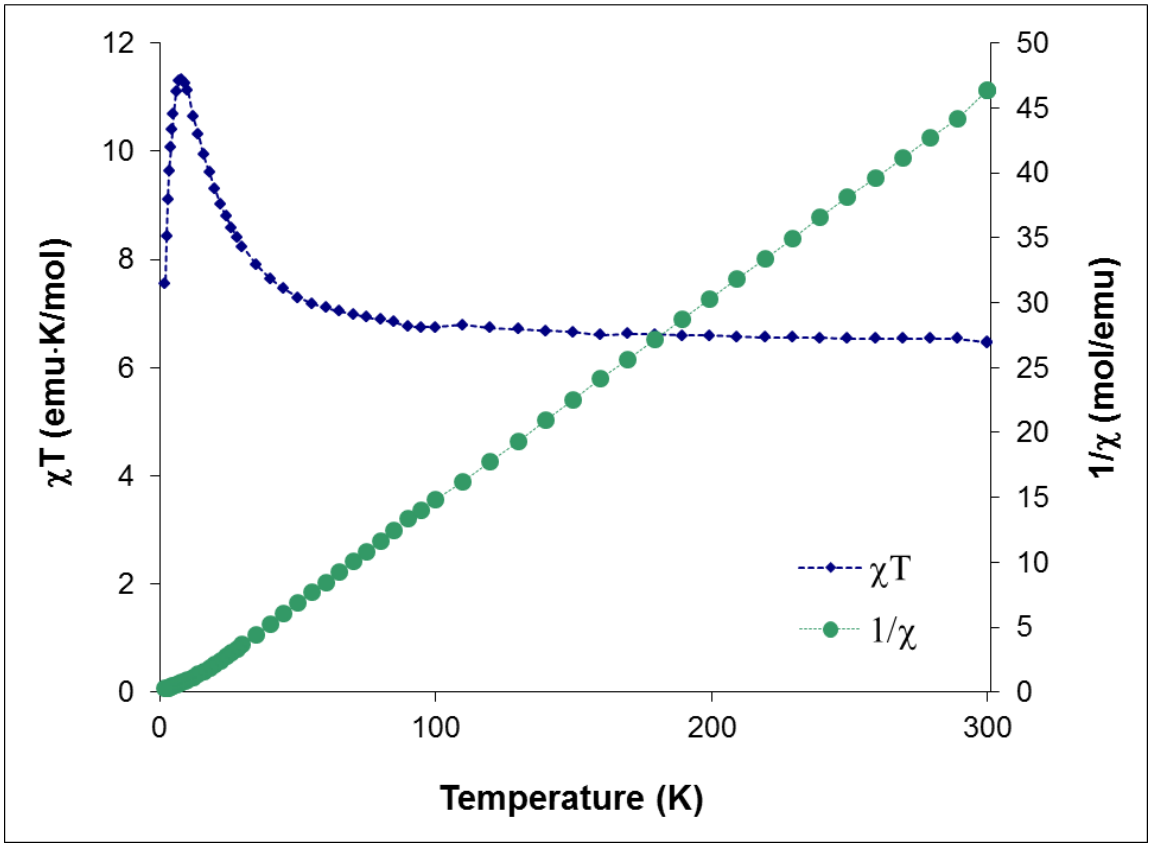

Figure 2.40 Temperature dependence of χT and $1/\chi$ for a "resolvated" sample of compound **2**. Solid lines are a guide for the eye.

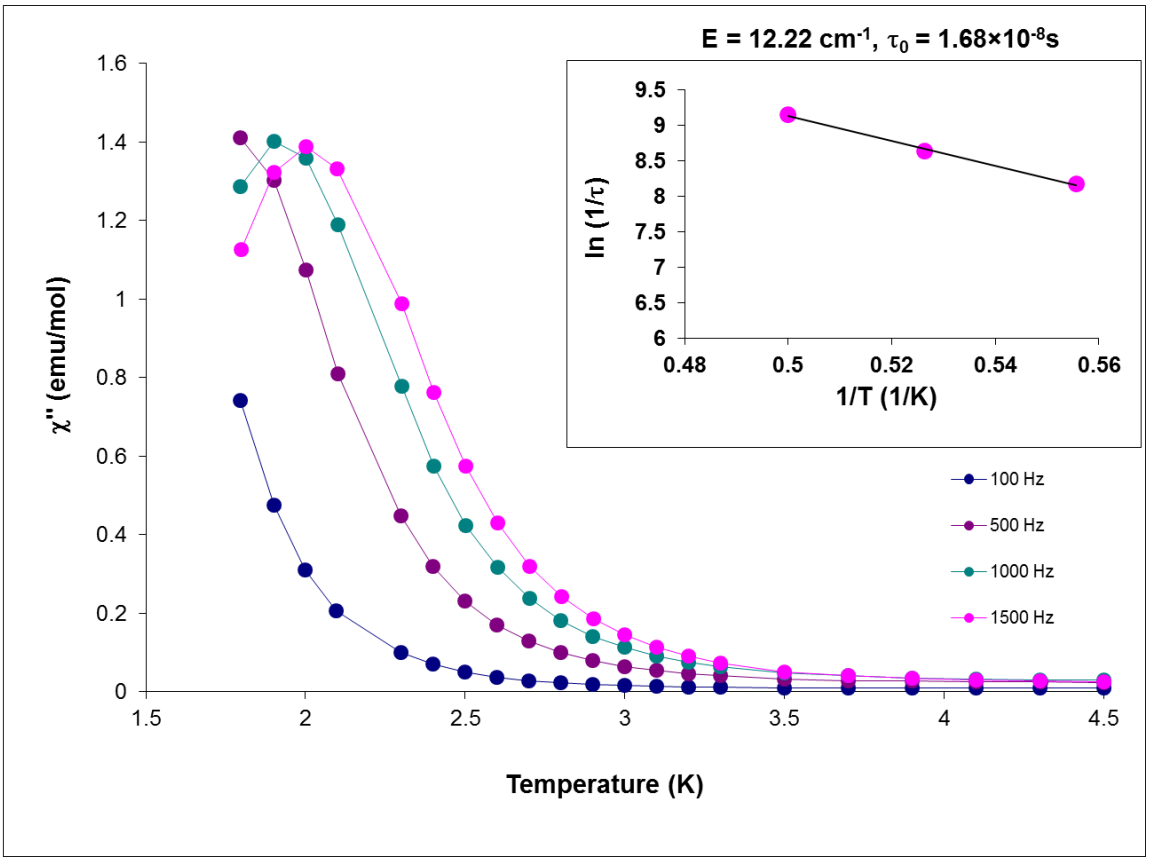

Figure 2.41 (a) Temperature dependence of the out-of-phase (χ") part of the ac susceptibility for a "resolvated" sample of **2** measured under various oscillating frequencies (100 – 1500 Hz). The solid lines are a guide for the eyes. Inset: dependence of the logarithm of the relaxation rate (1/τ) on the inverse temperature (1/T). The solid line is a best linear fit to the Arrhenius law (U_{eff} = 12.22 cm^{-1}, τ_0 = 1.68 x 10^{-8} s).

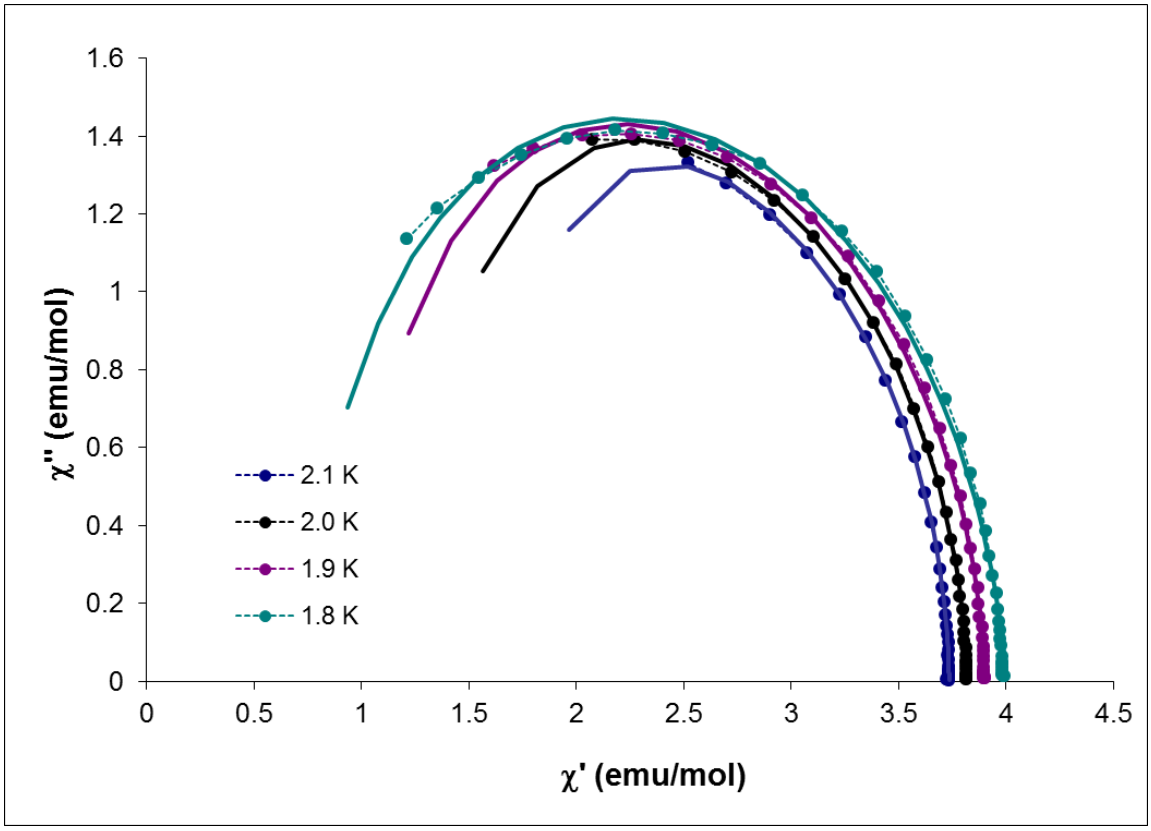

Figure 2.42 Cole-Cole plot for a "resolvated" sample of compound **2** at various temperatures (1.8 – 2.1 K). The solid lines are an extrapolation fit.

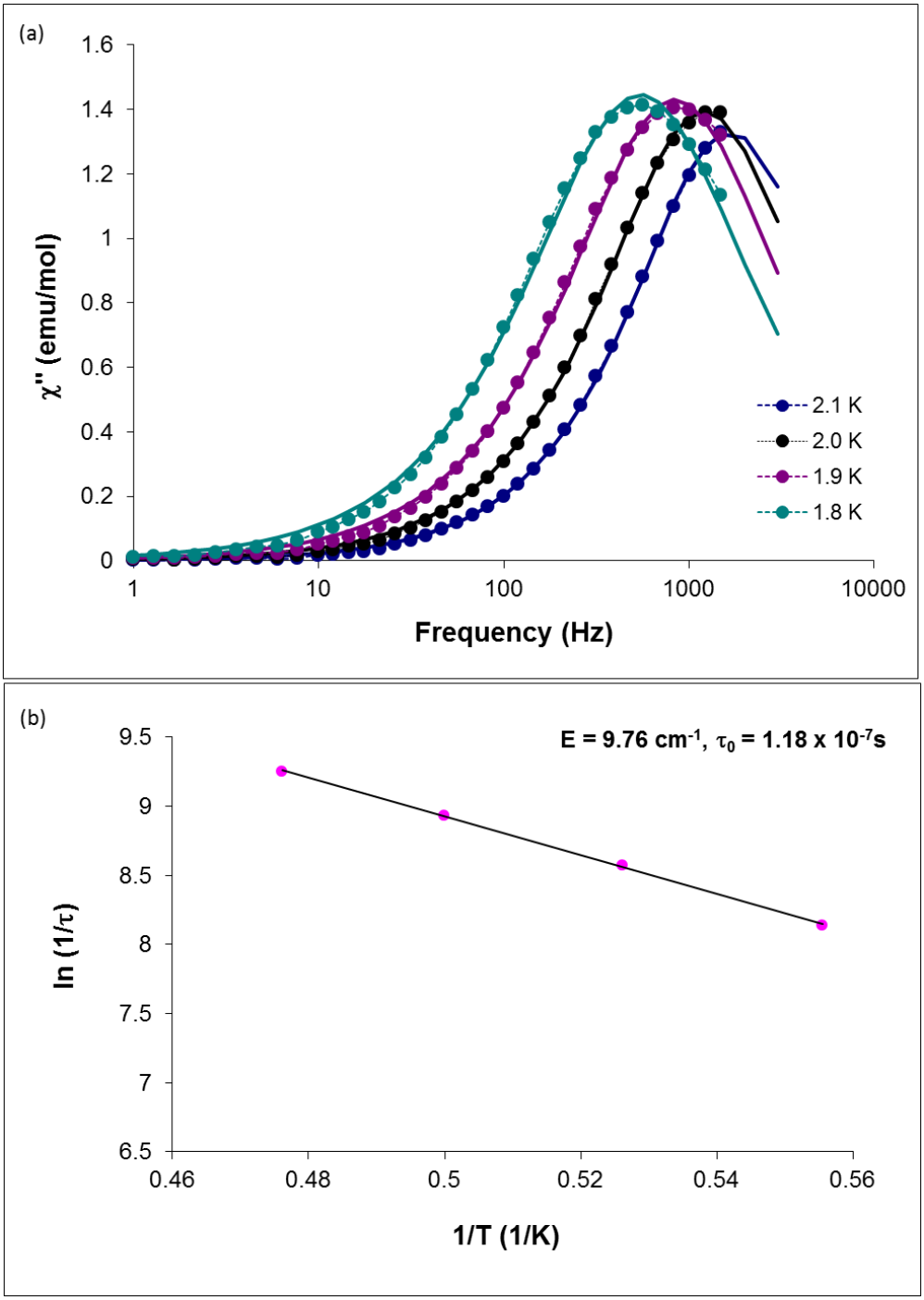

Figure 2.43 (a) Frequency dependence of the imaginary (χ") part of the ac susceptibility for a "resolvated" sample of **2** measured at various temperatures (1.8 – 2.1 K). (b) Dependence of the logarithm of the relaxation rate (1/τ) on the inverse temperature (1/T). The solid line is a best linear fit to the Arrhenius law (U_{eff} = 9.76 cm^{-1}, τ_0 = 1.18 x 10^{-7} s).

ac susceptibility measurements of the solvated and desolvated forms, that **2** exists in both an exchange bias state and a classical SMM form.

Reversibility of 2 and 2·4MeOH. To ascertain whether the exchange bias behavior for the Fe^{III} congener is reversible, as is the case for the Os^{III} congener, magnetic measurements were performed on a previously dried sample of **2** that was soaked under methanol for several hours and the measurements taken with the sample under solvent. The behavior of the χT plot (Figure 2.40) matches that of the other compounds measured with the value of χT increasing as the temperature is lowered to reach a maximum at ~8K. The ac magnetic susceptibility data under a zero applied DC field exhibits slow relaxation of the magnetization (Figure 2.41) and the χ_M" data indicates a blocking temperature, T_B, of 2 K at 1.5 kHz. The shape of the Cole-Cole plot (Figure 2.42) indicates that a single relaxation time, τ, can be considered and a complete conversion of the dried exchange bias **2** to the SMM **2**·4MeOH has occurred. A plot of $\ln(1/\tau)$ vs. 1/T (Figure 2.41, inset) when fit to an Arrhenius law, gives a least-squares fit with the values $\tau_o = 1.68 \times 10^{-8}$ s and $U_{eff} = 12.2$ cm^{-1}. The out-of-phase signal, χ", vs. frequency was also measured and (Figure 2.41a) the relaxation times plotted (Figure 2.43b) and fit to an Arrhenius relationship with the least-squares fit giving the values $U_{eff} = 9.76$ cm^{-1} with $\tau_0 = 1.18 \times 10^{-7}$ s.

The measurements of compound **2** soaked under solvent reveal that the Fe^{III} compound, as in the case of the Os^{III} congener, exhibits SMM behavior with reversible exchange bias behavior.

Conclusion

Two trinuclear compounds, (PPN){[Mn(salphen)(solv)]$_2$[M(CN)$_6$]} (M = Fe and Os), were prepared and subjected to detailed structural and magnetic measurements. During the course of these studies it was determined that fresh crystals of both compounds exhibit typical SMM properties but that exchange bias behavior of the SMMS is dominant when the crystals are dried which leads to loss of interstitial methanol. These compounds are the first cases for which the exchange bias phenomenon has been noted for cyanide bridged molecules. The ac magnetic data indicate that PPN{[Mn(salphen)(MeOH)]$_2$[M(CN)$_6$]} salts with M = Fe and Os both exhibit slow relaxation of the magnetization but that the blocking temperatures increase for the 5d metal ion analogue owing to the more diffuse orbitals and increased anisotropy. In fact T_B values increase by ~90% for the exchange biased samples of Os versus Fe. The packing diagrams of the compounds reveal that the choice of the salphen ligand and the PPN^+ cation results in hydrogen-bonding interactions between outer-sphere and coordinated methanol molecules and the salphen phenyl rings of the trinuclear SMM anions. The phenyl rings also participate in intermolecular π-π stacking interactions. While this π-π interaction combined with the hydrogen bonding interactions with interstitial methanol was initially proposed by Carolina Avendaño as the mechanism by which the exchange bias behavior is mediated,[190] the systematic study of these molecules presented here demonstrates unambiguously that the exchange bias SMM behavior in these molecules can be controlled by the extent of solvation of the compounds and was even demonstrated to be reversible. This pseudo 1D network of exchange coupled

SMMs further underscores the recently established fact that QTM in SMMS can be controlled with weak exchange interactions and opens up new horizons for the implementation of specific ancillary groups to regulate the quantum properties of molecular nanomagnets. More importantly, this study promotes the fact that the behavior of SMMs can be manipulated by fine-tuning the ligand properties vis-à-vis their ability to direct self-association of individual molecules, an important issue for the future use of SMMs in devices.

CHAPTER III

TRIGONAL BIPYRAMIDAL MOLECULES INCORPORATING HEXACYANOMOLYBDATE(III)

Introduction

In contrast to the magnetic coupling between two 3d transition metals which has been studied extensively, the coupling between 3d metal-based spins with those of 4d or 5d metal spins has been far less explored. The second and third row transition metal ions exhibit much higher anisotropy than their 3d counterparts owing to strong spin-orbit coupling effects and their more diffuse orbitals leads to increased overlap and, in principle, stronger interactions. Other attractive features are their ability to exist in multiple oxidation states with different coordination numbers[25,209] which leads to a diversity of geometries. Importantly, SMMs of the heavier congeners of Groups 6, 7 and 8 based on precursors such as $[(Me_3tacn)Mo^{III}(CN)_3]$,[210] $[Mo^{V}(CN)_8]^{3-}$,[114-116] $[W^{V}(CN)_8]^{3-}$,[114-116] $[Re^{IV}(CN)_7]^{3-}$,[110] $[(triphos)Re^{II}(CN)_3]^{-}$ [118] and $[Os(CN)_6]^{3-}$ [112] have appeared in the recent literature which bodes well for the future of this area.

Of particular interest in the field of molecular magnetism are the cyanomolybdate anions of general formula $[Mo(CN)_m]^{n-}$ (m = 6, n=3; m = 7, n = 4 and m = 8, n = 3). The $[Mo^{V}(CN)_8]^{3-}$,[114,115,33] anion is, by far, the most widely studied member of this class of homoleptic cyanides with a large variety of compounds having being reported. The heptacyanomolybdate derivative, $[Mo^{III}(CN)_7]^{4-}$, has been receiving renewed attention in the literature after years of sparse activity largely because of recent predictions that the

incorporation of this anion could lead to high T_B SMMs due to its large spin-orbit coupling parameter (800 cm^{-1})[33] and strong anisotropic exchange interactions.[100,211] Research in the chemistry of $[Mo^{III}(CN)_7]^{4-}$ in the 1990's by the Kahn group led to fascinating results including a number of 3D magnets with Mn^{II} ions,[130] but low dimensional compounds incorporating this anion remained unknown until recent years.[139] Among the reports of 2-D and 3-D magnets incorporating $[Mo^{III}(CN)_7]^{4-}$ is a recent discovery by our group of two 3-D phases that undergo a crystal-to-crystal transformation exhibiting extreme changes in the magnetic ordering properties.[133,134,137] The first molecular compound containing the $[Mo^{III}(CN)_7]^{4-}$ anion was also reported by the Dunbar group and was found to be a large spin molecule (S = 31) with strong intermolecular dipole interactions that suppress SMM behavior.[139]

Even fewer studies have focused on the chemistry of the related octahedral $[Mo^{III}(CN)_6]^{3-}$ species and, in fact, it was not until 2002 that the synthesis and characterization of this anion was reported by Beauvais and Long.[140] Extraordinarily strong magnetic interactions between $[Mo(CN)_6]^{3-}$ and the early 3d metal centers V^{II} and Cr^{II} have been predicted by theoretical calculations.[126] In fact it has been predicted that Prussian Blue phases based on Mo^{III}-CN-V^{II} and Mo^{III}-CN-Cr^{II} combinations should exhibit critical temperatures higher than the $Cr^{III}V^{II}$ derivatives $(V^{II}_{0.42}V^{III}_{0.58}[Cr^{III}(CN)_6]_{0.86}\cdot 2.8H_2O$, T_C = 315 K and $K_{0.058}V^{II/III}[Cr^{III}(CN)_6]_{0.79}\cdot(SO_4)_{0.058}\cdot 0.93\ H_2O$, T_c = 372 K),[41,42] namely 552 K for $Mo^{III}V^{II}$ and 308 K for $Mo^{III}Cr^{II}$. Unfortunately, the $[Mo^{III}(CN)_6]^{3-}$ anion is extremely unstable being sensitive to both oxygen and light. Presumably because of these

complications it was not until 2009 that the first magnetic molecule containing the $[Mo^{III}(CN)_6]^{3-}$ species was reported. The compound has a V_4Mo core and the reported coupling between the V^{II} and Mo^{III} spins of J = -61 cm^{-1} is the strongest antiferromagnetic coupling reported to date through a cyanide bridge.[110] While this is extremely strong coupling for a cyanide compound, the interaction is not nearly as high as the interaction predicted by theoretical calculations of model dimers made by Ruiz and Alvarez.[126] It remains to be seen whether those predictions will be borne out by experimental findings.

Previously our group reported two new members of the TBP family based on $[Mo(CN)_6]^{3-}$.[212] The products were isolated from reactions involving the $[Mo(CN)_7]^{4-}$ precursor which undergoes a loss of a cyanide ligand. The compounds are $[M(tmphen)_2]_3[Mo(CN)_6]_2$ (solvent) (M^{II} = Co, Ni) which were fully characterized by X-ray crystallography and magnetic studies constitute rare examples of molecular compounds containing $[Mo(CN)_6]^{3-}$.[212] Both of the reported TBPs exhibit ferromagnetic coupling between the Mo^{III} ions and the Co^{II}/Ni^{II} ions. In this work, three new members of the TBP family are reported in which the octahedral anion $[Mo(CN)_6]^{3-}$ is combined with the divalent 3d metal ions V^{II}, Mn^{II} and Fe^{II}.

Syntheses

Starting materials. Commercially available 18-crown-6 (Aldrich), tmphen (Aldrich), $MoCl_5$ (Aldrich), VCl_3, $Mn(CH_3COO)_2$ (Fisher Scientific) $NaBPh_4$ and Sn powder were used as received. Acetonitrile (ACS reagent grade, EMD Chemicals) was dried over 3 Å molecular sieves and distilled before use. Methanol (ACS reagent grade, EMD

Chemicals) was dried over 4 Å molecular sieves and distilled before use. Dichloromethane (ACS reagent grade, EMD Chemicals) was dried over phosphorous pentoxide and distilled before use. Distilled water and ethanol (200 proof, Koptec) were deoxygenated by boiling for at least three hours while bubbling N_2 through the solvent.

$[V(CH_3CN)_6][BPh_4]_2$. This salt was synthesized using a modification of a previously published procedure.[213,214] The reaction was carried out under dry N_2 using Schlenk techniques. A quantity of VCl_3 (3 g, 19.2 mmol) was stirred in 200 mL of dry acetonitrile at 75° C for three days. To the cooled green solution, a solution of $NaBPh_4$ (19.8 g, 57.8 mmol) in 40 mL acetonitrile was added *via* cannula. A white precipitate was formed to form instantaneously. The slurry was stirred for 3 hours and the solvent was removed under reduced pressure to obtain a green precipitate which was transferred to a Soxhlet thimble and extracted for three days to obtain a bright green solution. Upon cooling, white flocculent precipitate and small green platelet crystals formed in the green solution. A 25 mL aliquot of acetonitrile was added and the solution was heated to 85° C to dissolve all of the white precipitate and green crystals. The solution was filtered while hot. Green platelet crystals formed in solution upon cooling; the solution was chilled to 10° C to induce further crystallization. The green crystals were collected *via* suction filtration and washed with diethyl ether (3 x 10 mL) and stored under dry N_2. (Yield 8.454 g, 47 %)

$K_4[Mo(CN)_7]$ was synthesized following a modification of a previously published procedure.[129] First, $MoCl_5$ is used to synthesize $MoCl_4(CH_3CN)_2$ followed by conversion to $MoCl_4(THF)_2$. The $MoCl_4(THF)_2$ is then reduced using tin metal to

$MoCl_3(THF)_3$ followed by coordination of cyanide ligands to form $K_4[Mo(CN)_7]$. Specific synthesis details follow.

$MoCl_4(CH_3CN)_2$. The reaction carried out under dry N_2 with dry acetonitrile (50 mL) being added slowly over 30 minutes to $MoCl_5$ (10 g). The resulting suspension was stirred overnight at room temperature. The suspension was filtered to collect an orange/brown solid which was washed with two portions of CH_3CN (5 mL) and dried *in vacuo*. (Yield 9.1 g, 77 %)

$MoCl_4(THF)_2$. Reaction carried out under dry N_2 using Schlenk techniques. Dry THF (40 mL) was added to $MoCl_4(CH_3CN)_2$ (10 g) and the suspension was stirred rapidly for 2 hours. The suspension was filtered to collect the yellow precipitate. The precipitate was washed with THF (3 x 5 mL) and dried under vacuum for one hour. (Yield 8.2 g, 67 %)

$MoCl_3(THF)_3$. The reaction carried out under dry N_2 using Schlenk techniques. A suspension of $MoCl_4(THF)_2$ (5.0 g) and coarse Sn powder (30 mesh, 10 g) in THF (60 mL) was stirred at room temperature for one hour. The resulting purple/red solution was filtered through a fritted Schlenk funnel to remove an undissolved brown solid and the unreacted tin powder. The brown solid was dissolved in dry CH_2Cl_2 and filtered. The filtrate from both filtrations were combined and reduced in volume under reduced pressure to 30 mL. Orange crystals formed in solution which were collected via suction filtration and dried under vacuum for one hour. (yield 3.8 g, 69 %)

$K_4Mo(CN)_7 \cdot 2H_2O$. The reaction was carried out under dry N_2 using Schlenk techniques. To a Schlenk flask containing KCN (12 g) and $MoCl_3(THF)_3$ was added 70 mL of

deoxygenated water. The solution was stirred at 45-50° C for 18 hours. The small amount of undissolved $MoCl_3(THF)_3$ was removed by filtration. Ethanol (30 mL) was added to the dark red solution. The solution was cooled in an ice water bath. Olive green crystals formed over 1-2 hours. The solution was decanted *via* cannula and the crystals washed with 80% ethanol (20 mL x 2) followed by 95% ethanol (20 mL x 2) and 100% ethanol (10 mL x 2) before being dried under vacuum for 10 hours. (yield 4.8 g, 71%)

$[Fe(tmphen)_2]_3[Mo(CN)_6]_2\cdot(MeCN)\cdot(MeOH)_8\cdot(H_2O)_2$ (**3**). The compounds $FeCl_2$ (39.8 mg, 0.2 mmol) and tmphen (106 mg, 0.45 mmol) were dissolved in 10 mL of methanol/acetonitrile (1: 3). A solution of $(18\text{-crown-6-K})_4[Mo(CN)_7]$ was prepared by stirring 18-crown-6 (1.08 g, 1.0 mmol) and $K_4[Mo(CN)_7]$ (470 mg, 1.0 mmol) in 10 mL of methanol. The above solutions were combined *via* slow diffusion in a thin tube with a buffer of MeOH:CH_3CN (1: 3). Red needle-like crystals were harvested in about two weeks.

$[Mn(tmphen)_2]_3[Mo(CN)_6]_2\cdot(MeCN)_2\cdot(MeOH)_7\cdot(H_2O)_4$ (**4**). The compounds $Mn(CH_3COO)_2$ (50 mg, 0.2 mmol) and tmphen (106 mg, 0.45 mmol) were dissolved in 8 mL of methanol/acetonitrile (1: 3). A solution of $(18\text{-crown-6-K})_4[Mo(CN)_7]$ was prepared by stirring 18-crown-6 (1.08 g, 1.0 mmol) and $K_4[Mo(CN)_7]$ (470 mg, 1.0 mmol) in 10 mL of methanol. The methanol solution of $(18\text{-Crown-6-K})_4Mo(CN)_7$ was slowly diffused into the solution of solution of $Mn(tmphen)_2$ in a thin tube with a methanol/acetonitrile (v:v = 1: 3) as a buffer. Green needle-like crystals were collected in approximately two weeks.

$[V(tmphen)_2]_3[Mo(CN)_6]_2(CH_3CN)_2(MeOH)_{12}$ (**5**). The starting materials $[V(CH_3CN)_6][BPh_4]_2$ (186 mg, 0.2 mmol) and tmphen (106 mg, 0.4 mmol) were dissolved in 8 mL of MeOH:CH_3CN (1:3) to form a dark blue solution. A solution of $(18\text{-crown-6-K})_4[Mo(CN)_7]$ was prepared by stirring 18-crown-6 (1.08 g, 1.0 mmol) and $K_4[Mo(CN)_7]$ (470 mg, 1.0 mmol) in 10 mL of methanol. Single crystals of 1 were synthesized by slow diffusion of the above solutions in a thin tube with a 1:3 MeOH:CH_3CN buffer solution. Dark blue rhombic-shapeed crystals formed over the course of several weeks. Yield = 58.6 mg. Elemental analysis: Calculated for $Mo_2V_3C_{124}H_{150}N_{26}O_{12}$: C, 58.60%; H, 5.95%; N, 14.33%; O, 7.55%; Found: C, 58.26%; H, 4.81%; N, 14.63%; O, 6.16%. IR (Nujol), $\nu(C\equiv N)$ cm^{-1}: 2095, 2118).

Single Crystal X-ray Diffraction Studies

Single crystals were measured by suspending the crystal in polybutene oil on a cryoloop under a N_2 cold stream. Single-crystal X-ray data were collected at 110 K using a Bruker APEX diffractometer with a CCD detector. The data sets were measured over four ω-scans of 606 frames with a 0.3° step width followed by integration using the Bruker SAINT[215] software suite and the absorption correction (SADABS).[216] The crystal structures were determined using the SHELX[217] programs with X-SEED[218] as the graphical interface. The structures were solved by direct methods to determine the location of the metal atoms and the majority of the C and N atoms. Alternating cycles of least-squares refinements and difference Fourier maps were used to find the remaining non-hydrogen atoms. Hydrogen atoms were placed at calculated positions. All non-hydrogen atoms were refined using anisotropic thermal parameters. A summary of

information concerning the unit cell parameters, data collection and refinements is provided in Table 3.1. A list of selected metal-ligand bond distances and angles are shown in Table 3.2.

Results and Discussion

Syntheses

Reactions of (18-crown-6-K)$_4$[Mo(CN)$_7$] and $FeCl_2$, $Mn(CH_3COO)_2$ or $[V(CH_3CN)_6][BPh_4]_2$ with 3,4,7,8-tetramethyl-1,10-phenanthroline in a 1:2:4 ratio afforded compounds **1**, **2** and **3**. For the preparation of the TBP clusters, the precursors were prepared *in situ* by stirring one equivalent of the metal salt with two equivalents of tmphen in 1:3 MeOH:CH_3CN. Crystalline forms of these compounds were obtained by layering a solution of the $[M(tmphen)_2]^{2+}$ precursor over a solution of the heptacyanomolybdate ion separated by a buffer solution of 1:3 MeOH:CH_3CN. Larger sample quantities can be synthesized by performing bulk reactions but it should be emphasized that the desired TBP compounds often co-crystallize with crystals of $M(tmphen)_2(CN_2)$ (M = V, Fe, Mn). To obtain pure TBP products the samples were soaked in CH_3CN to dissolve the co-crystallized impurity.

Single Crystal X-Ray Studies

Single crystal X-ray diffraction studies revealed that compounds **3 - 5** are isostructural and crystallize in the monoclinic space group $P2_1/c$. The molecular structures consist of a pentanuclear core composed of cyanide bridged M^{II} and Mo^{III} ions

	Fe_3Mo_2 (**3**)	Mn_3Mo_2 (**4**)	V_3Mo_2 (**5**)
Formula	$Fe_3Mo_2C_{118}H_{135}N_{25}O_{10}$	$Mn_3Mo_2C_{119}H_{138}N_{26}O_{11}$	$V_3Mo_2C_{124}H_{150}N_{26}O_{12}$
Space group	$P2_1/c$	$P2_1/c$	$P2_1/c$
Unit cell	a = 19.550(3) Å	a = 19.5979(10) Å	a = 19.550(3) Å
	b = 25.687(4) Å	b = 26.0756(14) Å	b = 25.687(4) Å
	c = 24.744(4) Å	c = 24.7543(13) Å	c = 24.744(4) Å
	B= 98.171(2)°	B= 98.658(3)°	B= 98.171(2)°
Unit cell volume, V/Å^3	12300(3)	12506(1)	12300(3)
Z	4	4	4
Density (calculated) ρ/g cm^{-1}	1.308 Mg/m^3	1.309 Mg/m^3	1.373 Mg/m^3
Abs. coeff., μ/mm^{-1}	0.609	0.556	0.488
Crystal color and habit	Red needle	Green needle	Blue needle
Crystal size /mm	0.42 x 0.24 x 0.14	0.32 x 0.14 x 0.08	0.32 x 0.22 x 0.10
Temperature /K	110	110	110
Radiation, λ/Å	Mo-K α, 0.71073	Mo-K α, 0.71073	Mo-K α, 0.71073
Min. and max. Θ/°	2.09 to 28.48	1.05 to 25.00	2.09 to 25.00
Reflections collected	132303	127029	112627
	[R_{int} = 0.0957]	[R_{int} = 0.0509]	[R_{int} = 0.1272]
Independent reflections	28497	22029	21644
Data/restraints/ parameters	28497 / 67 / 1438	22029 / 896 / 1455	21644 / 110 / 1504
R[$F_o > 4\sigma(F_o)$]	R_1 = 0.0847	R_1 = 0.0764	R_1 = 0.1004
	wR_2 = 0.2254	wR_2 = 0.2157	wR_2 = 0.2322
G.o.f. on F^2	1.016	1.066	1.197
Max., min. residual densities /e Å^{-3}	1.543, -0.595	2.111, -0.571	2.067, -0.789

Table 3.1 Crystal structure and refinement parameters for compounds **3-5**.

Fe_3Mo_2 TBP (**3**)	Distance (Å)		Angle (°)
$Fe(1)–N_{(N\equiv C)}$	1.965(6)	Fe(1)–N≡C	166.2(5)
$Fe(2)–N_{(N\equiv C)}$	1.959(5)	Fe(2)–N≡C	170.8(6)
$Fe(3)–N_{(N\equiv C)}$	1.957(6)	Fe(3)–N≡C	171.7(5)
Mo(1)–C	2.188(8)	$Mo(1)–C\equiv N_{bridging}$	168.6(6)
Mo(2)–C	2.202(8)	$Mo(2)–C\equiv N_{bridging}$	168.4(5)
$C\equiv N_{bridging}$	1.165(8)		
$C\equiv N_{terminal}$	1.172(10)		
Mn_3Mo_2 TBP (**4**)	Distance (Å)		Angle (°)
$Mn(1)–N_{(N\equiv C)}$	2.238(6)	Mn(1)–N≡C	162.2(5)
$Mn(2)–N_{(N\equiv C)}$	2.235(6)	Mn(2)–N≡C	163.8(5)
$Mn(3)–N_{(N\equiv C)}$	2.232(6)	Mn(3)–N≡C	163.0(3)
Mo(1)–C	2.171(7)	$Mo(1)–C\equiv N_{bridging}$	175.8(7)
Mo(2)–C	2.164(7)	$Mo(2)–C\equiv N_{bridging}$	175.2(7)
$C\equiv N_{bridging}$	1.143(8)		
$C\equiv N_{terminal}$	1.148(10)		
V_3Mo_2 TBP (**5**)	Distance (Å)		Angle (°)
$V(1)–N_{(N\equiv C)}$	2.037(10)	V(1)–N≡C	163.8(9)
$V(2)–N_{(N\equiv C)}$	2.046(12)	V(2)–N≡C	166.1(10)
$V(3)–N_{(N\equiv C)}$	2.007(12)	V(3)–N≡C	167.3(10)
Mo(1)–C	2.152(15)	$Mo(1)–C\equiv N_{bridging}$	172.7(11)
Mo(2)–C	2.165(14)	$Mo(2)–C\equiv N_{bridging}$	173.6(11)
$C\equiv N_{bridging}$	1.158(15)		
$C\equiv N_{terminal}$	1.139(17)		

Table 3.2 Important bond distances and bond angles in the crystal structures of **3-5**.

(Figure 3.1). The two $[Mo(CN)_6]^{3-}$ ions occupy the axial positions of the TBP core. Three CN^- ligands from each hexacyanomolybdate ion act as bridges while the other three terminal CN^- ligands point away from the cluster. The three equatorial M^{II} ions are in pseudo-octahedral environments consisting of two bidentate tmphen ligands with the coordination sphere being completed by two bridging N-bound CN^- ligands. Each tmphen ligand bound to the M(3) center is engaged in intramolecular π-π contacts with a tmphen ligand from a neighboring M(1) or M(2) (Figure 3.2a). Only one tmphen from each of the M(1)/M(2) centers is involved in an intramolecular π-π interaction with a tmphen ligand bound to the M(3) center. The tmphen ligands from M(1) and M(2) that are not involved in and intramolecular π-π interaction, are involved in π-π stacking with the corresponding tmphen ligands from a neighboring cluster, the four stacked tmphen ligands forming a supramolecular dimer (Figure 3.2b). The three equatorial metal sites in one TBP molecule exhibit the same chirality (Δ or Λ). Each dimer contains both enantiomers, resulting in a centrosymmetric space group.

Magnetic Properties

Analysis of the magnetic data was performed with the assistance of Dr. Andrey Prosvirin of the Dunbar group. The magnetic properties of compounds **4** and **5** were investigated by magnetic susceptibility measurements over the temperature range of 1.8 - 400 K; field dependent magnetization measurements were performed under applied fields up to 7 Tesla. Measurements were carried out on crushed crystals and, in the case of the V_3Mo_2 TBP, on crystals in a sealed quartz tube. DC measurements were measured under an applied magnetic field of 1000 G.

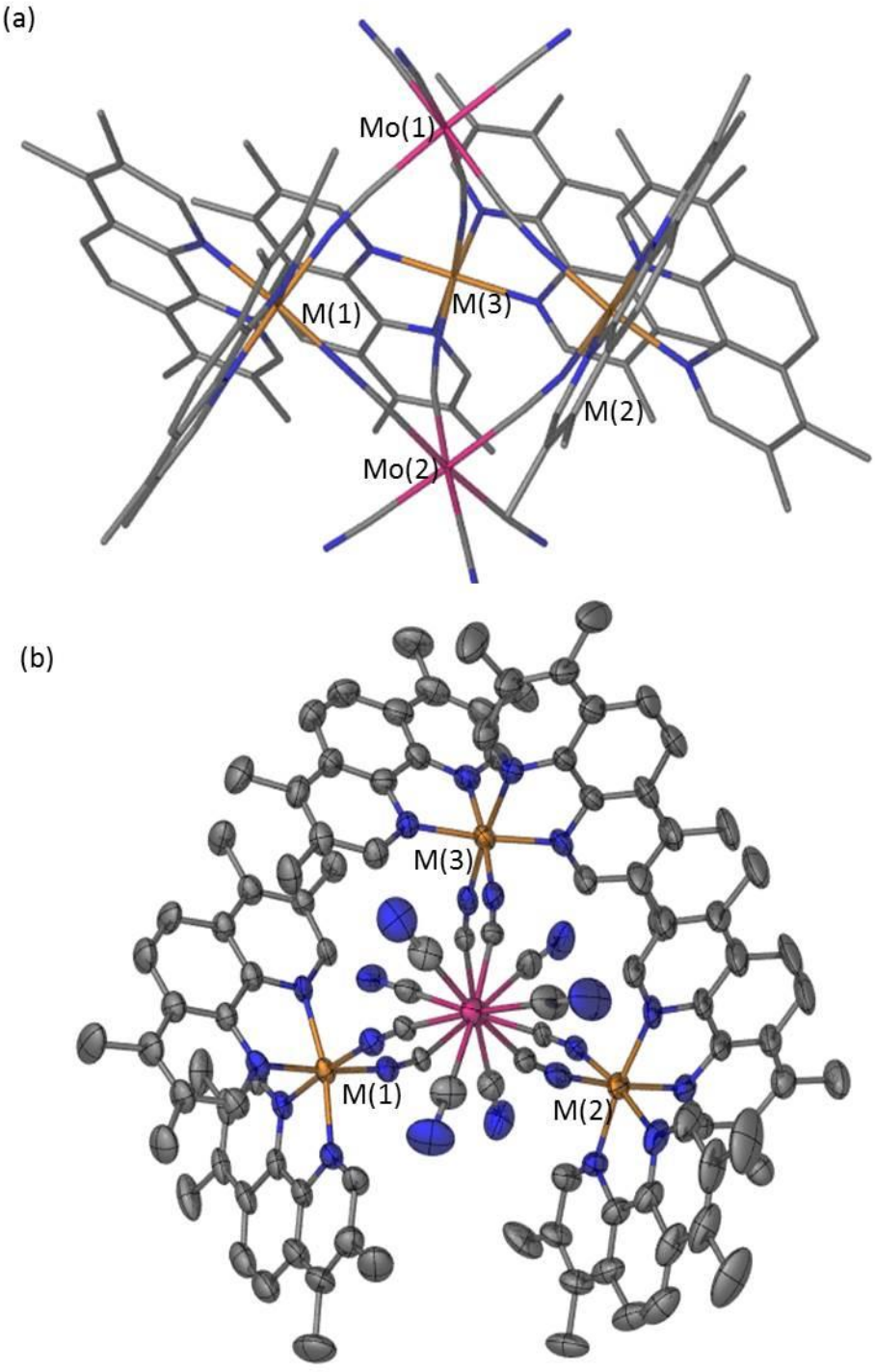

Figure 3.1 Molecular representation of (a) equatorial view of the core in the trigonal bipyramidal molecule **3 – 5.** (b) axial view of the thermal ellipsoid plot of compounds **3 – 5**, drawn at 50% probability level. (H-atoms omitted for the sake of clarity)

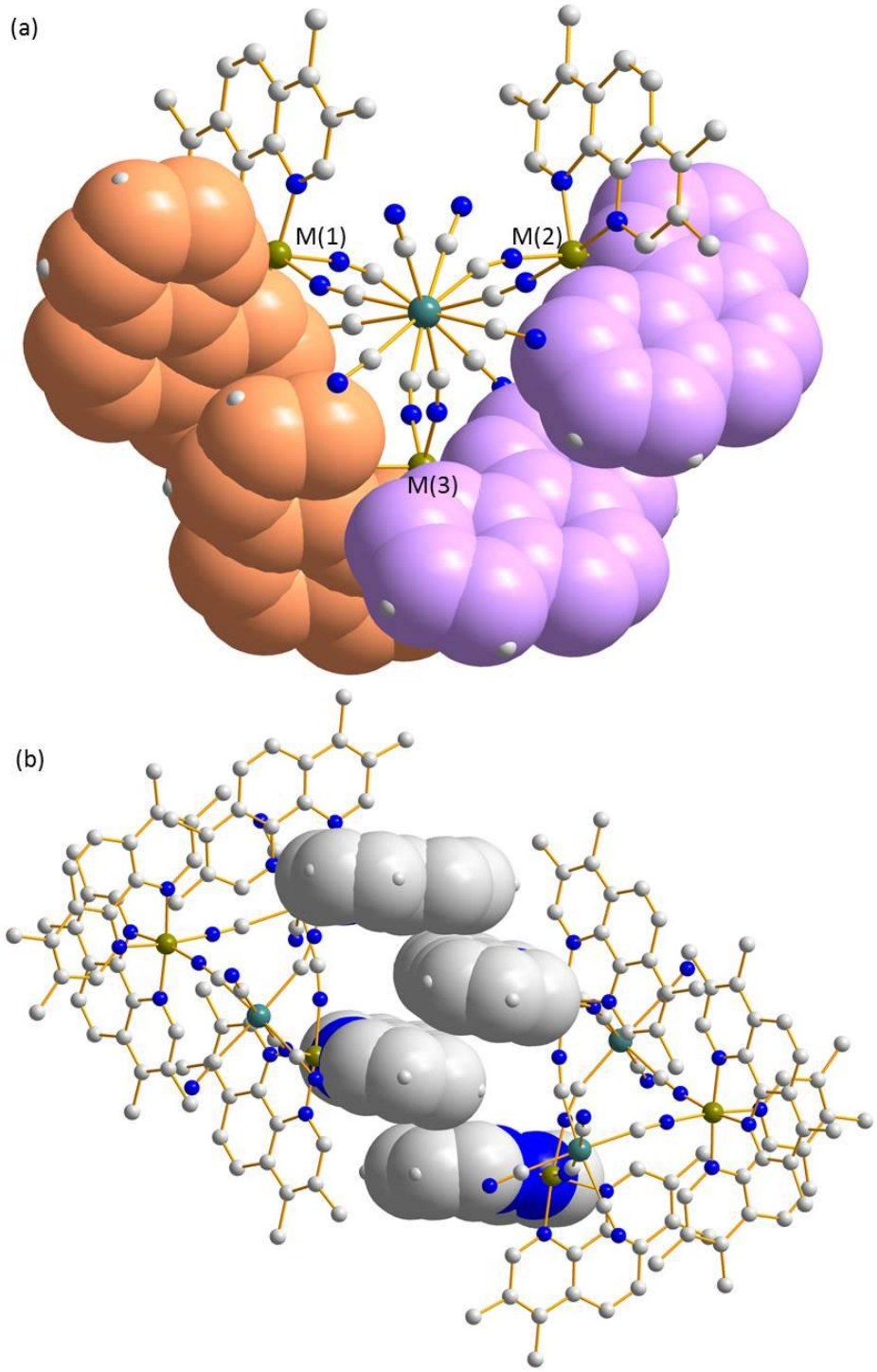

Figure 3.2 Molecular representation of compounds **3 – 5** (a) axial view showing itramolecular π-π interactions. (b) intermolecular π-π interactions between two neighboring molecules in the π-stacked dimer.

$[Mn(tmphen)_2]_3[Mo(CN)_6]_2 \cdot (MeCN)_2 \cdot (MeOH)_7 \cdot (H_2O)_4$ (**4**). Temperature dependent magnetic susceptibility data for **5** indicate antiferromagnetic coupling between the high spin S = 5/2 Mn^{II} ions and the S = 3/2 Mo^{III} ions (Figure 3.3). The room temperature χT vs. T value (14.6 emu·K·mol^{-1}) is lower than the expected value for three isolated Mn^{II} ions and two isolated Mo^{III} ions (16.8 emu·K·mol^{-1}). This discrepancy can be partly attributed to the g value not being 2.0 for this molecule. The values of χT first decrease as the temperature is lowered and then increase to a maximum of 21.1 emu·K·mol^{-1} at ~8K. The $1/\chi$ data above 100 K obey the Curie-Weiss law with a Curie constant C = 16.9 cm^3·mol^{-1}·K and a Weiss temperature Θ = -47 K. The shape of the χT curve and the negative value of the Weiss constant are indications of antiferromagnetic coupling between the Mn^{II} and Mo^{III} ions leading to a ferrimagnetic ground state. The field dependence of the magnetization at 1.8 K saturated at 11.5 B.M which suggests a ground state of S ~ 6, higher than expected for an antiferromagnetically coupled system (S = 9/2) (Figure 3.4). Although it can be seen from the magnetic data that an antiferromagnetic interaction is occurring between the Mn^{II} and Mo^{III} ions, a fitting of the magnetic data was not possible due to factors such as magnetic anisotropy.

$[V(tmphen)_2]_3[Mo(CN)_6]_2(CH_3CN)_2(MeOH)_{12}$ (**5**). The temperature dependence of the magnetic susceptibility data gives a room temperature χT value of 2.03 emu·K·mol^{-1} which is significantly smaller than the spin only value expected for three isolated V^{II} ions and two isolated Mo^{III} ions in the absence of magnetic interactions (9.38 emu·K·mol^{-1}). The χT value decreases slightly as temperature is lowered until ~6 K (Figure 3.5). The sharp decrease of χT below 6K is attributed to zero field splitting

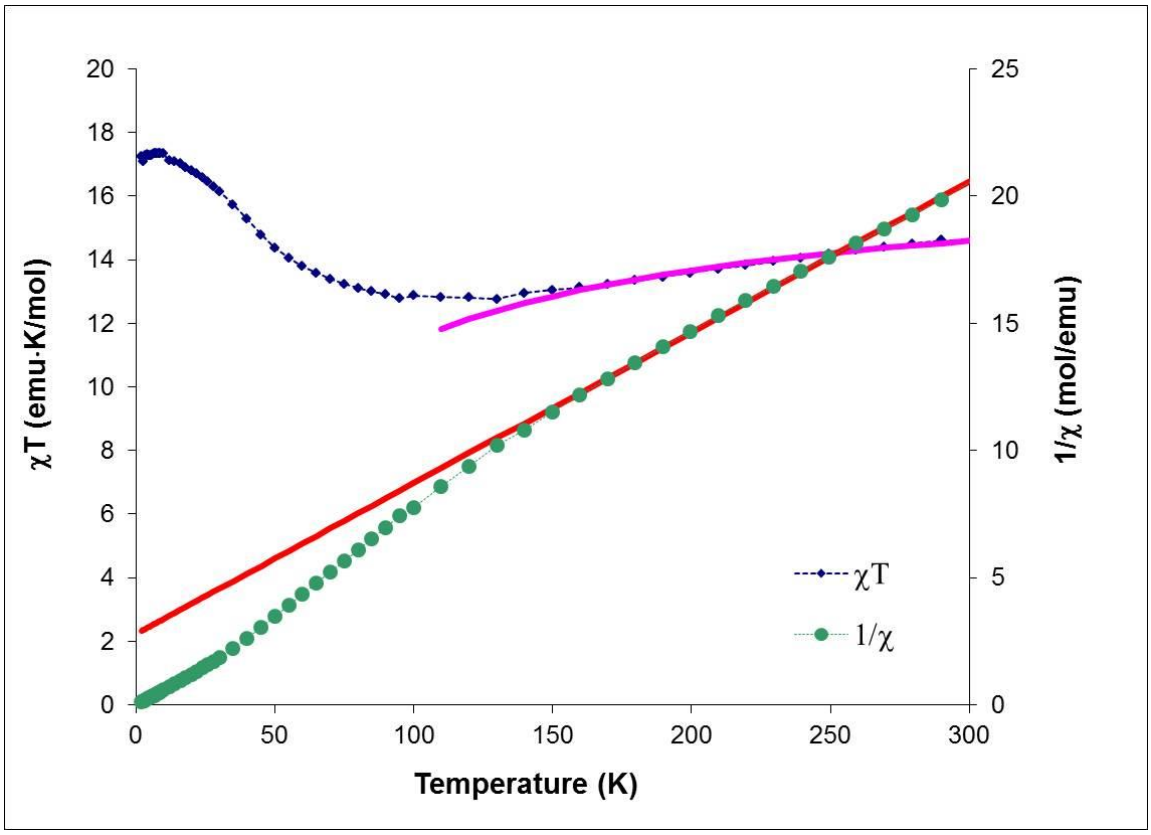

Figure 3.3 Temperature dependence of the χT product (blue diamonds) and 1/χ (green dots) for **4**. Pink line represents a Curie-Weiss simulation of the χT data above 100 K for 3 Mn^{II} S = 5/2 ions and 2 Mo^{III} S = 3/2 ions. Red line represents the Curie-Weiss Law fit above 100 K with C = 16.9 $cm^3 \cdot mol^{-1} \cdot K$ and Θ = -47 K.

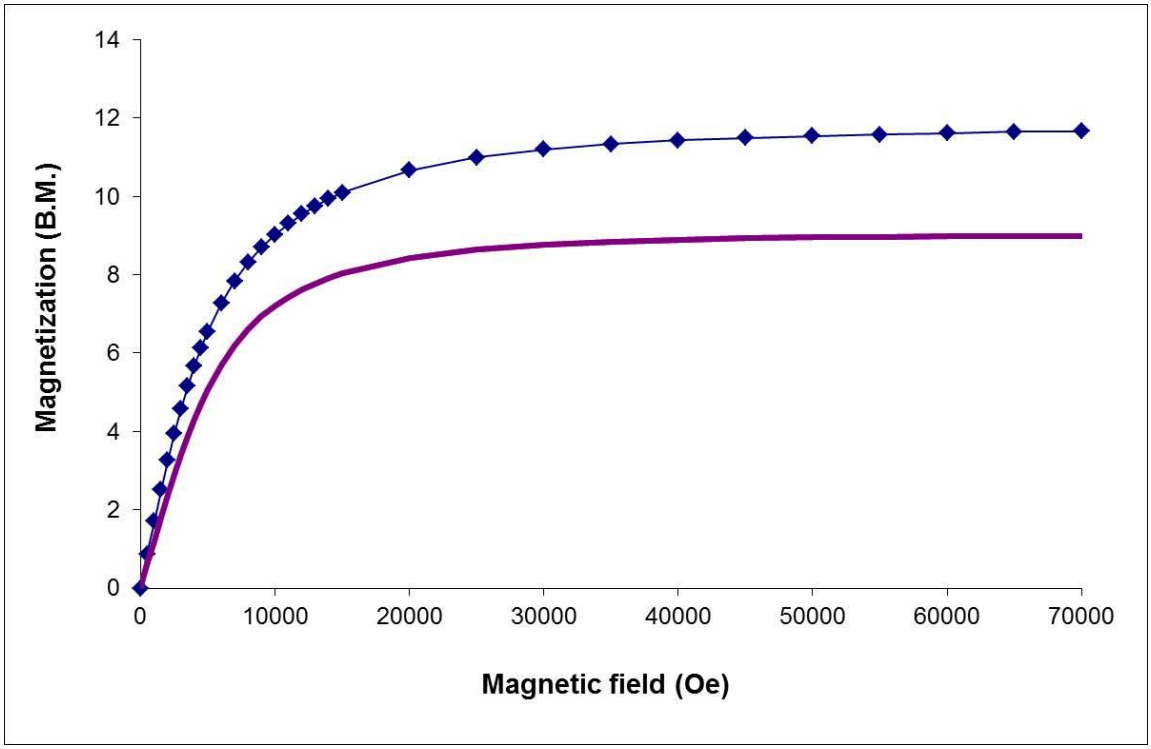

Figure 3.4 Field dependent magnetization for compound **4**. The purple line represents the Brillouin function for S = 9/2, g_{avg} = 2.0.

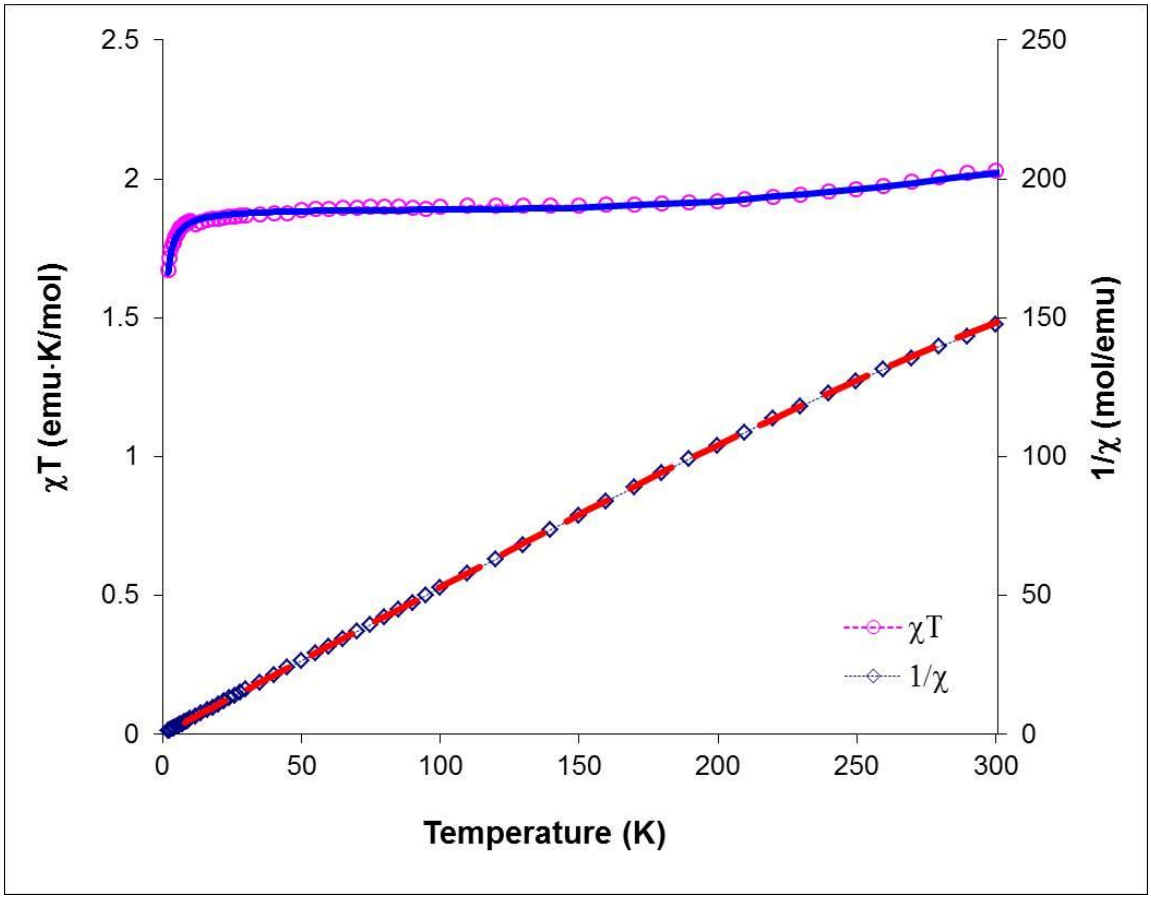

Figure 3. 5 Temperature dependence of the χT product for **5**. The solid line corresponds to the MAGPACK simulation (g_{Mo} = 2.01, g_V = 2.01, J = -130 cm^{-1}, zJ' = 0.15 cm^{-1}).

and/or molecular interactions. The continued rise of χT as the temperature approaches 300 K and the room temperature value being considerably smaller than the spin-only value is evidence that the system is already fully coupled at room temperature. To investigate this further, magnetic measurements were performed up to 350 K (Figure 3.6). Simulation of the magnetic data to 350 K was carried out using the isotropic Heisenberg-Dirac-Van Vleck Hamiltonian:

$$H = -2J_{V\text{-}Mo}(S_{Mo1} + S_{Mo2})(S_{V1} + S_{V2} + S_{V3}) + \mu_B H[g_{avg}(S_{Mo1} + S_{Mo2} + S_{V1} + S_{V2} + S_{V3})] - 3D[S^{Z}{}_{V}{}^{2} - (1/3)S_V(S_V + 1)] \quad \text{(Eq.3.1)}$$

Simulation of the data using MAGPACK and Eq. 3.1 resulted in the best fit parameters: $J = -130\ cm^{-1}$, $zJ' = -0.20\ cm^{-1}$, $g_V = 2.01$, $g_{Mo} = 2.01$, $D = 4\ cm^{-1}$. The field dependence of the magnetization saturates at 2.6 μ_B which is in good agreement with an S = 3/2 ground state from an antiferromagnetically coupled system of three S = 3/2 V^{II} ions and two S = 3/2 Mo^{III} ions (Figure 3.7).

In order to probe the magnetic properties further and investigate the extraordinarily strong coupling exhibited by compound 5, the magnetic data were analyzed by our collaborator, Prof. V. S. Mironov at Russian Acadamy of Sciences. His analysis involved theoretical modeling of the experimental data using a fixed value for the g-factor of molybdenum ($g_{Mo} = 1.96$) based on the experimental value previously reported by Beauvais and Long.[140] Then, the values for g_V and J were allowed to vary with the root mean square criterion for the experimental χT curve from 100 to 350 K. The best fit parameters gave $J = -134\ cm^{-1}$, $g_{Mo} = 1.96$, $g_V = 1.985$ and $D_{Mo} = +4\ cm^{-1}$ (Figure 3.8). The g values obtained from the calculation fit well with reported

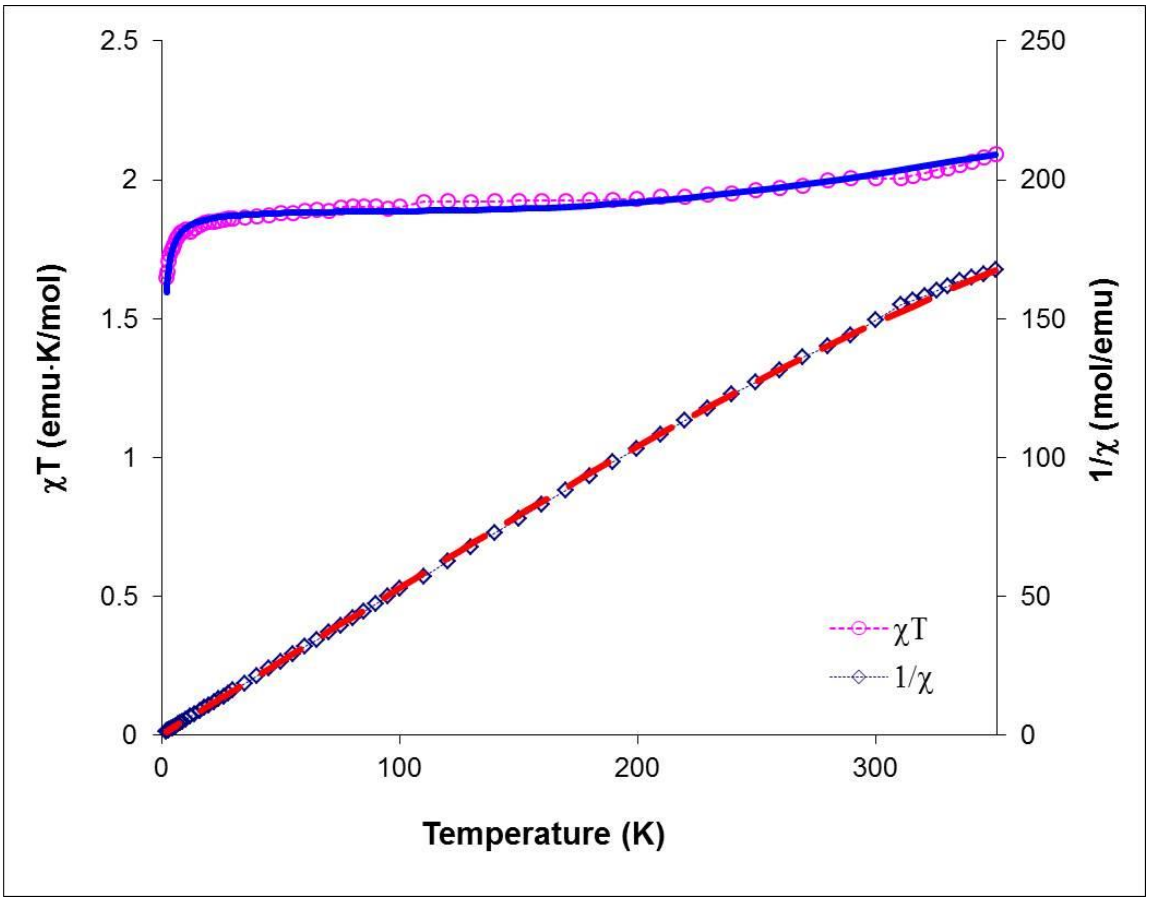

Figure 3.6 Temperature dependence of the χT product to 350 K for **5**. The solid line corresponds to the MAGPACK simulation (g_{Mo} = 2.01, g_V = 2.01, J = -130 cm^{-1}, zJ' = 0.20 cm^{-1}).

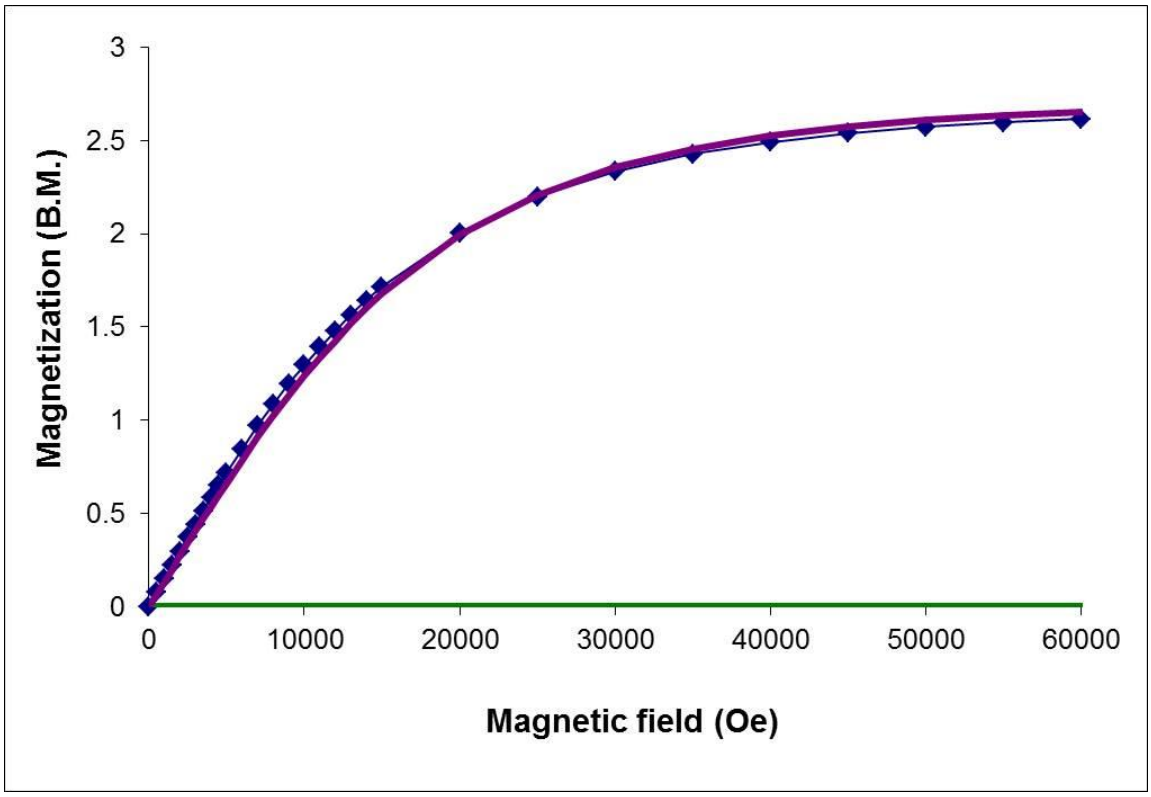

Figure 3.7 Field dependent magnetization for compound **5**. The solid line corresponds to the Brillouin function (S = 3/2, g_{avg} = 2.01).

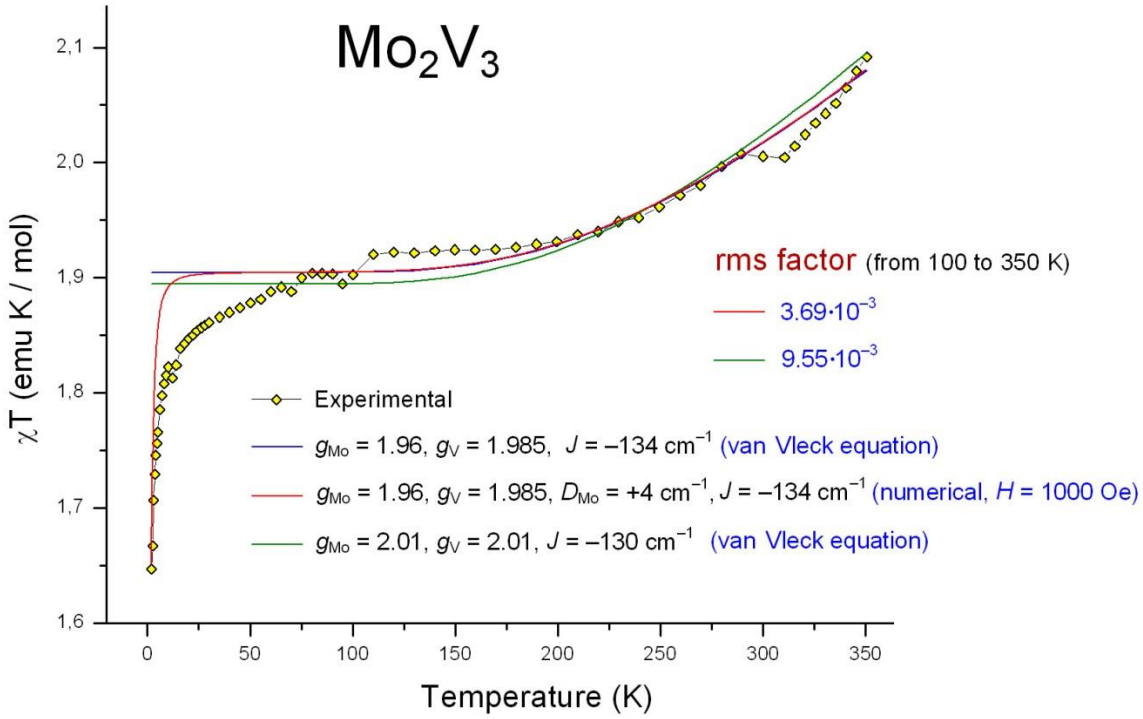

Figure 3.8 Experimental and theoretical temperature dependence of the χT product to 350 K for **5**. The blue line represents the best fit from 100 – 300 K with parameters J = -134 cm^{-1}, g_{Mo} = 1.96, g_V = 1.985 and D_{Mo} = +4 cm^{-1}. The red line is a numerical calculation using the same parameters to simulate the data at low temperatures (1.8 – 100 K).

experimental g values for V^{II} ions in an octahedral environment.[141] Numerical calculations were performed using the same parameters at 1000 Oe with zero-field splitting energy added to $[Mo(CN)_6]^{3-}$ to simulate the data to low temperatures. The drop in the χT curve below 20 K can be attributed to the ZFS energy of Mo^{III}, as illustrated by the red line in Figure 3.8. The decrease in the χT curve between 100 and 20 K can be attributed to variations of the g_{Mo} and g_V values upon cooling. To illustrate this, calculations were carried out where the values of both g_{Mo} and g_V were fixed and the value of J was allowed to vary. As seen in Figure 3.9, even small changes between calculations in the g values of Mo^{III} and V^{II} result in pronounced changes in the simulated χT curve, however, the calculated magnetic exchange parameter remains large regardless of the changes in the g-values.

Compound **5** is extraordinary in that it exhibits, by far, the strongest antiferromagnetic exchange coupling observed for a cyano-bridged compound. The previous record for a non-zero spin ground state in a cyano-bridged cluster (also exhibited by coupling between V^{II} and Mo^{III}) is for the previously mentioned compound $[(PY5Me_2)_4V_4Mo(CN)_6](PF_6)_5$ ($J = -61\ cm^{-1}$).[141] The coupling is stronger even than the strongest reported coupling for an S = 0 ground state compound, the record being held by $[Mo_2(CN)_{11}]^{5-}$ with $J = -113\ cm^{-1}$.[140] The fact that these record coupling parameters are all from compounds containing Mo^{III} ions lends valuable experimental support to the body of theoretical work which has predicted that Mo^{III} cyanide bridges to early 3d transition metals in magnetic materials will engender strong magnetic interactions.[41,42,126]

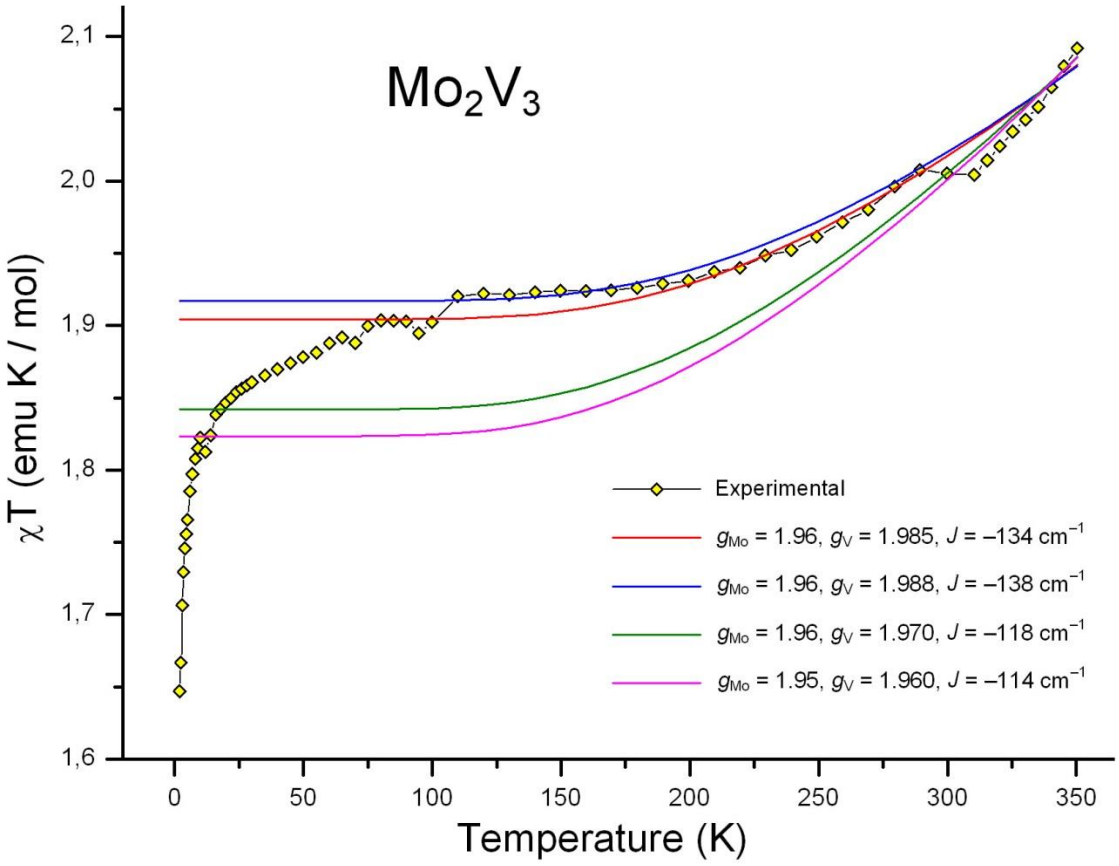

Figure 3.9 Experimental and theoretical temperature dependence of the χT product to 350 K for **5.** Solid lines represent fittings with the fixed values of g_{Mo} and g_V (listed on the plot) and the resultant calculated J parameter illustrating how dependent the χT curve is on the g-values of the Mo^{III} and V^{II} ions.

Conclusions

Three TBP molecules containing $[Mo(CN)_6]^{3-}$ were synthesized by *in situ* generation of $[Mo(CN)_6]^{3-}$ from $[Mo(CN)_7]^{4-}$. The compounds reported in this chapter constitute key additions to the small subset of magnetic compounds containing the octahedral hexacyanomolybdate(III) anion. The Mn_3Mo_3 TBP exhibits antiferromagnetic interactions between Mn^{II} and Mo^{III} through cyanide bridges. Theoretical predictions indicate that superexchange between $[Mo(CN)_6]^{3-}$ and the early 3d metal ions (V^{II} and Cr^{II}) through the cyanide bridge should be extremely strong. Synthesizing new compounds containing these theoretically studied anisotropic building blocks is important for addressing the validity of the predictions. Our new experimental support in this field, especially the extraordinarily large coupling parameter (J = -134 cm^{-1}) between Mo^{III} and V^{II}, heralds a bright future for an improved understanding of the magnetic interactions involving cyanide ligands and provides precious data to correlate theory and experiment.

CHAPTER IV

NEW CYANIDE BRIDGED COMPOUNDS INCORPORATING OCTACYANOTUNGSTATE(V)

Introduction

As stated earlier, one of the ways to introduce anisotropy into molecular magnets is to synthesize compounds with 4d and 5d transition metals that possess significant unquenched orbital angular momentum. Among the most widely investigated compounds in this category are those containing the pentavalent octacyanometallates, $[M^{V}(CN)_8]^{3-}$ (M = W, Mo) .[114-116,121-125,219-244] The $[W^{V}(CN)_8]^{3-}$ ion has produced a myriad of structural motifs ranging from 3-D extended structures[219-221], 2-D nets[222-231], 1-D chains[232-234] and 0-D discrete multinuclear compounds[114,115,123-125,235-242]. It has been predicted by DFT calculations that discrete molecules containing $[W^{V}(CN)_8]^{3-}$ and divalent metals such as Co^{II}, Ni^{II} and Mn^{II}, will result in a negative D value making these compounds good candidates for exhibiting SMM behavior. Most compounds containing the $[W^{V}(CN)_8]^{3-}$ building block are of the form M_9W_6, a pentadecanuclear six-capped body-centered cube (M = Mn, Ni, Co).[114,115,123-125,235-237] While this motif has led to interesting magnetic properties including several examples that exhibit SMM behavior[114,123], many of the reported M_9W_6 clusters are capped by coordinated alcohol molecules which renders them unstable under conditions required to perform magnetic measurements, *i.e.* vacuum conditions, leading to difficulty in interpreting the magnetic data. An efficient strategy to preparing more stable molecules containing the

$[W^V(CN)_8]^{3-}$ ion is to employ the use of a blocking ligand to control the binding by capping the peripheral sites of growing molecule. The Dunbar group has been highly successful at the approach, a prime example of which is the syntheses of a large family of trigonal-bipyramidal (TBP) molecules using the tmphen ligand (tmphen = 3,4,7,8-tetramethyl-1,10-phenanthroline). These neutral TBP molecules have general formula of $\{[M(tmphen)_2]_3[M'(CN)_6]_2\}$ which is the general metal ion ratio for PB analogs and as such, these molecules tend to mimic PB properties and many of the metal combinations have led to interesting properties that were previously observed only in extended PB-type materials. Highlights of these studies include SMM behavior, charge-transfer induced spin transition (CTIST), temperature-induced low-spin (LS) to high-spin (HS) transition, and cyanide linkage isomerism.[44,50,54,61,245-247] Our group recently reported the first instance in which the octacyanotungstate building block led to a TBP complex, namely $[Ni^{II}(tmphen)_2]_3[W^V(CN)_8]_2 \bullet 8CH_3OH \bullet 2H_2O$ which exhibits ferromagnetic coupling between the Ni^{II} and W^V ions and has a negative zero-field splitting parameter, $D = -0.24 cm^{-1}$. Micro-SQUID measurements on a single crystal, however, revealed that the compound is not a SMM.[116]

The work presented herein constitutes the second instance in which the octacyanotungstate ion has been incorporated into the TBP geometry. The product, $[Mn(tmphen)_2]_3[W^V(CN)_8]_2$, undergoes further reactions to form an open pentanuclear molecule with the same chemical composition and a 1-D chain, $\{[Mn_4(tmphen)_4(MeOH)_6(DMF)W^V_2(CN)_{16}]^{2+}[Mn_2(tmphen)_2(MeOH)_2(H_2O)_2W^V_2(CN)_{16}]^{2-}\}_\infty$. In addition to these compounds, the trinuclear molecule, $[Cu(tmphen)_2]_2[W(CN)_8]CF_3SO_3$,

was also synthesized. All four compounds were characterized by X-ray crystallography and magnetic studies of compounds 6, 8 and 9 were undertaken. The TBP molecule shows evidence of an out-of-phase signal when subjected to ac measurements in zero applied field. Magnetic measurements of the 1-D chain also reveal evidence for the beginning of an out-of-phase signal under zero applied field which hints at single chain magnet behavior.

Syntheses

Starting Materials. The tmphen ligand, $MnCl_2 \cdot 4H_2O$, $Na_2WO_4 \cdot 2H_2O$, KCN, KBH_4 and $Cu(CF_3SO_3)_2$ were purchased from Aldrich and used without further purification. The compound $[(C_4H_9)_3NH]_3W(CN)_8$ was prepared according to published procedure.[248-250]

$K_4W(CN)_8 \cdot 2H_2O$. The compound was prepared following an adaptation of a previously published procedure.[248,249] A quantity of $Na_2WO_4 \cdot 2H_2O$ (24.7 g, 0.075 mol), KCN (87.5 g, 1.35 mol) and KBH_4 (8.9 g, 0.165 mol) were dissolved in water. Acetic acid was added slowly (over 30 minutes) to the stirring solution causing the solution to change from colorless to yellow. The solution was heated for 20 minutes and then cooled to room temperature. Ethanol was added to the solution to precipitate $K_4W(CN)_8 \cdot 2H_2O$. The green product which was collected *via* suction filtration was dissolved in water and boiled with activated charcoal for 10 minutes. The solution was filtered to remove charcoal and the product was precipitated with ethanol. Yellow crystals of $K_4W(CN)_8 \cdot 2H_2O$ were collected *via* suction filtration. Yield = 28.1 g (64.1%).

$[(C_4H_9)_3NH]_3[W(CN)_8]$. The compound was prepared according to a previously published procedure.[250] A quantity of $K_4W(CN)_8 \cdot 2H_2O$ (2.409 g, 4.12 mmol) was dissolved in H_2O (8 mL) to form a yellow solution. Concentrated nitric acid (10 mL) was added dropwise affording a color change to green and then to reddish orange. The solution was diluted with 40 mL of water and then treated with tributylamine (2.85 mL, 12 mmol) by dropwise addition, which led to an instantaneous formation of a yellow precipitate. An additional 30 mL of water was added to precipitate more product. The yellow precipitate was collected *via* suction filtration and washed with three portions of cold water and then dissolved in 100 mL of methanol to form a yellow solution which was boiled with activated carbon for 10 minutes and allowed to cool to room temperature. The solution was filtered quickly to remove activated carbon and the resulting purple solution was reduced to dryness using a rotary evaporator to obtain a purple powder. Yield = 2.1 g (53%)

$[Mn(tmphen)_2]_3[W^V(CN)_8]_2$ (6) TBP. A solution of $MnCl_2 \cdot 4H_2O$ (40 mg, 0.2 mmol) in 6 mL of a 1:2 MeOH:H_2O v/v was added to a solution of tmphen (105 mg, 0.4 mmol) in 8 mL of MeOH to form a yellow solution. An aliquot of DMF (4 mL) was added to the solution and $[(C_4H_9)_3NH]_3[W(CN)_8]$ (190 mg, 0.2 mmol) in 16 mL of methanol to form a pale purple solution. In two separate vials, 8 mL aliquots of the $[(C_4H_9)_3NH]_3[W(CN)_8]$ solution were layered over 10 mL portions of the$MnCl_2$/tmphen solution. The solutions were stored in the dark to prevent decomposition by light. Brown block crystals began forming within two days.

$[Mn(tmphen)_2]_3[W^V(CN)_8]_2$ (7) open pentamer. Yellow platelet crystals of **7** were formed by leaving solutions containing crystals of **6** sitting in the dark at room temperature for approximately one month. The brown block crystals of **6** slowly dissolve as yellow plate crystals of **7** are formed.

$[Mn_4(tmphen)_4(MeOH)_6(DMF)W^V_2(CN)_{16}]^{2+}[Mn_2(tmphen)_2(MeOH)_2(H_2O)_2W^V_2(CN)_{16}]^{2-}\}_\infty$ (8). Tan needles of **8** were obtained by leaving solutions of **6** sitting at room temperature for longer than two months. The open pentamers, formed as compound **7**, self-assemble into 1D chains with time.

$[Cu(tmphen)_2]_2[W(CN)_8]CF_3SO_3$ (9). A solution of 26.4 mg (0.1 mmol) of tmphen in 3 mL of MeOH was added to a solution of $Cu(CF_3SO_3)_2$ (36.2 mg, 0.1 mmol) in 6 mL MeOH:DMF (1:1 v/v). The resulting green solution was layered with a solution of $[(C_4H_9)_3NH]_3[W(CN)_8]$ (95 mg, 0.1 mmol) in 9 mL of MeOH to form a lavender solution. The reaction was stored in the dark to prevent decomposition by light. Green needle-like crystals were obtained after a week.

Single Crystal X-Ray Crystallography

Single-crystal X-ray data were collected on a Bruker APEX diffractometer equipped with a CCD detector at 110 K in a procedure similar to that described in chapter III. A summary of pertinent information relating to unit cell parameters, data collection and refinements for compounds **6-9** is provided in Table 4.1. Selected metal-ligand bond distances and angles for compounds **6-9** are provided in Table 4.2.

Formula	Mn_3W_2 (**6**)	Mn_3W_2 (**7**)	$[Mn_3W_2]_\infty$ (**8**)	Cu_2W (**9**)
Space group	$P2_1/c$	P-1	P-1	P-1
Unit cell	a = 19.363(4) Å	a = 13.283(3) Å	a = 11.847(2) Å	a = 13.528(3)
	b = 25.486(5) Å	b = 13.376(3) Å	b = 15.230(3) Å	b = 13.526(3)
	c = 24.956(5) Å	c = 36.028(7) Å	c = 26.120(5) Å	c = 43.098(9)
	β = 104.79(3)°	α = 88.98(3)°	α = 99.14(3)°	α = 81.95(3)°
		β= 86.20(3)°	β = 95.34(3)°	β = 82.10(3)°
		γ = 78.01(3)°	γ = 106.50(3)°	γ = 77.74(3)°
Unit cell volume, V/Å^3	11907(4)	6248(2)	4413(1)	7583(3)
Z	5	3	2	2
Density (calculated) ρ/g cm^{-1}	1.376 Mg/m^3	1.344 Mg/m^3	1.547 Mg/m^3	1.427 Mg/m^3
Abs. coeff., μ/mm^{-1}	2.295	2.190	3.083	2.161
Crystal color and habit	Brown block	Yellow plate	Brown plate	Green needle
Crystal size /mm	0.31 x 0.24 x 0.12	0.12 x 0.06 x 0.01	0.43 x 0.43 x 0.04	0.20 x 0.06 x 0.04
Temperature /K	110	110	110	110
Radiation, λ /Å	Mo-K α, 0.71073	Mo-K α, 0.71073	Mo-K α, 0.71073	Mo-K α, 0.71073
Min. and max. Θ /°	1.09 to 28.38	1.56 to 15.14	1.42 to 28.27	1.44 to 28.26
Reflections collected	118048	18441	28182	32724
	[R_{int} = 0.0619]	[R_{int} = 0.0826]	[R_{int} = 0.0343]	[R_{int} = 0.0712]
Independent reflections	29023	5121	20048	26674
Data/restraints/ parameters	29023 / 0 / 1376	5121 / 0 / 672	20048 / 0 / 1079	26674 / 0 / 1618
R[$F_o > 4\sigma(F_o)$]	R_1 = 0.0710	R_1 = 0.0933	R_1 = 0.0574	R_1 = 0.1423
	wR_2 = 0.1956	wR_2 = 0.2497	wR_2 = 0.1585	wR_2 = 0.3397
G.o.f. on F^2	1.042	1.077	1.028	1.121
Max., min. residual densities /e Å^{-3}	3.066 and -1.870	2.612 and -0.533	4.860 and -2.990	2.851 and -3.797

Table 4.1 Crystal structure and refinement parameters for compounds **6** – **9**.

Mn_3W_2 TBP (**6**)	Distance (Å)		Angle (°)
$Mn(1)–N_{(N\equiv C)}$	2.211(9)	Mn(1)–N≡C	164.4(8)
$Mn(2)–N_{(N\equiv C)}$	2.196(12)	Mn(2)–N≡C	161.4(9)
$Mn(3)–N_{(N\equiv C)}$	2.197(9)	Mn(3)–N≡C	163.2(8)
W(1)–C	2.163(11)	$W(1)–C\equiv N_{bridging}$	178.9(9)
W(2)–C	2.160(12)	$W(2)–C\equiv N_{bridging}$	176.5(10)
$C\equiv N_{bridging}$	1.141(13)		
$C\equiv N_{terminal}$	1.132(15)		
Mn_3W_2 open pentamer (**7**)	Distance (Å)		Angle (°)
$Mn(1)–N_{(N\equiv C)}$	2.20(4)	Mn(1)–N≡C	159(3)
$Mn(2)–N_{(N\equiv C)}$	2.14(4)	Mn(2)–N≡C	163(3)
Mn(2)–O	2.22(3)	Mn(3)–N≡C	160(3)
$Mn(3)–N_{(N\equiv C)}$	2.29(4)	$W(1)–C\equiv N_{bridging}$	175(3)
Mn(3)–O	2.13(6)	$W(1)–C\equiv N_{terminal}$	177(4)
$W(1)–C_{(C\equiv N\ bridging)}$	2.27(4)	$W(2)–C\equiv N_{bridging}$	174(3)
$W(1)–C_{(C\equiv N\ terminal)}$	2.18(5)	$W(2)–C\equiv N_{terminal}$	177(4)
$W(2)–C_{(C\equiv N\ bridging)}$	2.13(5)		
$W(2)–C_{(C\equiv N\ terminal)}$	2.13(7)		
$C\equiv N_{bridging}$	1.13(4)		
$C\equiv N_{terminal}$	1.15(3)		
$[Mn_4W_2][Mn_2W_2]_\infty$ (**8**)[a]	Distance (Å)		Angle (°)
$Mn(1)–N_{(N\equiv C)}$	2.201(5)	Mn(1)–N≡C	157.1(5)
Mn(1)–O	2.166(5)	Mn(2)–N≡C	176.7(5)
$Mn(2)–N_{(N\equiv C)}$	2.167(6)	Mn(3)–N≡C	176.4(6)
Mn(2)–O	2.177(7)	$W(1)–C\equiv N_{bridging}$	177.3(5)
$Mn(3)–N_{(N\equiv C)}$	2.197(5)	$W(2)–C\equiv N_{bridging}$	178.3(5)
Mn(3)–O	2.205(5)		
$W(1)–C_{(C\equiv N\ bridging)}$	2.155(6)		
$W(1)–C_{(C\equiv N\ terminal)}$	2.158(7)		
$W(2)–C_{(C\equiv N\ bridging)}$	2.161(7)		
$W(2)–C_{(C\equiv N\ terminal)}$	2.166(6)		
$C\equiv N_{bridging}$	1.149(8)		
$C\equiv N_{terminal}$	1.145(9)		
Cu_2W (**9**)	Distance (Å)		Angle (°)
$Cu(1)–N_{(N\equiv C)}$	1.95(6)	Cu(1)–N≡C	168.1(2)
$Cu(2)–N_{(N\equiv C)}$	1.98(2)	Cu(2)–N≡C	172.9(5)
$W(1)–C_{(C\equiv N\ bridging)}$	2.17(8)	$W(1)–C\equiv N_{bridging}$	173.4(6)
$W(1)–C_{(C\equiv N\ terminal)}$	2.16(9)		

Table 4.2 Average metal-ligand bond distances (Å) and bond angles (°) obtained from the single crystal structures for compounds **6–9**. *a*- symmetry transformations used to generate equivalent atoms #1 -x + 1, -y + 2, -z + 1; #2 –x + 2, -y + 2, -z; #3 –x + 3, -y + 3, -z; #4 –x + 1, -y + 1, -z + 1

Results and Discussion

Syntheses

Reactions of $[(C_4H_9)_3NH]_3[W(CN)_8]$ and $MnCl_2$ with 3,4,7,8-tetramethyl-1,10-phenanthroline in a 1:1:2 ratio carried out in the dark afforded compound **6**. In the preparation of the TBP cluster, the precursors were formed *in situ* by stirring one equivalent of the metal salt with two equivalents of tmphen in 1:1:4 H_2O:DMF:MeOH. Crystalline forms of these compounds were obtained by bulk reactions, layering a solution of the $[Mn(tmphen)_2]^{2+}$ precursor over a solution of the octacyanotungstate ion in methanol. Brown block crystals of **6** were obtained over the course of a week. When crystals of compound **6** are left to stand in the mother liquor for longer than two weeks, the brown block crystals of **6** begin to dissolve and yellow platelet crystals of **7** form in solution. The TBP molecules disassemble and crystallize as an open pentanuclear molecule with the same molecular formula as **6**. Moreover, if the solutions are left standing in the dark for longer than two months, the yellow platelet crystals of **7** dissolve and tan needle-like crystals form in solution which are compound **8**.

Compound **9** was prepared by reacting $Cu(CF_3SO_3)_2$ and 3,4,7,8-tetramethyl-1,10-phenanthroline and $[(C_4H_9)_3NH]_3[W(CN)_8]$ in a 1:1:1 molar ratio. The reactions were carried out in ambient air in a 5:1 MeOH:DMF solution. Single crystals of compound **9** were obtained by layering solutions in thin tubes. Crystals of **9** can also be synthesized by bulk reaction, but a green insoluble powder is often present in this case. The reactions were stored in the dark to prevent decomposition by light. Green needle-like crystals were obtained after about a week.

Single Crystal Diffraction Studies

Four crystal structures of new compounds incorporating the octacyanotungstate anion were determined from single crystal X-ray diffraction measurements. Compound **6** crystallizes in the monoclinic space group $P2_1/c$. The molecular structure consists of a pentanuclear core composed of CN-bridged Mn^{II} and W^{V} ions (Figure 4.1). The two $[W(CN)_8]^{3-}$ ions occupy the axial positions of a TBP core. Three CN^- ligands from each octacyanotungstate ion act as bridges while the other five terminal CN^- ligands point away from the cluster. The three equatorial Mn^{II} ions are in pseudo-octahedral coordination environments consisting of two bidentate tmphen ligands and two bridging CN^- ligands. Each tmphen on the Mn(2) center is engaged in intramolecular π-π contact with a tmphen ligand from the neighboring Mn(1) or Mn(3) centers (Figure 4.2a). Only one tmphen from each of the Mn(1)/Mn(3) centers is involved in an intramolecular π-π interaction with a tmphen ligand bound to the Mn(2) center. The tmphen ligands from Mn(1) and Mn(2) that are not involved in an intramolecular π-π interaction are involved in π-π stacking with the corresponding tmphen ligands from a neighboring cluster, the four stacked tmphen ligands forming a supramolecular dimer (Figure 4.2b). A packing diagram along the c-axis (Figure 4.3) shows the intermolecular interactions of the TBP molecules.

An unexpected product was encountered in the course of these studies which was isolated as only a few crystals. The structure was determined but the limited quantity precluded the evaluation of physical and magnetic properties. Specifically, when crystals of compound **6** were left in the mother liquor for longer than two weeks, the

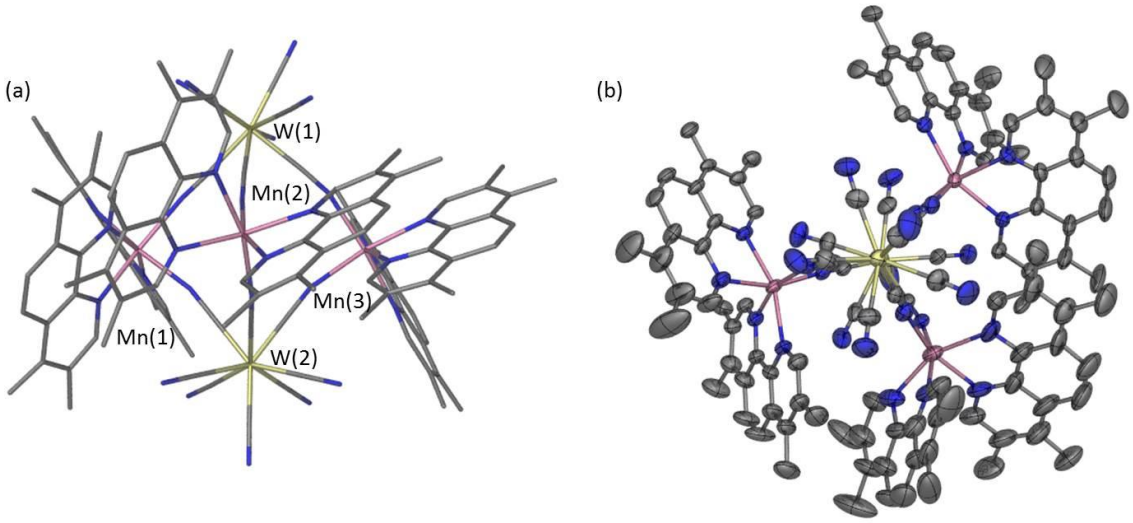

Figure 4.1 (a) Equatorial view of the core in the trigonal bipyramidal molecule **6**. (b) Axial view of the thermal ellipsoid plot of compound **6**, drawn at 50% probability level. (hydrogen atoms omitted for the sake of clarity)

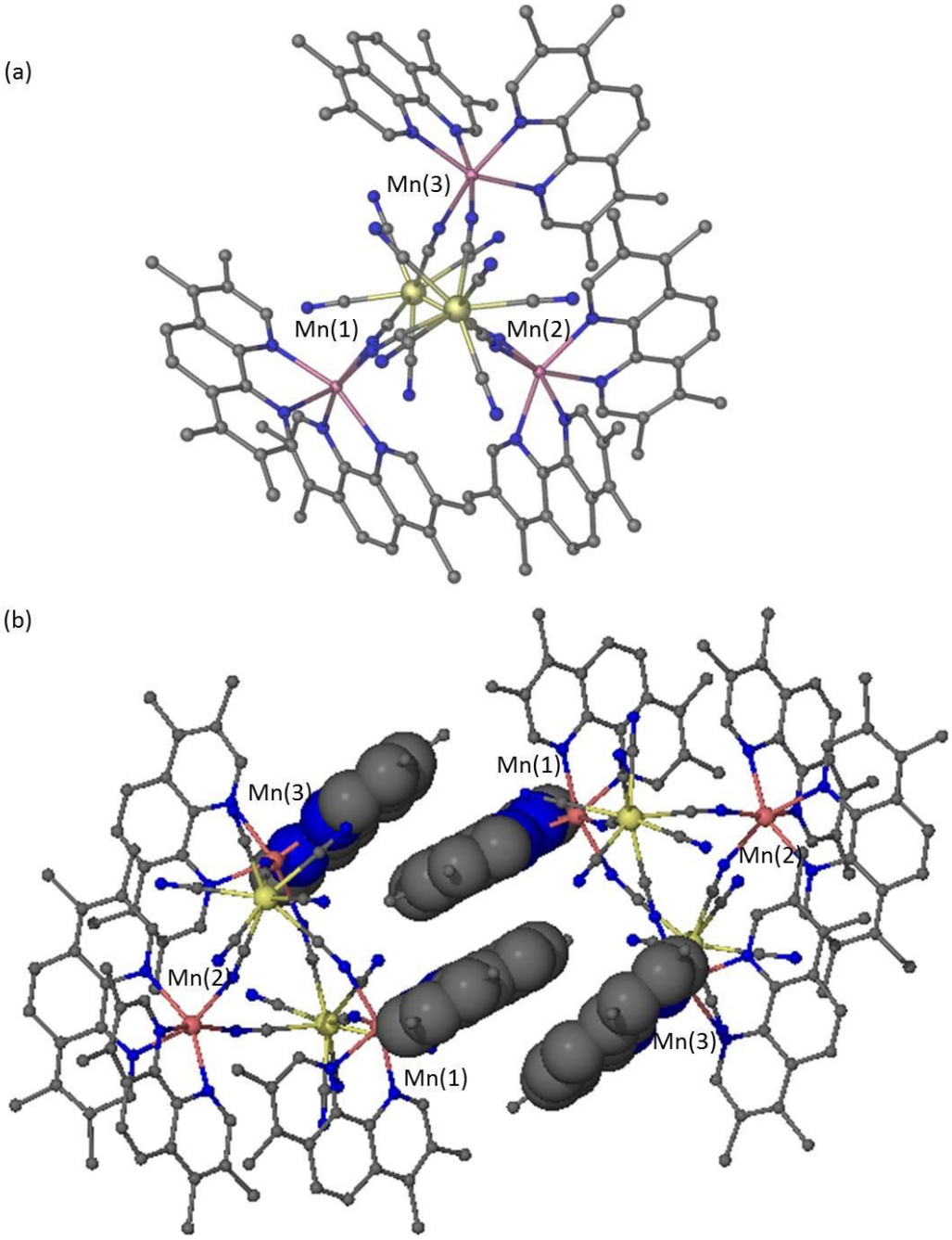

Figure 4.2 (a) Axial view of compound **6** emphasizing intramolecular π-π interactions. (b) The intermolecular π-π interactions between two neighboring molecules in the π-stacked dimer.

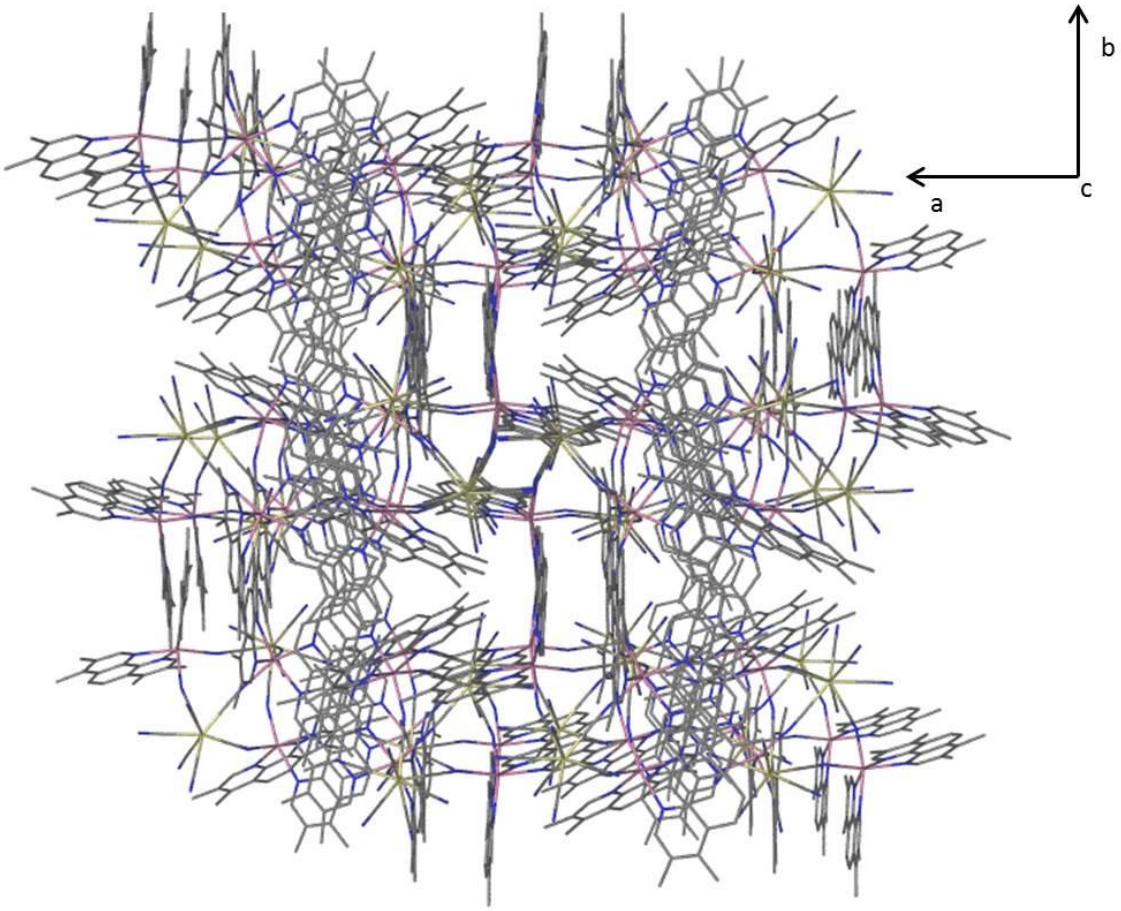

Figure 4.3 Packing diagram of compound **6** viewed down the c-axis. The intermolecular π-π interactions between TBP molecules form the 3-D packing of the compound.

previously discussed TBP compound dissolved and reformed a low yield of yellow platelet crystals of an open pentanuclear molecule. Compound **7** has the same molecular formula, but the TBP has become "unzipped" molecule to form a compound with the alternating metal backbone Mn(3)-W(2)-Mn(1)-Mn(2) which cups a centrally located DMF molecule (Figure 4.4). Each $[W(CN)_8]^{3-}$ ion acts as a bridge between two Mn^{II} ions with two CN^- ligands from each with the other six cyanides acting as terminal ligands. The three Mn^{II} ions are in pseudo-octahedral coordination environments consisting of two bidentate tmphen ligands and two N-bound bridging CN^- ligands. Each tmphen ligand is involved in a π-π interaction with a tmphen molecule from a neighboring molecule as illustrated in the packing diagram in Figure 4.5. These intermolecular π-π interactions between the tmphen molecules define the 3-D packing of the pentanuclear molecule.

Single crystal X-ray studies revealed that compound **8** is a one-dimensional polymer of CN^- bridged octacyanotungstate and Mn^{II} ions with complex counterions consisting of a square of two W^V and two Mn^{II} ions (Figure 4.6). The chain has a 2+ charge with a backbone of $\{Mn^{II}_4[W(CN)_8]_2\}^{2+}$. Four of the CN^- ligands coordinated to the $[W(CN)_8]^{3-}$ centers act as bridges whereas the other four terminal CN^- ligands complete the coordination sphere. Within the chain there are two different types of Mn^{II} ions, all in pseudo-octahedral environments. The Mn(1) is bound to one tmphen ligand, two cis N-bound CN^- ligands and two trans coordinated solvent molecules, namely DMF and MeOH. The Mn(2) centers are in a similar environment to Mn(1), having tmphen and two cis bridging CN^- ligands, but with two trans MeOH ligands rather than two

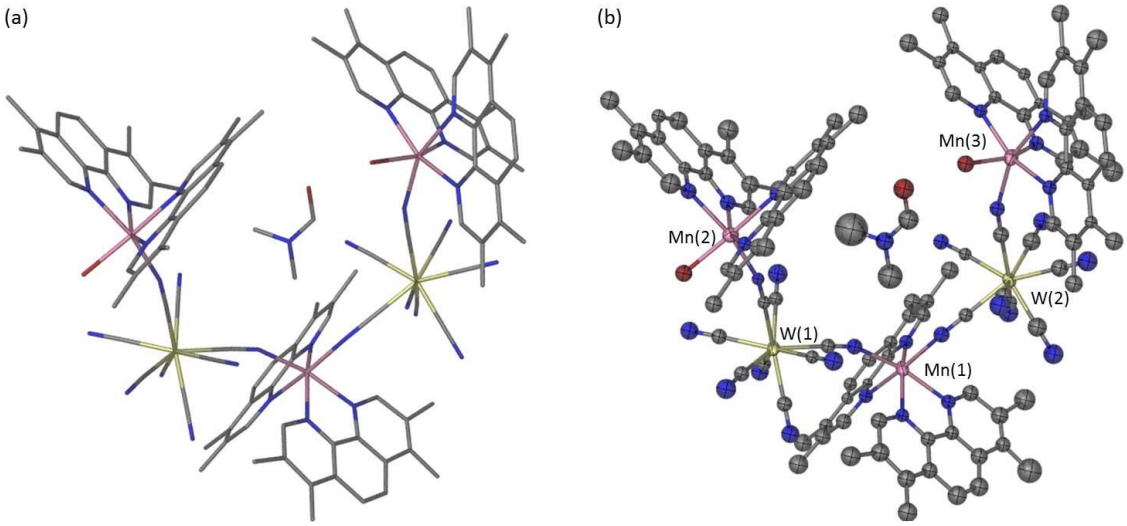

Figure 4.4 (a) Molecular representation of compound **7**. (b) Thermal ellipsoid plot of **7**, drawn at the 50% probability level. H-atoms are omitted for the sake of clarity. Os = yellow, Mn = pink, N = dark blue, C = grey, O = red.

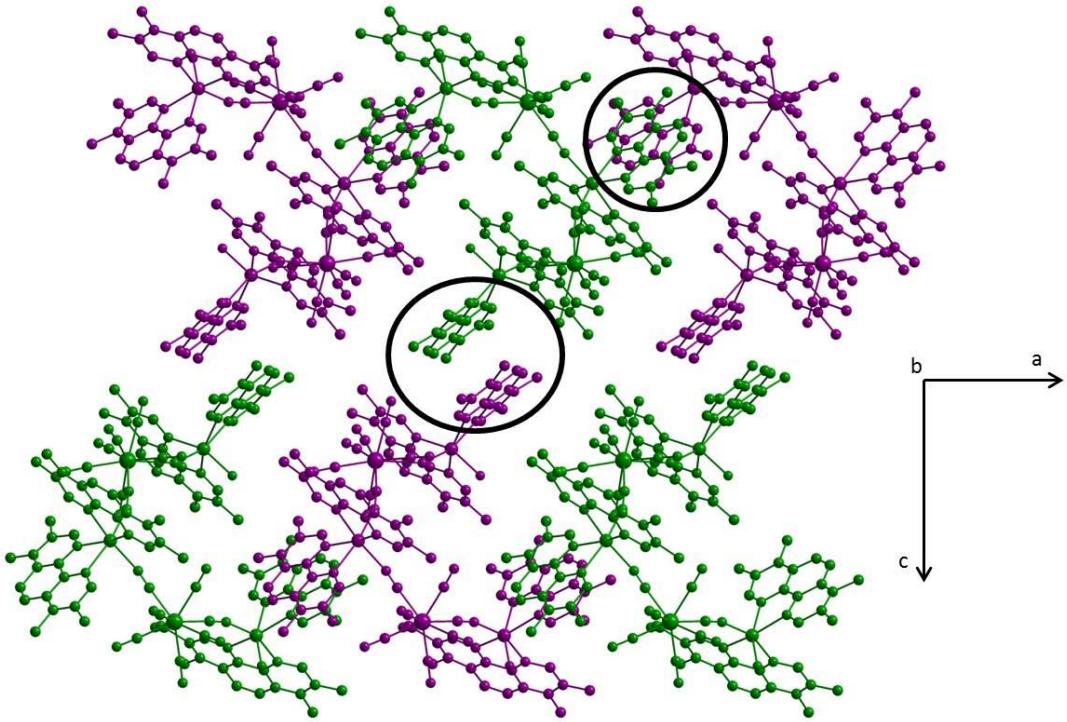

Figure 4.5 Molecular representation of the crystal packing of **7** viewed down the b-axis. The black circles highlight the intermolecular π-π interactions between neighboring clusters.

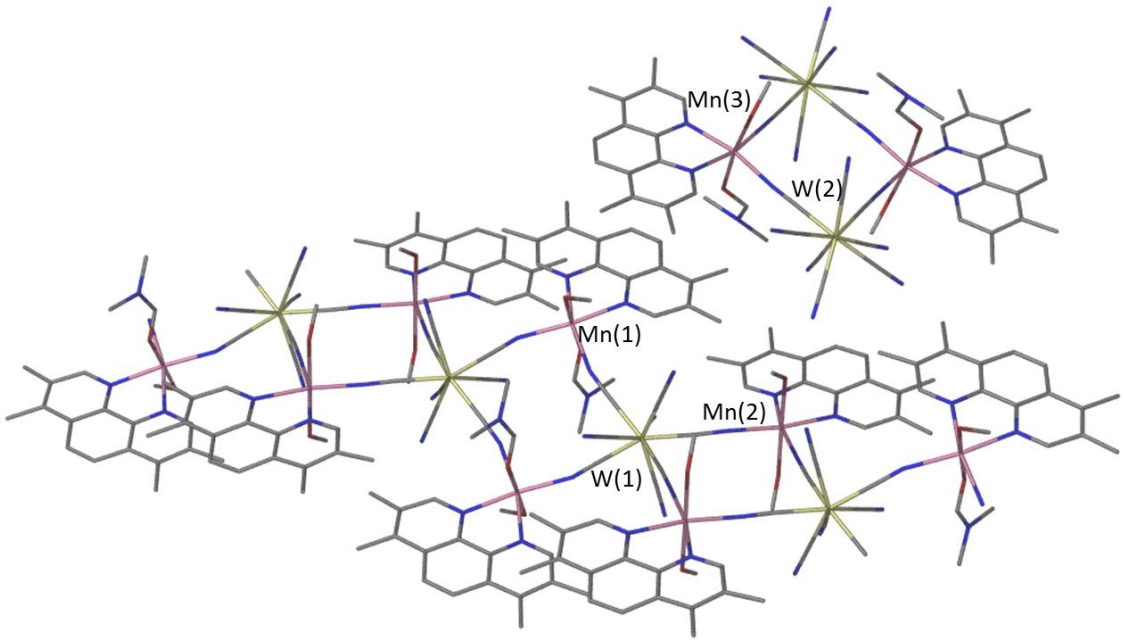

Figure 4.6 Molecular representation of the 1-D chain and the complex counteranion in **8**. H-atoms are omitted for the sake of clarity. Os = yellow, Mn = pink, N = dark blue, C = grey, O = red.

different solvent molecules. The charge balance of the chain is provided by tetranuclear anions consisting of $\{Mn^{II}_2[W(CN)_8]_2\}^{2-}$. The $[W(CN)_8]^{3-}$ units have two bridging CN^- ligands and six terminal cyanide ligands. The Mn(3) centers exhibit an environment similar to Mn(1) with one coordinated tmphen ligand, two cis ligands and two trans DMF and MeOH ligands. The tmphen ligand bound to the Mn(3) centers in the anion is involved in a π-π interaction with the tmphen ligands bound to the Mn(1) and Mn(2) centers in the chain (Figure 4.7).

Compound **9** is a trinuclear molecule with the formula $[Cu(tmphen)_2]_2[W(CN)_8]CF_3SO_3$. The trinuclear core is composed of a central octacyanotungstate anion bound to two $[Cu(tmphen)_2]^{2+}$ units resulting in a molecule with an overall positive charge (Figure 4.8). The Cu^{II} centers are bound through the nitrogen ends of bridging CN^- ligands. The coordination around the 5-coordinate Cu^{II} ion is completed by two bidentate tmphen ligands. The trinuclear molecule is bent due to the 8-coordinate W^V center giving rise to a C(1)-W-C(2) angle of 140.6°. One tmphen ligand coordinated to Cu(4) is involved in a π-π interaction with a tmphen ligand bound to the corresponding Cu^{II} ion on a neighboring molecule while the other tmphen on Cu(4) is involved in a π-π stacking with a tmphen ligand on Cu(3) of a different neighboring molecule (Figure 4.9). One tmphen ligand coordinated to Cu(2) is involved in a π-π interaction with the tmphen ligand bound to the corresponding Cu^{II} ion on a neighboring cluster while the other tmphen is involved in a π-π stacking with the tmphen on Cu(1) of a different neighboring molecule. The zigzag nature of the π-π-stacking

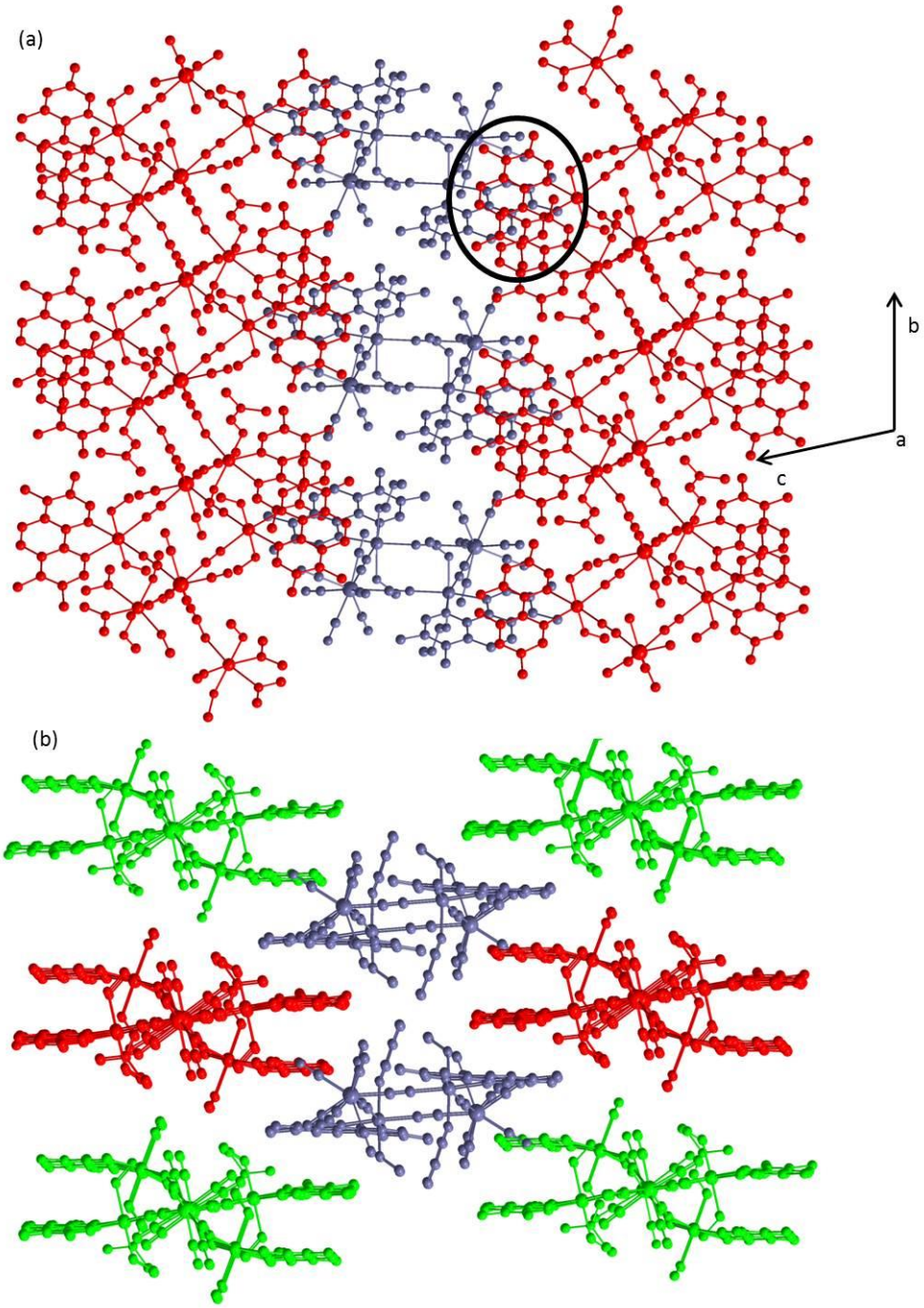

Figure 4.7 Molecular representation of the packing of **8** (a) in the bc-plane where the chains are red and the complex anions are in grey. The black circle highlights the π-π interactions between the tmphen ligands of the chain and of the complex anion. (b) along the chain direction where the red and green highlighted parts illustrate the alternating layers of 1-D chains.

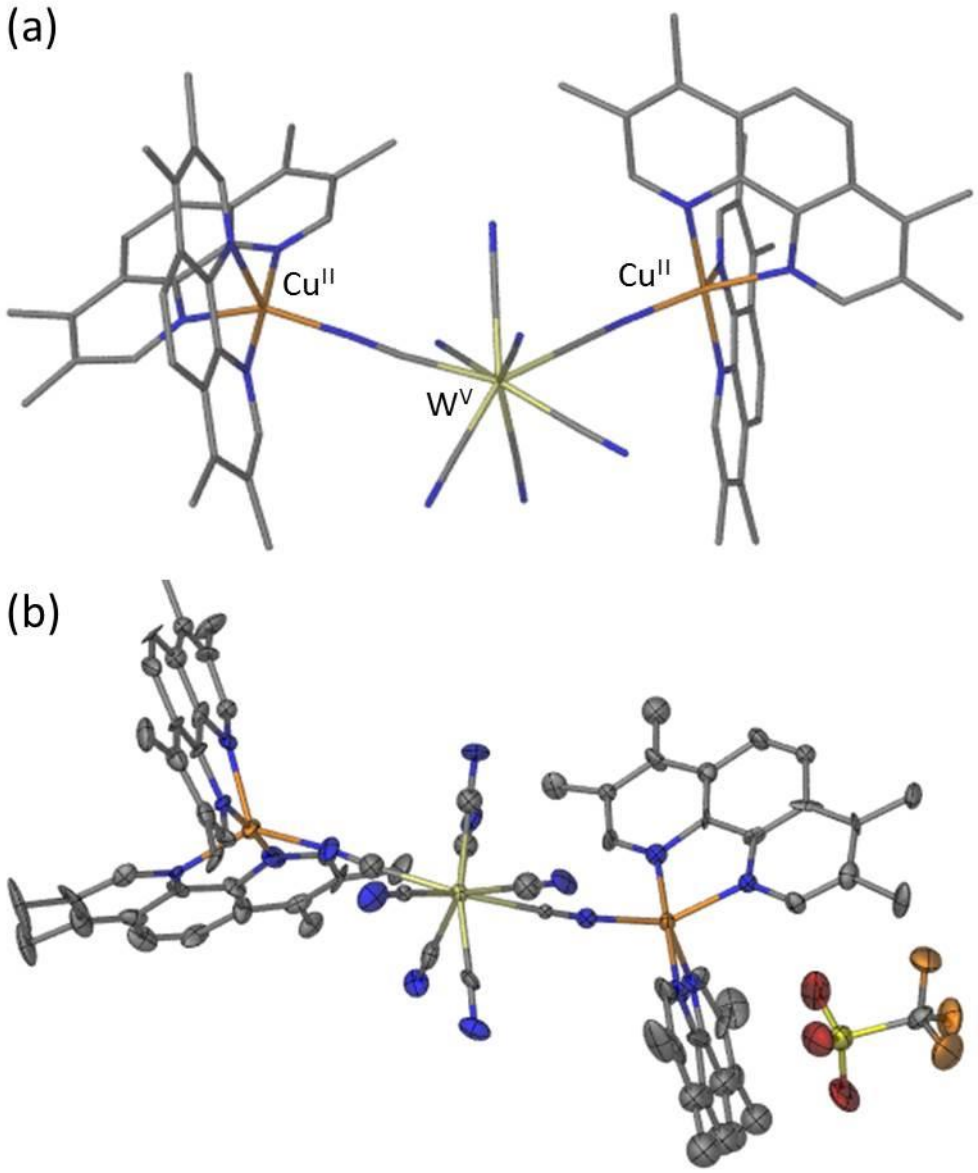

Figure 4.8 (a) Molecular representation of the trinuclear unit of **9**. (b) Thermal ellipsoid of **9** projected at the 50% probability level. H-atoms are omitted for the sake of clarity.

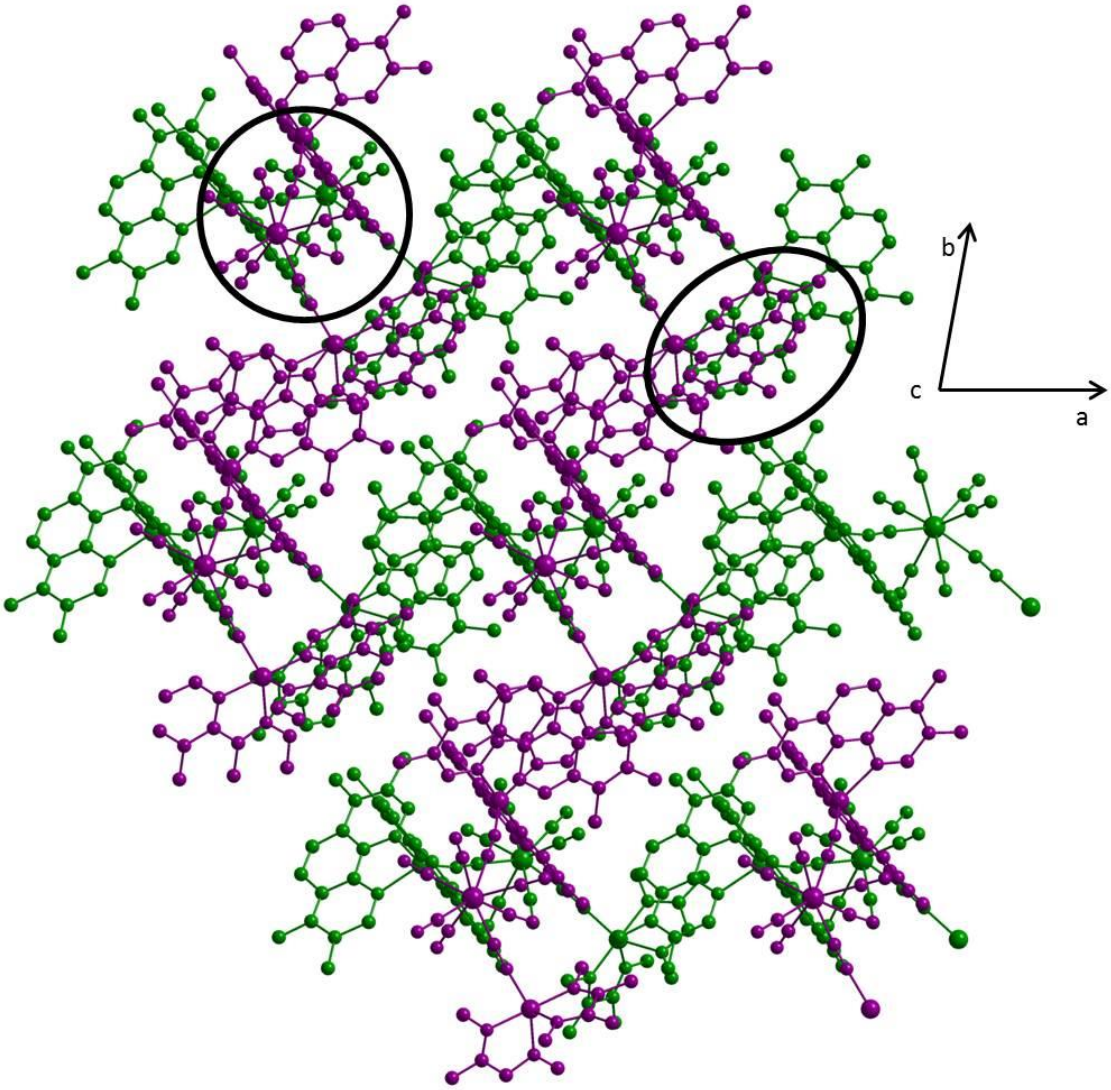

Figure 4.9 Molecular representation of the crystal packing of compound **9** illustrating the intermolecular π-π interactions between neighboring trinuclear molecules. The H-atoms and $[CF_3SO_3]^-$ anions are omitted for the sake of clarity.

interactions between trinuclear molecules creates the extended 3D packing network (Figure 4.10).

Magnetic Studies

The magnetic properties of compounds **6**, **8** and **9** were measured by DC magnetic susceptibility measurements in the temperature range of 2-300 K at an applied field of 1000 Oe. Field dependent DC magnetization measurements were performed from 0 to 7 Tesla. Measurements were carried out on crushed crystals encased in a polyethelene bag.

$[Mn(tmphen)_2]_3[W^V(CN)_8]_2$ (6). A room temperature χT value of 13.7 emu·K·mol^{-1} was observed for the trigonal bipyramidal molecule which is consistent with the expected value for three S = 5/2 and two S = 1/2 spin centers in the absence of magnetic interactions (13.8 emu·K·mol^{-1}, Figure 4.11). A plot of χT versus T shows a slight decrease followed by a sharp increase as the temperature is lowered and reaches a maximum of 27 emu·K·mol^{-1} at 2 K. This behavior is indicative of antiferromagnetic interactions between the Mn^{II} and W^V ions resulting in a ferrimagnetic ground state. The magnetic properties were modeled using the isotropic Heisenberg-Dirac Van Vleck Hamiltonian:

$$H = 2J_{Mn\text{-}W}(S_{W1} + S_{W2})(S_{Mn1} + S_{Mn2} + S_{Mn3}) + \mu_B H[g_W(S_{W1} + S_{W2}) + g_{Mn}(S_{Mn1} + S_{Mn2} + S_{Mn3})] - 3D[S^z{}_{Mn}{}^2 - (1/3)S_{Mn}(S_{Mn} + 1)] \quad \text{(Eq. 4.1)}$$

The simulation of the χT vs. T curves using this Hamiltonian and the program MAGPACK[207] resulted in the best fit parameters $g_W = 1.9$, $g_{Mn} = 2.02$, $J = -9.1$ cm^{-1}, $zJ' = 0.005$ cm^{-1}, $D = 0.3$ cm^{-1}. The field dependent magnetization curve of 5 at 1.8 K

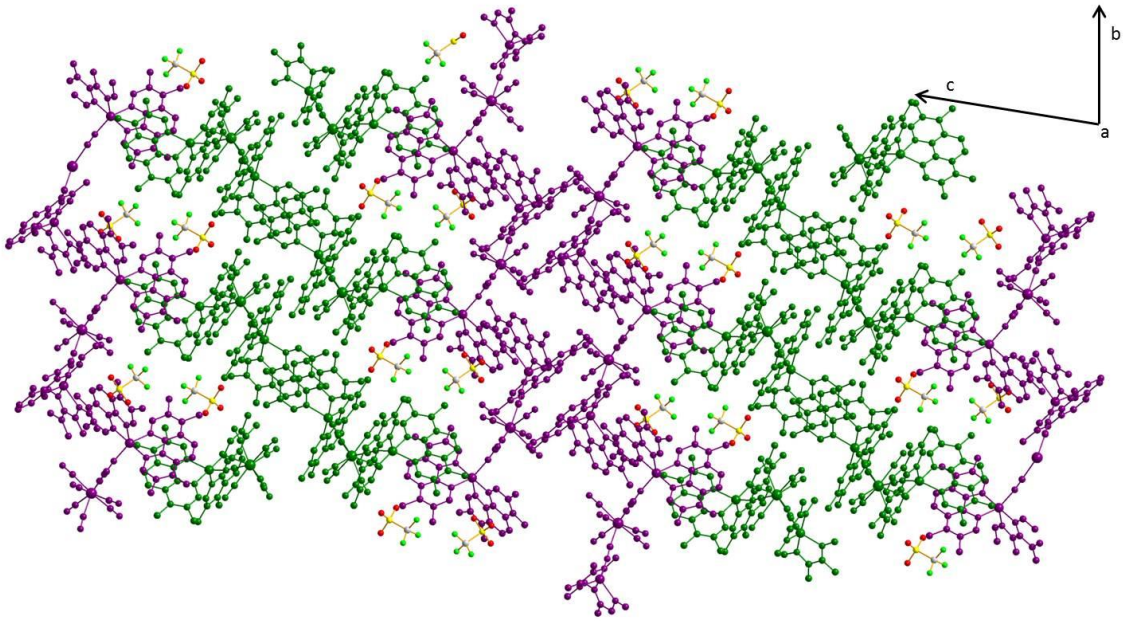

Figure 4.10 Molecular representation of the crystal packing of compound **9** in the bc-plane showing the extended 3-D π-π interactions between the trinuclear cations.

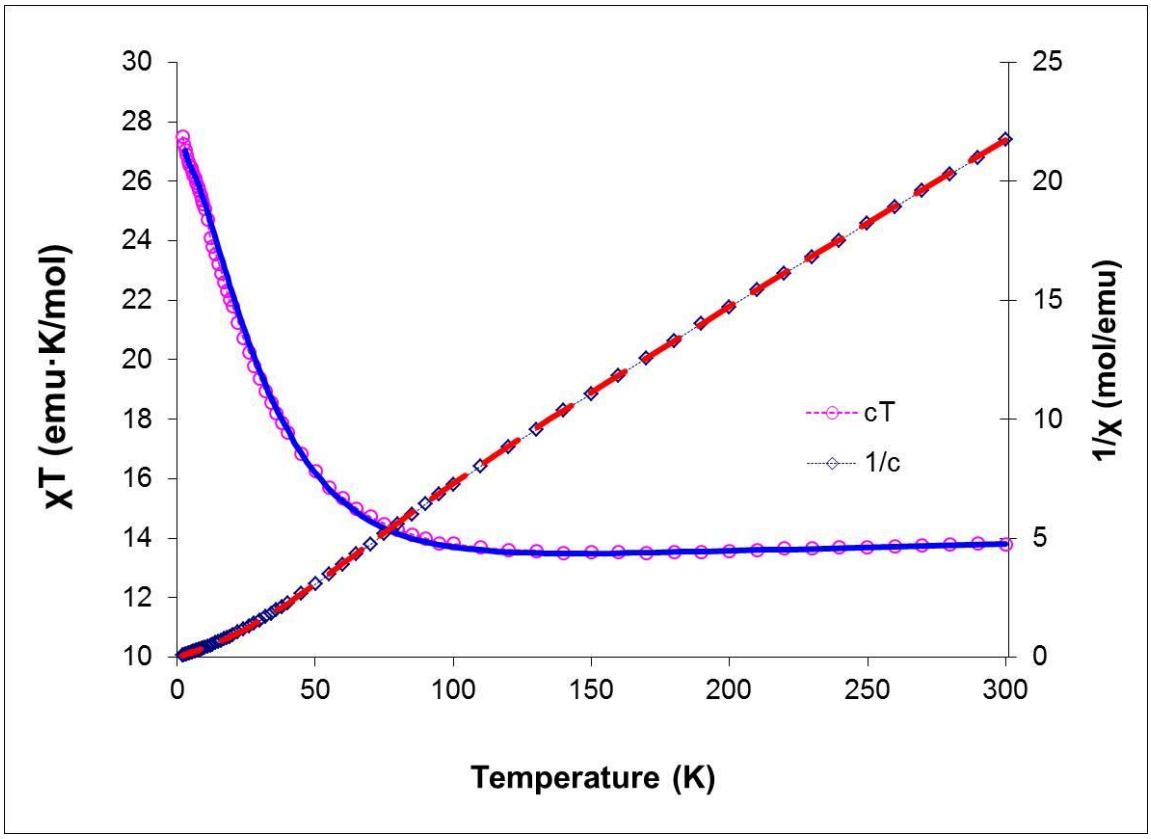

Figure 4.11 Temperature dependence of χT (O) and 1/χ (□) for **6**. The solid lines correspond to the MAGPACK simulation (g_W = 1.9, g_{Mn} = 2.02, J = -9.1 cm^{-1}, zJ' = 0.005 cm^{-1}, D = -0.3 cm^{-1}).

saturates at high fields to 13 B.M. which is in good agreement with the antiferromagnetically coupled compound with a spin ground state of S = 13/2 (Figure 4.12).

Given that previously reported cyanide compounds containing tungsten ions have been reported to exhibit SMM properties,[114,123] compound **6** was probed with ac magnetic susceptibility measurements. The ac susceptibility data under a zero applied field show a weak frequency dependent out-of-phase signal which hints at possible SMM behavior (Figure 4.13). The presence of an out-of-phase signal does not necessarily mean that a molecule is an SMM, especially when there is no maximum in the χ" vs. T plot, as is the case for compound **6**. To further explore the relaxation dynamics of 5, dc magnetization versus field scans on single crystals of **6** were carried out on a micro-SQUID apparatus. Temperature and sweep rate dependent scans, down to 0.04 K, revealed that there is no hysteresis (Figure 4.14). The micro-SQUID measurements provide evidence that compound **6** is not an SMM despite exhibiting a weak frequency dependent signal in the ac scans. As has been pointed out by others in the field, the beginning of an out-of-phase signal in the ac experiment is not sufficient evidence for concluding that a molecule is a SMM and this is a case where these data alone would have led to a false conclusion.

$[Mn_4(tmphen)_4(MeOH)_6(DMF)W^V_2(CN)_{16}]^{2+}[Mn_2(tmphen)_2(MeOH)_2(H_2O)_2W^V_2(CN)_{16}]^{2-}\}_\infty$ (8). Temperature dependent magnetic susceptibility data for compound **7** indicate antiferromagnetic coupling between the Mn^{II} ions and the W^V ions. The room temperature χT value is 13.6 emu·K·mol^{-1} (Figure 4.15) which is in good agreement to

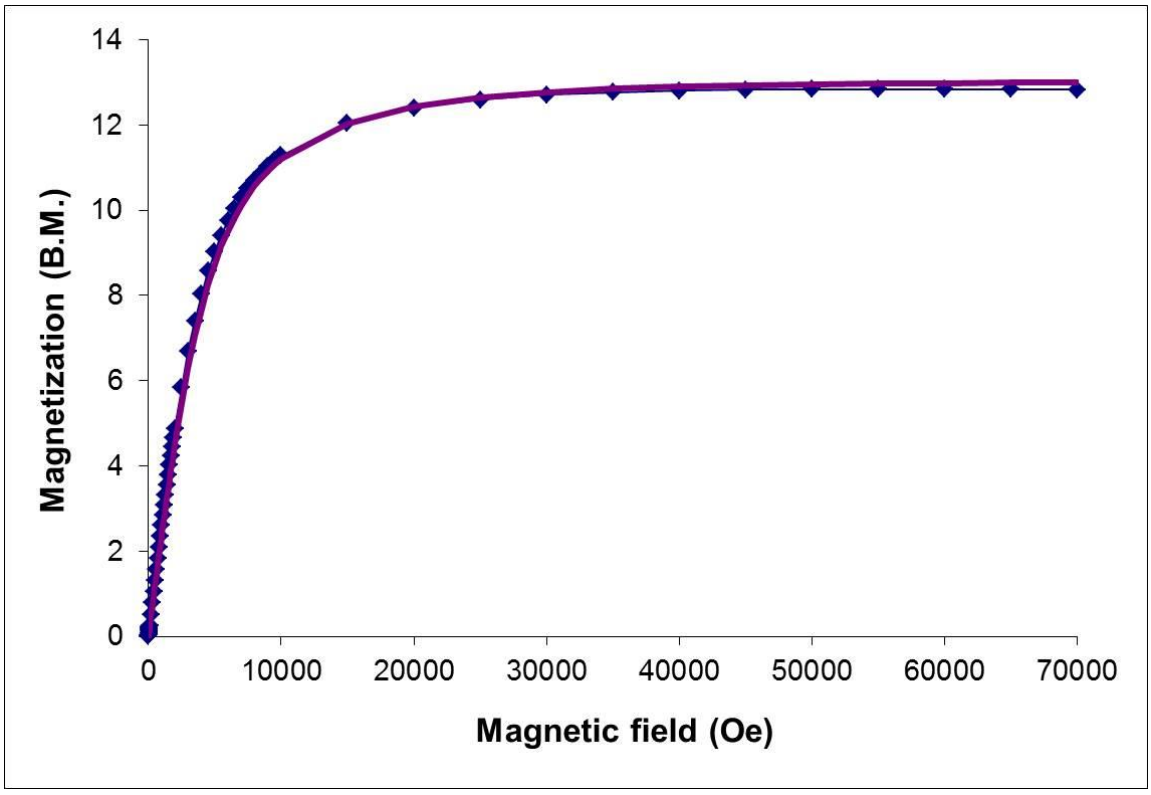

Figure 4.12 Field dependent magnetization for compound **6**. The solid line corresponds to the Brillouin function for S = 13/2, g_{avg} = 2.0.

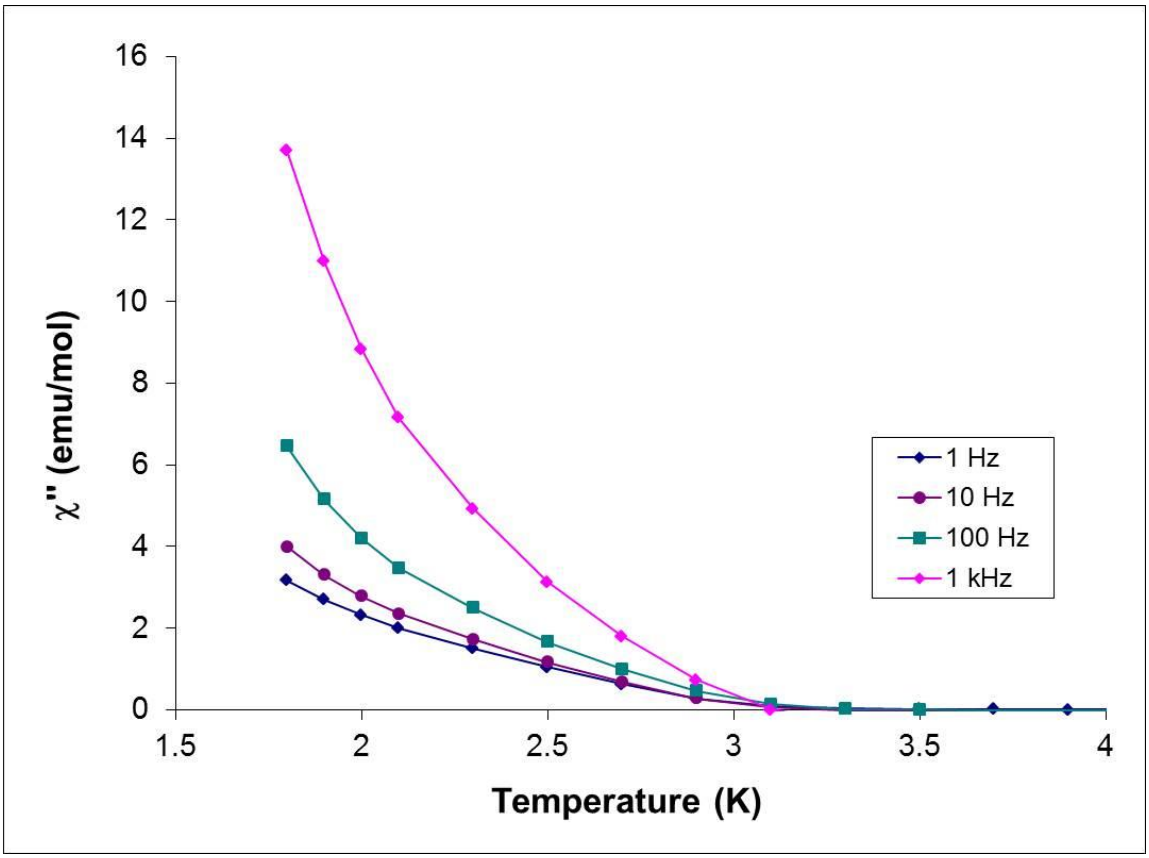

Figure 4.13 Temperature dependence of the imaginary (χ") part of the ac susceptibility for **6** with zero applied field measured under various oscillating frequencies (1 – 1500 Hz). The solid lines are a guide for the eye.

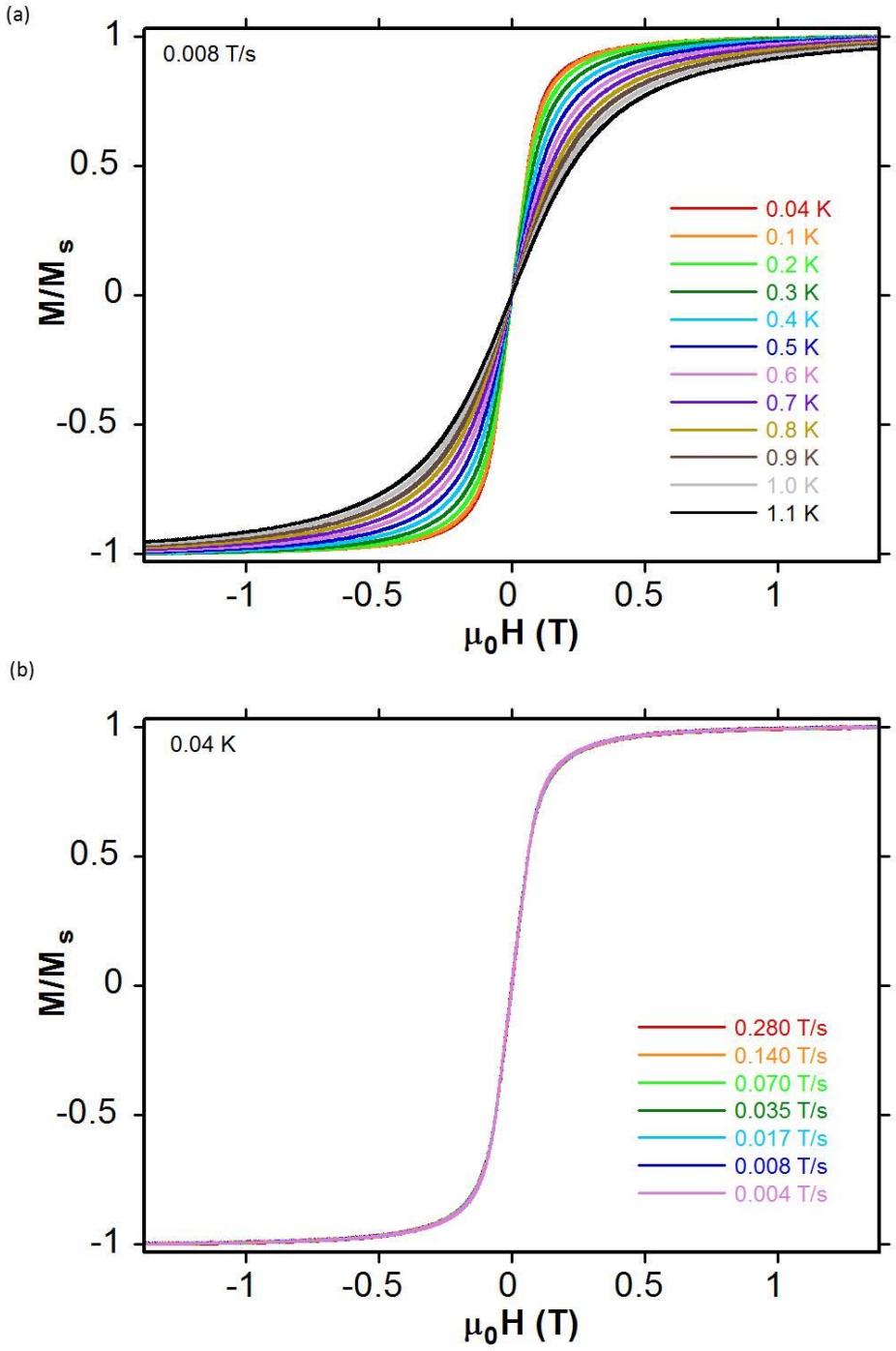

Figure 4.14 Micro-SQUID data where the field dependence of the magnetization of a single crystal of **6** is plotted (a) below 1.1 K with a sweep field rate of 0.008 T/s and (b) below a sweep rate of .280 T/s at 0.04 K.

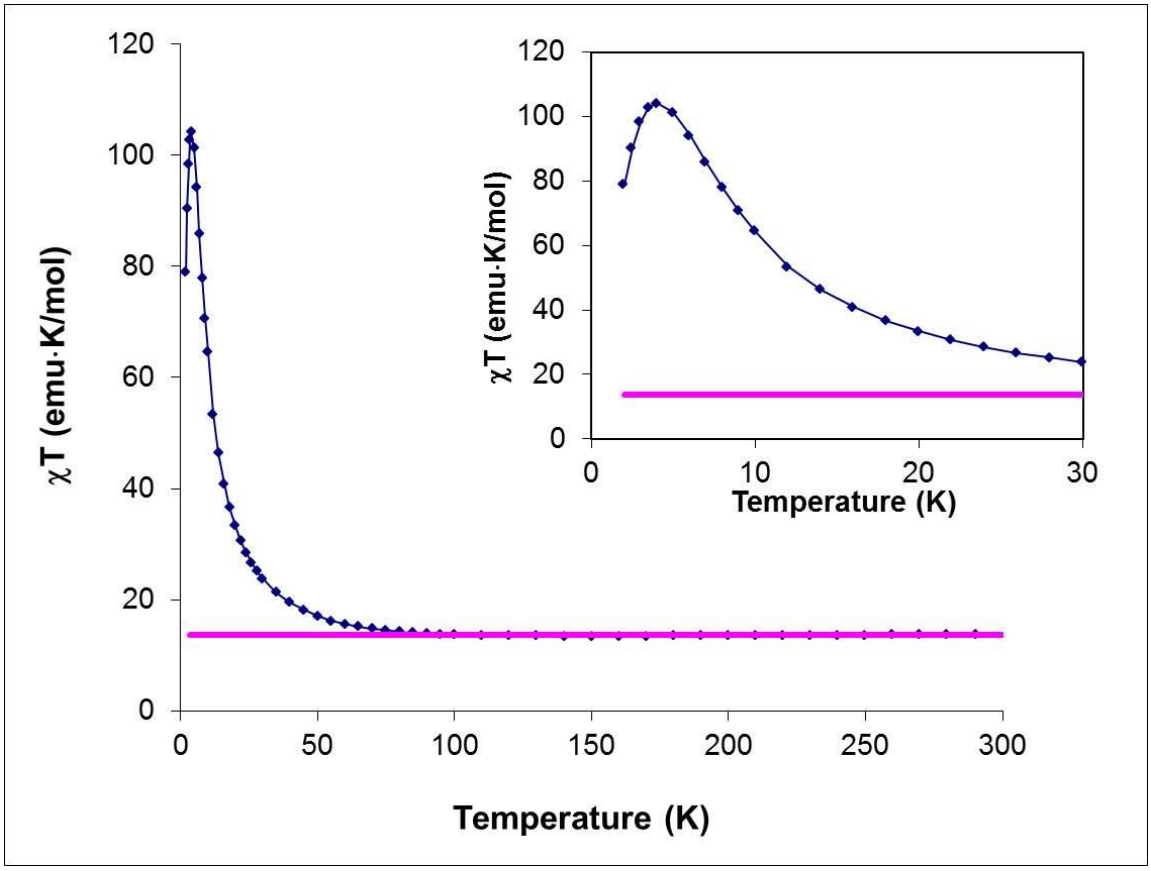

Figure 4.15 Temperature dependence of χT for **8**. The pink line serves as a guide for the eye for the room temperature value of 13.6 emu·K·mol^{-1}. Inset: Zoom of χT from 2 – 30 K which highlights the shape of the curve at low temperatures.

the spin-only value for three S = 5/2 Mn^{II} ions and two S = ½ W^{V} ions without magnetic interaction (13.8 emu·K·mol^{-1}). The χT value at 300 K for compound **8** is close to that of compound **6**, showing that the 1D chain has the same magnetic unit as the TBP molecule (3 Mn^{II} ions and 2 W^{V} ions). As the temperature is lowered, χT first decreases slightly, then increases sharply to a maximum of 104 emu·K·mol^{-1} at 4 K which is a sign of ferrimagnetic behavior with a large maximum for χT indicating that the chain may be approaching ordering. The field dependent magnetization curve of **8** at 1.8 K saturates at 7 T to a value 13 B.M. which shows the chain is an antiferromagnetically coupled system consisting of a metal core of three S = 5/2 Mn^{II} ions and two S = ½ W^{V} ions which gives a spin ground state of S = 13/2 (Figure 4.16). Compound **8** was also probed with ac susceptometry in a zero-applied field. The χ" vs. T plot of varying frequencies (1 – 1000 Hz) is shown in Figure 4.17 and exhibits a weak frequency dependent out-of-phase signal indicating a slow relaxation of the magnetization, common in chain molecules that behave as Single Chain Magnets (SCMs). As with compound **6**, the fact that there is no peak present in the ac signal, despite the fact that there is a beginning of an out-of-phase signal, is not conclusive evidence that compound **8** is a SCM.

$[Cu(tmphen)_2]_2[W(CN)_8]CF_3SO_3$ (9). Temperature dependent magnetic susceptibility data for **9** indicate ferromagnetic interactions between the S = ½ Cu^{II} ions and the S = ½ W^{V} ion (Figure 4.18). The room temperature χT vs. T value is 1.61 emu·K·mol^{-1} which is slightly higher than expected for two isolated Cu^{II} ions and one isolated W^{V} ion (1.37 emu·K·mol^{-1}). The values of χT increase as temperature decreases to reach a maximum value of 2.47 emu·K·mol^{-1}, indicative of ferromagnetic interactions. The decrease in χT

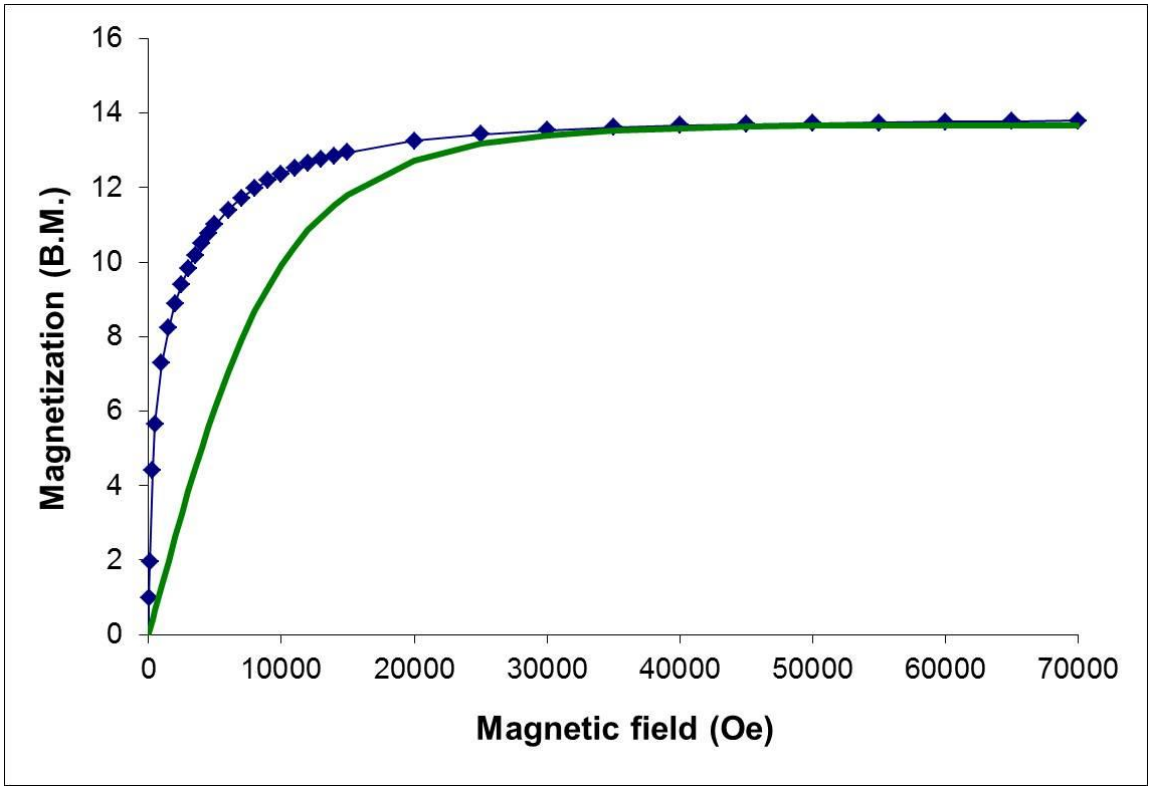

Figure 4.16 Field dependent magnetization for compound **8**. The solid line corresponds to the Brillouin function for S = 13/2, g_{avg} = 2.0.

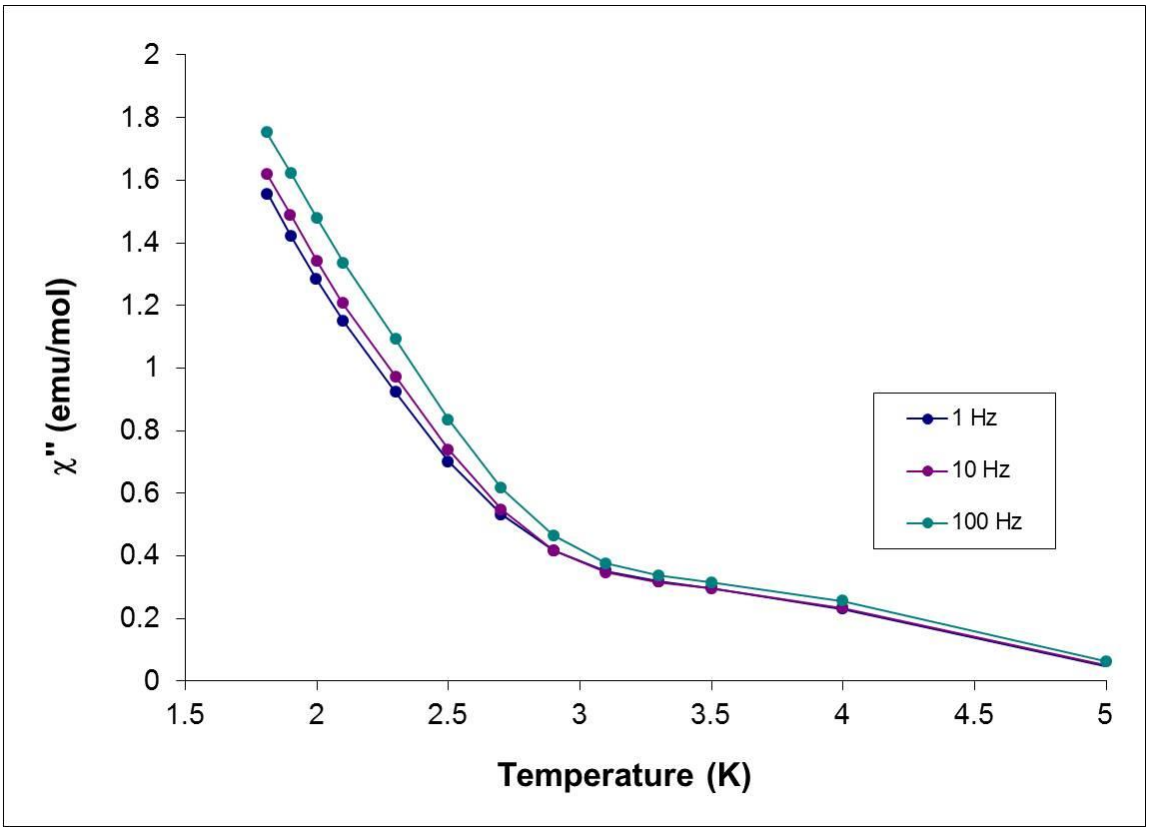

Figure 4.17 Temperature dependence of the imaginary (χ") part of the ac susceptibility for **8** with zero applied field measured under various oscillating frequencies (1 – 100 Hz). The solid lines are a guide for the eye.

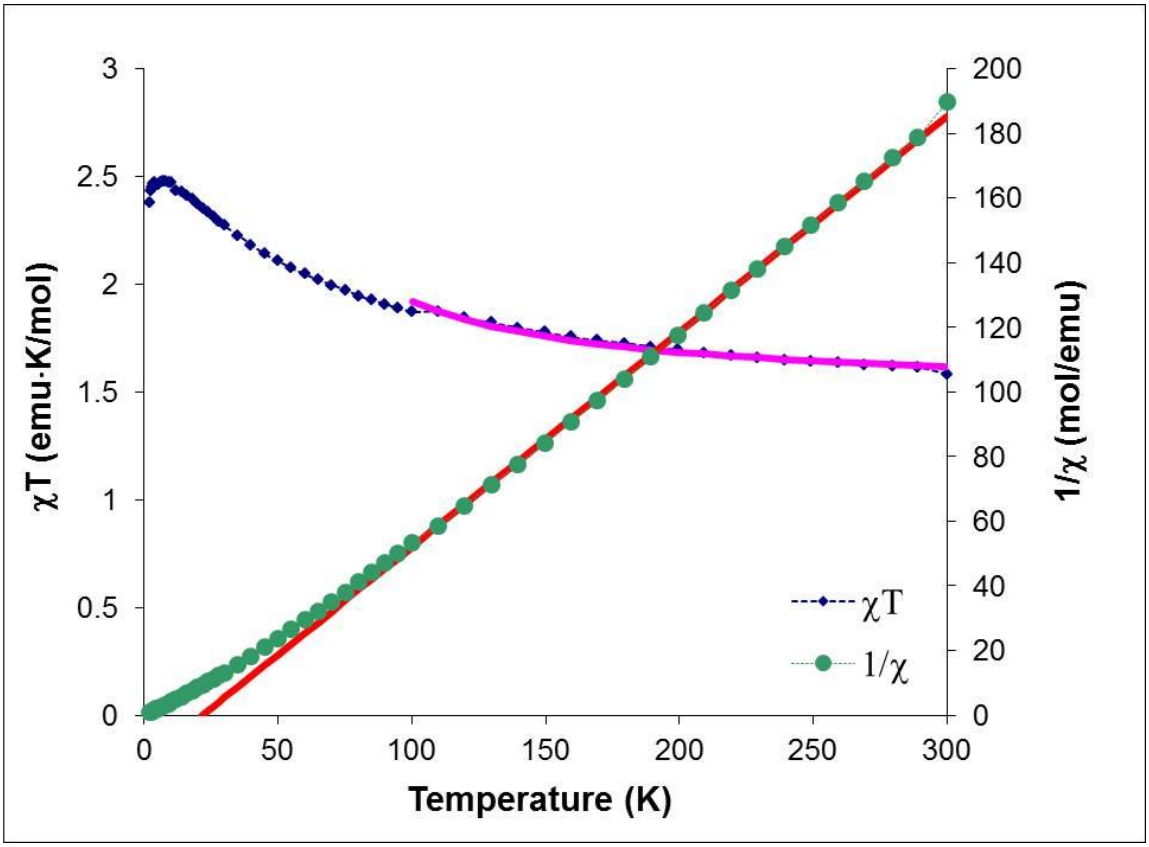

Figure 4.18 Temperature dependence of the χT product (blue diamonds) and 1/χ (green dots) for **9**. Pink line represents a Curie-Weiss simulation of the χT data above 100 K for 2 Cu^{II} S = 1/2 ions and 1 W^{IV} S = 1/2 ions. Red line represents the Curie-Weiss Law fit above 100 K with C = 1.6 $cm^3 \cdot mol^{-1} \cdot K$ and Θ = +22 K.

at low temperatures is attributed to zero-field splitting and/or intermolecular interactions. The $1/\chi$ data above 100 K obey the Curie-Weiss law with a Curie constant C = 1.6 $cm^3 \cdot mol^{-1} \cdot K$ and a Weiss temperature Θ = +22 K. The shape of the χT curve and the negative value of the Weiss constant are indications of ferromagnetic coupling between the Mn^{II} and Mo^{III} ions leading to an S = 3/2 ground state. The field dependent magnetization curve of **9** at 1.8 K saturates at high fields to 3.8 B.M. (Figure 4.19) which is higher than the expected value of 3 B.M. for the ferromagnetically coupled trinuclear molecule with a spin ground state of S = 3/2 which can be attributed to the variance of the g values at low temperature.

Conclusions

Four new complexes containing the octacyanometallate anion $[W^V(CN)_8]^{3-}$ were prepared and structurally characterized. The compounds exhibit several different structural motifs including three 0-D molecular compounds (two pentanuclear molecules and a linear trinuclear molecule) and a 1-D chain, illustrating the structural versatility of the octacyanotungstate(V) ions. A series of three compounds containing Mn^{II} ions and W^V ions were synthesized by self-assembly reactions from which the initial TBP molecule that was isolated converted into an open pentanuclear molecule which, remarkably, eventually self-assembles into a 1-D chain. The compound, $[Mn(tmphen)_2]_3[W^V(CN)_8]_2$, represents only the second time $[W(CN)_8]^{3-}$ has been incorporated into a trigonal bipyramidal molecule. Both the TBP molecule and the 1-D chain, $\{[Mn_4(tmphen)_4(MeOH)_6(DMF)W^V_2(CN)_{16}]^{2+}[Mn_2(tmphen)_2(MeOH)_2(H_2O)_2\text{-}W^V_2(CN)_{16}]^{2-}\}_\infty$, were subjected to detailed magnetic studies and exhibit the beginning

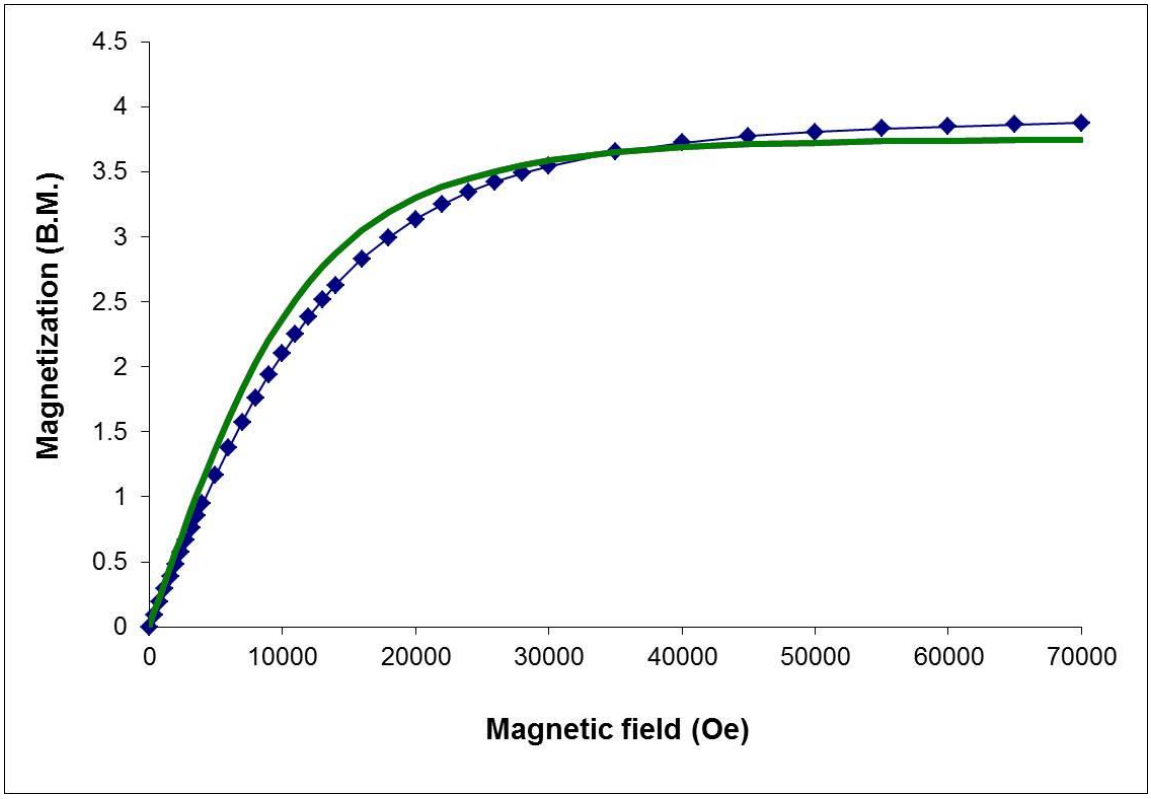

Figure 4.19 Field dependent magnetization at 1.8 K for compound **9**. The green solid line corresponds to the Brillouin function (S = 3/2, g_{Cu} = 2.4, g_W = 2.0).

of out-of-phase frequency dependent signals in the ac susceptibility measurements, an indication of slow relaxation of the magnetization. The trinuclear compound, $[Cu(tmphen)_2]_2[W(CN)_8]CF_3SO_3$, exhibits ferromagnetic coupling between the Cu^{II} ions and W^{V} ion. Ongoing studies in our laboratories are aimed at the synthesis of other compounds containing the $[W(CN)_8]^{3-}$ ion, particularly TBP molecules containing Cr^{II}, Fe^{II}, Co^{II} and Cu^{II} ions to explore their magnetic properties. This research is essential to adding to the knowledge and understanding of the magnetochemistry of octacyanotungstate ions. Moreover this study highlights the importance of kinetic products in cyanide chemistry and how it is relates to compounds of similar stabilities for the same building blocks, a topic that prevails in this area of research.

CHAPTER V

CONCLUSIONS AND FUTURE OUTLOOK

The rational design of molecular magnets is an immensely active field of research which is driven, in great measure, by the quest for improved devices for future technologies. With the discovery of Single Molecule Magnets in the 1990's came the realization that these bistable molecules with both quantum and classical behavior could provide a means for the miniaturization of technology.[16,63,64,69,71] Much research in the intervening years has focused on synthesizing SMMs with higher blocking temperatures and longer relaxation times. In response to the inherent challenges of enhancing SMM properties, researchers have turned to increasing anisotropy, with considerable success in preparing numerous small molecule and even mononuclear SMMs. One strategy that is being used in this vein is the incorporation of 4d and 5d transition metal ions into mixed metal complexes. These ions are characterized by large spin-orbit coupling (SOC) parameters which contribute to the orbital angular momenta and also, depending on the symmetry of the complex, lead to anisotropic exchange interactions.[4] Of importance in this context is the fact that theoretical work has predicted that single ion anisotropy originating from spin-orbit coupling will lead to higher blocking temperatures, T_B, for SMMs.[100-107,126] A convenient method for testing this hypothesis is to target cyanide-bridged complexes of heavier elements combined with 3d transition metals. In this vein, the work presented in this dissertation focuses on exploring the magnetic properties of

cyanide bridged materials containing the anisotropic 4d and 5d metal ions, Mo^{III}, W^{V} and Os^{III}.

A recent development in the field of molecular magnetism is the exploration of how the assembly and interaction of SMMs can be by exploited by introducing weak interactions such as hydrogen bonds.[74] These non-covalent intermolecular interactions modify the intrinsic SMM properties and provide new magnetic behavior. In Chapter II, two molecules were prepared with the purpose of investigating the effect that incorporation of 5d metal ions has on the barrier height of an SMM as compared to 3d metal ions and how intermolecular interactions between the SMMS affect the observed magnetic properties. Magnetic measurements on fresh solvated crystals of the trinuclear molecules, (PPN){[Mn(salphen)(MeOH)]$_2$[M(CN)$_6$]} (M = Fe and Os) exhibit typical SMM behavior with blocking temperatures (Mn_2Fe T_B = 11.5 cm^{-1} and Mn_2Os T_B = 13.2 cm^{-1}) comparable to other linear trinuclear species based on Mn^{III} Schiff base terminal units bridged by hexacyanometallates.[112] Measurements of dried crystals of the trinuclear compounds show pronounced enhancement of the T_B of both molecules (Mn_2Fe T_B = 17.0 cm^{-1} and Mn_2Os T_B = 28.2 cm^{-1}), moreover the blocking temperature increase by ~90% for the 5d metal analogue due to the more diffuse orbitals and magnetic anisotropy. In addition to enhanced blocking temperatures, measurements of dried crystals of the compounds on a micro-SQUID apparatus revealed a shift of the QTM from zero field, evidence of exchange bias behavior. The removal of the interstitial solvent promotes increased intermolecular interactions between the molecules and in turn, promotes enhanced magnetic properties. These results provide firm

evidence that interactions between SMMs can have significant effect on the observed properties. Furthermore, these properties can be manipulated by fine-tuning of the supporting ligands; one can design molecules with ligands that have the ability to direct self-association of molecules through weak interactions. This approach toward enhancing intrinsic SMM properties has great potential for producing materials for applications in information storage and molecular electronic devices. Further work in our labs will focus on the synthesis of additional trinuclear molecules with different $[Mn(Schiff\text{-}base)]^{+}$ units for the purpose of investigating supramolecular interactions between the SMMs. Attempts are also ongoing to synthesize the Ru^{III} analogue in order to complete the group 8 triad of compounds.

Of the known 4d and 5d cyanometallates, the $[Mo(CN)_6]^{3-}$ ion is the least studied. The compounds presented in Chapter III represent valuable additions to the small library of compounds containing the octahedral hexycyanomolybdate(III) ion. Three new trigonal bipyramidal molecules, $[M(tmphen)_2]_3[Mo(CN)_6]_2$ ($M = V^{II}$, Mn^{II} and Fe^{II}), were prepared and characterized by X-ray crystallography and, whenever the yield permitted, by magnetic measurements.

The Dunbar group previously published a large family of TBP molecules of the type $[M(tmphen)_2]_3[M'(CN)_6]_2$ (Table 5.1) with many exhibiting interesting properties such as SMM behavior, spin-crossover and charge transfer induced spin transition.[44,50,61,116,142,143,212,245-247] Working with such a large homologous family of molecules provides advantages in that one can make a direct comparison between different cyanometallate building blocks with the same co-ligands and metal ions. In

	V^{II}	Cr^{II}	Mn^{II}	Fe^{II}	Co^{II}	Ni^{II}	Zn^{II}
Cr^{III}		✓	✓	✓	✓	✓	✓
Mn^{III}			✓				
Fe^{III}			✓	✓	✓	✓	✓
Co^{III}			✓	✓	✓	✓	✓
Mo^{III}	✓		✓	✓	✓	✓	
W^{V}			✓			✓	
Ru^{III}		✓	✓	✓	✓	✓	
Os^{III}			✓	✓	✓	✓	

Table 5.1 Representative $M_3M'_2$ TBP molecules synthesized by the Dunbar group.

addition, the topology of the cluster remains the same throughout the series of these Prussian Blue analogues allowing for the establishment of extensive structure-property relationships. The Mn_3Mo_2 TBP exhibits antiferromagnetic interactions between the Mn^{II} and Mo^{III} ions through cyanide bridges. Theoretical predictions indicate that Mo^{III} ions would likely engender extremely strong magnetic coupling through a cyanide bridge with a variety of 3d transition metal ions, particularly the early 3d metal ions Cr^{II} and V^{II}.[126] Recently, Long's group reported the record antiferromagnetic coupling parameter for a cyanide bridged compound with J = -61 cm^{-1} between Mo^{III} and V^{II} lending support to these theoretical calculations. The TBP molecule V_3Mo_2 exhibits a much stronger antiferromagnetic coupling parameter (J = -134 cm^{-1}) between Mo^{III} and V^{II} ions through the cyanide bridge and the experimental data is supported by theoretical calculations by Mironov. These experimental results are important for assessing the validity of current theoretical predictions and adds to the body of work directed at understanding the magnetic interactions through cyanide ligands. Continued efforts in our laboratories will be directed at completing the family of TBP molecules containing $[Mo(CN)_6]^{3-}$, particularly the Cr_3Mo_2 analogue.

Chapter IV describes four new compounds incorporating the well-known octacyanometallate $[W^V(CN)_8]^{3-}$. The diversity of the compounds synthesized (two pentanuclear and one trinuclear 0-D molecular compounds and a 1-D chain) nicely illustrate the structural versatility of compounds based on the octacyanotungstate(V) anion. The molecule $[Mn(tmphen)_2]_3[W(CN)_8]$ represents the second time that the $[W(CN)_8]^{3-}$ ion has been incorporated into the TBP geometry. The TBP molecule

undergoes further reaction and is converted into an open pentanuclear molecule which eventually self-assembles into a 1-D chain. This series of compounds containing Mn^{II} and W^{V} ions illustrates the importance of kinetic products in cyanide chemistry given that each of these compounds was synthesized using the same reaction conditions with the reaction time being the only variable. Both the TBP molecule and the 1-D chain were subjected to magnetic studies and found to exhibit the beginning of out-of-phase signals in the AC measurements, which indicates slow relaxation of the magnetization. The fourth compound synthesized is a trinuclear molecule $[Cu(tmphen)_2]_2[W(CN)_8]CF_3SO_3$. The molecule exhibits antiferromagnetic interactions between the Cu^{II} and W^{V} ions. These results are important for understanding magnetic interactions involving the octacyanotungstate ions, particularly with the diversity of binding modes that were observed in this family of compounds. Research efforts in our laboratories continue to focus on the expansion of the family of TBP compounds containing $[W(CN)_8]^{3-}$, in particular those containing divalent metal ions Cr^{II}, Fe^{II}, Co^{II} and Cu^{II}.

The molecules presented in this dissertation provide clear evidence for the effectiveness of 4d and 5d metal ions in improving magnetic interactions in molecular materials. The detailed magnetic studies of the exchange biased trinuclear compounds show that incorporation of $[Os(CN)_6]^{3-}$ ions significantly improves the SMM properties as compared to the 3d analogue. In addition, the results support the contention that, by judicious choice of ligands, chemists can exert fine control over intermolecular interactions that influence magnetic properties. The continued studies of these issues

will allow for a deeper understanding of the subtleties of self-assembled SMMs with the eventual goal being to tailor these interactions for use in devices. There is a need for fundamental research to add to the understanding of the nature magnetic interactions of 4d and 5d metal ions to be able to develop more precise theoretical models for predicting the behavior of magnetic materials based on them. Given the small body of existing experimental work on $[Mo(CN)_6]^3$, the new chemistry presented in this dissertation will be valuable for comparing the intriguing theoretical predictions of magnetic interactions with experimental results. With the improved magnetic communication afforded by these 4d and 5d metal ions and the possibility of fine-tuning interactions by ligand design, the potential to form functional magnetic materials is becoming closer to reality.

REFERENCES

(1) Shatruk, M.; Avendaño, C.; Dunbar, K. R. In *Progress in Inorganic Chemistry, Vol 56*; John Wiley & Sons, Inc.: New York 2009; Vol. 56, p 155.

(2) Gatteschi, D.; Sessoli, R.; Villain, J. *Molecular Nanomagnets*; Oxford University Press: Oxford, 2006.

(3) Kahn, O. *Accounts of Chemical Research* **2000**, *33*, 647.

(4) Wang, X.-Y.; Avendano, C.; Dunbar, K. R. *Chem. Soc. Rev.* **2011**, *40*, 3213.

(5) Day, P. *Science* **1993**, *261*, 431.

(6) Gatteschi, D.; Sessoli, R. *Journal of Magnetism and Magnetic Materials* **2004**, *272–276, Part 2*, 1030.

(7) Miller, J. S.; Gatteschi, D. *Chem. Soc. Rev.* **2011**, *40*, 3065.

(8) Miller, J. S. *Adv. Mat.* **1990**, *2*, 98.

(9) Alivisatos, P.; Barbara, P. F.; Castleman, A. W.; Chang, J.; Dixon, D. A.; Klein, M. L.; McLendon, G. L.; Miller, J. S.; Ratner, M. A.; Rossky, P. J.; Stupp, S. I.; Thompson, M. E. *Adv. Mat.* **1998**, *10*, 1297.

(10) Miller, J. S. *Adv. Mat.* **1993**, *5*, 587.

(11) Gatteschi, D. *Adv. Mat.* **1994**, *6*, 635.

(12) Tejada, J.; Chudnovsky, E. M.; Barco, E. d.; Hernandez, J. M.; Spiller, T. P. *Nanotechnology* **2001**, *12*, 181.

(13) Troiani, F.; Affronte, M. *Chem. Soc. Rev.* **2011**, *40*, 3119.

(14) Bogani, L.; Wernsdorfer, W. *Nat Mater* **2008**, *7*, 179.

(15) Stamp, P. C. E.; Gaita-Arino, A. *Journal of Materials Chemistry* **2009**, *19*, 1718.

(16) Wolf, S. A.; Awschalom, D. D.; Buhrman, R. A.; Daughton, J. M.; von Molnár, S.; Roukes, M. L.; Chtchelkanova, A. Y.; Treger, D. M. *Science* **2001**, *294*, 1488.

(17) Rocha, A. R.; Garcia-suarez, V. M.; Bailey, S. W.; Lambert, C. J.; Ferrer, J.; Sanvito, S. *Nat Mater* **2005**, *4*, 335.

(18) Ardavan, A.; Rival, O.; Morton, J. J. L.; Blundell, S. J.; Tyryshkin, A. M.; Timco, G. A.; Winpenny, R. E. P. *Physical Review Letters* **2007**, *98*, 057201.

(19) Cheon, J.; Lee, J.-H. *Accounts of Chemical Research* **2008**, *41*, 1630.

(20) Bohigas, X.; Tejada, J.; Torres, F.; Arnaudas, J. I.; Joven, E.; del Moral, A. *Applied Physics Letters* **2002**, *81*, 2427.

(21) Ohkoshi, S.-i.; Fujishima, A.; Hashimoto, K. *J. Am. Chem. Soc.* **1998**, *120*, 5349.

(22) Verdaguer, M.; Bleuzen, A.; Marvaud, V.; Vaissermann, J.; Seuleiman, M.; Desplanches, C.; Scuiller, A.; Train, C.; Garde, R.; Gelly, G.; Lomenech, C.; Rosenman, I.; Veillet, P.; Cartier, C.; Villain, F. *Coord. Chem. Rev.* **1999**, *190–192*, 1023.

(23) Kurmoo, M. *Chem. Soc. Rev.* **2009**, *38*, 1353.

(24) Coronado, E.; Day, P. *Chemical Reviews* **2004**, *104*, 5419.

(25) Atanasov, M.; Comba, P.; Hausberg, S.; Martin, B. *Coord. Chem. Rev.* **2009**, *253*, 2306.

(26) Tasiopoulos, A. J.; Perlepes, S. P. *Dalt. Trans.* **2008**, *0*, 5537.

(27) Goswami, T.; Misra, A. *J. Phys. Chem. A* **2012**, *116*, 5207.

(28) Sieklucka, B.; Podgajny, R.; Pinkowicz, D.; Nowicka, B.; Korzeniak, T.; Balanda, M.; Wasiutynski, T.; Pelka, R.; Makarewicz, M.; Czapla, M.; Rams, M.; Gawel, B.; Lasocha, W. *CrystEngComm* **2009**, *11*, 2032.

(29) Karadas, F.; Schelter, E. J.; Shatruk, M.; Prosvirin, A. V.; Bacsa, J.; Smirnov, D.; Ozarowski, A.; Krzystek, J.; Telser, J.; Dunbar, K. R. *Inorg. Chem.* **2008**, *47*, 2074.

(30) *Bimetallic Magnets: Present and Perspectives*; Wiley-VCH: Weinheim, 2003; Vol. IV.

(31) Sato, O.; Tao, J.; Zhang, Y.-Z. *Angew. Chem. Int. Ed.* **2007**, *46*, 2152.

(32) Siretanu, D.; Li, D.; Buisson, L.; Bassani, D. M.; Holmes, S. M.; Mathonière, C.; Clérac, R. *Chem. Eur. J.* **2011**, *17*, 11704.

(33) Carlin, R. L. *Magnetochemistry*; Springer-Verlag: West Berlin, Heidelberg: New York, Tokyo, 1986.

(34) Kahn, O. *Molecular Magnetism*; Wiley-VCH, 1993.

(35) Goodenough, J. B. *Journal of Physics and Chemistry of Solids* **1958**, *6*, 287.

(36) Goodenough, J. B. *Magnetism and the Chemical Bond*; Interscience-Wiley: New York, 1963; Vol. 1.

(37) Kanamori, J. *Journal of Physics and Chemistry of Solids* **1959**, *10*, 87.

(38) Van Vleck, J. H. *The Theory of Electric and Magnetic Susceptibilities*; reprint ed.; Oxford University Press, 1965.

(39) Manriquez, J. M.; Yee, G. T.; Mclean, R. S.; Epstein, A. J.; Miller, J. S. *Science* **1991**, *252*, 1415.

(40) Ferlay, S.; Mallah, T.; Ouahes, R.; Veillet, P.; Verdaguer, M. *Nature* **1995**, *378*, 701.

(41) Dujardin, E.; Ferlay, S.; Phan, X.; Desplanches, C.; Moulin, C. C. D.; Sainctavit, P.; Baudelet, F.; Dartyge, E.; Veillet, P.; Verdaguer, M. *J. Am. Chem. Soc.* **1998**, *120*, 11347.

(42) Hatlevik, O.; Buschmann, W. E.; Zhang, J.; Manson, J. L.; Miller, J. S. *Adv. Mat.* **1999**, *11*, 914.

(43) Verdaguer, M.; Girolami, G. S. *Magnetic Prussian Blue Analogs*; Wiley-VCH: Weinheim, 2005; Vol. V.

(44) Funck, K. E.; Hilfiger, M. G.; Berlinguette, C. P.; Shatruk, M.; Wernsdorfer, W.; Dunbar, K. R. *Inorg. Chem.* **2009**, *48*, 3438.

(45) Pejakovic, D. A.; Manson, J. L.; Miller, J. S.; Epstein, A. J. *J. App. Phys.* **2000**, *87*, 6028.

(46) Sato, O.; Einaga, Y.; Fujishima, A.; Hashimoto, K. *Inorg. Chem.* **1999**, *38*, 4405.

(47) Sato, O.; Iyoda, T.; Fujishima, A.; Hashimoto, K. *Science* **1996**, *272*, 704.

(48) Verdaguer, M. *Science* **1996**, *272*, 698.

(49) Li, D.; Clérac, R.; Roubeau, O.; Harté, E.; Mathonière, C.; Le Bris, R.; Holmes, S. M. *J. Am. Chem. Soc.* **2007**, *130*, 252.

(50) Funck, K. E.; Prosvirin, A. V.; Mathonière, C.; Clérac, R.; Dunbar, K. R. *Inorg. Chem.* **2011**, *50*, 2782.

(51) Kosaka, W.; Nomura, K.; Hashimoto, K.; Ohkoshi, S.-i. *J. Am. Chem. Soc.* **2005**, *127*, 8590.

(52) Papanikolaou, D.; Kosaka, W.; Margadonna, S.; Kagi, H.; Ohkoshi, S.-i.; Prassides, K. *J. Phys. Chem. C* **2007**, *111*, 8086.

(53) Papanikolaou, D.; Margadonna, S.; Kosaka, W.; Ohkoshi, S.-i.; Brunelli, M.; Prassides, K. *J. Am. Chem. Soc.* **2006**, *128*, 8358.

(54) Shatruk, M.; Dragulescu-Andrasi, A.; Chambers, K. E.; Stoian, S. A.; Bominaar, E. L.; Achim, C.; Dunbar, K. R. *J. Am. Chem. Soc.* **2007**, *129*, 6104.

(55) Le Guennic, B.; Borshch, S.; Robert, V. *Inorg. Chem.* **2007**, *46*, 11106.

(56) Shimamoto, N.; Ohkoshi, S.-i.; Sato, O.; Hashimoto, K. *Inorg. Chem.* **2002**, *41*, 678.

(57) Bleuzen, A.; Lomenech, C.; Escax, V.; Villain, F.; Varret, F.; Cartier dit Moulin, C.; Verdaguer, M. *J. Am. Chem. Soc.* **2000**, *122*, 6648.

(58) Bleuzen, A.; Marvaud, V. r.; Mathoniere, C.; Sieklucka, B.; Verdaguer, M. *Inorg. Chem.* **2009**, *48*, 3453.

(59) Escax, V.; Bleuzen, A.; Cartier dit Moulin, C.; Villain, F.; Goujon, A.; Varret, F.; Verdaguer, M. *J. Am. Chem. Soc.* **2001**, *123*, 12536.

(60) Sato, O.; Einaga, Y.; Iyoda, T.; Fujishima, A.; Hashimoto, K. *J. Elect. Soc.* **1997**, *144*, L11.

(61) Berlinguette, C. P.; Dragulescu-Andrasi, A.; Sieber, A.; Güdel, H.-U.; Achim, C.; Dunbar, K. R. *J. Am. Chem. Soc.* **2005**, *127*, 6766.

(62) Dunbar, K. R.; Achim, C.; Shatruk, M. In *Spin-Crossover Materials*; John Wiley & Sons Ltd: 2013, p 171.

(63) Sessoli, R.; Gatteschi, D.; Caneschi, A.; Novak, M. A. *Nature* **1993**, *365*, 141.

(64) Sessoli, R.; Tsai, H. L.; Schake, A. R.; Wang, S.; Vincent, J. B.; Folting, K.; Gatteschi, D.; Christou, G.; Hendrickson, D. N. *J. Am. Chem. Soc.* **1993**, *115*, 1804.

(65) *Nanosized Magnetic Materials*; Wiley-VCH: Weinheim, 2002; Vol. III.

(66) Thomas, L.; Lionti, F.; Ballou, R.; Gatteschi, D.; Sessoli, R.; Barbara, B. *Nature* **1996**, *383*, 145.

(67) Aubin, S. M. J.; Dilley, N. R.; Pardi, L.; Krzystek, J.; Wemple, M. W.; Brunel, L.-C.; Maple, M. B.; Christou, G.; Hendrickson, D. N. *J. Am. Chem. Soc.* **1998**, *120*, 4991.

(68) Sangregorio, C.; Ohm, T.; Paulsen, C.; Sessoli, R.; Gatteschi, D. *Physical Review Letters* **1997**, *78*, 4645.

(69) Barbara, B.; Thomas, L.; Lionti, F.; Chiorescu, I.; Sulpice, A. *Journal of Magnetism and Magnetic Materials* **1999**, *200*, 167.

(70) Lecren, L.; Roubeau, O.; Coulon, C.; Li, Y.-G.; Le Goff, X. F.; Wernsdorfer, W.; Miyasaka, H.; Clérac, R. *J. Am. Chem. Soc.* **2005**, *127*, 17353.

(71) Wernsdorfer, W.; Sessoli, R. *Science* **1999**, *284*, 133.

(72) Bagai, R.; Christou, G. *Chem. Soc. Rev.* **2009**, *38*, 1011.

(73) Gatteschi, D.; Sessoli, R. *Angew. Chem. Int. Ed.* **2003**, *42*, 268.

(74) Jeon, I.-R.; Clerac, R. *Dalt. Trans.* **2012**, *41*, 9569.

(75) Lis, T. *Acta Crystallographica Section B* **1980**, *36*, 2042.

(76) Caneschi, A.; Gatteschi, D.; Sessoli, R.; Barra, A. L.; Brunel, L. C.; Guillot, M. *J. Am. Chem. Soc.* **1991**, *113*, 5873.

(77) Friedman, J. R.; Sarachik, M. P.; Tejada, J.; Ziolo, R. *Physical Review Letters* **1996**, *76*, 3830.

(78) Christou, G. *Poly.* **2005**, *24*, 2065.

(79) Christou, G.; Gatteschi, D.; Hendrickson, D. N.; Sessoli, R. *MRS Bulletin* **2000**, *25*, 66.

(80) Foguet-Albiol, D.; O'Brien, T. A.; Wernsdorfer, W.; Moulton, B.; Zaworotko, M. J.; Abboud, K. A.; Christou, G. *Angew. Chem. Int. Ed.* **2005**, *44*, 897.

(81) Torres, F.; Hernández, J. M.; Bohigas, X.; Tejada, J. *Applied Physics Letters* **2000**, *77*.

(82) Eppley, H. J.; Tsai, H.-L.; de Vries, N.; Folting, K.; Christou, G.; Hendrickson, D. N. *J. Am. Chem. Soc.* **1995**, *117*, 301.

(83) Pederson, M. R.; Khanna, S. N. *Physical Review B* **1999**, *60*, 9566.

(84) Arom, G.; Aubin, S. M. J.; Bolcar, M. A.; Christou, G.; Eppley, H. J.; Folting, K.; Hendrickson, D. N.; Huffman, J. C.; Squire, R. C.; Tsai, H.-L.; Wang, S.; Wemple, M. W. *Poly.* **1998**, *17*, 3005.

(85) Tasiopoulos, A. J.; Wernsdorfer, W.; Abboud, K. A.; Christou, G. *Inorg. Chem.* **2005**, *44*, 6324.

(86) Soler, M.; Wernsdorfer, W.; Sun, Z.; Ruiz, D.; Huffman, J. C.; Hendrickson, D. N.; Christou, G. *Poly.* **2003**, *22*, 1783.

(87) Brockman, J. T.; Abboud, K. A.; Hendrickson, D. N.; Christou, G. *Poly.* **2003**, *22*, 1765.

(88) Murugesu, M.; Wernsdorfer, W.; Abboud, K. A.; Brechin, E. K.; Christou, G. *Dalt. Trans.* **2006**, *0*, 2285.

(89) Chakov, N. E.; Lee, S.-C.; Harter, A. G.; Kuhns, P. L.; Reyes, A. P.; Hill, S. O.; Dalal, N. S.; Wernsdorfer, W.; Abboud, K. A.; Christou, G. *J. Am. Chem. Soc.* **2006**, *128*, 6975.

(90) Chakov, N. E.; Abboud, K. A.; Zakharov, L. N.; Rheingold, A. L.; Hendrickson, D. N.; Christou, G. *Poly.* **2003**, *22*, 1759.

(91) Soler, M.; Wernsdorfer, W.; Sun, Z.; Huffman, J. C.; Hendrickson, D. N.; Christou, G. *Chem. Commun.* **2003**, *0*, 2672.

(92) King, P.; Wernsdorfer, W.; Abboud, K. A.; Christou, G. *Inorg. Chem.* **2005**, *44*, 8659.

(93) Soler, M.; Artus, P.; Folting, K.; Huffman, J. C.; Hendrickson, D. N.; Christou, G. *Inorg. Chem.* **2001**, *40*, 4902.

(94) Artus, P.; Boskovic, C.; Yoo, J.; Streib, W. E.; Brunel, L.-C.; Hendrickson, D. N.; Christou, G. *Inorg. Chem.* **2001**, *40*, 4199.

(95) Tsai, H.-L.; Eppley, H. J.; de Vries, N.; Folting, K.; Christou, G.; Hendrickson, D. N. *Journal of the Chemical Society, Chemical Communications* **1994**, *0*, 1745.

(96) Milios, C. J.; Vinslava, A.; Wernsdorfer, W.; Moggach, S.; Parsons, S.; Perlepes, S. P.; Christou, G.; Brechin, E. K. *J. Am. Chem. Soc.* **2007**, *129*, 2754.

(97) Ako, A. M.; Hewitt, I. J.; Mereacre, V.; Clérac, R.; Wernsdorfer, W.; Anson, C. E.; Powell, A. K. *Angew. Chem. Int. Ed.* **2006**, *45*, 4926.

(98) Murugesu, M.; Takahashi, S.; Wilson, A.; Abboud, K. A.; Wernsdorfer, W.; Hill, S.; Christou, G. *Inorg. Chem.* **2008**, *47*, 9459.

(99) Tasiopoulos, A. J.; Vinslava, A.; Wernsdorfer, W.; Abboud, K. A.; Christou, G. *Angew. Chem. Int. Ed.* **2004**, *43*, 2117.

(100) Mironov, V. *Dokl. Phys. Chem.* **2006**, *408*, 130.

(101) Mironov, V. S. *Dokl. Phys. Chem.* **2007**, *415*, 199.

(102) Mironov, V. S.; Chibotaru, L. F.; Ceulemans, A. *J. Am. Chem. Soc.* **2003**, *125*, 9750.

(103) Ostrovsky, S. M.; Klokishner, S. I.; Palii, A. V.; Dunbar, K. R. *J. Mol. Struct.* **2007**, *838*, 138.

(104) Palii, A.; Ostrovsky, S. M.; Klokishner, S. I.; Tsukerblat, B. S.; Dunbar, K. R. *ChemPhysChem* **2006**, *7*, 871.

(105) Palii, A. V.; Ostrovsky, S. M.; Klokishner, S. I.; Tsukerblat, B. S.; Schelter, E. J.; Prosvirin, A. V.; Dunbar, K. R. *Inorg. Chim. Acta* **2007**, *360*, 3915.

(106) Waldmann, O. *Inorg. Chem.* **2007**, *46*, 10035.

(107) Ruiz, E.; Cirera, J.; Cano, J.; Alvarez, S.; Loose, C.; Kortus, J. *Chem. Commun.* **2008**, *0*, 52.

(108) Oshio, H.; Nakano, M. *Chem. Eur. J.* **2005**, *11*, 5178.

(109) Neese, F.; Pantazis, D. A. *Faraday Discussions* **2011**, *148*, 229.

(110) Freedman, D. E.; Jenkins, D. M.; Iavarone, A. T.; Long, J. R. *J. Am. Chem. Soc.* **2008**, *130*, 2884.

(111) Pedersen, K. S.; Dreiser, J.; Nehrkorn, J.; Gysler, M.; Schau-Magnussen, M.; Schnegg, A.; Holldack, K.; Bittl, R.; Piligkos, S.; Weihe, H.; Tregenna-Piggott, P.; Waldmann, O.; Bendix, J. *Chem. Commun.* **2011**, *47*, 6918.

(112) Pedersen, K. S.; Schau-Magnussen, M.; Bendix, J.; Weihe, H.; Palii, A. V.; Klokishner, S. I.; Ostrovsky, S.; Reu, O. S.; Mutka, H.; Tregenna-Piggott, P. L. W. *Chem. Eur. J.* **2010**, *16*, 13458.

(113) Palii, A.; Tsukerblat, B.; Klokishner, S.; Dunbar, K. R.; Clemente-Juan, J. M.; Coronado, E. *Chem. Soc. Rev.* **2011**, *40*, 3130.

(114) Lim, J. H.; Yoon, J. H.; Kim, H. C.; Hong, C. S. *Angew. Chem. Int. Ed.* **2006**, *45*, 7424.

(115) Song, Y.; Zhang, P.; Ren, X.-M.; Shen, X.-F.; Li, Y.-Z.; You, X.-Z. *J. Am. Chem. Soc.* **2005**, *127*, 3708.

(116) Hilfiger, M. G.; Zhao, H. H.; Prosvirin, A.; Wernsdorfer, W.; Dunbar, K. R. *Dalt. Trans.* **2009**, 5155.

(117) Venkatakrishnan, T. S.; Sahoo, S.; Bréfuel, N.; Duhayon, C.; Paulsen, C.; Barra, A.-L.; Ramasesha, S.; Sutter, J.-P. *J. Am. Chem. Soc.* **2010**, *132*, 6047.

(118) Schelter, E. J.; Karadas, F.; Avendaño, C.; Prosvirin, A. V.; Wernsdorfer, W.; Dunbar, K. R. *J. Am. Chem. Soc.* **2007**, *129*, 8139.

(119) Schelter, E. J.; Prosvirin, A. V.; Dunbar, K. R. *J. Am. Chem. Soc.* **2004**, *126*, 15004.

(120) Schelter, E. J.; Prosvirin, A. V.; Reiff, W. M.; Dunbar, K. R. *Angew. Chem. Int. Ed.* **2004**, *43*, 4912.

(121) Sieklucka, B.; Podgajny, R.; Korzeniak, T.; Nowicka, B.; Pinkowicz, D.; Kozieł, M. *European Journal of Inorganic Chemistry* **2011**, *2011*, 305.

(122) Sieklucka, B.; Podgajny, R.; Przychodzen, P.; Korzeniak, T. *Coord. Chem. Rev.* **2005**, *249*, 2203.

(123) Lim, J. H.; Yoo, H. S.; Yoon, J. H.; Koh, E. K.; Kim, H. C.; Hong, C. S. *Poly.* **2008**, *27*, 299.

(124) Zhang, Y.-Q.; Luo, C.-L. *Inorg. Chem.* **2009**, *48*, 10486.

(125) Zhang, Y.-Q.; Luo, C.-L. *Dalt. Trans.* **2008**, *0*, 4575.

(126) Ruiz, E.; Rodríguez-Fortea, A.; Alvarez, S.; Verdaguer, M. *Chem. Eur. J.* **2005**, *11*, 2135.

(127) Entley, W. R.; Treadway, C. R.; Girolami, G. S. *Molecular Crystals and Liquid Crystals Science and Technology. Section A. Molecular Crystals and Liquid Crystals* **1995**, *273*, 153.

(128) Weihe, H.; Güdel, H. U. *Comments on Inorganic Chemistry* **2000**, *22*, 75.

(129) Young, R. C. *J. Am. Chem. Soc.* **1932**, *54*, 1402.

(130) Kahn, O.; Larionova, J.; Ouahab, L. *Chem. Commun.* **1999**, *0*, 945.

(131) Gillon, B.; Goujon, A.; Willemin, S.; Larionova, J.; Desplanches, C.; Ruiz, E.; André, G.; Stride, J. A.; Guérin, C. *Inorg. Chem.* **2007**, *46*, 1090.

(132) Larionova, J.; Clérac, R.; Donnadieu, B.; Guérin, C. *Chem. Eur. J.* **2002**, *8*, 2712.

(133) Milon, J.; Daniel, M.-C.; Kaiba, A.; Guionneau, P.; Brandès, S.; Sutter, J.-P. *J. Am. Chem. Soc.* **2007**, *129*, 13872.

(134) Tomono, K.; Tsunobuchi, Y.; Nakabayashi, K.; Ohkoshi, S.-i. *Inorg. Chem.* **2010**, *49*, 1298.

(135) Larionova, J.; Clérac, R.; Sanchiz, J.; Kahn, O.; Golhen, S.; Ouahab, L. *J. Am. Chem. Soc.* **1998**, *120*, 13088.

(136) Tanase, S.; Tuna, F.; Guionneau, P.; Maris, T.; Rombaut, G.; Mathonière, C.; Andruh, M.; Kahn, O.; Sutter, J.-P. *Inorg. Chem.* **2003**, *42*, 1625.

(137) Wang, Q.-L.; Southerland, H.; Li, J.-R.; Prosvirin, A. V.; Zhao, H.; Dunbar, K. R. *Angew. Chem. Int. Ed.* **2012**, *51*, 9321.

(138) Kaur Sra, A.; Andruh, M.; Kahn, O.; Golhen, S.; Ouahab, L.; Yakhmi, J. V. *Angew. Chem. Int. Ed.* **1999**, *38*, 2606.

(139) Wang, X.-Y.; Prosvirin, A. V.; Dunbar, K. R. *Angew. Chem. Int. Ed.* **2010**, *49*, 5081.

(140) Beauvais, L. G.; Long, J. R. *J. Am. Chem. Soc.* **2002**, *124*, 2110.

(141) Freedman, D. E.; Jenkins, D. M.; Long, J. R. *Chem. Commun.* **2009**, *0*, 4829.

(142) Hilfiger, M. G.; Chen, M.; Brinzari, T. V.; Nocera, T. M.; Shatruk, M.; Petasis, D. T.; Musfeldt, J. L.; Achim, C.; Dunbar, K. R. *Angew. Chem. Int. Ed.* **2010**, *49*, 1410.

(143) Hilfiger, M. G.; Shatruk, M.; Prosvirin, A.; Dunbar, K. R. *Chem. Commun.* **2008**, 5752.

(144) Tregenna-Piggott, P. L. W.; Sheptyakov, D.; Keller, L.; Klokishner, S. I.; Ostrovsky, S. M.; Palii, A. V.; Reu, O. S.; Bendix, J.; Brock-Nannestad, T.; Pedersen, K.; Weihe, H.; Mutka, H. *Inorg. Chem.* **2008**, *48*, 128.

(145) Dreiser, J.; Pedersen, K. S.; Schnegg, A.; Holldack, K.; Nehrkorn, J.; Sigrist, M.; Tregenna-Piggott, P.; Mutka, H.; Weihe, H.; Mironov, V. S.; Bendix, J.; Waldmann, O. *Chem. Eur. J.* **2013**, *19*, 3693.

(146) AlDamen, M. A.; Cardona-Serra, S.; Clemente-Juan, J. M.; Coronado, E.; Gaita-Ariño, A.; Martí-Gastaldo, C.; Luis, F.; Montero, O. *Inorg. Chem.* **2009**, *48*, 3467.

(147) AlDamen, M. A.; Clemente-Juan, J. M.; Coronado, E.; Martí-Gastaldo, C.; Gaita-Ariño, A. *J. Am. Chem. Soc.* **2008**, *130*, 8874.

(148) Boulon, M.-E.; Cucinotta, G.; Luzon, J.; Degl'Innocenti, C.; Perfetti, M.; Bernot, K.; Calvez, G.; Caneschi, A.; Sessoli, R. *Angew. Chem. Int. Ed.* **2013**, *52*, 350.

(149) Ishikawa, N.; Sugita, M.; Ishikawa, T.; Koshihara, S.-y.; Kaizu, Y. *J. Am. Chem. Soc.* **2003**, *125*, 8694.

(150) Ishikawa, N.; Sugita, M.; Ishikawa, T.; Koshihara, S.-y.; Kaizu, Y. *The Journal of Physical Chemistry B* **2004**, *108*, 11265.

(151) Lin, P.-H.; Korobkov, I.; Burchell, T. J.; Murugesu, M. *Dalt. Trans.* **2012**, *41*, 13649.

(152) Suzuki, K.; Sato, R.; Mizuno, N. *Chemical Science* **2013**, *4*, 596.

(153) Blagg, R. J.; Muryn, C. A.; McInnes, E. J. L.; Tuna, F.; Winpenny, R. E. P. *Angew. Chem. Int. Ed.* **2011**, *50*, 6530.

(154) Coutinho, J. T.; Antunes, M. A.; Pereira, L. C. J.; Bolvin, H.; Marcalo, J.; Mazzanti, M.; Almeida, M. *Dalt. Trans.* **2012**, *41*, 13568.

(155) Rinehart, J. D.; Long, J. R. *J. Am. Chem. Soc.* **2009**, *131*, 12558.

(156) Freedman, D. E.; Harman, W. H.; Harris, T. D.; Long, G. J.; Chang, C. J.; Long, J. R. *J. Am. Chem. Soc.* **2010**, *132*, 1224.

(157) Harman, W. H.; Harris, T. D.; Freedman, D. E.; Fong, H.; Chang, A.; Rinehart, J. D.; Ozarowski, A.; Sougrati, M. T.; Grandjean, F.; Long, G. J.; Long, J. R.; Chang, C. J. *J. Am. Chem. Soc.* **2010**, *132*, 18115.

(158) Jurca, T.; Farghal, A.; Lin, P.-H.; Korobkov, I.; Murugesu, M.; Richeson, D. S. *J. Am. Chem. Soc.* **2011**, *133*, 15814.

(159) Lin, P.-H.; Smythe, N. C.; Gorelsky, S. I.; Maguire, S.; Henson, N. J.; Korobkov, I.; Scott, B. L.; Gordon, J. C.; Baker, R. T.; Murugesu, M. *J. Am. Chem. Soc.* **2011**, *133*, 15806.

(160) Ruamps, R.; Maurice, R.; Batchelor, L.; Boggio-Pasqua, M.; Guillot, R.; Barra, A. L.; Liu, J.; Bendeif, E.-E.; Pillet, S.; Hill, S.; Mallah, T.; Guihéry, N. *J. Am. Chem. Soc.* **2013**, *135*, 3017.

(161) Vallejo, J.; Castro, I.; Ruiz-García, R.; Cano, J.; Julve, M.; Lloret, F.; De Munno, G.; Wernsdorfer, W.; Pardo, E. *J. Am. Chem. Soc.* **2012**, *134*, 15704.

(162) Zadrozny, J. M.; Atanasov, M.; Bryan, A. M.; Lin, C.-Y.; Rekken, B. D.; Power, P. P.; Neese, F.; Long, J. R. *Chemical Science* **2013**, *4*, 125.

(163) Zadrozny, J. M.; Long, J. R. *J. Am. Chem. Soc.* **2011**, *133*, 20732.

(164) Zhu, Y.-Y.; Cui, C.; Zhang, Y.-Q.; Jia, J.-H.; Guo, X.; Gao, C.; Qian, K.; Jiang, S.-D.; Wang, B.-W.; Wang, Z.-M.; Gao, S. *Chemical Science* **2013**.

(165) Rinehart, J. D.; Fang, M.; Evans, W. J.; Long, J. R. *J. Am. Chem. Soc.* **2011**, *133*, 14236.

(166) Luzon, J.; Sessoli, R. *Dalt. Trans.* **2012**, *41*, 13556.

(167) Papatriantafyllopoulou, C.; Wernsdorfer, W.; Abboud, K. A.; Christou, G. *Inorg. Chem.* **2010**, *50*, 421.

(168) Tanase, S.; Ferbinteanu, M.; Cimpoesu, F. *Inorg. Chem.* **2011**, *50*, 9678.

(169) Habib, F.; Long, J.; Lin, P.-H.; Korobkov, I.; Ungur, L.; Wernsdorfer, W.; Chibotaru, L. F.; Murugesu, M. *Chemical Science* **2012**, *3*, 2158.

(170) Cornia, A.; Mannini, M.; Sainctavit, P.; Sessoli, R. *Chem. Soc. Rev.* **2011**, *40*, 3076.

(171) Domingo, N.; Bellido, E.; Ruiz-Molina, D. *Chem. Soc. Rev.* **2012**, *41*, 258.

(172) Gatteschi, D.; Cornia, A.; Mannini, M.; Sessoli, R. *Inorg. Chem.* **2009**, *48*, 3408.

(173) Gonidec, M.; Biagi, R.; Corradini, V.; Moro, F.; De Renzi, V.; del Pennino, U.; Summa, D.; Muccioli, L.; Zannoni, C.; Amabilino, D. B.; Veciana, J. *J. Am. Chem. Soc.* **2011**, *133*, 6603.

(174) Mannini, M.; Pineider, F.; Sainctavit, P.; Danieli, C.; Otero, E.; Sciancalepore, C.; Talarico, A. M.; Arrio, M.-a.; Cornia, A.; Gatteschi, D.; Sessoli, R. *Nature Materials* **2009**, *8*, 194.

(175) Moro, F.; Biagi, R.; Corradini, V.; Evangelisti, M.; Gambardella, A.; De Renzi, V.; del Pennino, U.; Coronado, E.; Forment-Aliaga, A.; Romero, F. M. *J. Phys. Chem. C* **2012**, *116*, 14936.

(176) Rogez, G.; Donnio, B.; Terazzi, E.; Gallani, J.-L.; Kappler, J.-P.; Bucher, J.-P.; Drillon, M. *Adv. Mat.* **2009**, *21*, 4323.

(177) Mannini, M.; Sainctavit, P.; Sessoli, R.; Cartier dit Moulin, C.; Pineider, F.; Arrio, M.-A.; Cornia, A.; Gatteschi, D. *Chem. Eur. J.* **2008**, *14*, 7530.

(178) Lecren, L.; Wernsdorfer, W.; Li, Y.-G.; Vindigni, A.; Miyasaka, H.; Clérac, R. *J. Am. Chem. Soc.* **2007**, *129*, 5045.

(179) Miyasaka, H.; Clérac, R.; Wernsdorfer, W.; Lecren, L.; Bonhomme, C.; Sugiura, K.-i.; Yamashita, M. *Angew. Chem. Int. Ed.* **2004**, *43*, 2801.

(180) Miyasaka, H.; Matsumoto, N.; Ōkawa, H.; Re, N.; Gallo, E.; Floriani, C. *J. Am. Chem. Soc.* **1996**, *118*, 981.

(181) Miyasaka, H.; Clérac, R.; Mizushima, K.; Sugiura, K.-i.; Yamashita, M.; Wernsdorfer, W.; Coulon, C. *Inorg. Chem.* **2003**, *42*, 8203.

(182) Ferbinteanu, M.; Miyasaka, H.; Wernsdorfer, W.; Nakata, K.; Sugiura, K.-i.; Yamashita, M.; Coulon, C.; Clérac, R. *J. Am. Chem. Soc.* **2005**, *127*, 3090.

(183) Sawada, Y.; Kosaka, W.; Hayashi, Y.; Miyasaka, H. *Inorg. Chem.* **2012**, *51*, 4824.

(184) Inglis, R.; Jones, L. F.; Milios, C. J.; Datta, S.; Collins, A.; Parsons, S.; Wernsdorfer, W.; Hill, S.; Perlepes, S. P.; Piligkos, S.; Brechin, E. K. *Dalt. Trans.* **2009**, *0*, 3403.

(185) Miyasaka, H.; Nakata, K.; Sugiura, K.-i.; Yamashita, M.; Clérac, R. *Angew. Chem. Int. Ed.* **2004**, *43*, 707.

(186) Toma, L. M.; Ruiz-Pérez, C.; Pasán, J.; Wernsdorfer, W.; Lloret, F.; Julve, M. *J. Am. Chem. Soc.* **2012**, *134*, 15265.

(187) Tiron, R.; Wernsdorfer, W.; Aliaga-Alcalde, N.; Christou, G. *Physical Review B* **2003**, *68*, 140407.

(188) Tiron, R.; Wernsdorfer, W.; Foguet-Albiol, D.; Aliaga-Alcalde, N.; Christou, G. *Physical Review Letters* **2003**, *91*, 227203.

(189) Wernsdorfer, W.; Aliaga-Alcalde, N.; Hendrickson, D. N.; Christou, G. *Nature* **2002**, *416*, 406.

(190) Avendaño, C. Dissertation, Texas A&M University, 2010.

(191) Bagai, R.; Wernsdorfer, W.; Abboud, K. A.; Christou, G. *J. Am. Chem. Soc.* **2007**, *129*, 12918.

(192) Boskovic, C.; Bircher, R.; Tregenna-Piggott, P. L. W.; Güdel, H. U.; Paulsen, C.; Wernsdorfer, W.; Barra, A.-L.; Khatsko, E.; Neels, A.; Stoeckli-Evans, H. *J. Am. Chem. Soc.* **2003**, *125*, 14046.

(193) Das, A.; Gieb, K.; Krupskaya, Y.; Demeshko, S.; Dechert, S.; Klingeler, R.; Kataev, V.; Büchner, B.; Müller, P.; Meyer, F. *J. Am. Chem. Soc.* **2011**, *133*, 3433.

(194) Guo, Y.-N.; Xu, G.-F.; Wernsdorfer, W.; Ungur, L.; Guo, Y.; Tang, J.; Zhang, H.-J.; Chibotaru, L. F.; Powell, A. K. *J. Am. Chem. Soc.* **2011**, *133*, 11948.

(195) Inglis, R.; Jones, L. F.; Mason, K.; Collins, A.; Moggach, S. A.; Parsons, S.; Perlepes, S. P.; Wernsdorfer, W.; Brechin, E. K. *Chem. Eur. J.* **2008**, *14*, 9117.

(196) Inglis, R.; Taylor, S. M.; Jones, L. F.; Papaefstathiou, G. S.; Perlepes, S. P.; Datta, S.; Hill, S.; Wernsdorfer, W.; Brechin, E. K. *Dalt. Trans.* **2009**, *0*, 9157.

(197) Nguyen, T. N.; Wernsdorfer, W.; Abboud, K. A.; Christou, G. *J. Am. Chem. Soc.* **2011**, *133*, 20688.

(198) Ramsey, C. M.; del Barco, E.; Hill, S.; Shah, S. J.; Beedle, C. C.; Hendrickson, D. N. *Nat Phys* **2008**, *4*, 277.

(199) Yang, E.-C.; Wernsdorfer, W.; Hill, S.; Edwards, R. S.; Nakano, M.; Maccagnano, S.; Zakharov, L. N.; Rheingold, A. L.; Christou, G.; Hendrickson, D. N. *Poly.* **2003**, *22*, 1727.

(200) Gomez-Coca, S.; Ruiz, E. *Dalt. Trans.* **2012**, *41*, 2659.

(201) Miyasaka, H.; Takahashi, H.; Madanbashi, T.; Sugiura, K.-i.; Clérac, R.; Nojiri, H. *Inorg. Chem.* **2005**, *44*, 5969.

(202) Dreiser, J.; Schnegg, A.; Holldack, K.; Pedersen, K. S.; Schau-Magnussen, M.; Nehrkorn, J.; Tregenna-Piggott, P.; Mutka, H.; Weihe, H.; Bendix, J.; Waldmann, O. *Chem. Eur. J.* **2011**, *17*, 7492.

(203) McAuliffe, C. A.; Nabhan, A.; Pritchard, R. G.; Watkinson, M.; Bermejo, M.; Sousa, A. *Acta Crystallogr., Sect. C* **1994**, *50*, 1676.

(204) Heintz, R. A. S., J. A.; Szalay, P. S.; Weisgerber, A.; Dunbar, K. R. *Homoleptic Transition Metal Acetonitrile Cations with Tetrafluoroborate or Trifluoromethanesulfonate Anions*; Wiley-Interscience: New York, 2002; Vol. 33.

(205) Hilfiger, M. G. Dissertation, Texas A&M University, 2010.

(206) Cauzzi, D. A.; Mori, G.; Predieri, G.; Tiripicchio, A.; Cavatorta, F. *Inorg. Chim. Acta* **1993**, *204*, 181.

(207) Borrás-Almenar, J. J.; Clemente-Juan, J. M.; Coronado, E.; Tsukerblat, B. S. *J. Comp. Chem.* **2001**, *22*, 985.

(208) Coulon, C.; Miyasaka, H.; Clérac, R. In *Single-Molecule Magnets and Related Phenomena*; Winpenny, R., Ed.; Springer Berlin Heidelberg: 2006; Vol. 122, p 163.

(209) Przychodzen, P.; Korzeniak, T.; Podgajny, R.; Sieklucka, B. *Coord. Chem. Rev.* **2006**, *250*, 2234.

(210) Sokol, J. J.; Hee, A. G.; Long, J. R. *J. Am. Chem. Soc.* **2002**, *124*, 7656.

(211) Mironov, V. S.; Chibotaru, L. F.; Ceulemans, A. *J. Am. Chem. Soc.* **2003**, *125*, 9750.

(212) Wang, X.-Y.; Hilfiger, M. G.; Prosvirin, A.; Dunbar, K. R. *Chem. Commun.* **2010**, *46*, 4484.

(213) Buschmann, W. E.; Miller, J. S. *Inorganic Synthesis*; John Wiley and Sons: New York, 2002; Vol. 33.

(214) Casey, A. T.; Clark, R. J. H.; Nyholm, R. S.; Scaife, D. E.; Boyd, T. E.; Rhine, W.; Stucky, G. In *Inorganic Syntheses*; John Wiley & Sons, Inc.: 2007, p 165.

(215) Siemens Analytical X-ray Instruments Inc.: Madison, 1996.

(216) Sheldrick, G. M.; University of Gottinggen: Gottinggen, 1996.

(217) Sheldrick, G. M. *Acta Crystallogr., Sect. A, Foundat. of Crystallogr.* **2008**, *64*, 112.

(218) Barbour, L. J. *J. of Supramol. Chem.* **2003**, *1*, 189.

(219) Clima, S.; Hendrickx, M. F. A.; Chibotaru, L. F.; Soncini, A.; Mironov, V.; Ceulemans, A. *Inorg. Chem.* **2007**, *46*, 2682.

(220) Li, D.-F.; Gao, S.; Zheng, L.-M.; Sun, W.-Y.; Okamura, T.-a.; Ueyama, N.; Tang, W.-X. *New Journal of Chemistry* **2002**, *26*, 485.

(221) Herrera, J. M.; Bleuzen, A.; Dromzée, Y.; Julve, M.; Lloret, F.; Verdaguer, M. *Inorg. Chem.* **2003**, *42*, 7052.

(222) Bałanda, M.; Korzeniak, T.; Pełka, R.; Podgajny, R.; Rams, M.; Sieklucka, B.; Wasiutyński, T. *Solid State Sciences* **2005**, *7*, 1113.

(223) Bałanda, M.; Pełka, R.; Wasiutyński, T.; Rams, M.; Nakazawa, Y.; Miyazaki, Y.; Sorai, M.; Podgajny, R.; Korzeniak, T.; Sieklucka, B. *Physical Review B* **2008**, *78*, 174409.

(224) Kaneko, S.; Tsunobuchi, Y.; Sakurai, S.; Ohkoshi, S.-i. *Chemical Physics Letters* **2007**, *446*, 292.

(225) Korzeniak, T.; Podgajny, R.; Alcock, N. W.; Lewiński, K.; Bałanda, M.; Wasiutyński, T.; Sieklucka, B. *Poly.* **2003**, *22*, 2183.

(226) Korzeniak, T.; Stadnicka, K.; Rams, M.; Sieklucka, B. *Inorg. Chem.* **2004**, *43*, 4811.

(227) Korzeniak, T.; Stadnicka, K.; Pelka, R.; Balanda, M.; Tomala, K.; Kowalski, K.; Sieklucka, B. *Chem. Commun.* **2005**, *0*, 2939.

(228) Ohkoshi, S.-i.; Arimoto, Y.; Hozumi, T.; Seino, H.; Mizobe, Y.; Hashimoto, K. *Chem. Commun.* **2003**, *0*, 2772.

(229) Podgajny, R.; Korzeniak, T.; Balanda, M.; Wasiutynski, T.; Errington, W.; Kemp, T. J.; Alcock, N. W.; Sieklucka, B. *Chem. Commun.* **2002**, *0*, 1138.

(230) Pratt, F. L.; Zieliński, P. M.; Bałanda, M.; Podgajny, R.; Wasiutyński, T.; Sieklucka, B. *Journal of Physics: Condensed Matter* **2007**, *19*, 456208.

(231) Sieklucka, B.; Korzeniak, T.; Podgajny, R.; Bałanda, M.; Nakazawa, Y.; Miyazaki, Y.; Sorai, M.; Wasiutyński, T. *Journal of Magnetism and Magnetic Materials* **2004**, *272–276, Part 2*, 1058.

(232) Podgajny, R.; Korzeniak, T.; Stadnicka, K.; Dromzee, Y.; Alcock, N. W.; Errington, W.; Kruczala, K.; Balanda, M.; Kemp, T. J.; Verdaguer, M.; Sieklucka, B. *Dalt. Trans.* **2003**, *0*, 3458.

(233) Podgajny, R.; Pełka, R.; Desplanches, C. d.; Ducasse, L.; Nitek, W.; Korzeniak, T.; Stefanczyk, O.; Rams, M.; Sieklucka, B.; Verdaguer, M. *Inorg. Chem.* **2011**, *50*, 3213.

(234) Zhao, H.; Shatruk, M.; Prosvirin, A. V.; Dunbar, K. R. *Chem. Eur. J.* **2007**, *13*, 6573.

(235) Bonadio, F.; Gross, M.; Stoeckli-Evans, H.; Decurtins, S. *Inorg. Chem.* **2002**, *41*, 5891.

(236) Larionova, J.; Gross, M.; Pilkington, M.; Andres, H.; Stoeckli-Evans, H.; Güdel, H. U.; Decurtins, S. *Angew. Chem. Int. Ed.* **2000**, *39*, 1605.

(237) Zhong, Z. J.; Seino, H.; Mizobe, Y.; Hidai, M.; Fujishima, A.; Ohkoshi, S.-i.; Hashimoto, K. *J. Am. Chem. Soc.* **2000**, *122*, 2952.

(238) Korzeniak, T.; Desplanches, C. d.; Podgajny, R.; Giménez-Saiz, C.; Stadnicka, K.; Rams, M.; Sieklucka, B. *Inorg. Chem.* **2009**, *48*, 2865.

(239) Podgajny, R.; Desplanches, C.; Sieklucka, B.; Sessoli, R.; Villar, V.; Paulsen, C.; Wernsdorfer, W.; Dromzée, Y.; Verdaguer, M. *Inorg. Chem.* **2002**, *41*, 1323.

(240) Ko, H. H.; Lim, J. H.; Yoo, H. S.; Kang, J. S.; Kim, H. C.; Koh, E. K.; Hong, C. S. *Dalt. Trans.* **2007**, *0*, 2070.

(241) Kou, H.-Z.; Zhou, Bei C.; Si, S.-F.; Wang, R.-J. *European Journal of Inorganic Chemistry* **2004**, *2004*, 401.

(242) Podgajny, R.; Korzeniak, T.; Przychodzeń, P.; Gimenez-Saiz, C.; Rams, M.; Kwaśniak, M.; Sieklucka, B. *European Journal of Inorganic Chemistry* **2010**, *2010*, 4166.

(243) Yoon, J. H.; Lim, J. H.; Kim, H. C.; Hong, C. S. *Inorg. Chem.* **2006**, *45*, 9613.

(244) Freedman, D. E.; Bennett, M. V.; Long, J. R. *Dalt. Trans.* **2006**, *0*, 2829.

(245) Berlinguette, C. P.; Galán-Mascarós, J. R.; Dunbar, K. R. *Inorg. Chem.* **2003**, *42*, 3416.

(246) Berlinguette, C. P.; Vaughn, D.; Cañada-Vilalta, C.; Galán-Mascarós, J. R.; Dunbar, K. R. *Angew. Chem. Int. Ed.* **2003**, *42*, 1523.

(247) Shatruk, M.; Chambers, K. E.; Prosvirin, A. V.; Dunbar, K. R. *Inorg. Chem.* **2007**, *46*, 5155.

(248) Leipoldt, J. G.; Bok, L. D. C.; Cilliers, P. J. *Z. anorg. allg. Chem.* **1974**, *407*, 350.

(249) Leipoldt, J. G.; Bok, L. D. C.; Cilliers, P. J. *Z. anorg. allg. Chem.* **1974**, *409*, 343.

(250) Bok, L. D. C.; Leipoldt, J. G.; Basson, S. S. *Z. anorg. allg. Chem.* **1975**, *415*, 81.